Dendritic Poly(3-hexylthiophene) Star Copolymer Systems for Next Generation Bulk Heterojunction Organic Photovoltaic Cells

Anne Lutgarde Djoumessi Yonkeu

BSc Chemistry, University of Buea, BSc Honours Chemistry, UWC (***Cum Laude)***

MSc Nanoscience, UWC (***Cum Laude***)

A thesis submitted in fulfilment of the requirements for the degree of

PHILOSOPHIAE DOCTOR

Department of Chemistry, Faculty of Natural Sciences, University of the Western Cape, South Africa

Supervisor: Professor Emmanuel I. Iwuoha

Co-supervisor: Professor Vera Cimrova

December 2018

ABSTRACT

The continuous increase in energy consumption and decrease in fossil fuels reserves are a primary concern worldwide; especially for South Africa. Therefore, there is an urgent need for alternative energy resources that will be sustainable, and environmentally friendly in order to tackle the ecological degradation generated by the use of fossil fuels. Among many energy 'niches', solar energy appears to be one of the most promising and reliable for the African continent because of the constant availability of sun light. Organic conjugated polymers have been identified as suitable materials to ensure proper design and fabrication of flexible, easy to process and cost-effective solar cells. Their tendency to exhibit good semiconducting properties and their capability to absorb photons from the sunlight and convert it into electrical energy are important features that justify their use in organic photovoltaic cells. Many different polymers have been investigated as either electron donating or electron accepting materials. Among them, poly(3-hexylthiophene) is one of the best electron donor materials that have been used in organic photovoltaic cells. It is a good light absorber and its Highest Occupied Molecular Orbital (HOMO) energy level is suitable to allow electron transfer into an appropriate electron acceptor. On the other hand, the molecular ordering found in dendrimers attracted some interest in the field of photovoltaics as this feature can ensure a constant flow of charges. In this work, I hereby report for the first time, the chemical synthesis of a highly crystalline dendritic star copolymer generation 1 poly(propylene thiophenoimine)-co-poly(3-hexylthiophene) (G1PPT-co-P3HT) with high molecular weight and investigate its application as donating material in bulk heterojunction organic photovoltaics. The crystalline nature of this macromolecule was conferred by 84 % regioregularity found in the

extended conjugation of poly(3-hexylthiophene). The star polymer exhibited good absorption properties with an optical energy band gap as low as 1.43 eV, which is in the spectral range for an ideal light absorber. The requirement that a donor material should have its highest occupied molecular orbital, HOMO below the air-oxidation energy level was also achieved by the star-copolymer whose HOMO energy level is found to be -5.53 eV. G1PPT-co-P3HT with particle size of less than 90 nm also demonstrated good semiconducting properties with phase degree slightly above 74; and good electron donating properties characterized by photo-induced intermolecular charge transfer to the acceptor copolymer, poly[N,N-bis(dodecyl)perylene-3,4,9,10-tetracarboxylic diimide-1,7-diyl-alt-9-(heptadecan-9-yl)carbazole-2,7-diyl] (PDI-co-Carbazole). Such property was exhibited when G1PPT-co-P3HT was blended in bulk heterojunction systems with this electron accepting, perylene-based copolymer through photoluminescence quenching. The acceptor was prepared by Suzuki coupling and also demonstrated good absorption and semiconducting properties. Even though, the two materials demonstrated good features toward photovoltaic application, the device characteristics of their bulk heterojunction active layer G1PPT-co-P3HT:PDI-co-Carbazole (2:1) were very poor with an open-circuit voltage V_{OC} below 10 mV and a short-circuit current J_{SC} in the microampere range. Förster resonance energy transfer, as observed from the donor emission and acceptor absorption spectral overlap and suggested to be accompanied by non-radiative charge carriers' recombination, is one of the main factors that led to such poor performances. Also, defects that act as traps, observed in their molecular structure as seen on their HRSEM images aided in these charge carriers' recombination.

Because charge transport constitutes an important step in the photovoltaic process, in the course of this work, the hole mobilities of a series of thienothiadiazole/fluorene-based copolymers were also investigated. The results obtained demonstrate that the extent of hole transport is strongly associated with the type of alkyl chains used as substituents - straight or branched, the molecular weight and the dispersity of the copolymers. Saturated hole mobility, μ_{sat}, as high as 2.4×10^{-2} cm^2/Vs was obtained from the longer, straight dodecyl substituent on the thienothiadiazole component.

KEY WORDS

Band gap

Bulk heterojunction

Conjugated polymers

Dendrimers

Hole mobilities

HOMO

LUMO

Molecular ordering

Organic field-effect transistors

Organic photovoltaics

Photoluminescence quenching

Poly(propylene thiophenoimine)-co-poly(ethylenedioxythiophene), generation 1

Power conversion efficiency

Thiophene

DECLARATION

I, hereby declare that "**Dendritic Poly(3-hexylthiophene) Star Copolymer Systems for Next Generation Bulk Heterojunction Organic Photovoltaic Cells**" is my own work; that it has not been previously submitted for any degree or examination in any other university or higher education; and that all the sources and quotations have been indicated and acknowledged by complete references.

Anne Lutgarde Djoumessi Yonkeu Date : December 2018

Signature :

DEDICATION

This work is dedicated to

My mom, **Melanie Tchounke Djoumessi**

and

My late dad, **Binjamen Djoumessi** …

ACKNOWLEDGEMENTS

To God Almighty be the Glory for without HIM, my maker and perfecter I would not have been able to come this far. I thank my Lord and Saviour Jesus for giving me the strength and wisdom through the Holy Spirit, to successfully complete this work. As, His word says, in Ecclesiastes 7,8 "Better is the end of a thing than the beginning thereof".

I am exceedingly grateful to my supervisor Prof. Emmanuel Iwuoha; and co-supervisor Prof. Vera Cimrova for their academic guidance, kindness and their patience. Special thanks to Prof. Emmanuel for the opportunity he gave me to be part of his research group and for trusting in me. I am mostly thankful because in him, I found not only a mentor and supervisor but a role model and father. I would have not asked for a better supervisor; you are the best a student and child could ever have.

I thank my parents, late dad, Binjamen Djoumessi and my mum, Melanie Tchounke Djoumessi for their unconditional love and support. They have been role models and source of inspiration all my life. This is just the result of their hard work and perseverance. Thanks especially to this prayer warrior that you are *maman*. You wanted me so badly to be a Doctor, so this dissertation is more yours than mine. I also extend my gratitude to the members of my entire family for their encouragement.

Dr B. Hollong, Gautier Djoumessi, Alain Ngatat, Marlene Djoumessi and Dimitri Djoumessi, where will I have been without you? Your constant check, words, encouragement, smile, trust and love gave me a reason never to give up. Thank you! Vanessa Djoumessi, my sister, my 'mother',

the ‘mother of Qerene’, I am pouring tears as I write these words. You showed me what it is meant to have a sister through your love, kindness, patience and above all constant prayers and I am forever grateful. May Our Almighty Father abundantly bless you. Qerene R. O. Hollong, my daughter, my ‘first PhD’, you came …and you gave me more reasons to pursue my dream. Now I look forward seeing you become a PhD.

To my beloved Estelle Tshouongang, Dr Gertrude Fomo, Judith Donang, Carole Kodjou, Etchu Esther, Miranda Ndipingwi and others, your love, care and support led me through. Be blessed!

To my spiritual family: Pastors Winifred and Daniel Anga’ama and all my brethren especially Mr Georges Mbuya and Mr Hans Anyikame, I extend my heartfelt thanks as your encouragement and prayers are rewarded here.

To all my SensorLab colleagues particularly Dr Chinwe, Dr Abdul, Dr Masikini, Dr Tesfaye, Candice Franke, Penny Mathumba, your assistance, advice and encouragement have always been a blessing and I will like you to receive my gratitude. To the rest of the Chemistry Department, especially to Prof P. Baker and Mrs W. Jackson; and E. Mc Donald (Electron Microscopy Unit), S. Magubane and Dr S. Halindintwali at the Department of Physics, I extend my gratitude.

Finally, I will like to thank the National Research Foundation (NRF) of South Africa for the award of Doctoral Scholarship through the South African Research Chair Initiative (SARChI) for NanoElectrochemistry and Sensor Technology of Prof E. Iwuoha. I am grateful to the Czech Academy of Science for funding of the IUPAC/UNESCO Postgraduate Course in Polymer Science done at the Institute of Macromolecular Chemistry, Prague, Czech Republic from October 2015 to July 2016.

LIST OF PUBLICATIONS

Anne L. Djoumessi Yonkeu, Abdalmoman Baleg, Miranda M. Ndipingwi, Ntuthuko W. Hlongwa, Nomxolisi Dywili, Masikini Milua, Emmanuel Iwuoha· Naphthalene Diimide Photoluminescent Quenching Effects on Poly(propylene thiophenoimine)-co-poly(ethylenedioxythiophene) Star Copolymer. *SN Applied Sciences*. Submitted.

Naledi Raleie, Penny Mathumba, Nomxolisi Dywili, Ntuthuko W. Hlongwa, **Anne Lutgarde Djoumessi Yonkeu**, Masikini Milua, Emmanuel Iwuoha. Novel benzothiadiazole metallo-polymers containing tin-based nanoalloys for high efficiency bulk heterojunction solar cells. *Electrocatalysis*. Submitted.

Ndipingwi, M. M, Ikpo, C. O., Hlongwa, N. W., Dywili, N., **Djoumessi Yonkeu, A. L**. & Iwuoha, E. I. Crystal chemistry and lithium-ion intercalation properties of lithium manganese silicate cathode for aqueous rechargeable Li-ion batteries. *Journal of Applied Electrochemistry* (2019). https://doi.org/10.1007/s10800-019-01296-0

Dywili, N.R.; Ntziouni, A.; Ikpo, C.; Ndipingwi, M.; Hlongwa, N.W.; **Yonkeu, A.L.D**.; Masikini, M.; Kordatos, K.; Iwuoha, E.I. Graphene Oxide Decorated Nanometal-Poly(Anilino-Dodecylbenzene Sulfonic Acid) for Application in High Performance Supercapacitors. Micromachines, 10 (2019). https://doi.org/10.3390/mi10020115

Hlamulo Makelane, Suru V. John, **Anne L. Djoumessi Yonkeu**, Tesfaye Waryo, Oluwakemi Tovide, and Emmanuel Iwuoha. Phase Selective Alternating Current Voltammetric Signalling Protocol: Application in Dendritic Co-polymer Sensor for Anthracene. *Electroanalysis*, 29, 1887 – 1893 (2017).

Nolubabalo Matinise, Noluthando Mayedwa, Chinwe O. Ikpo, Ntuthuko Wonderboy Hlongwa, Miranda M. Ndipingwi, Lerato Molefe, Nomxolisi Dywili, **Anne Lutgarde Djoumessi Yonkeu**, Tesfaye Waryo, Priscilla Gloria Lorraine Baker, Emmanuel Iheanyichukwu IwuohaBimetallic Nanocomposites of Palladium (100) and Ruthenium for Electrooxidation of Ammonia. *Journal of Nano Research*, 44, 100-113 (2016).

Nomxolisi Dywili, Njagi Njomo, Chinwe O. Ikpo, **Anne Lutgarde Djoumessi Yonkeu**, Suru Vivian John, Ntuthuko Wonderboy Hlongwa, Naledi Raleie, Emmanuel Iheanyichukwu Iwuoha. Anilino-Functionalized Graphene Oxide Intercalated with Pt Metal Nanoparticles for Application as Supercapacitor Electrode Material. *Journal of Nano Research*, 44, 79-89 (2016).

Abd Almonam Baleg, Nazeem Jahed, **Anne L. Djoumessi Yonkeu**, Njagi Njomo, Gcineka Mbambisa, Kerileng M. Molapo, Xolile G. Fuku, Gertrude Fomo,Hlamulo Makelane, Abebaw Tsegaye, Tesfaye T. Waryo, Priscilla Baker,Sibulelo Vilakazi, Robert Tshikhudo, Emmanuel I. Iwuoha. Impedimetry and microscopy of electrosynthetic poly(propyleneimine)-co-polypyrrole conducting dendrimeric star copolymers. *Electrochimica* Acta 128, 448–457 (2014).

Anne L. Djoumessi Yonkeu, O. Rasoga, M. Socol, C. Breazu, N. Preda, A. Stanculescu, F. Stanculescu, E. Iwouha. On the optical and electrical properties of organic heterostructures based on star-shaped dendritic polymer donor and naphthalene diimide derivative acceptor. Journal of Materials Science. In preparation.

Anne L. Djoumessi Yonkeu, Abd Almoman Baleg, Emmanuel Iwouha. Photophysical and electroanalytical investigation of highly crystalline first-time chemically prepared poly(propylene thiophenoimine)-co-poly(3-hexylthiophene) Star Copolymer. Macromolecular, Materials and engineering. In preparation.

Anne Lutgarde Djoumessi Yonkeu, Naledi Raleie, Penny Mathumba, Abd Almoman Baleg, Emmanuel Iwouha. Optical, photophysical, electronic and photovoltaic characteristics of poly(perylene diimide-co-carbazole)/poly(propylene thiephenoimine)-co-poly(3-hexylthiophene) bulk heterojunction nanocomposites. SN Applied Sciences. In preparation.

Anne Lutgarde Djoumessi Yonkeu, Veřa Cimrová, Drahomír Výprachtický, Veronika Pokorná, Emmanuel Iwouha. Hole mobilities in alkylated thienothiadiazole/fluorene copolymers. Polymer. In preparation.

CONFERENCES AND WORKSHOPS

CONFERENCES

April 2018: 4th International Symposium on Electrochemistry, "Pure and Applied Electrochemistry", Johannesburg, South Africa. (Poster presentation).

October 2016: Nanoscience Symposium, Cape Town, South Africa. (Oral Presentation).

WORKSHOPS

July 2016: Career in Polymers Workshop at the Institute of Macromolecular Chemistry, Prague, Czech Republic. (Oral Presentation).

May 2015: MAPET 2015 Workshop, University of the Western Cape, Cape Town, South Africa. (Poster presentation).

RESEARCH VISITS

January-April 2017: Research visit at the Institute of Macromolecular Chemistry, Prague, Czech Republic.

October 2015– July 2016: Postgraduate Course in Polymer Science at the Institute of Macromolecular Chemistry, Prague, Czech Republic.

November-December 2014: Research visit at the National Institute of Materials Physics, Bucharest-Magurele, Romania.

September -October 2014: Research Exchange Program with LaborQ laboratory in the frame of European project FP7 Marie Curie International Research Staff Exchange, at University of Bucharest, Bucharest, Romania.

TABLE OF CONTENTS

LIST OF FIGURES

LIST OF TABLES

LIST OF SCHEMES

I can all things through Christ which strengtheneth me

Ph 4:13

CHAPTER ONE

Conjugated polymers at the rescue of energy shortage

1.1 Background

Over the past decades, conjugated polymers have attracted an increasing amount of attention mainly because they have demonstrated outstanding properties towards soft, processable, easy-to-manufacture, stretchable, large-area and cheaper electronic devices[1,2] for applications in areas such as organic field-effect transistors (OFETs)[2–4] and organic photovoltaic cells (OPVs)[5–8] (Figure 1.1 shows their characteristic device images). This is possible, thanks to the conjugated electronic and polymeric structures of the polymers, resulting in semiconducting properties with good solution processability, mechanical properties and thermal stability.[9,10] In order to afford new conjugated polymers with excellent photoelectrical properties, appropriate design and synthesis of the macromolecules with different architectures and functional moieties are crucial.[11] Among conjugated polymers, polymers consisting of alternating electron donor (D) and electron acceptor (A),[12–19] known as D–A conjugated polymers and low-band gap polymers have been extensively investigated recently. Indeed, varying the electron donating or electron withdrawing component in

these conjugated polymers results in the effective tunability of the electronic absorptions; highest occupied molecular orbital/lowest unoccupied molecular orbital (HOMO/LUMO) energies, and band gap energy, E_g; inter-chain interactions and thin-film morphologies of these conjugated polymers[12–19] which in turn, has an impact on the semiconductors performances. As such, n-type, p-type or even ambipolar polymeric semiconductors with high charge carrier mobilities have been designed and prepared based on D–A and low band-gap conjugated polymers.[20–23]

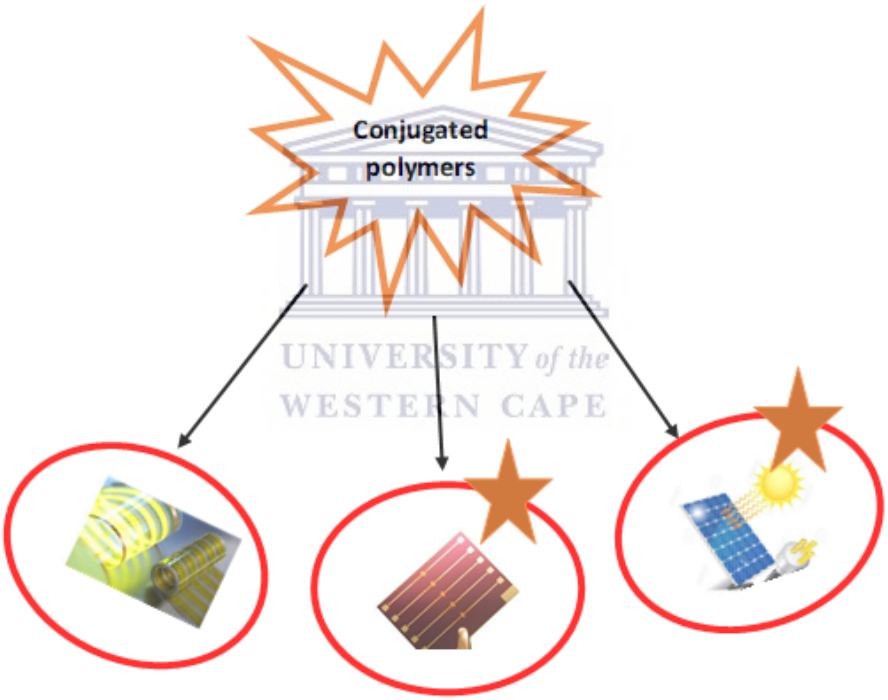

Figure 1.1 Applications of conjugated polymers in electronics and photonics

1.2 Problem statement: the world facing an energy shortage crisis

Leaving in a more industrialized and digitalized era where there is an unceasingly growing demand for energy and more developed electronics, the world is in need of alternative sustainable solutions.[24] Especially when considering that over the past centuries, the world energy consumption has been majorly based on *fossil fuels* – this term refers to a group of energy sources consisting of oil, coal and natural gas- whose usage has exponentially increased with the growing world population.[25] Fossil fuels are not renewable, and as such it is expected that the world will reach a point at which their reserves will be completely depleted. Shafiee and Topal, for instance, in the report of their investigation published in 2009, demonstrated that the fossil fuels predicted complete depletion time is 35, 107 and 37 years for oil, coal and gas, respectively.[26] The other disadvantage of the use of these energy resources is their environmental impact that include the degradation of the sea fauna and flora and the destruction of the ozone layer. Thus, the indisputable urgent need to look for alternative environmental friendly, clean and renewable sources of energy.[27] Over the past decennia, a lot of research has been conducted to develop and/or improve new energy carriers such as biomass, biofuel, wind energy, hydrothermal power and solar energy as potentially good replacements for fossil fuels.[27,28] Among all these renewable energy sources, solar energy has captured much more interest compared to other energy sources. Indeed, besides its renewability and ecological advantages, the continuous irradiation of sunlight throughout the year and almost all over the earth justifies such interest. For many years now, through constant development and improvement of materials, solar energy has been able to contribute considerably

to the decrease in fossil fuels dependency. Figure 1.2 shows the different energy sources arranged in two main categories: renewable and non-renewable.

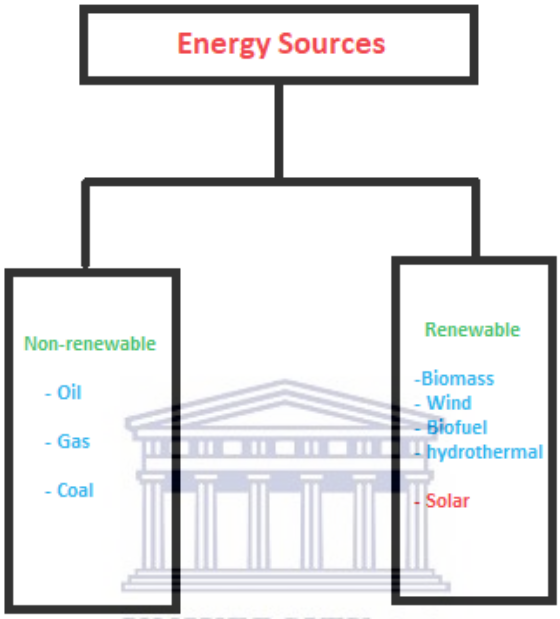

Figure 1.2 Types of energy sources

1.3 Rationale: Solar Cells, a field always developing, contribution of conjugated polymers

Even though the *photovoltaic effect* was discovered in 1839,[29] it is only many years later that practical photovoltaic power became a possibility. Indeed, the first group of solar cells as reported by Chapman, Fuller, and Pearson was made of p-n junctions in crystalline Silicon (c-Si) with a

typical conversion efficiency of about 6%.[30] At that time, available literature also reported that c-Si could only attain a maximum power conversion efficiency (PCE) of about 24%, which could solely be achieved by highly pure materials.[29] This use of Si as the unique solar cell material of choice was due to its great features such as non-toxicity, abundance and availability – Si being the element mostly present on earth, besides oxygen. As a quite new technology, Si-based solar panels faced the challenge of extremely high cost. Nevertheless, developments during the 1950s and 1960s led to the application of silicon photovoltaic technology in areas going from satellites to rooftops. And despite high cost issue, c-Si solar cells till to date remain the most efficient and stable type of solar cells; thanks to the wide photons absorption over visible and infrared regions and the high mobility of generated charge carriers.[29] The disadvantages faced by these c-Si solar panels are associated with the high fabrication cost of large-area c-Si wafers, faster rates of the charge carriers' recombination, and the loss as heat of an important amount of energy of high-energy photons (with ultraviolet and blue wavelengths). These drawbacks led to the need for developing new types of photovoltaic cells materials: the 'second generation of solar cells' that englobes thin-film solar cells based on amorphous silicon (a-Si); quantum dots materials such as cadmium telluride (CdTe) or copper indium gallium diselenide (CIGS), gallium-arsenide (GaAs); and the Grätzel cells, generally referred to as Dye-sensitized solar cells (DSSC) based on the sensitized absorption of nanocrystalline titanium dioxide (TiO_2) and other nanocrystalline molecules.[30–33] Although this second category of solar cells could afford thin-films being fabricated on a big range of substrates, including flexible substrates and textiles, and a reduced production cost; power conversion efficiency far lower than c-Si cells remains the main issue. This

brought up the era of the 'third generation of solar cells': Organic photovoltaic cells denoted, OPVs. Figure 1.3 summarizes the different types of solar cells.[34]

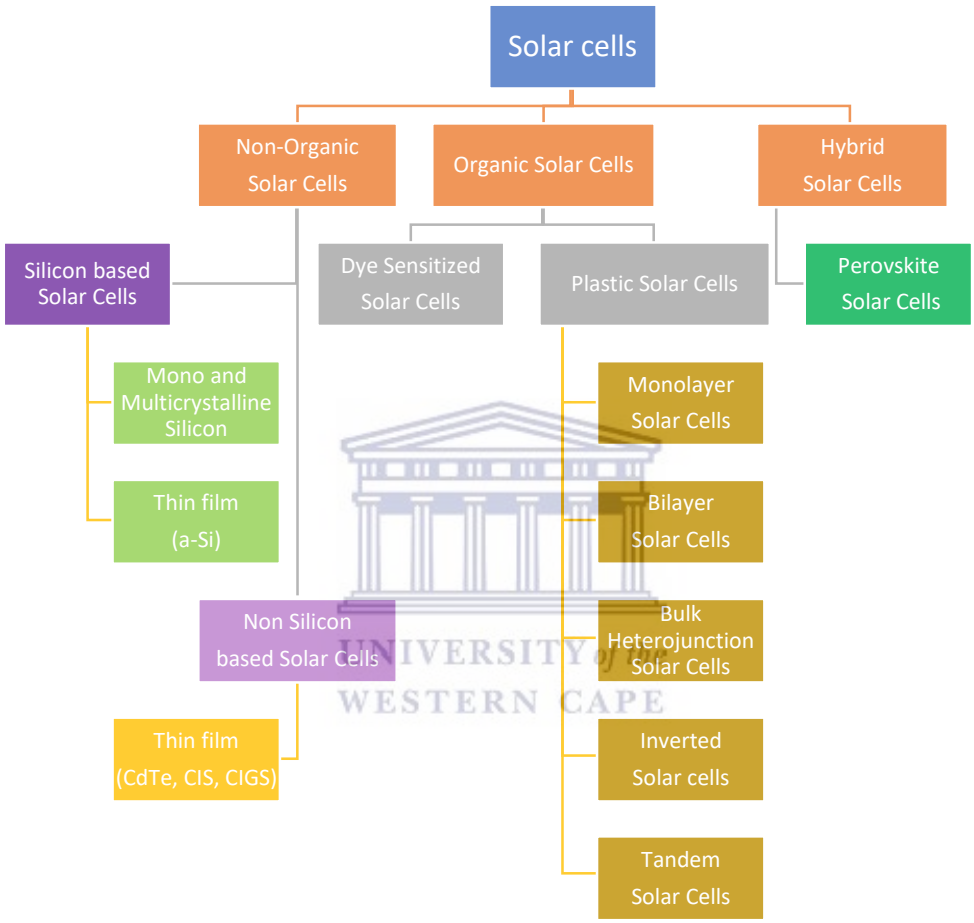

Figure 1.3 Types of solar cells[34]

During the past four decades, an important effort has been put into developing organic solar cells as they offer more sustainable advantages compared to silicon and other photovoltaic

technologies.[35] This field began with the use of small organic molecules such as pigments;[36,37] and with the development of semiconducting polymers which have been playing a big role in designing OPVs with remarkable improvement. The great potential of organic semiconductors lies in their ability to absorb light in the ultraviolet – visible (UV-Vis) region of the solar spectrum as a result of the sp^2-hybridization of their carbon atoms, and in their ability to transport electric current. An important downfall of organic semiconducting materials over their inorganic counterparts is generally the poor (lower order of magnitude) charge-carrier mobility in organic materials[38] which in turn has a greater effect on OPVs' design and efficiency. Nevertheless, their relatively strong absorption coefficients (usually 10^5 cm^{-1}) partly balance the low mobility; therefore, giving rise to high absorption even with thin devices with dimensions less than 100 nm[30]. Another important difference to inorganic, crystalline semiconductors, is the quite small length of diffusion of primary photoexcitations (referred to as excitons) compare to the rather amorphous and disordered molecular structure found in organic materials.[39] Being very important intermediates in the solar energy conversion process, these excitons usually require strong electric fields to be separated into free charge carriers - the final products of outermost importance for photovoltaic conversion. This is because exciton binding energies usually exceed those of inorganic semiconductors.[40] Such features of organic semiconducting materials generally lead to devices with layer thicknesses of the order of 100 nm. Most organic semiconductors are hole-conductors (electron donors or p-type materials) and have their optical band gap around 2 eV, much higher than that of silicon; resulting in the restriction of the harvesting of the solar spectrum to a great extent. Nonetheless, the chemical flexibility allowing for modifications of organic semiconductors via synthetic methods; as well as

the perspective of low cost, large-scale production drives the research in this field in academia and industry.[30]

The attractive features of organic photovoltaic cells can be summarized as below,[41]

- flexible and semi-transparent,
- Can be manufactured via continuous printing process,
- printing on large surfaces,
- Ease to integrate in various devices
- Environmentally-friendly and cost-effective

1.4 Thesis statement

Conjugated polymers with low band gap energy and/or with alternating donor and acceptor are extensively used for the design of flexible, low-cost and highly efficient optoelectronic and photonic devices. Study of the charge carrier mobility of some thienothiadiazole/fluorene copolymers and investigation of the power conversion efficiency of a novel dendritic bulk heterojunction nanocomposite might bring a new insight into organic transistors and photovoltaic fields.

1.5 Research questions

The following research questions have been set in order to establish a guideline to efficiently conduct this work.

- What is the effect of alkyl substitution on the charge transport properties of thienothiadiazole-fluorene copolymers?
- Do parameters such as alkyl substitution, molecular weight, dispersity, temperature, thickness affect the transport properties in thienothiadiazole-fluorene copolymers?
- How do optical, photophysical and electronic properties determine the potential applicability of Poly[N,N'-bis(dodecyl)perylene-3,4,9,10-tetracarboxylicdiimide-1,7-diyl-alt-9(heptadecan-9-yl)carbazole-2,7-diyl] (PDI) copolymer as an electron acceptor in organic photovoltaics?
- How do parameters such as molecular ordering, crystallinity and light absorption determine the qualification of generation 1 poly(propylene thiopheneoime)-co-poly(3-hexylthiophene) (G1PPT-co-P3HT) as a good donor material in organic photovoltaics?
- What are the photovoltaic properties exhibited by G1PPT-co-P3HT:PDI bulk heterojunction systems and what is the morphology-performance relationship?

1.6 Aim and objectives of the study

1.6.1 Aim of the study

Investigating the effects of alkyl substitution, molecular weight, dispersity, device thickness on the charge carrier transport properties of thienothiadiazole-fluorene copolymers in organic field effect transistors; preparing a novel bulk heterojunction nanocomposite system comprising poly (propylene thiophenoimine) dendritic star copolymer and a perylene-based copolymer and investigate its performance in organic photovoltaic cell.

1.6.2 Objectives of the study

The objectives of the study were to

1. investigate charge carrier mobilities in alkylated thienothiadazole-fluorene copolymers.
2. synthesize a conjugated D-A copolymer based on dodecyl perylene diimide and carbazole via Suzuki coupling.
3. chemically prepare novel poly(propylene thiophenoimine) -co-poly(3-hexylthiophene) star copolymer via oxidative condensation using $FeCl_3$.

4. interrogate the spectroscopic, morphological, structural, electrochemical/electronic and optical characteristics of the synthesized macromolecules.

5. understand the performance/structure - morphology relationship in the fabricated bulk heterojunction devices.

1.7 Thesis Structure

The thesis is divided into eight chapters.

CHAPTER ONE gives the background, problem statement, rationale and motivation, research questions, thesis statement, aims and objectives of the research as well as the thesis structure.

CHAPTER TWO presents a detailed review on conjugated polymers for organic photovoltaic cells and organic field-effect transistors and parameters affecting charge transport properties and photovoltaic performances.

CHAPTER THREE gives details on the materials used, describes the major reaction processes employed for monomer preparation and functionalization; and synthesis of the copolymers; the general experimental procedures, and a detailed methodology of the research.

CHAPTER FOUR presents the results on the hole mobilities of copolymers based on 4,6-bis(3'-alkylthien-2'-yl)thieno[3,4-c][1,2,5]thiadiazole and 9,9-dioctylfluorene with different alkyl substitutions.

CHAPTER FIVE elaborates on the synthesis and characterization of Poly[N,N'-bis(dodecyl)perylene-3,4,9,10-tetracarboxylic diimide-1,7-diyl-alt-9-(heptadecan-9-yl)carbazole-2,7-diyl] (PDI-co-Carbzole).

CHAPTER SIX reports on the morphological, optical, photophysical and electrochemical investigation of highly crystalline chemically prepared poly(propylene thiophenoimine)-co-poly(3-hexylthiophene) star-copolymer (G1PPT-co-P3HT).

CHAPTER SEVEN discusses the intermolecular charge transfer, photoluminescence quenching effects, photovoltaic properties and morphology-performance relationship of G1PPT-co-P3HT / PDI-co- Carbazole bulk heterojunction systems.

CHAPTER EIGHT summarizes the findings of this work and gives recommendations for future work.

References

1. Luo, H., Liu, Z. & Zhang, D. Conjugated D–A terpolymers for organic field-effect transistors and solar cells. *Polymer Journal* **50,** 21–31 (2017).

2. Lei, T., Pochorovski, I. & Bao, Z. Separation of semiconducting carbon nanotubes for flexible and stretchable electronics using polymer removable method. *Accounts of Chemical Research* **50,** 1096–1104 (2017).

3. Sirringhaus, H. 25th Anniversary Article: Organic field-effect transistors: the path beyond amorphous silicon. *Advanced Materials* **26,** 1319–1335 (2014).

4. Lüssem, B., Keum, C.-M., Kasemann, D., Naab, B., Bao, Z. & Leo, K. Doped organic transistors. *chemical reviews* **116,** 13714–13751 (2016).

5. Li, Y. Molecular Design of photovoltaic materials for polymer solar cells: toward suitable electronic energy levels and broad absorption. *Accounts of Chemical Research* **45,** 723–733 (2012).

6. Yao, H., Ye, L., Zhang, H., Li, S., Zhang, S. & Hou, J. Molecular design of benzodithiophene-based organic photovoltaic materials. *Chemical Reviews* **116,** 7397–7457 (2016).

7. Lo, W.-Y., Zhang, N., Cai, Z., Li, L. & Yu, L. Beyond Molecular wires: design molecular electronic functions based on dipolar effect. *Accounts of Chemical Research* **49,** 1852–1863 (2016).

8. Heeger, A. J. 25th Anniversary Article: bulk heterojunction solar cells: understanding the mechanism of operation. *Advanced Materials* **26,** 10–28 (2014).

9. Guo, X., Facchetti, A. & Marks, T. J. Imide- and amide-functionalized polymer semiconductors. *Chemical Reviews* **114,** 8943–9021 (2014).

10. Zhao, X. & Zhan, X. Electron transporting semiconducting polymers in organic electronics. *Chemical Society Reviews* **40,** 3728 (2011).

11. Peng, H., Sun, X., Weng, W., Fang, X., Peng, H., Sun, X., Weng, W. & Fang, X. 2 – Synthesis and Design of Conjugated Polymers for Organic Electronics. In *Polymer Materials for Energy and Electronic Applications* 9–61 (Academic Press, 2017).

12. Han, A.-R., Dutta, G. K., Lee, J., Lee, H. R., Lee, S. M., Ahn, H., Shin, T. J., Oh, J. H. & Yang, C. ε -Branched flexible side chain substituted diketopyrrolopyrrole-containing polymers designed for high hole and electron mobilities. *Advanced Functional Materials* **25,** 247–254 (2015).

13. Kang, I., Yun, H.-J., Chung, D. S., Kwon, S.-K. & Kim, Y.-H. Record high hole mobility in polymer semiconductors via side-chain engineering. *Journal of the American Chemical Society* **135,** 14896–14899 (2013).

14. Kim, G., Kang, S.-J., Dutta, G. K., Han, Y.-K., Shin, T. J., Noh, Y.-Y. & Yang, C. A Thienoisoindigo-naphthalene polymer with ultrahigh mobility of 14.4 cm^2 /v·s that substantially exceeds benchmark values for amorphous silicon semiconductors. *Journal of the American Chemical Society* **136,** 9477–9483 (2014).

15. Sun, B., Hong, W., Yan, Z., Aziz, H. & Li, Y. Record high electron mobility of 6.3 $cm^2 v^{-1} s^{-1}$ achieved for polymer semiconductors using a new building block. *Advanced Materials* **26,** 2636–2642 (2014).

16. Guo, X., Zhou, N., Lou, S. J., Hennek, J. W., Ponce Ortiz, R., Butler, M. R., Boudreault, P.-L. T., Strzalka, J., Morin, P.-O., Leclerc, M., López Navarrete, J. T., Ratner, M. A., Chen, L. X., Chang, R. P. H., Facchetti, A. & Marks, T. J. Bithiopheneimide–dithienosilole/dithienogermole copolymers for efficient solar cells: information from structure–property–device performance correlations and comparison to thieno[3,4- *c*]pyrrole-4,6-dione analogues. *Journal of the American Chemical Society* **134,** 18427–18439 (2012).

17. Liu, X., Hsu, B. B. Y., Sun, Y., Mai, C.-K., Heeger, A. J. & Bazan, G. C. High thermal stability solution-processable narrow-band gap molecular semiconductors. *Journal of the American Chemical Society* **136,** 16144–16147 (2014).

18. Stuart, A. C., Tumbleston, J. R., Zhou, H., Li, W., Liu, S., Ade, H. & You, W. Fluorine substituents reduce charge recombination and drive structure and morphology development in polymer solar cells. *Journal of the American Chemical Society* **135,** 1806–1815 (2013).

19. Steckler, T. T., Henriksson, P., Mollinger, S., Lundin, A., Salleo, A. & Andersson, M. R. Very low band gap thiadiazoloquinoxaline donor–acceptor polymers as multi-tool conjugated polymers. *Journal of the American Chemical Society* **136,** 1190–1193 (2014).

20. Luo, H., Yu, C., Liu, Z., Zhang, G., Geng, H., Yi, Y., Broch, K., Hu, Y., Sadhanala, A., Jiang, L., Qi, P., Cai, Z., Sirringhaus, H. & Zhang, D. Remarkable enhancement of charge

carrier mobility of conjugated polymer field-effect transistors upon incorporating an ionic additive. *Science Advances* **2,** e1600076: 1–10 (2016).

21. Yao, J., Yu, C., Liu, Z., Luo, H., Yang, Y., Zhang, G. & Zhang, D. Significant improvement of semiconducting performance of the diketopyrrolopyrrole–quaterthiophene conjugated polymer through side-chain engineering via hydrogen-bonding. *Journal of the American Chemical Society* **138,** 173–185 (2016).

22. Gao, X. & Hu, Y. Development of n-type organic semiconductors for thin film transistors: a viewpoint of molecular design. *Journal of Materials Chemistry C* **2,** 3099–3117 (2014).

23. Yang, J., Wang, H., Chen, J., Huang, J., Jiang, Y., Zhang, J., Shi, L., Sun, Y., Wei, Z., Yu, G., Guo, Y., Wang, S. & Liu, Y. Bis-diketopyrrolopyrrole moiety as a promising building block to enable balanced ambipolar polymers for flexible transistors. *Advanced Materials* **29,** 1606162 (2017).

24. Asif, M. & Muneer, T. Energy supply, its demand and security issues for developed and emerging economies. *Renewable and Sustainable Energy Reviews* **11,** 1388–1413 (2007).

25. Höök, M. & Tang, X. Depletion of fossil fuels and anthropogenic climate change-A review. *Energy Policy* **52,** 797–809 (2013).

26. Shafiee, S. & Topal, E. When will fossil fuel reserves be diminished? *Energy Policy* **37,** 181–189 (2009).

27. Mazzio, K. A. & Luscombe, C. K. The future of organic photovoltaics. *Chemical Society Reviews* **44,** 78–90 (2015).

28. Jaymand, M., Hatamzadeh, M. & Omidi, Y. Modification of polythiophene by the incorporation of processable polymeric chains: recent progress in synthesis and applications. *Progress in Polymer Science* **47,** 26–69 (2015).

29. Allen, N. S. *Photochemistry and Photophysics of Polymer Materials* (Wiley, 2010).

30. Hoppe, H. & Sariciftci, N. S. Organic solar cells: an overview. *Journal of Materials Research* **19,** 1924–1945 (2004).

31. Su'ait, M. S., Rahman, M. Y. A. & Ahmad, A. Review on polymer electrolyte in dye-sensitized solar cells (DSSCs). *Solar Energy* **115,** 452–470 (2015).

32. Rahman, M. Y. A., Umar, A. A., Taslim, R., Roza, L., Saad, S. K. M. & Salleh, M. M. TiO 2 and ZnO thin film nanostructure for photoelectrochemical cell application : A Brief Review. **2,** 4–7 (2014).

33. Veerapandian, S., Amudha, S., Suthanthiraraj, S. A., Rahman, M. A. & Nasar, A. S. Enhanced performance of a nanocrystalline dye-sensitized solar cell based on polyurethane dendrimers. *RSC Advances* **5,** 31404–31409 (2015).

34. Ganesamoorthy, R., Sathiyan, G. & Sakthivel, P. Review: Fullerene based acceptors for efficient bulk heterojunction organic solar cell applications. *Solar Energy Materials and Solar Cells* **161,** 102–148 (2017).

35. Darling, S. B. & You, F. The case for organic photovoltaics. *RSC Advances* **3,** 17633 (2013).

36. Kumavat, P. P., Sonar, P. & Dalal, D. S. An overview on basics of organic and dye sensitized solar cells , their mechanism and recent improvements. *Renewable and*

Sustainable Energy Reviews **78,** 1262–1287 (2017).

37. Lee, T. D. & Ebong, A. U. A review of thin film solar cell technologies and challenges. *Renewable and Sustainable Energy Reviews* **70,** 1286–1297 (2017).

38. Dimitrakopoulos, C. D. & Mascaro, D. J. Organic thin-film transistors: a review of recent advances. *IBM Journal of Research and Development* **45,** 11–27 (2001).

39. Peumans, P., Yakimov, A. & Forrest, S. R. Small molecular weight organic thin-film photodetectors and solar cells. *Journal of Applied Physics* **93,** 3693–3723 (2003).

40. Gregg, B. A. & Hanna, M. C. Comparing organic to inorganic photovoltaic cells: theory, experiment, and simulation. *Journal of Applied Physics* **93,** 3605–3614 (2003).

41. Brabec, C. J. Organic photovoltaics: technology and market. *Solar Energy Materials and Solar Cells* **83,** 273–292 (2004).

CHAPTER TWO

Parameters affecting conjugated polymers performances in organic field-effect transistors and photovoltaic cells

Summary

The continuous depletion of fossil fuels and the environmental impact associated with their exploitation and use have become a concern of primary importance over the years. If the consumption of these non-renewable energy resources continues at the fast rate at which it is nowadays, the world will face a major energy crisis in the years to come, worse than the situation at present. This therefore calls for all parties, going from environmentalists to scientists through policies makers and government members, to come up with ideas and methods on how to identify, develop and implement new energy carriers. These energy carriers need to be easy to process, low-cost, sustainable and most especially ecological-friendly. Among many, solar energy has been identified as one of the most sustainable, as the earth surface is constantly illuminated by sunlight. Solar technology has undergone a lot of phases in terms of development of appropriate materials for solar cells with good power conversion efficiency, flexible and at affordable prices.

'Conjugated polymers' falls within the category of materials that could efficiently fulfill such requirements if properly designed; and a lot of work from scientists across different fields have made possible not only to design new materials but to constantly improve them in order to achieve increasing performances. D-A conjugated polymers consisting of alternating electron donating and withdrawing repeating units constitute the best type of conjugated polymers due to their interesting features. Many D-A copolymers based on monomers such as diketopyrrolopyrrole (DPP), benzothiadiazole (BTZ), fluorene (F), carbazole (C), thiophene (T), perylene diimide (PDI) have been prepared as n-type, p-type or ambipolar semiconductors and investigated for optoelectronic and photovoltaic applications. This review aims at presenting some outstanding D-A copolymers that have been recently investigated as organic field-effect transistors and in organic photovoltaic cells, and discusses how parameters such as side-chain, molecular weight, interfacial layers and morphology affect the performances of these devices.

2.1 Introduction

Solar energy has been identified as one of the ideal solutions to fulfill our needs regarding green and renewable energy while saving our environment from pollution.[1] Among all materials that have been involved in solar technology, conjugated polymers with electro-and photo-activity are considered to constitute the most promising way to decrease the price of the energy generated by solar cells. Different device architectures have been used for the fabrication of organic

photovoltaic devices;[2,3] of which the most efficient is the Bulk Heterojunction (BHJ), a blend of donor p-type and acceptor n-type materials. The bulk heterojunction morphology is characterized by bi-continuous three-dimensional interpenetrating network[4] (Figure 2.1) with donor-acceptor phase separation at least in a 80-100 nm length scale range.[5] There exists four main steps characterizing the photovoltaic process in BHJ (Figure 2.2): a) light absorption and excitation, b) exciton formation and diffusion, c) exciton dissociation/ separation and d) charges transport and collection at the electrodes.[6]

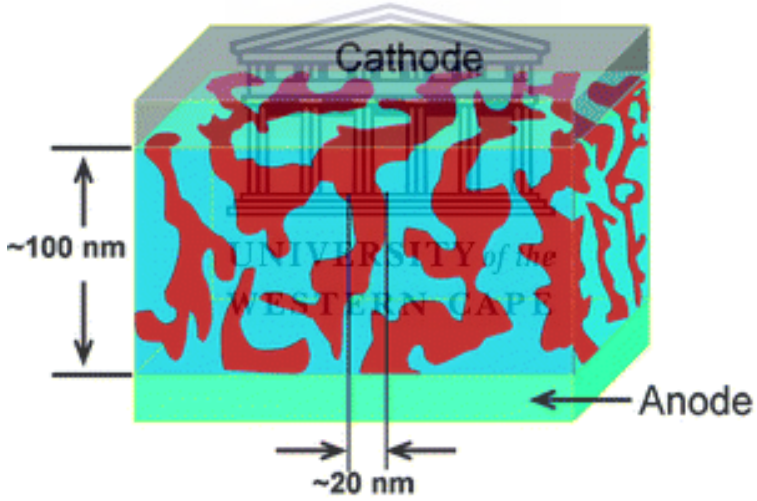

Figure 2.1 Conceptual morphology model of BHJ[4]

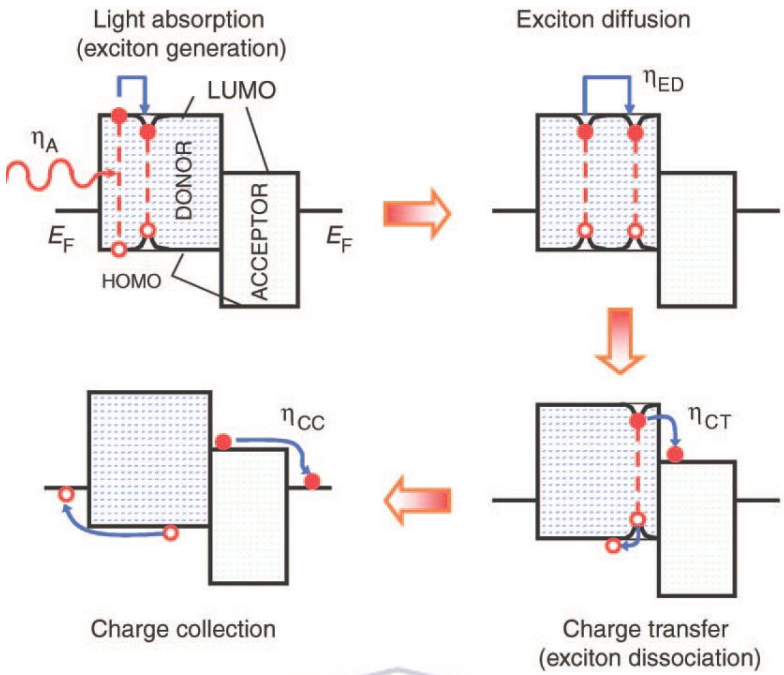

Figure 2.2 Steps in the BHJ photovoltaic process[6]

Organic conductive materials were already in existence and being used in xerographic applications (photocopiers)[7]; but it was not a breakthrough at the time. It is through a discovery by Alan Heeger, Alan MacDiarmid, and Hideki Shirakawa in 1977 - for which a Noble prize in Chemistry was awarded in 2000[8] - that organic semiconductors became popular. Indeed, they found that the electrical conductivity of a semiconductor, namely polyacetylene, could be tuned to over 7 orders of magnitude.[9] This is often regarded as the beginning of 'organic electronics'. The electrical conductivity in organic semiconductors results from conjugation characterized by the presence of alternating single (σ-bond) and double bonds (π-bond) between subsequent carbon atoms[10]. As such, in conjugated polymers, the delocalization is not restricted to two carbon atoms, but the π-

electrons are shared over the whole conjugated path. The band gap of a conjugated molecule is relatively small as a result of this delocalization, and keeps decreasing with increasing conjugation length.[11] Still, the conjugated macromolecule will remain a semiconductor as Peierls distortion[12,13] inhibits the extinction of the band gap. Rapidly after this discovery, many researchers invested themselves into developing and investigating more stable polymers.

These polymeric materials attracted more attention compared to inorganic semiconductors due to their decreased cost of production, flexibility, easy processability, as well as the tunability of their optical, physical and electronic properties[1,14–17] through chemical engineering. These superior properties therefore made them good advanced candidates for photonics and optoelectronics.[18,19] Many classes of conjugated polymers, classified according to the structure of their conjugated backbone, have been studied for optoelectronic device applications. These include: polyacetylene (PA), poly(para-phenylene)s (PPPs), poly(para-phenylenesulfide)s (PPSs), polythiophenes (PTs), polyaniline (PANI), poly(ethylenedioxythiophene) (PEDOT), polypyrroles (PPs), polycarbazoles (PCs), polyfluorenes (PFs) (Table 2.1). Incorporation of side-chains on these polymers main chains decreases their backbone rigidity while increasing the solubility; which in turn helps in the preparation of films through inexpensive, facile, solution-based methods such as spin-coating[20]. Variations observed in the photophysical and electrochemical properties of these polymers are also attributed to these ramifications.

Table 2.1 Summary of some conducting polymers and their chemical structures

Name	Structure	Conductivity (S cm^{-2})	Type of doping
Polyacetylene	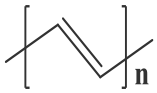	200 – 1000	n, p
Polypyrrole	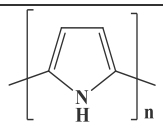	40 – 200	p
Polythiophene	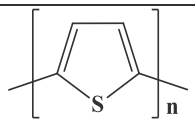	10 – 100	p
Poly(ethylenedioxythiophene)	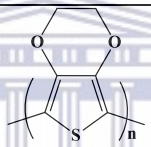	10 – 600	p
Poly(para-phenylene)		500	n, p
Poly(para-phenylene sulphide)	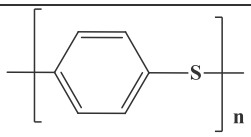	3 -500	p
Polyaniline	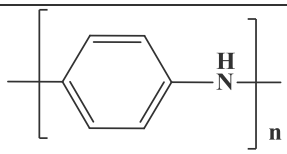	5 – 200	n, p

2.2 Conjugated polymers in organic field-effect transistors (OFETs) for various applications.

The first field-effect transistors based on a polymeric semiconductor were presented in 1980's.[21] Indeed, polythiophene based OFETs, initially produced by electrochemical polymerization directly onto the source and drain electrodes, were reported in the late 1980s. To be good candidates for OFET applications, conjugated polymers need to possess some critical properties. The first requirement is the long-term environmental stability[22] of the semiconducting polymers, which depends on the highest occupied molecular orbital (HOMO) whose energy level value must be lower than -5.2 eV to be air-stable. Even though stability is important, the main factor that allows conjugated polymers to exhibit high mobility is their potential to form highly organized films. Indeed, the closer is the π-stacking, the better is the charge carrier mobility. Therefore, to produce polymer with good packing, planar conjugated units could be used, which will drive an efficient π-stacking. To obtain processable materials, alkyl chains are added along the conjugated backbone.[20] Adding alkyl chain is not necessarily effective for efficient π-stacking; but we have to keep in mind that the aim is to find a compromise between the need of substituents for solubility and the π-stacking to ascertain good mobility in solution-processed technologies. Another very important point for polymer chain stacking in OFETs is how these stacks of polymer chains are positioned versus the substrate. According to reports, perpendicular/parallel orientations of these polymer packings with respect to the surface affect good charge diffusion through the source and the drain electrodes.[23] Also, careful choice of the repeating donor and acceptor units provides a certain extent of control over HOMO and lowest unoccupied molecular orbital (LUMO) energy levels of polymers.[24] In line with these prerequisites, Li *et al.*, 2012[25] studied conjugated

alternating D-A polymers consisting of relatively strong donor moiety, dithienylthieno[3,2-b]thiophene (DTT) and a comparatively weaker acceptor moiety, N-alkyldiketopyrrolopyrrole (DPP) (Figure 2.3 A), a promising building block for the design of high-mobility polymeric semiconductors, for p-type semiconductor design. Their research allowed them to find that DPP-DTT-based conjugated polymer with different molecular weights, could exhibit extremely high hole mobility of 10.5 cm^2/Vs, via synthesis and processing optimizations, a world record for a stable, solution-processed polymer semiconductor at the time. Many reports on conjugated DPP-based D-A polymer semiconductors are found in literature within mobility range from 0.1 cm^2/Vs to close to 2 cm^2/Vs.[26–31] Recently, Park *et al.*,[32] reported n-type charge-transport property with electron mobilities as high as 2.36 cm^2/Vs in alternating copolymers consisting of DPP and a fluorinated phenyl unit (Figure 2.3 B); the number of fluorine substituents on phenylene varies from one to four for OFET application. Their investigation demonstrated that in these alternating D-A copolymers, the increased mobilities were related to the larger number of fluorine substitutions. More fluorine attachments, decreased the LUMO energy level of the polymer, which in turn favored the face-on orientation thereby, switching the charge-transport behavior of the transistor from p-type to n-type. Some polymers with mobilities exceeding 1 cm^2/Vs as reported in literature are depicted in Figure 2.3; obviously, they exhibit the right combination of processability, π-stacking and polymer chain orientations onto the substrates.

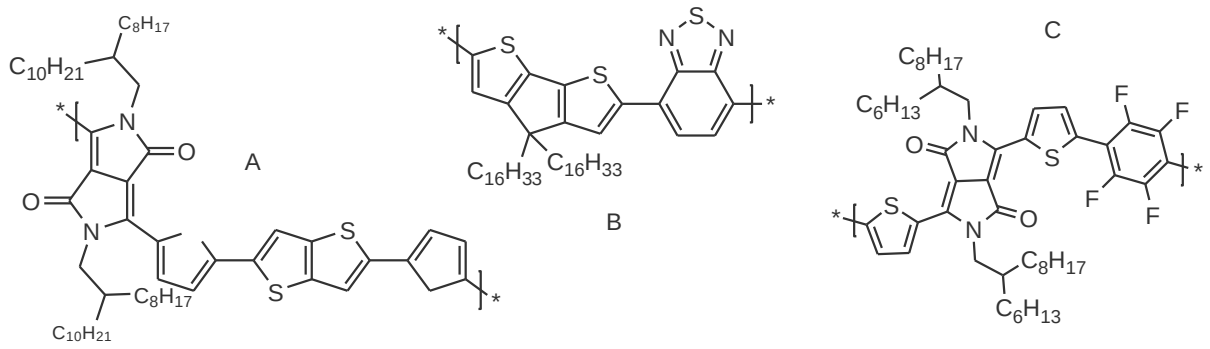

Figure 2.3 Efficient conjugated polymers for p-type and/or n-type OFETs[36]

Figure 2.4 depicts the progress in charge transport mobilities of the different classes of semiconducting materials that have evolved over the years. Short-contact polymers include those containing DPP and benzothiadiazole (BTZ) in their backbone.

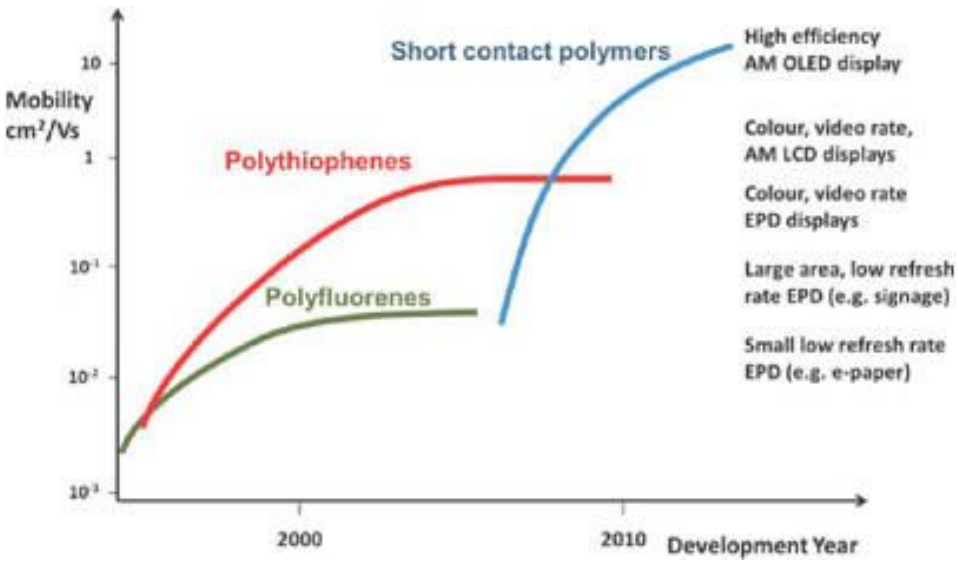

Figure 2.4 Evolution in charge carrier mobilies[34]

2.2.1 Thiadiazole-containing polymers

Although diketopyrrolopyrroles remain one of the most versatile group of high performing materials explored for OFETs, D–A conjugated polymers based on thiadiazole, and its derivatives, especially benzothiadiazole[24] (BTZ) have been explored. Oh *et al*.,[35] in 2011 reported on some copolymers based on dithienylbenzobis(thiadiazole), PCPBBT, with carbazole as donating counterpart which exhibited ambipolar characteristics with hole mobilty, $\mu_h = 7.1 \times 10^{-4}$ cm^2/Vs and electron mobility, $\mu_e = 3.3 \times 10^{-3}$ cm^2/Vs for an optical band-gap of 1.01 eV. The same year, Yuen *et al*.,[36] investigated the transport properties of donor-acceptor copolymers based on diketopyrrolopyrrole (DPP) coupled to various accepting units: benzene (B), benzothiadiazole (BT), benzobisthiadiazole

(BBT). In this work, they studied the effects of donor - acceptor interactions. The best properties were exhibited by the copolymer denoted PBBT12DPP where DPP was coupled with the strong acceptor BBT. This material displayed strong ambipolar characteristics with equivalent p-type and n-type mobilities of 1.17 and 1.32 cm^2/Vs, respectively. These D-A conjugated polymers exhibited better charge transport properties compared to other conjugated polymers due to strong effect on interchain interactions. Indeed, ambipolar behavior with mobilities values as low as 1.8×10^{-2} and 1.9×10^{-2} cm^2/Vs for hole and electron mobilities, respectively, was reported by Zhang *et al*.,[37] in a copolymer containing dithienocoronenediimide (DTCDI) and benzothiadiazole. Moreover, lower mobilities with maximum values of 1.04×10^{-2} cm^2/Vs were reported by the same authors when DTCDI was replaced by benzo[1,2-c;3,4- c0]bis[1,2,5]thiadiazole (BBT).[38] On the other hand, BTZ-based materials displaying p-type behavior have also been investigated.[39–41] Bathula *et al.*,[42], reported that a new conjugated polymer denoted PTBDTPT could exhibit hole mobility of 1.92×10^{-2} cm^2/Vs when the triisopropylsilylethynyl(TIPS)benzo[1,2-b:4,5-b′]dithiophene unit was attached to dithienothiadiazole[3,4-c]pyridine. Another series of p-type polymeric semiconductors consisting of a strong-donor-*alt*-strong acceptor denoted PDFBT-*alt*-DTP prepared by Efrem *et al*.,[43] showed low hole mobility of 1.4×10^{-2} cm^2/Vs.

More interestingly, few studies on the transport properties of macromolecules consisting of fluorene and benzothiadiazole in D-A conjugation have been reported.[44,45] Watters *et al.*,[44] reported on the hole transport of a newly synthesized a fluorene/benzothiadiazole copolymer (PFDT2BT-8) namely poly[9,9-dioctylfluorene-4,7-alt-(5,6-bis(octyloxy)-4,7-di(2,2′-bithiophen-5yl)benzo[c] [1,2,5] thiadiazole)-5,5-diyl]. With a good solubility in common organic solvents, the material mobility was 5.03×10^{-3} cm^2/Vs with a deep lying HOMO level of −5.33 eV. Pearson

et al.,[45] also worked on the same class of copolymers where the dithienyl group was replaced by a fused thienothiophene. The materials denoted PCDTTBT-8 and PFDTTBT-8 (chemical structures shown in Figure 2.5) were prepared via Suzuki coupling reaction of thienothiophene - octyloxybenzothiadazole with carbazole and fluorine, respectively. Their report showed that copolymer PFDTTBT-8 exhibited a lower charge carrier mobility than the dithienyl derivative PFDT2BT-8 with values of 7×10^{-4} cm^2/Vs and $4.3 \times x\ 10^{-3}$ cm^2/Vs, respectively. Whereas their carbazole counterparts displayed an order of magnitude higher mobility of 2.1×10^{-3} cm^2/Vs for PCDT2BT-8 and 2.4×10^{-3} cm^2/Vs for PCDTTBT-8, showing that PFDT2BT-8 is the best semiconducting material.

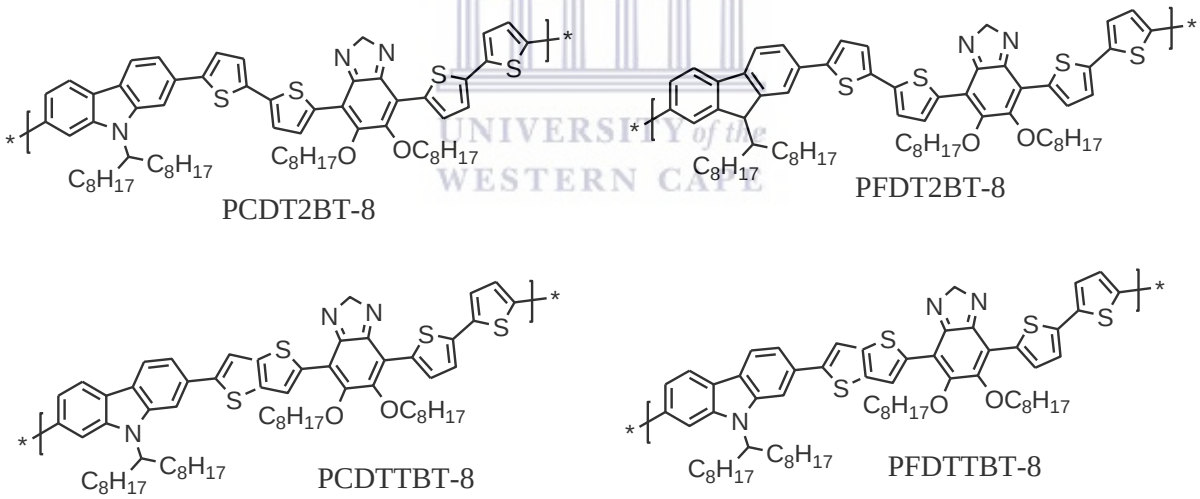

Figure 2.5 Chemical structures of PCDT2BT-8, PCDTTBT-8, PFDT2BT-8, PFDTTBT-8[45]

2.3 Conjugated polymers in organic photovoltaic cells

Just like in organic field-effect transistors, the first successfully applied organic semiconductors in solar cells were presented in the 1980s.[46–48] Since then, tremendous effort from different scientists across various fields have been put together and we are now far away from the firstly reported power conversion efficiency of 1% by Tang, 1986[49] with efficiencies now exceeding 10%.[50,51] Also, the first polymer-based OPV device is already available on the market.[52]

Depending on their constituents being either small or large molecules (polymers), OPVs are classified into two main groups. This classification is mainly based on the processes used for their synthesis, purification and device fabrication. While small-molecule solar cells require thermal evaporation deposition in a high-vacuum environment, Polymer solar cells (PSCs) are simply prepared from organic solvents.[53] PSCs are attractive owing to a number of advantageous features including their morphology in thin-films, low material utilization conferred by their high coefficient of absorption,[14,16] their use of organic materials strictly, the use of efficient solution processes and low manufacturing energy consumption; as well as their mechanical flexibility, low specific weight, tunable material properties and high transparency. One of the major forces currently driving materials innovation lies in the fact that performances of polymer solar cells (PSCs) are still far below the commercially available Si solar cells. One of the most studied and efficient OPV BHJ blends is the mixture poly(3-hexyl thiophene) (P3HT) and [6,6]-phenyl-C 61 -butyric acid methyl ester (PCBM);[54–56] but devices made from these materials without further processing or optimization, often exhibit poor PCE; therefore, subsequent treatments such as

thermal annealing or solvent vapor annealing are of uttermost importance.[57–65] Besides poly(alkylthiophenes), other one-dimension (1D) polymers consisting of the same repeating monomeric unit such as polyfluorenes, polycarbazoles and others have been used in PSCs as reported by a review of Guo *et al*.[66] But D-A conjugated polymers comprising different building blocks (Figure 2.6) have also attracted a lot of attention. Isoindigo-based D-A polymer solar cells, for example, since their first use in PSCs in 2010 have demonstrated relatively good efficiencies up to ∼ 8 % depending on the type of the donor unit they are attached to, which include terthiophene, dithienocarbazole or benzodithiophene as reported in literature.[67–69] Park *et al.*,[24] reported a 6% power conversion efficiency with an internal quantum efficiency close to 100% using the alternating D-A copolymer, poly[N-9″-hepta-decanyl-2,7-carbazole-alt-5,5-(4′,7′-di-2-thienyl-2′,1′,3′-benzothiadiazole) (PCDTBT) in bulk heterojunction composites with the fullerene derivative [6,6]-phenyl C_{70}-butyric acid methyl ester ($PC_{70}BM$). More recently, Xiao *et al.*,[70] reported efficiency as high as 7.25 % resulting from a BHJ blend of a D-A polymer poly{4,8-di(2,3-dioctylthiophene-5-yl)-2,6- benzo[1,2-b:4,5-b´]dithiophene-alt-5,5-[5´,8´-di-2-thienyl-(6´-fluoro- 2´,3´-bis-(3´´-octyloxyphenyl)-quinoxaline)]} (PBDTTFTQ-DO) with $PC_{71}BM$.

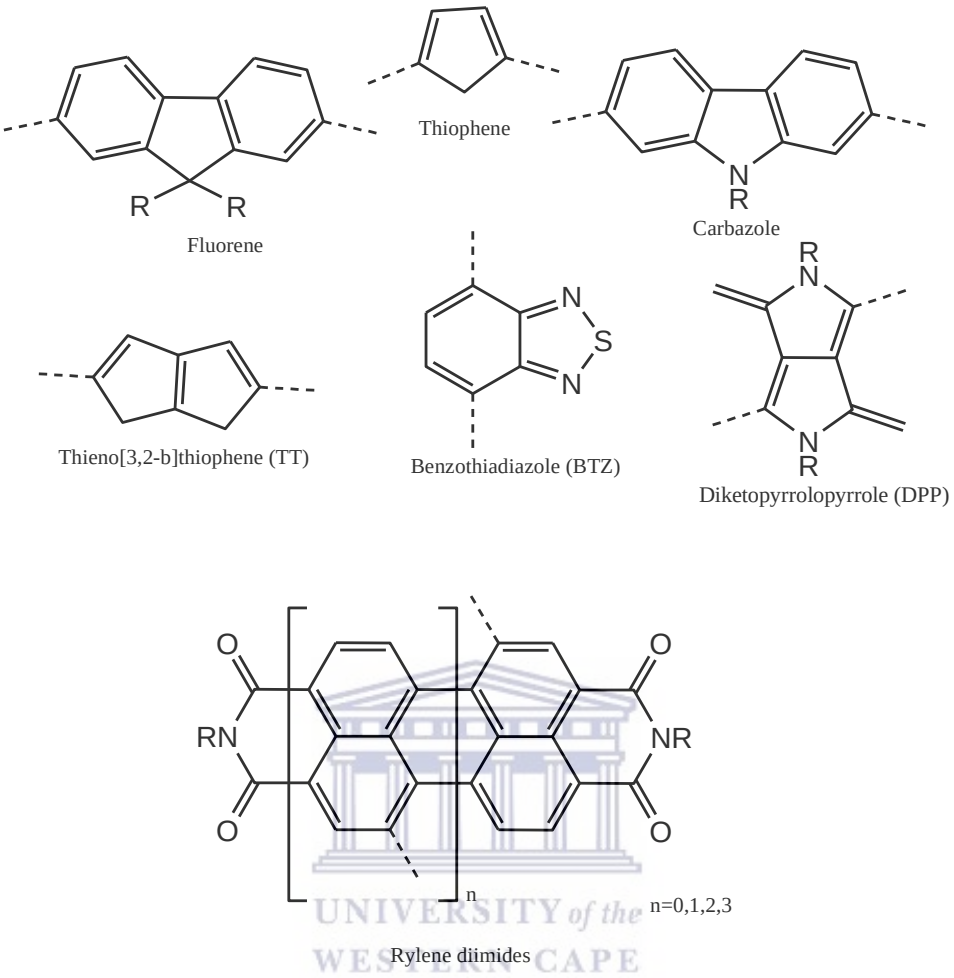

Figure 2.6 Some typical building blocks for OPVs[66]

2.3.1 Dendrimers and dendritic polymers as electron donors in OPVs

The interesting characteristics and electrical properties observed in fullerene,[71] have given room to the investigation of three-dimensional (3D) dendrimers electrical and optical properties and their potential application in optoelectronics and photovoltaics.[72] Among dendritic macromolecules of

the most important conjugated polymeric materials that have been investigated,[73,74] we count poly(phenyleneethynylene),[75] poly(phenylenevinylene) and poly(phenylene), poly(azomethine)s (PAZs), [76] polythiophenes and their derivatives[77]. Zhang *et al.*,[78] for instance, have synthesized new star-shaped D-π-A molecules made of triphenylamine (TPA) as core and donor unit and dicyanovinyl (DCN) as end group and acceptor unit; and used them as donor materials in OPV devices where the fullerene derivative $PC_{70}BM$ was the acceptor. These devices were able to achieve power conversion efficiencies (PCE) of up to 3.0 %. Schulz *et al.*,[79] designed donor materials by incorporating pyrazinoquinoxaline into thiophene-based conjugated dendrimers and the fabricated photovoltaics devices demonstrated PCE of maximum 1.7 % with $PC_{71}BM$ compare to slightly lower efficiencies when $PC_{61}BM$ was used. Recently, Gao *et al*.,[77] designed a series of thiophene-based dendrimers and achieved power conversion efficiencies up to 1.33 %. On the other hand, Iwan *et al.*,[76] in their review attempted to understand the effect of liquid crystalline(LC) PAZs on the photovoltaic parameters of some polymer solar cells and find the optimum parameters necessary to produce smart BHJ devices when liquid crystalline compounds are incorporated in polymer solar cells.

2.3.2 Perylene-containing polymers as electron acceptors in OPVs

Even though most of the research works go into the development of donating copolymers, more new accepting semiconducting materials are emerging.[80] Perylene diimide (PDI)-based polymers

constitute one of the new classes of n-type polymers for application in PSCs as a replacement of the 'super acceptor' fullerene. Indeed, the first PDI-based polymer was used in all-PSC in 2007 by Zhan and co-workers, using a copolymer based on PDI and dithienothiophene denoted P(PDI2DD-DTT), as the acceptor. Approximately 3.9 and 5.9 eV were the obtained HOMO/LUMO energies of P(PDI2DD-DTT) as estimated by cyclic voltammetry. Their prepared thin film showed good absorption throughout the visible into the near-IR region. PSCs were fabricated using bis(thienylenevinylene)-substituted polythiophene, BTV-PT as donating component and PCEs slightly above 1% were obtained.[81] Further optimization of PDI-based materials coupled to device structure engineering have allowed to obtain photovoltaic device performances with PCE 6 %.[82–85] Because PDI is electron-deficient, it can be easily coupled with a wide variety of electron-rich (donor) units in order to tune the optoelectronic properties of the resulting polymers. Zhou *et al.*,[86] developed and investigated a series of six PDI-based D-A copolymers with carbazole (C), fluorene (F), vinylene (V), thiophene (T), dithieno[3,2-b:2',3'-d]pyrrole (DTP), and dibenzosilole (DBS) as n-type component (Figure 2.7) and blended with two polythiophene derivatives P3HT and PT1 in solar cells applications. They obtained PCE as high as 2.23%, based on PT1/PC–PDI BHJ blend, which at the time was one of the best obtained efficiencies for polymer/polymer blend photovoltaic devices.

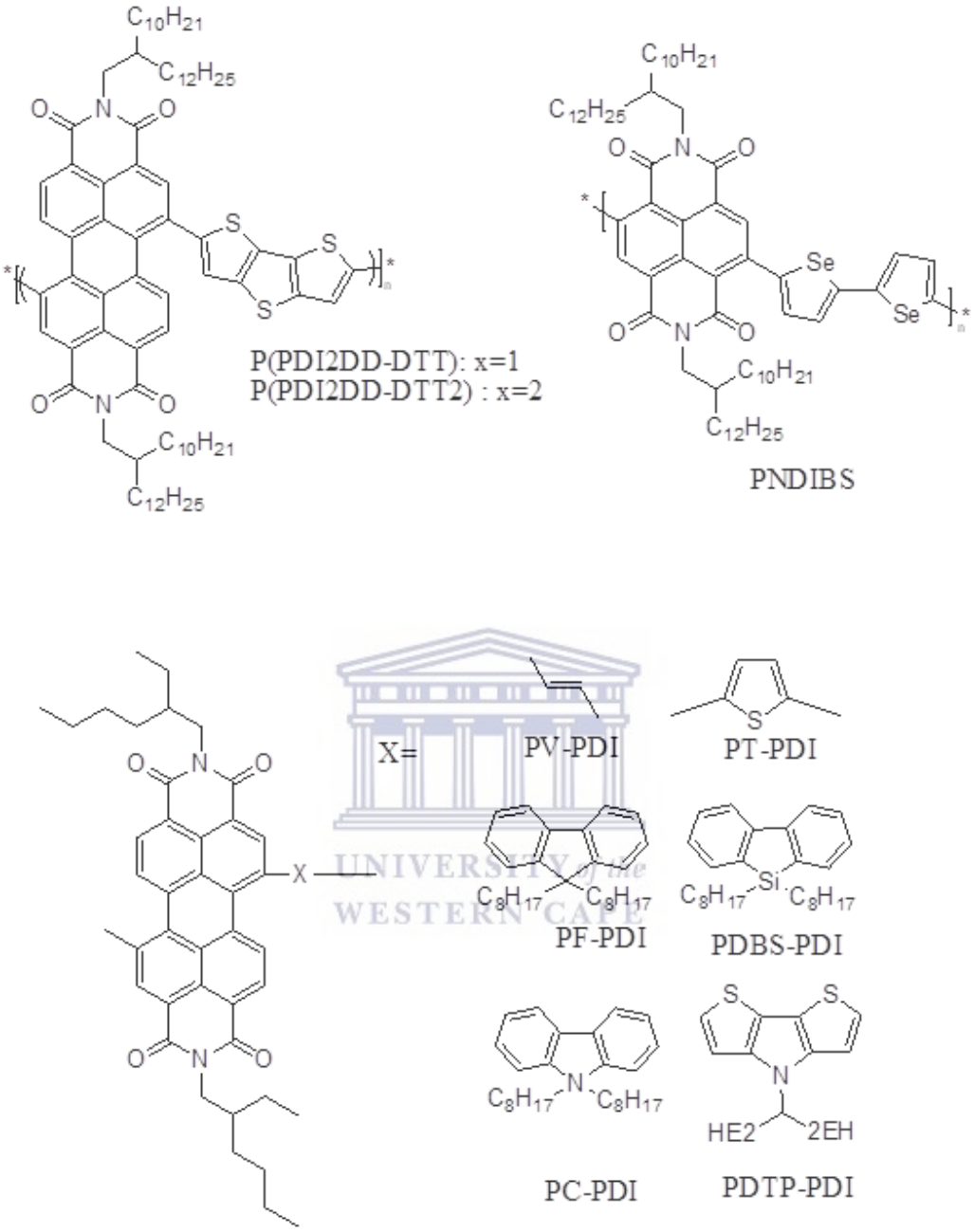

Figure 2.7 Some PDI-based D-A copolymers[87]

Using an alternating PDI-phenylenevinylene copolymer (P(PDI-PEPEP) acceptor and poly(3-phenyl hydrazone thiophene) (PPHT) donor, Mikroyannidis *et al.*,[88]obtained a PCE of 2.3% under white-light illumination. Other works on PDI-based copolymer include that of Zhang *et al*.,[89] who investigated the PCE of Donor-acceptor diblock copolymers, composed of regioregular poly(3-hexylthiophene) (rrP3HT) as electron donating block and poly(perylene diimide acrylate) (PPDA) as electron accepting (Figure 2.8). Measured PCE of 0.49% of the annealed devices fabricated from the polymer was higher compare to blends of P3HT and N,N′-bis(1-ethylpropryl)-3,4,9,10-perylene bis(tetracarboxyl diimide) (EP-PTC) (0.4%), which was due to the nanostructured nature of the rrP3HT-block-PPDA copolymer. We suggest that this low efficiency compared to reported efficiencies was probably due to substitution at the core of the PDI moiety instead of the common bay-substitution. Steric hinderance caused by bulky attachment probably created some distortion in the macromolecule planarity resulting in poor stacking.

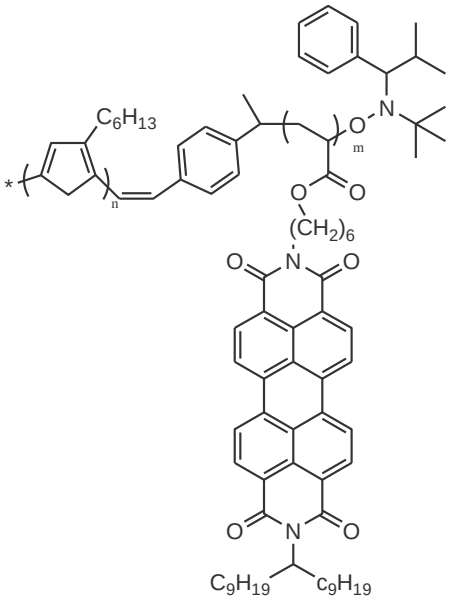

Figure 2.8 Donor-Acceptor diblock rrP3HT-block-PPDA

2.4 Strategy for optimized Donor – Acceptor (D-A) conjugated polymers

Combined efforts of physicists, chemists, and engineers for the design of better optoelectronic devices and organic solar cells motivated the shift of research focus from the preparation of highly conducting polymers to the design of stable semiconducting polymers with improved performances. This idea is mainly motivated by the goal to set up the so-called 'plastic electronics' where micro-electronic devices can be printed on different substrates. But polymer design for PSCs present key issues[90,91] that include: engineering of energy levels and bandgap that can allow for high short-circuit current density, J_{SC} and open-circuit Voltage, V_{OC}; improving planarity to

maximize carrier mobility; and materials processability and stability. Unfortunately, all these issues are interrelated. Ideally, all these factors should be optimized in a single polymer, but this remains a big challenge.[53] It therefore becomes important to chemically tune the electronic properties of existing polymers in order to obtain low bandgap semiconducting materials. This can be done through the rigidification of the conjugated backbone, the attachment of electron-withdrawing or electron-donating side substituents, or maybe increasing of the quinoid (versus aromatic) character of the main chain.[92] However, the most successful approach to obtain low band gap polymers is a copolymerized D-A structure[88] involving the utilization of electron-rich or electron-poor units leading to alternating "push-pull" architecture[93]. Combination of these two different moieties in a copolymer results in hybridization between the molecular orbitals of the donating and accepting units, causing a significant modulation of the copolymer bandgap (Figure 2.9). Usually, while the LUMO energy level is mainly influenced by the electron-poor unit, the energy level of the HOMO of the resulting D-A polymer is determined by the electron-rich unit.[94]

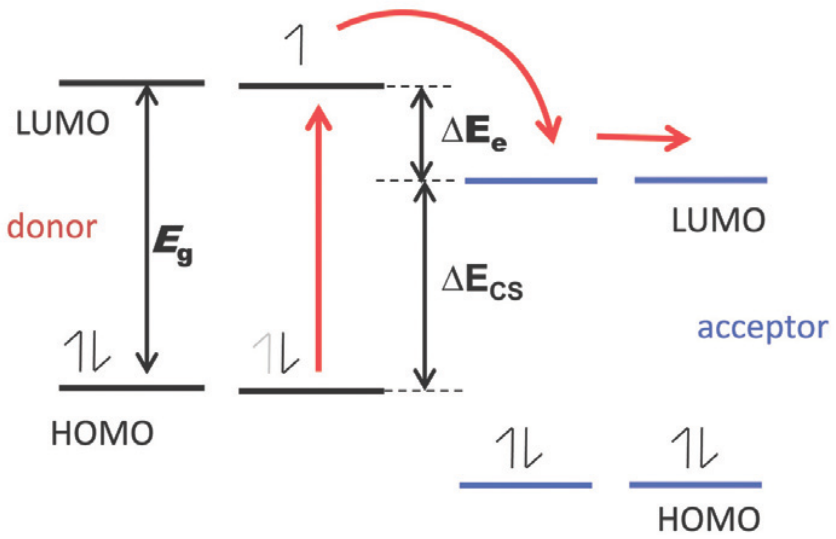

Figure 2.9 HOMO-LUMO energy levels hybridization in donor-acceptor BHJ active layer[94]

Over the years, this 'third generation of semiconducting copolymers[95] has evolved to meet the needs of various electronic applications. An example is a series of several different polyfluorene copolymers prepared and tested in solar cells[96–99] among which is the APFO (APFO: alternating polyfluorene) polymers group prepared by Zhang *et al*.[100] This class of polymers demonstrated a low band gap with photosensitivity down to 1 mm while displaying various HOMO/LUMO levels positions. The APFO family is therefore a successful demonstration of the donor–acceptor approach, and proves the high potential for PSCs of PF-based materials.[14]

Since in Conjugated D-A polymers, the majority of carriers is determined by the relative strengths of their electron donating and withdrawing components, they are fundamentally ambipolar

transport semiconductors i.e. stronger acceptor will majorly lead to electron transport, while stronger donor to hole transport. Thus, the suitable molecular design to generate the appropriate material should be a D-A copolymer where a strong acceptor is attached to a comparatively weak donor or vice versa to develop a n-channel or p-channel semiconductor, respectively.[25] Also, a relatively good planarity of the polymer backbone structure to enhance closer π-π stacking of polymer chains is ideal as tighter π-π stacking would instead allow charge transport by hopping.[101] Another essential parameter is the functionalization of the polymer core via attachment of side-chains to enhance solubility, essential requirement for cheap solution-processed manufacturing[102] as well as for solid state core interactions enhancement.[103,104] Other important parameters for efficient D-A polymer design for PSCs include molecular weight (M_W) and the dispersity (Đ)[81]; type of interfacial layers used and morphology.

2.4.1 Side-chain substitution

When it comes to D-A, low band gap conjugated copolymers engineering, many factors have to be taken into consideration to obtain better materials for optimized device performances. One of the factors on which the performance of these macromolecules relies is the variation of the substituent(s) grafted[105–107] onto the aromatic unit in the polymer backbone. By doing this, the solubility can be tuned and the molecular orbitals effectively perturbed, as well as polymer physical properties such as phase behavior, structural order and charge transport properties.[108] In

2002, Egbe *et al.*,[109] reported that depending on the size, number, geometry, and position of alkoxy side chains attached on the backbone, poly(p-phenylenevinylene)/poly(p-phenyleneethylene), PPV/PPE hybrid polymer could afford good solubility. This, in turn had effects on the optical properties of the materials in solution and solid states. Colladet *et al.*,[110] investigated a series of four D-A polymers among which two of the polymers had alkyl side-chain attached. The alkyl substitution effectively increased the solubility of these two polymers. But also lowered their M_Ws as a result of steric hindrance during the polymerization. Liang *et al.*,[111] found that replacing an alkyl side chain by an alkoxy group on a copolymer consisting of alternating thieno[3,4-b]thiophene and benzodithiophene units, PTB made the HOMO energy level to be lowered by 0.1 eV. Cimrova *et al.*,[112–114] studied the effect of alkyl (branched and linear) substitution on D-A copolymers based on thienothiadiazole and fluorene and they found that copolymers denoted CEHTF with branched ethylhexyl groups exhibited lower power conversion efficiencies compared to CDTF with dodecyl substituents. More interestingly they found that when replacing the fluorene donating unit with an alkoxy-substituted dioxaborinanylbenzene, the solubility of the new copolymer CEHTP was restricted to a certain type of solvent but both copolymers showed PCE between 0.2-0.3 %. More recently, this same group[115] again investigated the effect of alkyl and alkoxy substituents but this time on thienthiadiazole-phenylene copolymers CDTDP and CDTDOP. The nature of the substituting group attached to the benzene ring affected their photophysical properties. While CDTDP was soluble in all common solvents, the solubility of CDTDOP was limited to toluene and chloroform. Also, they reported that even though CDTDOP had a broader absorption, up to the IR region, it exhibited more pronounced aggregation in solid-state, which was already observed in liquid state. Also, CDTDOP showed a lower HOMO energy

level compared to CDTDP (4.9 eV) due to its stronger electron donating ability. While CDTP had a PCE of 1.05 %, CDTDOP was only 0.19 %. The efficiency of the later is almost similar to that of its fluorene counterpart already reported.[114]

2.4.2 Molecular weight (M_w) and dispersity index (*Đ*)

When it comes to developing new D-A conjugated polymers, other key polymer parameters to be considered for good device performances are the molecular weight (M_W) and the dispersity index (Đ) since they tend to influence solubility, solution aggregation, and formulation rheology, as well as thin films formation and morphology.[81] Increased molecular weight had also been linked to improved charge transport arising from better inter-grain connectivity.[25] Cimrova *et al*., [116] investigated the photovoltaic characteristics of a series of thienothiadiazole-fluorene copolymers denoted CEHTF8 prepared with different M_W from 60 000 to 220 000 g/mol but similar PDI 1.4-1.5. They noticed that the M_W did really have an effect on the devices' performances; as all conjugated polymers demonstrated almost similar ionization potentials and electron affinities at 5.04 eV and 3.53 eV, respectively. Also, all PSCs showed PCE in the range 1.3-1.9 %. The group of Chu *et al*.,[117] has developed a new class of low-band gap D-A copolymers consisting of dithienosilole and poly(N -9′-heptadecanyl-2,7-carbazole- alt -5,5-thienopyrrolodione) (PDTSTPDs) and studied the effect of M_Ws on the octyl-substituted derivative denoted PDTSTPD-8. They demonstrated that increasing M_Ws from 10000 to 31000 g/mol resulted in increased PCE

from 3.1 to 7.7%. Kang *et al*.,[118] also showed that an increase in M_W improves PCE when they investigated the photovoltaic performances of a series of all-PSCs devices based on poly[(2,5-bis(2-hexyldecyloxy)phenylene)-alt-(5,6-difluoro-4,7-di(thiophen-2-yl)benzo[c][1,2,5]thiadiazo-le)], (PPDT2FBT). Indeed, three copolymers were prepared with M_Ws 12, 24 and 40 kg/mol and exhibited efficiencies of 1.34, 2.39 and 3.59 %, respectively.

2.4.3 New design of interfacial layers

In PSCs, after they are generated and dissociated, the free charge carriers need to diffuse to their respective electrodes (anode or cathode) to be collected.[119] The charge collection efficiency can be tuned depending on the type of materials used on the anode covered with an electron blocking, hole transporting layer (HTL) and, on the cathode covered with a hole blocking layer.[108] The band offset of the hole-transporting layer in a BHJ is critical to establish the device polarity.[120] When it comes to anode materials for PSCs, the conducting polymer poly(3,4-ethylenedioxythiophene): poly(styrenesulfonate) (PEDOT:PSS), has been widely used as the material of choice in normal BHJ[116,121] and more recently in inverted BHJ[109] PSCs. While serving as a hole-injecting layer, PEDOT:PSS also helps as an electron blocking layer (EBL) when deposited on the ITO electrode. PEDOT:PSS helps to reduce the dark current in these devices while acting as a lower resistance contact for hole extraction.[120,122] This dual character is mainly due to the band gap of PEDOT:PSS with a low-lying LUMO therefore providing an energy barrier to the transport of electrons to the

anode.[123] Despite all these advantages, PEDOT:PSS stability is an issue as it degrades and limits device performance in multiple ways[124] due to oxygen and/or moisture presence in the air.[125] These limitations drive the urge for investigating how PEDOT:PSS properties can be enhanced by various methods such as solvent treatments;[126] embedding of metal oxides[127] and doping;[128] or design of materials[129] such as graphene oxide[130,131] or metal oxides[119–121] to effectively replace PEDOT:PSS as the HTL in OPV devices.

2.4.4 Morphology control in Bulk heterojunctions (BHJ)

Bulk heterojunction architecture offers a powerful solution for addressing the issue of exciton dissociation. But, it was found that the morphology control of the conjugated polymer (the donor–acceptor phase separation) is of great importance in achieving proper charge transport paths for collection of the holes and electrons at the electrodes, and improve PSCs performances.[53,135] Ideally, the morphology of the active layer BHJ should be an interpenetrating network of the electron donating and electron accepting materials, with exciton diffusion length domain sizes or around 10 nm.[136,137] Basically, for effective dissociation of a large number of excitons while ensuring a constant charge transport channeling to the electrodes, the BHJ layer should have enough interfacial area. However, effective application of this principle is a bit more complex and does not really happen in reality; which is the reason motivating researchers in trying to understand how the nanostructure of the BHJ layer can be manipulated in order to improve photovoltaic

performances. In PSCs, the type of solvent used; donor/acceptor concentrations; solvent annealing conditions[138]; thermal annealing temperatures and duration; additives[139], and the interlayer surface energies are typical parameters that influence the active layer morphology.

Thermal annealing[140] and solvent annealing are currently the mostly used for morphology control. Indeed, Wang *et al*.,[141] and Goh *et al*,[142] showed that both thermal and solvent annealing could be used to improve PSCs efficiency by a significant amount. But in 2001, Shaheen *et al*.,[143] already reported that processing poly(2-methoxy-5-(3′,7′-dimethyloctyloxy)-p-phenylene vinylene) MDMO-PPV/PCBM active layer from chlorobenzene rather than toluene increased the device performance because thin film formed from chlorobenzene solution was more intimately mixed with small domain sizes. Following this, in an attempt to understand the correlation between solvent, solvent loading, and blend composition, Hoppe *et al.*,[16] by varying weight ratios of MDMO-PPV:PCBM in chlorobenzene and toluene realized that by increasing the ratio of PCBM, the films processed from toluene displayed an increasingly large amount of PCBM aggregates surrounded by a thin skin of MDMO-PPV. But better phases' mixing was observed when casting from chlorobenzene for all ratio and PCBM aggregation was only observed from ratio 1:6 and the clusters formed were even smaller compare to when formed with toluene.

Also, Vanlaeke *et al*.,[144,145] demonstrated that the efficiency of BHJ solar cells based on Poly(3-hexylthiophene) (P3HT) and 1-(3-methoxycarbonyl)-propyl-1-phenyl-(6,6)C_{61} ester (PCBM) prepared from chlorobenzene solution can be improved by annealing. Layers from 1:2 wt. ratio of P3HT and PCBM revealed an undesirable amorphous phase in the as-produced cells but after

thermal treatment, a more desirable crystalline phase was obtained. More interestingly, they obtained a PCE of 3.6% through variation of the processing solvent without the need of annealing with evidence that the as-produced BHJ layer is crystalline.

2.5 Conclusion

Alternating donor-acceptor (D-A) conjugated polymers have been extensively studied to investigate their charge transport properties in organic field effect transistors and in polymer solar cells applications over the past years. Internetworking phase separation between the donor and acceptor in bulk heterojunction layer constitutes the best material architecture to use for this type of macromolecules. Several electron-rich and electron-poor monomeric units have been studied and copolymerized using various routes in different solvents and under different temperature conditions; and fabricated devices demonstrated different power conversion efficiencies.[65,146,147] Despite their solution processability and their low manufacturing cost, these materials still face the challenge of not sufficiently good power conversion efficiency to overthrow the long-time used c-Silicon solar cells. Indeed, in order to be efficient, D-A copolymers need to meet a certain number of requirements such a narrower energy bandgap, E_g and broad absorption in ultraviolet-visible region through IR region, relatively lower-lying HOMO (highest occupied molecular orbital) level, and higher electron and/or hole mobilities. This could be achieved by amending a certain number of factors. Addition of substituents on the main chain backbone, for instance, has been proven to

not only help with solubility improvement; but can also to a certain extent, help with the rigidification of the macromolecules which could increase their planarity, which in turn will favor the diffusion of the positive and negative charges and ascertain better efficiency.[148,149] Increased molecular weight and appropriate dispersity of these copolymers, on the other hand have demonstrated to be parameters not to be neglected in the optimization of the performances of these polymers.[117,150] Another very important aspect to consider is the optimization of the interfacial layers which is very essential to ensure the dissociated charges diffuse to the right electrodes.[125] Above all, the parameter which is of outermost importance if the control of the morphology which can be achieved through thermal annealing, varying solvent conditions, doping, or addition of additives.

References

1. Mazzio, K. A. & Luscombe, C. K. The future of organic photovoltaics. *Chemical Society Reviews* **44,** 78–90 (2015).

2. Yumusak, C. & M. Egbe, D. A. Organic Bulk Heterojunction Solar Cells Based on Poly(p-Phenylene-Vinylene) Derivatives. In *Solar Cells - New Aspects and Solutions*, 415–432 (Intech, 2011).

3. Antohe, S., Iftimie, S., Hrostea, L., Antohe, V. A. & Girtan, M. A critical review of photovoltaic cells based on organic monomeric and polymeric thin film heterojunctions. *Thin Solid Films* **642,** 219–231 (2017).

4. Zhao, J., Song, D., Qiao, B., Xu, Z., Huang, D., Wang, M., Zhang, X., Li, Y., Zhu, Y. & Zhao, S. Regulating the polymer crystallize behavior via the synergistic additives towards high-performance bulk heterojunction solar cells. Organic Electronics: physics, materials, applications 58, 178–184 (2018).

5. Alessandri, R., Uusitalo, J. J., De Vries, A. H., Havenith, R. W. A. & Marrink, S. J. Bulk heterojunction morphologies with atomistic resolution from coarse-grain solvent evaporation simulations. Journal of the American Chemical Society 139, 3697–3705 (2017).

6. Forrest, S. R. The limits to organic photovoltaic cell efficiency. *MRS Bulletin* **30,** 28–32 (2005).

7. Mozer, A. J. & Sariciftci, N. S. Conjugated polymer photovoltaic devices and materials. *Comptes Rendus Chimie* **9,** 568–577 (2006).

8. Wang, Y. *Low Threshold Organic Semiconductor Lasers*. (Springer, 2014).

9. Terao, J. Synthesis of Conjugated Polyrotaxanes and Its Application to Molecular Wires. In *Molecular Architectonics*, 487–512 (Springer, 2017).

10. Feixas, F., Matito, E., Poater, J. & Solà, M. Understanding conjugation and hyperconjugation from electronic delocalization measures. *The Journal of Physical Chemistry A* **115,** 13104–13113 (2011).

11. Brondijk, J. J. Device physics of solution-processed organic field-effect transistors: s.n. (Dissertaion, 2012).

12. Rhyee, J., Lee, K. H., Lee, S. M., Cho, E., Kim, S. Il, Lee, E., Kwon, Y. S., Shim, J. H. & Kotliar, G. Peierls distortion as a route to high thermoelectric performance in $In_4Se_{3-\delta}$ crystals. *Nature* **459,** 965–968 (2009).

13. Torres, A. E., Flores, R., Fomine, S., Investigaciones, I. De, Nacional, U., México, A. De & Postal, A. A comparative study of one and two dimensional systems. *Synthetic Metals* **213,** 78–87 (2016).

14. Dennler, G., Scharber, M. C. & Brabec, C. J. Polymer-fullerene bulk-heterojunction solar cells. *Advanced Materials* **21,** 1323–1338 (2009).

15. Lyons, B. P., Clarke, N. & Groves, C. The relative importance of domain size, domain purity and domain interfaces to the performance of bulk-heterojunction organic

photovoltaics. *Energy & Environmental Science* **5,** 7657 (2012).

16. Lyons, B. P., Clarke, N. & Groves, C. The relative importance of domain size, domain purity and domain interfaces to the performance of bulk-heterojunction organic photovoltaics. Energy & Environmental Science 5, 7657 (2012).

17. Servaites, J. D., Ratner, M. A. & Marks, T. J. Organic solar cells: A new look at traditional models. *Energy & Environmental Science* **4,** 4410 (2011).

18. Shinar, R. & Shinar, J. *Organic electronics in sensors and biotechnology*. (McGraw-Hill, 2009).

19. Gómez, R. & Segura, J. L. Handbook of Organic Electronics and Photonics. (American Scientific Pub, 2007).

20. Cai, Y., Huo, L. & Sun, Y. Recent Advances in Wide-Bandgap Photovoltaic Polymers. Advanced Materials 29, 1605437: 1–38 (2017).

21. Mori, T. Electronic properties of organic conductors. (Springer, 2016)

22. Pan, Y., Lv, A. & Chi, L. Analysis of influencing factors on air-stable organic field-effect transistors (OFETs). *Materials Science* **24,** 148–158 (2018).

23. Mori, T., Oyama, T., Komiyama, H. & Yasuda, T. Solution-grown unidirectionally oriented crystalline thin films of a U-shaped thienoacene-based semiconductor for high-performance organic field-effect transistors. *Journal of Materials Chemistry C* **5,** 5872–5876 (2017).

24. Park, S. H., Roy, A., Beaupré, S., Cho, S., Coates, N., Moon, J. S., Moses, D., Leclerc, M., Lee, K. & Heeger, A. J. Bulk heterojunction solar cells with internal quantum efficiency

approaching 100%. *Nature Photonics* **3,** 297–302 (2009).

25. Li, J., Zhao, Y., Tan, H. S., Guo, Y., Di, C. A., Yu, G., Liu, Y., Lin, M., Lim, S. H., Zhou, Y., Su, H. & Ong, B. S. A stable solution-processed polymer semiconductor with record high-mobility for printed transistors. *Scientific Reports* **2,** 1–9 (2012).

26. Nelson, T. L., Young, T. M., Liu, J., Mishra, S. P., Belot, J. A., Balliet, C. L., Javier, A. E., Kowalewski, T. & McCullough, R. D. Transistor paint: high mobilities in small bandgap polymer semiconductor based on the strong acceptor, diketopyrrolopyrrole and strong donor, dithienopyrrole. *Advanced Materials* **22,** 4617–4621 (2010).

27. Li, Y., Sonar, P., Singh, S. P., Soh, M. S., van Meurs, M. & Tan, J. Annealing-free high-mobility diketopyrrolopyrrole−quaterthiophene copolymer for solution-processed organic thin film transistors. *Journal of the American Chemical Society* **133,** 2198–2204 (2011).

28. Bronstein, H., Chen, Z., Ashraf, R. S., Zhang, W., Du, J., Durrant, J. R., Shakya Tuladhar, P., Song, K., Watkins, S. E., Geerts, Y., Wienk, M. M., Janssen, R. A. J., Anthopoulos, T., Sirringhaus, H., Heeney, M. & McCulloch, I. Thieno[3,2-*b*]thiophene−diketopyrrolopyrrole-containing polymers for high-performance organic field-effect transistors and organic photovoltaic devices. *Journal of the American Chemical Society* **133,** 3272–3275 (2011).

29. Zhang, X., Richter, L. J., DeLongchamp, D. M., Kline, R. J., Hammond, M. R., McCulloch, I., Heeney, M., Ashraf, R. S., Smith, J. N., Anthopoulos, T. D., Schroeder, B., Geerts, Y. H., Fischer, D. A. & Toney, M. F. Molecular packing of high-mobility diketo pyrrolo-pyrrole polymer semiconductors with branched alkyl side chains. *Journal of the American*

Chemical Society **133,** 15073–15084 (2011).

30. Ha, J. S., Kim, K. H. & Choi, D. H. 2,5-Bis(2-octyldodecyl)pyrrolo[3,4- *c*]pyrrole-1,4-(2 *H* ,5 *H*)-dione-based donor–acceptor alternating copolymer bearing 5,5′-di(thiophen-2-yl)-2,2′-biselenophene exhibiting 1.5 $cm^{2-1}s^{-1}$ hole mobility in thin-film transistors. *Journal of the American Chemical Society* **133,** 10364–10367 (2011).

31. Kim, J.-H., Lee, M., Yang, H. & Hwang, D.-H. A high molecular weight triisopropylsilylethynyl (TIPS)-benzodithiophene and diketopyrrolopyrrole-based copolymer for high performance organic photovoltaic cells. *Journal of Materials Chemistry A* **2,** 6348 (2014).

32. Park, J. H., Jung, E. H., Jung, J. W. & Jo, W. H. A fluorinated phenylene unit as a building block for high-performance n-type semiconducting polymer. *Advanced Materials* **25,** 2583–2588 (2013).

33. Wang, S., Kappl, M., Liebewirth, I., Müller, M., Kirchhoff, K., Pisula, W. & Müllen, K. Organic field-effect transistors based on highly ordered single polymer fibers. *Advanced Materials* **24,** 417–420 (2012).

34. Holliday, S., Donaghey, J. E. & McCulloch, I. Advances in charge carrier mobilities of semiconducting polymers used in organic transistors. *Chemistry of Materials* **26,** 647– 663 (2014).

35. Oh, H. S., Kim, T.-D., Koh, Y.-H., Lee, K.-S., Cho, S., Cartwright, A. & Prasad, P. N. Synthesis and characterization of dithienylbenzobis(thiadiazole)-based low band-gap polymers for organic electronics. *Chemical Communications* **47,** 8931–8933 (2011).

36. Yuen, J. D., Fan, J., Seifter, J., Lim, B., Hufschmid, R., Heeger, A. J. & Wudl, F. High performance weak donor-acceptor polymers in thin film transistors: Effect of the acceptor on electronic properties, ambipolar conductivity, mobility, and thermal stability. *Journal of the American Chemical Society* **133,** 20799–20807 (2011).

37. Zhang, C., Zhao, G., Zeng, W., Tian, K., Dong, H., Hu, W., Qin, J. & Yang, C. Ambipolar copolymer of dithienocoronenedi-imide and benzo(bis)thiadiazole with balanced hole and electron mobility. *Organic Electronics* **16,** 101–108 (2015).

38. Zhang, C., Chen, Z., Zeng, W., Yu, G. & Yang, C. Narrow band-gap copolymers with two acceptors of benzo[1,2-c;3,4-c′]bis[1,2,5]thiadiazole and benzo[c][1,2,5] thiadiazole: synthesis, characteristics and application in field-effect transistors. *Dyes and Pigments* **130,** 291–297 (2016).

39. Cameron, J., Nanson, L., Blouin, N., Findlay, N. J., Inigo, A. R. & Skabara, P. J. Solution-processable 2,1,3-benzothiadiazole containing compound based on the novel 1-dodecyl-6-dodecoxynaphthyridine-2-one unit for organic field-effect transistors. *Organic Electronics: physics, materials, applications* **49,** 400–405 (2017).

40. Tabi, G. D., Nketia-yawson, B., Kang, S. & Yang, C. High performance p-type chlorinated-benzothiadiazole-based polymer electrolyte gated organic field-effect transistors. *Organic Electronics* **54,** 255–260 (2018).

41. Tabi, G. D., Nketia-yawson, B., Lee, J. Y., Cho, K., Lim, B. & Noh, Y. Fluorinated benzothiadiazole and indacenodithieno[3,2-b]thiophene based regioregular-conjugated copolymers for ambipolar organic field-effect transistors and inverters. *RSC Advances* **7**,

1110–1117 (2017).

42. Bathula, C., Lee, S. K., Kalode, P., Badgujar, S., Belavagi, N. S., Khazi, I. A. M. & Kang, Y. Synthesis and photophysical studies of thiadiazole[3,4-c]pyridine copolymer based organic field-effect transistors. *Journal of Fluorescence* **26,** 1045–1052 (2016).

43. Efrem, A., Wang, K. & Wang, M. Facile synthesis of a narrow-bandgap strong-donor-alt-strong-acceptor copolymer of poly(5,6-difluorobenzo-[c][1,2,5]-thiadiazole-alt-5H-dithieno[3,2-b:2′,3’-d]pyran) via direct C-H arylation polymerization. *Dyes and Pigments* **145,** 331–338 (2017).

44. Watters, D. C., Yi, H. N., Pearson, a J., Kingsley, J., Iraqi, a & Lidzey, D. Fluorene-based co-polymer with high hole mobility and device performance in bulk heterojunction organic solar cells. *Macromolecular Rapid Communications* **34,** 1157–1162 (2013).

45. Pearson, A. J., Watters, D. C., Yi, H., Sarjadi, M. S., Reynolds, L. X., Marchisio, P. P., Kingsley, J., Haque, S. A., Iraqi, A. & Lidzey, D. G. Impact of dithienyl or thienothiophene units on the optoelectronic and photovoltaic properties of benzo[1,2,5]thiadiazole based donor-acceptor copolymers for organic solar cell devices. *RSC Advances* **4,** 43142–43149 (2014).

46. Kumavat, P. P., Sonar, P. & Dalal, D. S. An overview on basics of organic and dye sensitized solar cells , their mechanism and recent improvements. *Renewable and Sustainable Energy Reviews* **78,** 1262–1287 (2017).

47. Stoltzfus, D. M., Donaghey, J. E., Armin, A., Shaw, P. E., Burn, P. L. & Meredith, P. Charge generation pathways in organic solar cells: assessing the contribution from the electron

acceptor. *Chemical Reviews* **116,** 12920–12955 (2016).

48. Cheng, P., Li, G., Zhan, X. & Yang, Y. Next-generation organic photovoltaics based on non-fullerene acceptors /639/301/299/946 /639/624/399 review-article. *Nature Photonics* **12,** 131–142 (2018).

49. Yan, C., Barlow, S., Wang, Z., Yan, H., Jen, A. K.-Y., Marder, S. R. & Zhan, X. Non-fullerene acceptors for organic solar cells. *Nature Reviews Materials* **3,** 18003 (2018).

50. Liu, Y., Zhao, J., Li, Z., Mu, C., Ma, W., Hu, H., Jiang, K., Lin, H., Ade, H. & Yan, H. Aggregation and morphology control enables multiple cases of high-efficiency polymer solar cells. *Nature Communications* **5,** 1–8 (2014).

51. Chen, C. C., Chang, W. H., Yoshimura, K., Ohya, K., You, J., Gao, J., Hong, Z. & Yang, Y. An efficient triple-junction polymer solar cell having a power conversion efficiency exceeding 11%. *Advanced Materials* **26,** 5670–5677 (2014).

52. Freitas, A. M., Gomes, R. A. M., Ferreira, R. A. M. & Porto, M. P. Experimental performance of commercial OPV panels tested outdoor. *Renewable Energy,* 1004–1012 (2019). doi:10.1016/j.renene.2018.12.051

53. Li, G., Zhu, R. & Yang, Y. Polymer solar cells. *Nature Photonics* **6,** 153–161 (2012).

54. Fukuda, T., Toda, A., Takahira, K., Suzuki, K., Liao, Y., Hirahara, M., Saito, M. & Osaka, I. Molecular ordering of spin-coated and electrosprayed P3HT:PCBM thin films and their applications to photovoltaic cell. *Thin Solid Films* **612,** 373–380 (2016).

55. Laquai, F., Andrienko, D., Mauer, R. & Blom, P. W. M. Charge carrier transport and

photogeneration in P3HT:PCBM photovoltaic blends. *Macromolecular Rapid Communications* **36,** 1001–1025 (2015).

56. González, D. M., Körstgens, V., Song, L., Roth, S. V, Müller-Buschbaum, P., Santoro, G. & Yao, Y. Improved power conversion efficiency of p3ht:pcbm organic solar cells by strong spin-orbit coupling-induced delayed fluorescence. *Advanced Energy Materials* **5,** 1401770: 1–10 (2015).

57. Motaung, D. E., Malgas, G. F. & Arendse, C. J. Insights into the stability and thermal degradation of P3HT:C60 blended films for solar cell applications. *Journal of Materials Science* **46,** 4942–4952 (2011).

58. Motaung, D. E., Malgas, G. F. & Arendse, C. J. Correlation between the morphology and photo-physical properties of P3HT:fullerene blends. *Journal of Materials Science* **45,** 3276–3283 (2010).

59. Kim, H. J., Lee, H. H. & Kim, J. J. Real time investigation of the interface between a P3HT:PCBM layer and an al electrode during thermal annealing. *Macromolecular Rapid Communications* **30,** 1269–1273 (2009).

60. Zhou, H., Zhang, Y., Seifter, J., Collins, S. D., Luo, C., Bazan, G. C., Nguyen, T. Q. & Heeger, A. J. High-efficiency polymer solar cells enhanced by solvent treatment. *Advanced Materials* **25,** 1646–1652 (2013).

61. Bavel, Svetlana S, V., Sourty, E., With, Gijsbertus, D. & Loos, J. Three-dimesional nanoscale organization of bulk heterojunction polymer solar cells. *Nano Letters* **9,** 507–513 (2009).

62. Pearson, A. J., Wang, T., Dunbar, A. D. F., Yi, H., Watters, D. C., Coles, D. M., Staniec, P. A., Iraqi, A., Jones, R. A. L. & Lidzey, D. G. Morphology development in amorphous polymer: Fullerene photovoltaic blend films during solution casting. *Advanced Functional Materials* **24,** 659–667 (2014).

63. Verploegen, E., Miller, C. E., Schmidt, K., Bao, Z. & Toney, M. F. Manipulating the morphology of P3HT-PCBM bulk heterojunction blends with solvent vapor annealing. *Chemistry of Materials* **24,** 3923–3931 (2012).

64. Hrostea, L., Girtan, M., Mallet, R. & Leontie, L. Optical and Morphological Properties of P3HT and P3HT: PCBM Thin Films Used in Photovoltaic Applications. *IOP Conference Series: Materials Science and Engineering* **374,** 1–6 (2018).

65. Wang, W., Song, L., Magerl, D., Moseguí González, D., Körstgens, V., Philipp, M., Moulin, J. F. & Müller-Buschbaum, P. Influence of solvent additive 1,8-octanedithiol on p3ht:pcbm solar cells. *Advanced Functional Materials* **28,** 1–9 (2018).

66. Guo, X., Baumgarten, M. & Müllen, K. Designing π-conjugated polymers for organic electronics. *Progress in Polymer Science* **38,** 1832–1908 (2013).

67. Wang, E., Mammo, W. & Andersson, M. R. 25th anniversary article: Isoindigo-based polymers and small molecules for bulk heterojunction solar cells and field effect transistors. *Advanced Materials* **26,** 1801–1826 (2014).

68. Ma, Z., Dang, D., Tang, Z., Gedefaw, D., Bergqvist, J., Zhu, W., Mammo, W., Andersson, M. R., Inganäs, O., Zhang, F. & Wang, E. A facile method to enhance photovoltaic performance of benzodithiophene- isoindigo polymers by inserting bithiophene spacer.

Advanced Energy Materials **4,** 1–6 (2014).

69. Deng, Y., Liu, J., Wang, J., Liu, L., Li, W., Tian, H., Zhang, X., Xie, Z., Geng, Y. & Wang, F. Dithienocarbazole and isoindigo based amorphous low bandgap conjugated polymers for efficient polymer solar cells. *Advanced Materials* **26,** 471–476 (2014).

70. Xiao, B., Zhang, M., Yan, J., Luo, G., Gao, K., Liu, J., You, Q., Wang, H. B., Gao, C., Zhao, B., Zhao, X., Wu, H. & Liu, F. High efficiency organic solar cells based on amorphous electron-donating polymer and modified fullerene acceptor. *Nano Energy* **39,** 478–488 (2017).

71. John, S. V., Mayedwa, N., Ikpo, C., Molefe, L. Y., Ndipingwi, M. M., Dywili, N. R., Van Wyk, J., Mapolie, S. F., Baker, P. & Iwuoha, E. Photoluminescence quenching of poly(octylfluorenylbenzothiadiazole) luminophore by n-type cobalt(II) salicylaldimine metallodendrimer. *Synthetic Metals* **220,** 114–122 (2016).

72. Rupert, B. & Rance, W. Pi-conjugated dendrimers for solar-energy harvesting. *SPIE Newsroom* 1–4 (2009).

73. Zhang, J., Li, G., Kang, C., Lu, H., Zhao, X., Li, C., Li, W. & Bo, Z. Synthesis of star-shaped small molecules carrying peripheral 1,8-naphthalimide functional groups and their applications in organic solar cells. *Dyes and Pigments* **115,** 181–189 (2015).

74. Stoltzfus, D. M., Ma, C. Q., Nagiri, R. C. R., Clulow, A. J., Bäuerle, P., Burn, P. L., Gentle, I. R. & Meredith, P. Thiophene dendrimer-based low donor content solar cells. *Applied Physics Letters* **109,** 103302: 1–5 (2016).

75. Fraix, A., Torrisi, V., Marletta, G., Sortino, S., Mineo, P. G., Tomaselli, G. A., Ballistreri, F. P., Trusso Sfrazzetto, G. & Pappalardo, A. Supramolecular polymer networks based on calix[5]arene chained poly(p-phenyleneethynylene) and C_{60} fulleropyrrolidine. *Supramolecular Chemistry* **28,** 485–492 (2016).

76. Iwan, A. An overview of LC polyazomethines with aliphatic-aromatic moieties: thermal, optical, electrical and photovoltaic properties. *Renewable and Sustainable Energy Reviews* **52,** 65–79 (2015).

77. Gao, W., Wang, J., Lin, Y., Luo, Q., Ma, Y., Dou, J., Tan, H., Ma, C. Q. & Cui, Z. Functionalization of diketopyrrolopyrrole with dendritic oligothiophenes: synthesis, photophysical properties, and application in solar cells. *Journal of Photochemistry and Photobiology A: Chemistry* **355,** 350–359 (2018).

78. Zhang, J., Deng, D., He, C., He, Y., Zhang, M., Zhang, Z. G., Zhang, Z. & Li, Y. Solution-processable star-shaped molecules with triphenylamine core and dicyanovinyl endgroups for organic solar cells. *Chemistry of Materials* **23,** 817–822 (2011).

79. Schulz, G. L., Mastalerz, M., Ma, C. Q., Wienk, M., Janssen, R. & Bäuerle, P. Synthesis and photovoltaic performance of pyrazinoquinoxaline containing conjugated thiophene-based dendrimers and polymers. *Macromolecules* **46,** 2141–2151 (2013).

80. Ogawa, S. *Organic Electronics Materials and Devices*. (Springer, 2015).

81. Facchetti, A. π-Conjugated polymers for organic electronics and photovoltaic cell applications. *Chemistry of Materials* **23,** 733–758 (2011).

82. Hwang, Y. J., Earmme, T., Courtright, B. A. E., Eberle, F. N. & Jenekhe, S. A. n-Type

semiconducting naphthalene diimide-perylene diimide copolymers: controlling crystallinity, blend morphology, and compatibility toward high-performance all-polymer solar cells. *Journal of the American Chemical Society* **137,** 4424–4434 (2015).

83. Kozma, E., Kotowski, D., Catellani, M., Luzzati, S., Cavazzini, M., Bossi, A., Orlandi, S. & Bertini, F. Design of perylene diimides for organic solar cell: effect of molecular steric hindrance and extended conjugation. *Materials Chemistry and Physics* **163,** 152–160 (2015).

84. Liu, M., Yang, J., Lang, C., Zhang, Y., Zhou, E., Liu, Z., Guo, F. & Zhao, L. Fused perylene diimide-based polymeric acceptors for efficient all-polymer solar cells. *Macromolecules* **50,** 7559–7566 (2017).

85. Pakseresht, M., Bodapati, J. B. & Icil, H. A New π-conjugated 1,7-diphenoxy-perylene bisimide: Synthesis, characterization, photophysical and electrochemical properties. *Journal of Photochemistry and Photobiology A: Chemistry* **360,** 270–277 (2018).

86. Zhou, E., Cong, J., Wei, Q., Tajima, K., Yang, C. & Hashimoto, K. All-polymer solar cells from perylene diimide based copolymers: Material design and phase separation control. *Angewandte Chemie - International Edition* **50,** 2799–2803 (2011).

87. Facchetti, A. Polymer donor-polymer acceptor (all-polymer) solar cells. *Materials Today* **16,** 123–132 (2013).

88. Mikroyannidis, J. A., Stylianakis, M. M., Sharma, G. D., Balraju, P. & Roy, M. S. A novel alternating phenylenevinylene copolymer with perylene bisimide units: synthesis, photophysical, electrochemical, and photovoltaic properties. *Journal of Physical Chemistry C* **113,** 7904–7912 (2009).

89. Zhang, Q., Cirpan, A., Russell, T. P. & Emrick, T. Donor - Acceptor poly(thiophene- block -perylene diimide) copolymers : synthesis and solar cell fabrication **42**, 1079-1082 (2009).

90. Cheng, Y.-J., Yang, S.-H. & Hsu, C.-S. Synthesis of conjugated polymers for organic solar cell applications. *Chemical Reviews* **109,** 5868–5923 (2009).

91. Liang, Y. & Yu, L. Development of semiconducting polymers for solar energy harvesting. *Polymer Reviews* **50,** 454–473 (2010).

92. Roncali, J. Molecular engineering of the band gap of π-conjugated systems: Facing technological applications. *Macromolecular Rapid Communications* **28,** 1761–1775 (2007).

93. Hendriks, K. H., Heintges, G. H. L., Gevaerts, V. S., Wienk, M. M. & Janssen, R. A. J. High-Molecular-Weight Regular Alternating diketopyrrolopyrrole- based terpolymers for efficient organic solar cells. *Angewandte Chemie, International Edetion* **52,** 8341–8344 (2013).

94. Nelson, J. Polymer: Fullerene bulk heterojunction solar cells. *Materials Today* **14,** 462–470 (2011).

95. Dang, M. T., Hirsch, L. & Wantz, G. P3HT:PCBM, best seller in polymer photovoltaic research. *Advanced Materials* **23,** 3597–3602 (2011).

96. Admassie, S., Inganäs, O., Mammo, W., Perzon, E. & Andersson, M. R. Electrochemical and optical studies of the band gaps of alternating polyfluorene copolymers. *Synthetic Metals* **156,** 614–623 (2006).

97. Slooff, L. H., Veenstra, S. C., Kroon, J. M., Moet, D. J. D., Sweelssen, J. & Koetse, M. M. Determining the internal quantum efficiency of highly efficient polymer solar cells through optical modeling. *Applied Physics Letters* **90,** 143506: 1–3 (2007).

98. Koetniyom, W., Keawprajak, A., Jiramitmongkon, K. & Asawapirom, U. The study of crystallization of polyfluorene and fullerene derivatives in semiconducting layer of organic solar cells. *Key Engineering Materials* **751,** 435–441 (2017).

99. Espinosa-Roa, A., Cruz-Carrillo, M. de J., Ledesma-Juárez, A., Montoya del Angel, A., Romero-Borja, D., Güizado-Rodríguez, M., Rodríguez, M., Galindo, R., Maldonado, J. L. & Barba, V. Synthesis of polyfluorenes by oxidative polymerization, their characterization and implementation in organic solar cells. *Journal of Materials Science: Materials in Electronics* **0,** 0 (2018). doi.org/10.1007/s1085 4-018-0547-2

100. Zhang, F., Inganäs, O., Zhou, Y. & Vandewal, K. Development of polymer-fullerene solar cells. *National Science Review* **3,** 222–239 (2016).

101. Berlin, Y. A., Hutchison, G. R., Rempala, P., Ratner, M. A. & Michl, J. Charge hopping in molecular wires as a sequence of electron-transfer reactions. *The Journal of Physical Chemistry A* **107,** 3970–3980 (2003).

102. Tsao, H. N., Cho, D. M., Park, I., Hansen, M. R., Mavrinskiy, A., Yoon, D. Y., Graf, R., Pisula, W., Spiess, H. W. & Müllen, K. Ultrahigh mobility in polymer field-effect transistors by design. *Journal of the American Chemical Society* **133,** 2605–2612 (2011).

103. Katz, H. E. Recent advances in semiconductor performance and printing processes for organic transistor-based electronics. *Chemistry of Materials* **16,** 4748–4756 (2004).

104. Allard, S., Forster, M., Souharce, B., Thiem, H. & Scherf, U. Organic semiconductors for solution-processable field-effect transistors (OFETs). *Angewandte Chemie - International Edition* **47,** 4070–4098 (2008).

105. Li, W., Hendriks, K. H., Furlan, A., Roelofs, W. S. C., Meskers, S. C. J., Wienk, M. M. & Janssen, R. A. J. Effect of the fibrillar microstructure on the efficiency of high molecular weight diketopyrrolopyrrole-based polymer solar cells. *Advanced Materials* **26,** 1565–1570 (2014).

106. Wang, Y., Xin, X., Lu, Y., Xiao, T., Xu, X., Zhao, N., Hu, X., Ong, B. S. & Ng, S. C. Substituent effects on physical and photovoltaic properties of 5,6-difluorobenzo[c][1,2,5]thiadiazole-based D-A polymers: Toward a donor design for high performance polymer solar cells. *Macromolecules* **46,** 9587–9592 (2013).

107. Zhang, Z. G., Fan, H., Min, J., Zhang, S., Zhang, J., Zhang, M., Guo, X., Zhan, X. & Li, Y. Synthesis and photovoltaic properties of copolymers of carbazole and thiophene with conjugated side chain containing acceptor end groups. *Polymer Chemistry* **2,** 1678–1687 (2011).

108. Xu, T. & Yu, L. How to design low bandgap polymers for highly efficient organic solar cells. *Materials Today* **17,** 11–15 (2014).

109. Egbe Mbi, Ayuk Daniel, Roll, C. P., Birckner, E., Grummt, U., Stockmann, R. & Klemm, E. Side Chain Effects in Hybrid PPV / PPE Polymers. *Macrolmolecules* **2,** 3825–3837 (2002).

110. Colladet, K., Fourier, S., Cleij, T. J., Lutsen, L., Gelan, J., Vanderzande, D., Imomec, D. V,

Diepenbeek, B.-, Nguyen, L. H., Neugebauer, H., Sariciftci, S., Aguirre, A., Janssen, G. & Goovaerts, E. Low Band Gap Donor - Acceptor Conjugated Polymers toward Organic Solar Cells Applications. *Macromolecules* **40,** 65–72 (2007).

111. Liang, Y., Feng, D., Wu, Y., Tsai, S. T., Li, G., Ray, C. & Yu, L. Highly efficient solar cell polymers developed via fine-tuning of structural and electronic properties. *Journal of the American Chemical Society* **131,** 7792–7799 (2009).

112. Cimrová, V., Kmínek, I., Pavlačková, P. & Výprachtický, D. Low-bandgap donor-acceptor copolymers with 4,6-bis(3′-(2-ethylhexyl) thien-2′-yl)thieno[3,4-c][1,2,5]thiadiazole: Synthesis, optical, electrochemical, and photovoltaic properties. *Journal of Polymer Science, Part A: Polymer Chemistry* **49,** 3426–3436 (2011).

113. Kminek, I., Vyprachticky, D., Kriz, J., Dybal, J. & Cimrova, V. Low-band gap copolymers containing thienothiadazole units: synthesis, optical, and electrochemical properties. *Journal of Polymer Science: Part A: Polymer Chemistry* **48,** 2743–2756 (2010).

114. Cimrová, V., Kmínek, I. & Výprachtický, D. Novel soluble fluorene-thienothiadiazole and fluorene-carbazole copolymers for optoelectronics. *Macromolecular Symposia* **295,** 65–70 (2010).

115. Cimrová, V., Pokorná, V. & Výprachtický, D. Effects of alkyl or alkyloxy side chains in poly[4,6-bis(3′-dodecylthien-2′-yl)thieno-[3,4- c][1,2,5]thiadiazole-5′,5′-diyl- alt -2,5-di(alkyl or alkyloxy)-1,4-phenylene]: Synthesis, photophysics, and spectroelectrochemical and photovoltaic properties. *Polymer* **118,** 180–191 (2017).

116. Cimrová, V., Kmínek, I., Výprachtický, D. & Pokorná, V. Short-time synthesis of poly[4,6-

bis(3′-(2-ethylhexyl)thien-2′-yl)thieno[3,4-c][1,2,5]thiadiazole-alt-9,9-dioctylfluorene], its photophysical, electrochemical and photovoltaic properties. *Polymer (United Kingdom)* **59,** 298–304 (2015).

117. Chu, T. Y., Lu, J., Beaupré, S., Zhang, Y., Pouliot, J. R., Zhou, J., Najari, A., Leclerc, M. & Tao, Y. Effects of the molecular weight and the side-chain length on the photovoltaic performance of dithienosilole/thienopyrrolodione copolymers. *Advanced Functional Materials* **22,** 2345–2351 (2012).

118. Kang, H., Uddin, M. A., Lee, C., Kim, K.-H., Nguyen, T. L., Lee, W., Li, Y., Wang, C., Woo, H. Y. & Kim, B. J. Determining the role of polymer molecular weight for high-performance all-polymer solar cells: its effect on polymer aggregation and phase separation **137**, 2359−2365 (2015).

119. Ganesamoorthy, R., Sathiyan, G. & Sakthivel, P. Review: fullerene based acceptors for efficient bulk heterojunction organic solar cell applications. *Solar Energy Materials and Solar Cells* **161,** 102–148 (2017).

120. Irwin, M. D., Buchholz, D. B., Hains, A. W., Chang, R. P. H. & Marks, T. J. p-Type semiconducting nickel oxide as an efficiency-enhancing anode interfacial layer in polymer bulk-heterojunction solar cells. *Proceedings of the National Academy of Sciences* **105,** 2783–2787 (2008).

121. Bouguerra, N., Ruìšžička, A., Ulbricht, C., Enengl, C., Enengl, S., Pokorná, V., Výprachtický, D., Tordin, E., Aitout, R., Cimrová, V. & Egbe, D. A. M. Synthesis and photophysical and electroluminescent properties of poly(1,4-phenylene-ethynylene)-alt-

poly(1,4-phenylene-vinylene)s with various dissymmetric substitution of alkoxy side chains. *Macromolecules* **49,** 455–464 (2016).

122. Shaheen, S. E., Ginley, D. S. & Jabbour, G. E. Organic-based photovoltaics: toward low-cost power generation. *MRS Bulletin* **30,** 10–19 (2005).

123. Steirer, K. X., Chesin, J. P., Widjonarko, N. E., Berry, J. J., Miedaner, A., Ginley, D. S. & Olson, D. C. Solution deposited NiO thin-films as hole transport layers in organic photovoltaics. *Organic Electronics: physics, materials, applications* **11,** 1414–1418 (2010).

124. Jørgensen, M., Norrman, K. & Krebs, F. C. Stability/degradation of polymer solar cells. *Solar Energy Materials & Solar Cells* **92,** 686–714 (2008).

125. Rafique, S., Abdullah, S. M., Sulaiman, K. & Iwamoto, M. Layer by layer characterisation of the degradation process in PCDTBT:PC71BM based normal architecture polymer solar cells. *Organic Electronics: physics, materials, applications* **40,** 65–74 (2017).

126. Hu, Z., Zhang, J. & Zhu, Y. Effects of solvent-treated PEDOT:PSS on organic photovoltaic devices. *Renewable Energy* **62,** 100–105 (2014).

127. Park, Y., Müller-Meskamp, L., Vandewal, K. & Leo, K. PEDOT:PSS with embedded TiO_2 nanoparticles as light trapping electrode for organic photovoltaics. *Applied Physics Letters* **108,** 253302:1–5 (2016).

128. Hu, Z., Zhang, J., Hao, Z. & Zhao, Y. Influence of doped PEDOT:PSS on the performance of polymer solar cells. *Solar Energy Materials and Solar Cells* **95,** 2763–2767 (2011).

129. Hains, A. W. & Marks, T. J. High-efficiency hole extraction/electron-blocking layer to

replace poly(3,4-ethylenedioxythiophene):poly(styrene sulfonate) in bulk-heterojunction polymer solar cells. *Applied Physics Letters* **92,** 023504:1–3 (2008).

130. Murray, I. P., Lou, S. J., Cote, L. J., Loser, S., Kadleck, C. J., Xu, T., Szarko, J. M., Rolczynski, B. S., Johns, J. E., Huang, J., Yu, L., Chen, L. X., Marks, T. J. & Hersam, M. C. Graphene oxide interlayers for robust, high-efficiency organic photovoltaics. *Journal of Physical Chemistry Letters* **2,** 3006–3012 (2011).

131. Li, S. S., Tu, K. H., Lin, C. C., Chen, C. W. & Chhowalla, M. Solution-processable graphene oxide as an efficient hole transport layer in polymer solar cells. *ACS Nano* **4,** 3169–3174 (2010).

132. Xu, M.-F., Cui, L.-S., Zhu, X.-Z., Gao, C.-H., Shi, X.-B., Jin, Z.-M., Wang, Z.-K. & Liao, L.-S. Aqueous solution-processed MoO 3 as an effective interfacial layer in polymer/fullerene based organic solar cells. *Organic Electronics* **14,** 657–664 (2013).

133. Janáky, C. & Rajeshwar, K. The role of (photo)electrochemistry in the rational design of hybrid conducting polymer/semiconductor assemblies: from fundamental concepts to practical applications. *Progress in Polymer Science* **43,** 96–135 (2015).

134. Betancur, R., Maymóc, Elias, X., Vuong, L. T. & Martorell, J. Sputtered NiO as electron blocking layer in P3HT:PCBM solar cells fabricated in ambient air. *Solar Energy Materials and Solar Cells* **95,** 735–739 (2011).

135. Yu, J., Zheng, Y. & Huang, J. Towards high performance organic photovoltaic cells: A review of recent development in organic photovoltaics. *Polymers* **6,** 2473–2509 (2014).

136. Markov, D. E., Amsterdam, E., Blom, P. W. M., Sieval, A. B. & Hummelen, J. C. Accurate measurement of the exciton diffusion length in a conjugated polymer using a heterostructure with a side-chain cross-linked fullerene layer. *Journal of Physical Chemistry A* **109,** 5266–5274 (2005).

137. Sim, M., Shin, J., Shim, C., Kim, M., Byeok Jo, S., Kim, J.-H. & Cho, K. Dependence of exciton diffusion length on crystalline order in conjugated polymers. *Journal of Physical Chemistry C* **118,** 760−766 (2014).

138. Zhang, F., Jespersen, K. G., Björström, C., Svensson, M., Andersson, M. R., Sundström, V., Magnusson, K., Moons, E., Yartsev, A. & Inganäs, O. Influence of solvent mixing on the morphology and performance of solar cells based on polyfluorene copolymer/fullerene blends. *Advanced Functional Materials* **16,** 667–674 (2006).

139. Peet, J., Kim, J. Y., Coates, N. E., Ma, W. L., Moses, D., Heeger, A. J. & Bazan, G. C. Efficiency enhancement in low-bandgap polymer solar cells by processing with alkane dithiols. *Nature Materials* **6,** 497–500 (2007).

140. Kwon, O. K., Uddin, M. A., Park, J. H., Park, S. K., Nguyen, T. L., Woo, H. Y. & Park, S. Y. A high efficiency nonfullerene organic solar cell with optimized crystalline organizations. *Advanced Materials* **28,** 910–916 (2016).

141. Wang, J. L., Liu, K. K., Yan, J., Wu, Z., Liu, F., Xiao, F., Chang, Z. F., Wu, H. Bin, Cao, Y. & Russell, T. P. Series of multifluorine substituted oligomers for organic solar cells with efficiency over 9% and fill factor of 0.77 by combination thermal and solvent vapor annealing. *Journal of the American Chemical Society* **138,** 7687–7697 (2016).

142. Goh, T., Huang, J. S., Bartolome, B., Sfeir, M. Y., Vaisman, M., Lee, M. L. & Taylor, A. D. Panchromatic polymer-polymer ternary solar cells enhanced by Förster resonance energy transfer and solvent vapor annealing. *Journal of Materials Chemistry A* **3,** 18611–18621 (2015).

143. Shaheen, S. E., Brabec, C. J., Sariciftci, N. S., Padinger, F., Fromherz, T. & Hummelen, J. C. 2.5% efficient organic plastic solar cells. *Applied Physics Letters* **78,** 841–843 (2001).

144. Vanlaeke, P., Vanhoyland, G., Aernouts, T., Cheyns, D., Deibel, C., Manca, J., Heremans, P. & Poortmans, J. Polythiophene based bulk heterojunction solar cells: Morphology and its implications. *Thin Solid Films* **511–512,** 358–361 (2006).

145. Vanlaeke, P., Swinnen, A., Haeldermans, I., Vanhoyland, G., Aernouts, T., Cheyns, D., Deibel, C., D'Haen, J., Heremans, P., Poortmans, J. & Manca, J. V. P3HT/PCBM bulk heterojunction solar cells: relation between morphology and electro-optical characteristics. *Solar Energy Materials and Solar Cells* **90,** 2150–2158 (2006).

146. Gu, K. L., Zhou, Y., Gu, X., Yan, H., Diao, Y., Kurosawa, T., Ganapathysubramanian, B., Toney, M. F. & Bao, Z. Tuning domain size and crystallinity in isoindigo/PCBM organic solar cells via solution shearing. *Organic Electronics: physics, materials, applications* **40,** 79–87 (2017).

147. Lee, J.-H., Kim, S., Kim, H. & Lee, J. Solvent-dependent performance of solution-processed small-molecule organic field-effect transistors. *Organic Electronics* **52,** 184–189 (2018).

148. Liu, Z., Zhang, G. & Zhang, D. Modification of Side Chains of Conjugated Molecules and Polymers for Charge Mobility Enhancement and Sensing Functionality. *Accounts of*

Chemical Research **51,** 1422–1432 (2018).

149. Duan, C., Willems, R. E. M., van Franeker, J. J., Bruijnaers, B. J., Wienk, M. M. & Janssen, R. A. J. Effect of side chain length on the charge transport, morphology, and photovoltaic performance of conjugated polymers in bulk heterojunction solar cells. *Journal of Materials Chemistry A* **4,** 1855–1866 (2016).

150. Sharma, B., Alam, F., Dutta, V. & Jacob, J. Synthesis and photovoltaic studies on novel fluorene based cross-conjugated donor-acceptor type polymers. *Organic Electronics: physics, materials, applications* **40,** 42–50 (2017).

CHAPTER THREE

Research materials and synthetic routes

3.1 Introduction

Details highlighted in this chapter includes the following:

- Materials: provides information on all the materials used including their source
- Methodology: Research design and synthetic routes with sequential steps taken to fulfill the aim of this research. The research processes section gives information on the types and steps of all the major reactions carried out in the course of the research.

For the effective investigation, characterization and application of the prepared macromolecules and/or devices, the following analytical techniques were used: Nuclear Magnetic Resonance (NMR) spectroscopy using Bruker Avance III HD 400 MHz Nanobay NMR spectrometer equipped with a 5 mm BBO using tetramethylsilane as internal standard; Gel Permeation

Chromatography in the form of Size Exclusion chromatography (GPC/SEC) was performed using an Agilent 1260 Quad Pump, with DMF as the mobile phase and DMAC (0.05 % BHT + 0.03 % LiCl) was used as eluent. Fourier-Transform Infra-Red (FTIR) spectroscopy was investigated on PerkinElmer model Spectrum 100 series equipment; while Ultraviolet-Visible (UV-Vis) spectroscopy measurements were performed in a quartz cuvette using a Nicolet Evolution 100 UV–Visible spectrometer (Thermo Electron, UK). Photoluminescence (PL) spectroscopy studies were done on Horiba NanoLog™ - TRIAX (USA), with double grating excitation and emission monochromators with a slit width of 5 nm, and on Ocean Optics equipment. Microscopic analyses were performed with: High Resolution Transmission Electron Microscopy (HRTEM) using Tecnai G2F2O X-Twin MAT 200 kV field emission transmission electron microscope from FEI-Thermo Fischer Scientific (USA) and Scanning Electron Microscopy (SEM) using ZEISS ULTRA scanning electron microscope equipped with an energy dispersive spectrometer. Small-Angle X-ray Scattering (SAXS) analysis was carried out on an Anton Paar SAXSpace system, Graz, Austria using copper Kα radiation (0,154 nm) equipped with a 1 D mythen 2 position sensitive detector and a beamstop alignment for particle size determination. Cyclic Voltammetry (CV), Square Wave Voltammetry (SWV) and Electrochemical Impedance Spectroscopy (EIS) were done on CH instruments, Austin-USA.

3.2 Materials

The materials used and their suppliers are compiled in Table 3.1

Table 3.1 List of materials used and their suppliers

Materials	**Suppliers**
1,2-dichlorobenzene	Acros
1,4,5,8-perylene tetracarboxylic dianhydride	Sigma Aldrich
2-ethylhexylbromide	Sigma Aldrich
2-thiophene carboxaldehyde	Sigma Aldrich
3-hexylthiophene	Sigma Aldrich
9-(heptadecan-9-yl)-2,7-bis(4,4,5,5-tetramethyl-1,3,2-dioxyborolan-2-yl)-9H-carbazole	Sigma Aldrich
Acetone	Sigma Aldrich
Acetonitrile	Sigma Aldrich
Aluminum	Sigma Aldrich
Bromine	Sigma Aldrich
chloroform	Sigma Aldrich
DAB-Am4, Poly(propylene) tetramine dendrimer, Generation 1	Sigma Aldrich

Dichlorobenzene	Sigma Aldrich
Ferric chloride	Sigma Aldrich
Ferrocene	Sigma Aldrich
Glacial acetic acid	Sigma Aldrich
Hellmanex solution	Ossila
Hexamethyldisilazane	Aesar
Iodine	Sigma Aldrich
Iron (III) chloride	Sigma Aldrich
ITO substrates for photovoltaics	Ossila
ITO substrates for transistors	Merck
Lithium perchlorate anhydrous	Sigma Aldrich
Methanol	Sigma Aldrich
N-dodecylamine	Sigma Aldrich
N-methyl-2-pyrrolidone	Sigma Aldrich
Oleum	Sigma Aldrich
Palladium (0) tetrakis- (triphenylphosphine)	Sigma Aldrich
Perylene-3,4,9,10-tetracarboxyic dianhydride	Sigma Aldrich
Phenylboronic acid pinacol ester	Sigma Aldrich
Poly(3,4-ethylenedioxythiphene):poly(styrenesulph-onate) (PEDOT:PSS)	Sigma Aldrich
Poly(3-hexylthiophene)	Sigma Aldrich
Poly(methylmethacrylate)	Sigma Aldrich

Silver nitrate	Sigma Aldrich
Sodium carbonate	Sigma Aldrich
Tetrabutylammonium hexafluorophosphate	Fluka
Tetrahydrofuran	Sigma Aldrich

3.3 Research design

The conception of the thesis was done through a series of consecutive steps. For confirmation of the prepared materials with regard to initially proposed structures, each newly prepared material underwent Nuclear magnetic resonance (NMR) spectroscopy analysis. After which, purification and characterization were carried out to investigate the properties of the materials for possible application in organic electronics; particularly, organic photovoltaic cells. The broad research design is summarized in the flow diagram shown in Scheme 3.1.

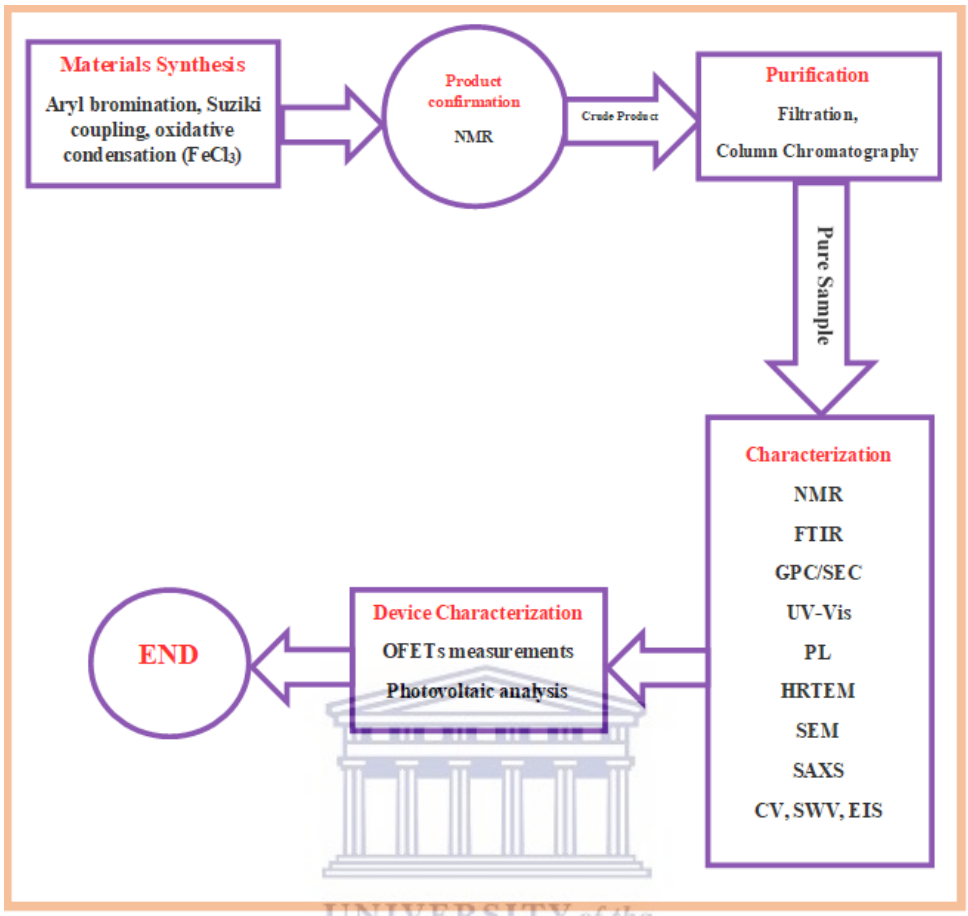

Scheme 3.1 Research design flow chart

The entire research based on the evaluation of the performances of conjugated polymers in organic field-effect transistors and organic photovoltaic cells is designed according to the following sequential steps:

- Materials synthesis: each route in the materials synthesis followed a set of well-known chemical reactions usually to give a crude product (with some side-products) which is then

isolated to get the pure sample. For co-polymerization, synthetic steps such as Suzuki coupling terminated by end-capping or oxidative condensation using $FeCl_3$ were used.

- Product confirmation: the crude product analyzed by ^1H NMR spectroscopy to confirm the success of the synthesis.

- Purification/Isolation: successful reactions were followed by purification either through column chromatography, or filtration or both of the above purification steps to obtain the pure product.

- Sample Characterization: desirable macromolecules were then investigated by nuclear magnetic resonance (NMR) and Fourier-Transform Infra-Red (FTIR) spectroscopy to confirm the chemical structures of the materials obtained. Ultraviolet-visible (UV-Vis) spectroscopy and Photoluminescence (PL) were used as means to elucidate the optical and photophysical properties of the materials which enabled the determination of the optical bang gap, E_{opt}. Scanning Electron Microscopy (SEM) and High-Resolution Transmission Electron Microscopy (HRTEM), were used for morphology interrogation. The later technique obtained results about the shape of the materials were then confirmed by SAXS analysis and interrogation of the materials' crystallinity was done using XRD technique. Electrochemical investigation through Cyclic Voltammetry (CV), Square Wave Voltammetry (SWV), Electrochemical Impedance Spectroscopy (EIS) enabled us to

determine the Highest Occupied Molecular Orbital (HOMO), Lowest Unoccupied Molecular orbital (LUMO) and electrochemical bang gap, E_g^{ec}, and investigate the conductivity of the materials and to ascertain their potential for device fabrication.

- Device Fabrication and Characterization: devices are fabricated and characterized to obtain the OFETs characteristics (Output and Transfer) and the photovoltaic current-voltage (I-V) curve, from where the device efficiency is derived.

3.4 Synthetic processes for the preparation of poly[N,N'-bis(dodecyl)perylene-3,4,9,10-tetracarboxylic diimide-1,7-diyl-alt-9-(heptadecane-9-yl)carbazole-2,7-diyl] (PDI-co-Carbazole)

3.4.1 Bromination of perylene-3,4,9,10-tetracarboxyic dianhydride (PTCDA)

Exactly, 7.85 g of perylene-3,4,9,10-tetracarboxylic dianhydride was weighed in a 250 mL three-neck round bottom flask and, 34 mL of 96% sulfuric acid, H_2SO_4 and 29 mL of oleum was added. The mixture was allowed to stir overnight. The catalyst I_2 (0.20 g) was then added. After which the reaction mixture temperature was raised to 85 °C, and bromine (Br_2) solution (2.5 mL) was introduced drop-wise over a period of 8 h. The reaction mixture was then stirred for additional 14 h (while temperature was kept 85 °C). Upon reaction completion, the mixture was left to cool down to room temperature, and Br_2 excess was removed using a gentle Argon (Ar) stream. Addition of

50 mL of water allowed for a precipitate to be formed; which was then filtered through an S3 frit using 30 mL of 70 % and 30 % sulfuric acid and a large amount of water consecutively. Collected sample was dried under vacuum for 48 h.[1] The reaction is depicted in Scheme 3.2.

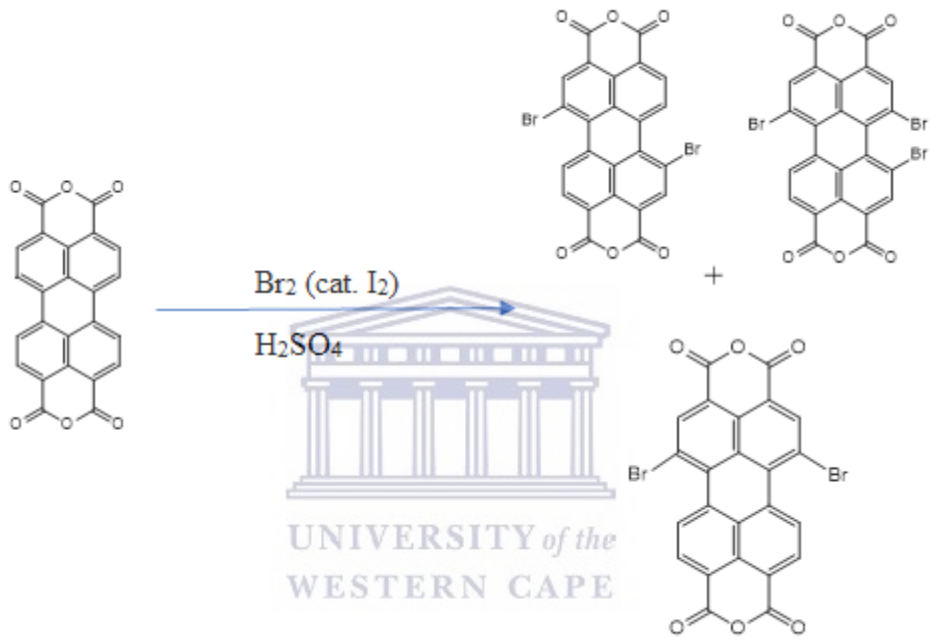

Scheme 3.2 Bromination of Perylene-3,4,9,10-tetracarboxyic dianhydride

3.4.2 Imidization of brominated PTCDA

Due to poor solubility of brominated-PTCDA, the material was used as obtained from preceding bromination reaction. 2 g of brominated perylene-3,4,9,10-tetracarboxylic dianhydride was introduced into a three-neck round bottom flask containing 40 mL of N-methyl-2-pyrrolidone (NMP), mixed with 10 mL of acetic acid, and purged under an Ar stream for 15 min. Reaction vessel temperature was raised to 60 °C for 25 min. Two (2) equivalences of N-dodecylamine dissolved in 1 mL of acetic acid were added to the heated mixture and temperature was increased to 120 °C and allowed to stir for 12 h. Upon completion of the reaction, the mixture was poured into 500 mL of water and filtered using professional filter paper with 4 -7 µm pore size and washed three (3) times with methanol. This reaction procedure (Scheme 3.3) is a slight modification of the procedure used by Vajiravelu *et al.*[2]

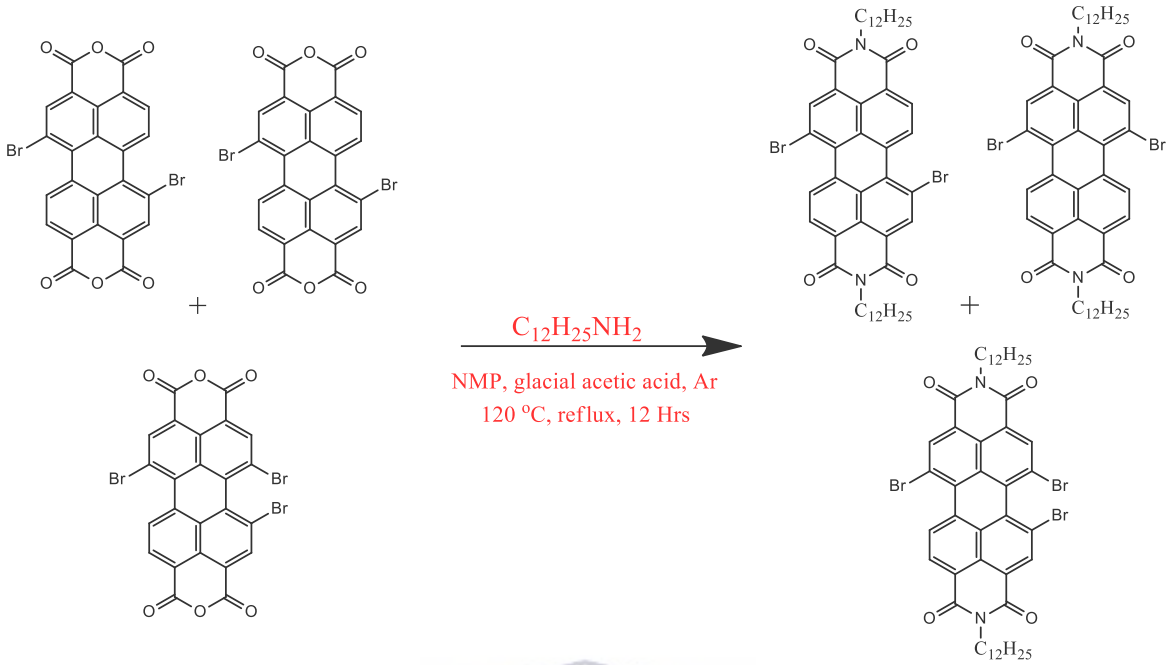

Scheme 3.3 Imidization of brominated PTCDA

3.4.3 Suzuki coupling reaction between 1,7-dibromo(N,N'-bis(dodecyl)perylene-3,4,9,10-tetracarboxylic diimide) (PDI-2Br) and 9-(heptadecan-9-yl)-2,7-bis(4,4,5,5-tetramethyl-1,3,2-dioxyborolan-2-yl)-9H-carbazole (Carbazole)

The reaction between an aryl/vinyl boronic acid (R-B$(OH)_2$) and an aryl/vinyl halide (R-X) in the presence of a Pd^0 complex is referred to as Suzuki coupling. Such coupling usually occurs in a basic medium, where the base helps in the enhancement of the transmetalation and the reductive elimination steps by increasing boronic acid reactivity toward the Pd-halide complex and converting it into the respective organoborate. Transition metal-catalyzed organic syntheses are

generally needed for the formation of a new carbon-carbon (C–C) bond. Palladium-catalyzed Suzuki reaction[3] has been identified as one of the most efficient procedure for C–C bond formation. Akira Suzuki and co-workers reported this coupling for the first time in 1979. This discovery coupled to the development of palladium-catalyzed cross couplings used in organic synthesis earned him and his colleagues, Richard F. Heck and Ei-ichi Negishi the 2010 Nobel Prize in Chemistry.[4] Many other coupling reactions that include Stille,[5] Sonogoshira,[6] Kumuda,[7] Heck and Hiyama[8] could be used to serve this purpose; but Suzuki coupling remains the mostly used. Indeed, its mild reaction conditions, the availability of various boronic acids on the market and their environmental safety compared to other organometallic reagents[9–12] justify the interest in this type of reaction. Stability, low toxicity and ease of preparation of boronic acid compounds have also led to new developments and progress in the reaction process of Suzuki coupling applications.[10,13] The ease in the removal of excess boron-containing products in comparison to other organometallic reagents and the facile reaction management gave another advantage of this coupling over the others.

Suzuki catalytic cycle is characterized by 3 main steps:[14]

1. Oxidative addition: Pd^0 is added in the reaction medium containing halide-substituted compound and is oxidized to Pd^{2+} while forming a brominated organopalladium complex.

2. Transmetalation: the later intermediate undergoes a transmetalation by reaction with the boronate complex (which is the base-activated boronic acid produced by the reaction of the boronic acid with base) to form the organopalladium species.

3. Reductive elimination allows for the generation of the desired product which ends the catalytic cycle and allows for regeneration of Pd^0.

In this work, 1,7-dibromo(N,N'-bis(dodecyl)perylene-3,4,9,10-tetracarboxylic diimide) (PDI-2Br) was copolymerized to 9-(Heptadecan-9-yl)-2,7-bis(4,4,5,5-tetramethyl-1,3,2-dioxyborolan-2-yl)-9H-carbazole (Carbazole), depicted in Scheme 3.4, according to the same synthetic route as reported by Zhou *et al*.[15] Approximately, 570 mg of PDI-2Br was weighed in a completely dried three-neck round bottom flask which was then connected to a condenser and flushed for 1 h under N_2 gas. 425 mg of carbazole was added in 35 mL degassed tetrahydrofuran (THF) and degassed 0.1 M aqueous Na_2CO_3 (30 mL) was also added. The reaction vessel was then allowed to be purged for 30 min to completely remove O_2 in the system. An excess of the catalyst $Pd(PPh_3)_4$ (3 mg, 20% per monomer) was also added in degassed THF and reaction mixture was allowed to stir for 72 h at 110 ℃ under refllux. End cappings, phenylboronic acid pinacol ester (50 mg) was introduced and left at 110 ℃ for 1 h; followed by 2-ethylhexylbromide (21 µL) left for 2 h at the same temperature. After cooling, the reaction mixture was transferred into an excess of methanol. The precipitated copolymer was filtered off, washed with water and methanol and dried in the vacuum.

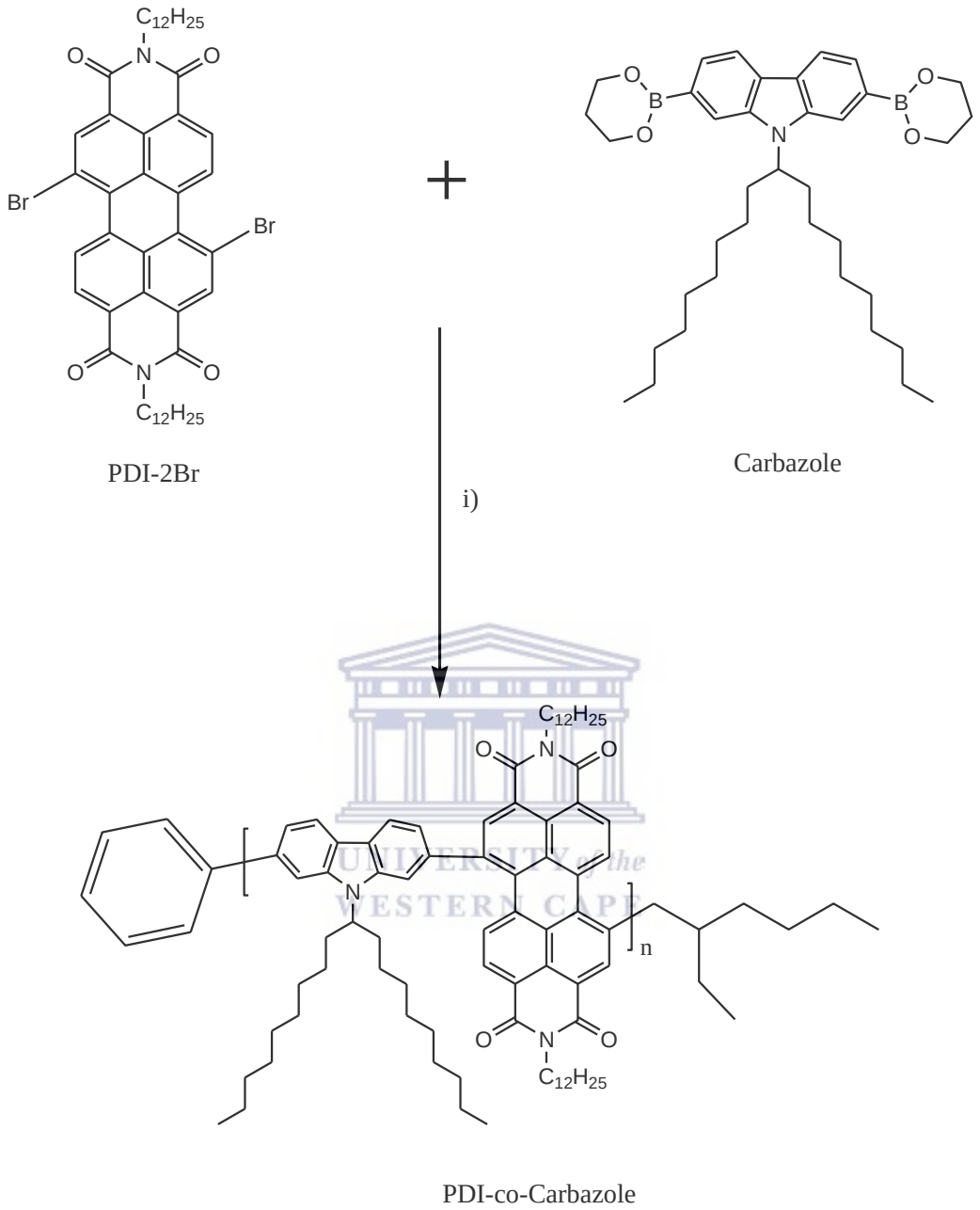

Scheme 3.4 Synthesis of PDI-co-Carbazole. i) THF, Na_2CO_3 (aq), $Pd(PPh_3)_4$, N_2, 72 h. End cappings: 1) phenylboronic pinacol ester, reflux 1 h, 2) ethylhexylbromide, reflux 2 h.

3.5 Synthetic processes for preparation of generation 1 poly(propylene thiophenoimine)-co-poly(3-hexylthiophene) (G1PPT-co-P3HT)

3.5.1 Generation 1 poly(propyleneimine) tetramine (G1PPI) functionalization

Prior to the functionalization of the dendrimer, a 250 mL 2-neck round bottom flask was washed, rinsed and dried for two (2) hours to remove all moisture. Then, the glassware was purged with nitrogen (N_2) gas. In order to functionalize the dendrimer, 0.3863 g (1.2205 mmol) of generation 1 poly(propyleneimine) tetramine dendrimer, G1PPI was dissolved in 25 mL of methanol (MeOH), then 472.55 µL (4.8821 mmol) of 2-thiophene carbaldehyde was added and the mixture was allowed to stir for 48 h under N_2 gas. G1PPT was thus functionalized into generation 1 poly(propylene thiophenoimine), G1PPT.[16] Upon completion of functionalization (Scheme 3.5), the solvent was completely removed by evaporation, after which 25 mL of dichloromethane and 25 mL of water were added to the functionalized dendrimer, transferred into a separation funnel, shaken for 10-15 min; then, the mixture was allowed to rest in order to separate the organic phase from the aqueous phase. This was done 5 times to ensure complete removal of any excess of 2-thiophene carbaldehyde. Water was removed, methanol evaporated and G1PPT was collected.

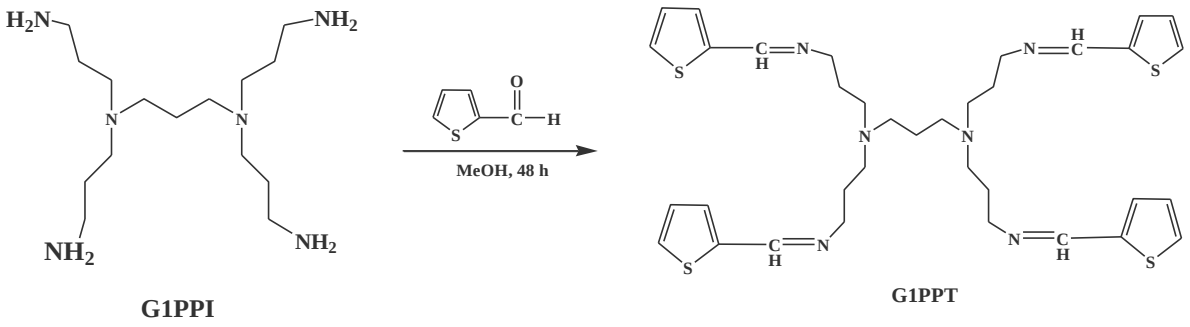

Scheme 3.5 Functionalization of G1PPI

3.5.2 Oxidative copolymerization of generation 1 poly(propylene thiophenoimine) (G1PPT) to 3-hexylthiophene (3-HT)

This copolymerization reaction depicted in Scheme 3.6 follows the procedure reported by Liu *et al.*,[17] for the polymerization of 3-hexylthiophene. 77.8 mg of G1PPT, 291 mg of $FeCl_3$ and chloroform ($CHCl_3$) were put in a 2-neck round bottom flask. 3-hexylthiophene (81 µL) was added dropwise to the magnetically stirred suspension and the reaction mixture was stirred for 48 h under N_2 atmosphere. 100 mL of methanol was added to quench the copolymerization. The prepared material was successively extracted with methanol (100 mL), acetone (100 mL), and $CHCl_3$ (100 mL) by filtration and G1PPT-co-P3HT copolymer was collected from $CHCl_3$.

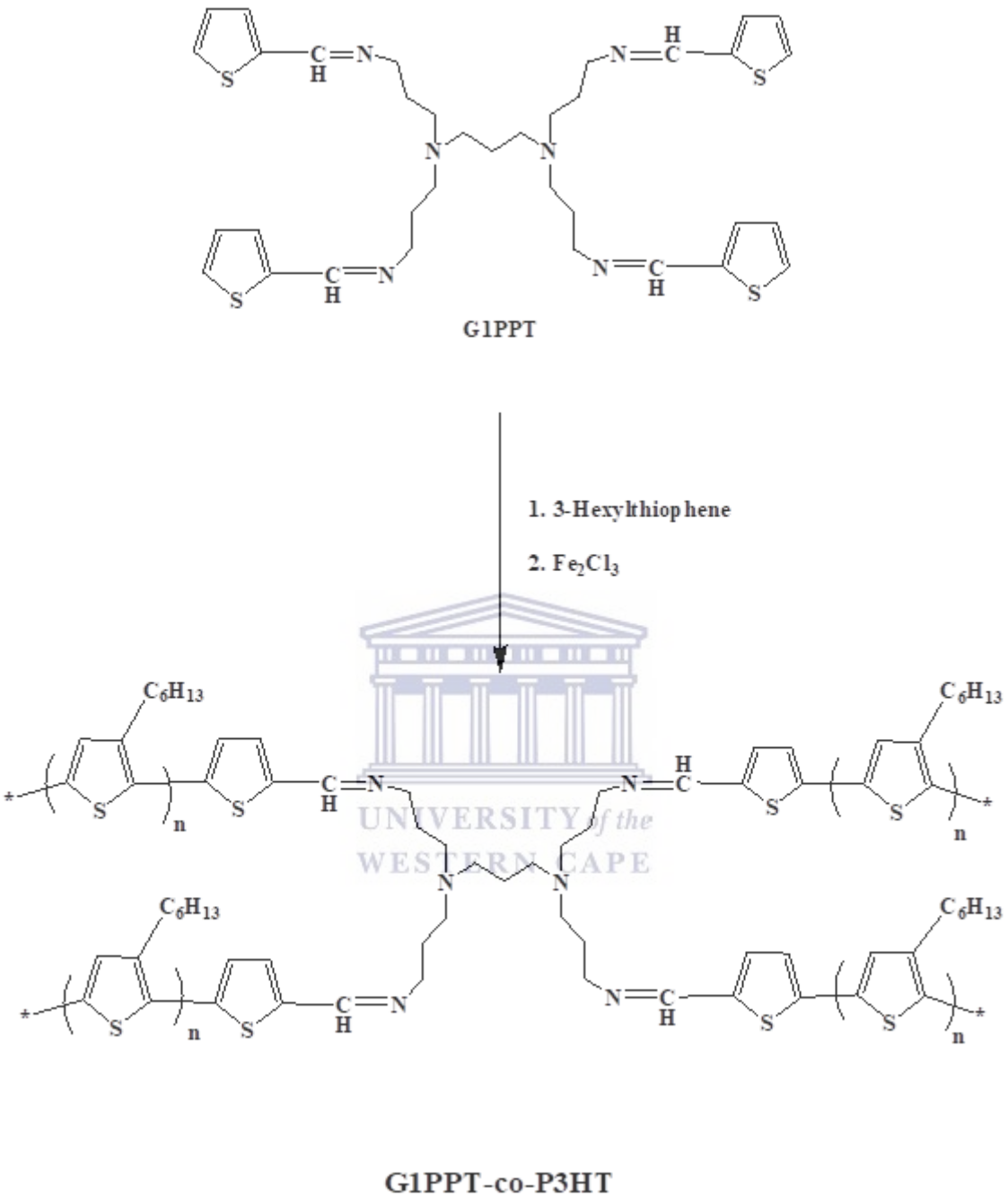

Scheme 3.6 Copolymerization of G1PPT and 3-hexylthiophene in the presence of $FeCl_3$ in chloroform

References

1. Würthner, F., Stepanenko, V., Chen, Z., Saha-Möller, C. R., Kocher, N. & Stalke, D. Preparation and characterization of regioisomerically pure 1,7-disubstituted perylene bisimide dyes. *Journal of Organic Chemistry* **69,** 7933–7939 (2004).

2. Vajiravelu, S., Ramunas, L., Juozas Vidas, G., Valentas, G., Vygintas, J. & Valiyaveettil, S. Effect of substituents on the electron transport properties of bay substituted perylene diimide derivatives. *Journal of Materials Chemistry* **19,** 4268–4275 (2009).

3. Efrem, A., Wang, K. & Wang, M. Facile synthesis of a narrow-bandgap strong-donor-alt-strong-acceptor copolymer of poly(5,6-difluorobenzo-[c][1,2,5]-thiadiazole-alt-5H-dithieno[3,2-b:2′,3’-d]pyran) via direct C-H arylation polymerization. *Dyes and Pigments* **145,** 331–338 (2017).

4. Devendar, P., Qu, R. Y., Kang, W. M., He, B. & Yang, G. F. Palladium-catalyzed cross-coupling reactions: a powerful tool for the synthesis of agrochemicals. *Journal of Agricultural and Food Chemistry* **66,** 8914–8934 (2018).

5. Tabi, G. D., Nketia-yawson, B., Lee, J. Y., Cho, K., Lim, B. & Noh, Y. Fluorinated benzothiadiazole and indacenodithieno[3,2-b]thiophene based regioregular-conjugated copolymers for ambipolar organic field-effect transistors and inverters. *RSC Advances* **7,** 1110–1117 (2017).

6. John, S. V., Cimrová, V., Ulbricht, C., Pokorná, V., Ružička, A., Giguère, J. B., Lafleur-

Lambert, A., Morin, J. F., Iwuoha, E. & Egbe, D. A. M. Poly[(arylene ethynylene)-alt-(arylene vinylene)]s based on anthanthrone and its derivatives: synthesis and photophysical, electrochemical, electroluminescent, and photovoltaic properties. *Macromolecules* **50,** 8357–8371 (2017).

7. Sharma, B., Alam, F., Dutta, V. & Jacob, J. Synthesis and photovoltaic studies on novel fluorene based cross-conjugated donor-acceptor type polymers. *Organic Electronics: physics, materials, applications* **40,** 42–50 (2017).

8. Jaymand, M., Hatamzadeh, M. & Omidi, Y. Modification of polythiophene by the incorporation of processable polymeric chains: recent progress in synthesis and applications. *Progress in Polymer Science* **47,** 26–69 (2015).

9. Meng, G. & Szostak, M. Palladium-catalyzed Suzuki-Miyaura coupling of amides by carbon-nitrogen cleavage: general strategy for amide N-C bond activation. *Organic and Biomolecular Chemistry* **14,** 5690–5707 (2016).

10. Rostamnia, S., Alamgholiloo, H. & Liu, X. Pd-grafted open metal site copper-benzene-1,4-dicarboxylate metal organic frameworks (Cu-BDC MOF's) as promising interfacial catalysts for sustainable Suzuki coupling. *Journal of Colloid and Interface Science* **469,** 310–317 (2016).

11. Nasrollahzadeh, M., Azarian, A., Maham, M. & Ehsani, A. Synthesis of Au/Pd bimetallic nanoparticles and their application in the Suzuki coupling reaction. *Journal of Industrial and Engineering Chemistry* **21,** 746–748 (2015).

12. Geiger, L., Nieger, M. & Bräse, S. Suzuki–Miyaura cross-coupling reactions of

tetrahydroxanthones and 4-chromanone lactones to heteromeric biaryls. *Advanced Synthesis and Catalysis* **359,** 3421–3427 (2017).

13. Alonso, F., Beletskaya, I. P. & Yus, M. Non-conventional methodologies for transition-metal catalysed carbon-carbon coupling: a critical overview. Part 2: The Suzuki reaction. *Tetrahedron* **64,** 3047–3101 (2008).

14. Das, P. & Linert, W. Schiff base-derived homogeneous and heterogeneous palladium catalysts for the Suzuki-Miyaura reaction. *Coordination Chemistry Reviews* **311,** 1–23 (2016).

15. Zhou, E., Cong, J., Wei, Q., Tajima, K., Yang, C. & Hashimoto, K. All-polymer solar cells from perylene diimide based copolymers: Material design and phase separation control. *Angewandte Chemie - International Edition* **50,** 2799–2803 (2011).

16. Makelane, H. R., John, S. V., Waryo, T. T., Baleg, A., Mayedwa, N., Rassie, C., Wilson, L., Baker, P. & Iwuoha, E. I. AC voltammetric transductions and sensor application of a novel dendritic poly(propylene thiophenoimine)-co-poly(3-hexylthiophene) star co-polymer. *Sensors and Actuators, B: Chemical* **227,** 320–327 (2016).

17. Liu, Y., Nishiwaki, N., Saigo, K. & Sugimoto, R. Polymerization of 3-hexylthiophene with $FeCl_3$ in aromatic solvents. *Polymer Bulletin* **72,** 1817–1826 (2015).

CHAPTER FOUR

Hole mobilities investigation in thienothiadazole/fluorene-based copolymers

Abstract

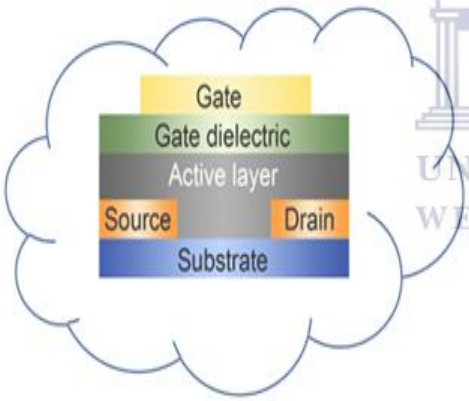

Denotation	R_1	R
CHTF	2-ethylhexyl	n-C_6H_{13}
CDTF	2-ethylhexyl	n-$C_{12}H_{25}$
CEHTF	2-ethylhexyl	2-ethylhexyl
CEHTF8	n-C_8H_{17}	2-ethylhexyl

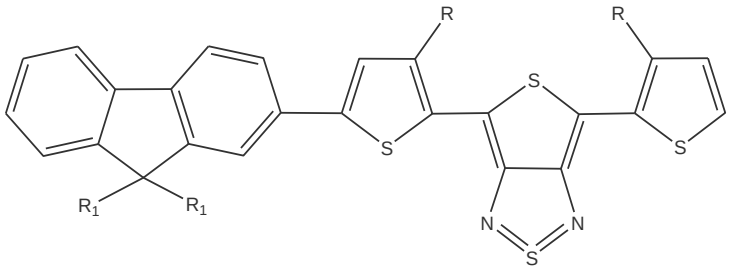

Graphical Abstract: OFET device architecture (top left), denotation of copolymers used and their substituents (top right), fluorene/thienothiadiazole copolymer backbone (bottom)

This chapter reports on the charge transport properties evaluation of the copolymers denoted CHTF, CDTF, CEHTF and CEHTF8 consisting of 4,6-bis(3'-alkylthien-2'-yl)thieno[3,4-c][1,2,5]thiadiazole and 9,9-dioctylfluorene with varying substituents on both donor and acceptor components. These polymers were prepared with various molecular weights in different solvents. Top-Gate organic field-effect transistors (OFETs) were prepared and their characteristics measured for hole mobilities. The polymeric films were spin-coated on substrates with inter-digitated indium-tin oxide (ITO) electrodes with preliminary surface treatment using hexamethyldisilazane (HMDS) or not. Poly(methylmethacrylate) (PMMA) used as gate dielectric layer was spin-coated on top of the polymer layer and finally a silver (Ag) gate electrode was thermally evaporated. This study revealed the effects of substitutions on either component of the main backbone with different side chains- straight and branched- result in the copolymers exhibiting similar hole mobilities characteristics in both linear and saturated regimes. Obtained results prove that the extent of hole mobility is associated with different factors that include the type of alkyl chain and their positions on either donating or electron withdrawing components of the backbone, molecular weight, and dispersity index. OFETs prepared based on materials with longer straight alkyl substitutions on the thienothiadiazole component exhibited higher mobilities up to 2.4 x10^{-2} cm^2/Vs.

KEY WORDS: Alkyl substitution, fluorene, hole mobilities, molecular weight, OFETs thienothiadiazole.

4.1 Introduction

The impressive innovations and progress in the synthesis, design, and processing of organic semiconductors have made organic electronics to be a continuous emerging technology.[1] Industrial applications that need large surface areas distribution on flexible plastic substrates are a good play ground for the applications of organic thin-film transistors. Field -effect transistor (FET) principle was first elaborated by Lilienfeld in 1930.[2] A FET basic operation is the same as that of a capacitor in which one plate is the gate electrode and the other plate is a conducting channel between two ohmic contacts, the source and drain electrodes. The voltage applied at the gate electrode modulates the density of charge carriers in the channel.[3] The first field-effect transistor, a silicon-based metal-oxide-semiconductor FET (MOSFET) was only fabricated in 1960 by Kahng and Atalla.[4] On the other hand, even though descriptions of the field-effect in organic semiconducting materials were made in the 1970s,[5] it is only after the report of Koezuka *et al.*,[6,7] that organic field-effect transistors (OFETs) were identified as potential elements of electronic devices. The intensive studies conducted in the domain of organic field-effect transistors in the recent years helped in generating the fundamentals of charge transport physics in small molecules as well as in π-conjugated polymers.[8] While clear guidelines for the design of high-mobility small-molecule semiconductors, which include extended π-π overlap in two or more spatial directions (ideally), close π – π stacking that help for high degree of crystallinity, decreased tendency of the materials to form static lattice defects and total quenching of thermal lattice fluctuations, have been presented;[8] charge carrier transport in polymeric field-effect transistors (PFETs) is known to be more complex to understand and predict, generally exhibiting low charge mobilities as a result of

the absence or poor macroscopic order, as well as poor molecular packing.[9] Indeed a major challenge to OFETs is the ability to monitor the film morphology, electronic structures and the properties of organic semiconducting devices through chemical modifications of their structures.[10] Nevertheless, more and more polymeric materials that fulfil the requirements of an ideal FET with high charge carrier mobilities have been reported.[11,12] Side-chain engineering[13–16] has been identified as one of the most important parameters to ascertain devices high charge carrier transport; mainly because polymers solubility and molecular packing are greatly affected by suitable side chain selection that includes side chain type and length, and branching point position.[17] In this work, I will therefore investigate the effects of side-chain substitutions on the charge carrier mobilities of a relatively new group of thienothiadiazole-fluorene copolymers.

4.2 Experimental

4.2.1 Materials and reagents

All materials under investigation were prepared via multi-step synthesis including Suzuki coupling by Cimrova *et al*., and are reported in literature.[18–24] Indium-tin Oxide (ITO) glass substrates were purchased from Merck. 1,2-Dichlorobenzene (DCB, 99%, extra purity grade) was purchased from Acros, hexamethyldisilazane (HMDS) was purchased from Aesar and Poly(methylmethacrylate) (PMMA) from Sigma Aldrich.

4.2.2 Sample preparation and characteristics measurement

The structure of the OFET devices was based on a Top-gate – Bottom contact (TGBC) architecture (Figure 4.1) and device preparation as well as characteristics measurements were done in an nitrogen inert atmosphere. Two types of top-gate/bottom-contact OFET samples were prepared and tested. Polymer layers were spin-coated on substrates with interdigitated indium-tin oxide (ITO) electrodes (5 various interelectrode spacings: 50, 75, 100, 150, 200 µm) from Ossila (UK) for the first type OFET samples (Figure 4.2, left). In the second case, HMDS was spin-coated on ITO substrate prior the polymer layer preparation. The thin polymer films were prepared by spin-coating from 1,2-dichlorobenzene solutions followed by annealing at 120 ^{o}C for 30 min in vacuum.

Then, PMMA, a dielectric layer was deposited on top of the polymer layer by spin-coating. A silver gate electrode was then thermally evaporated as the last stage of the transistor fabrication. All devices were then inserted in the OFETs board (Figure 4.2, right) for charge-carrier mobilities evaluation.

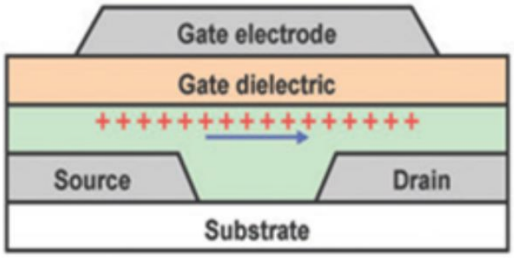

Figure 4.1 Top gate- Bottom contact architecture in OFETs

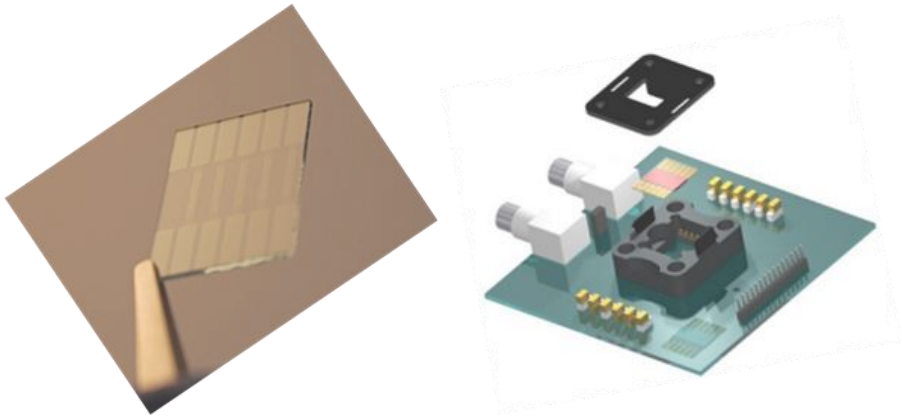

Figure 4.2 Inter-digitated ITO glass substrates (left) and OFETs board (right)

4.3 Results and discussion

The charge-carrier transport properties of the copolymers were investigated in the source-drain voltage (V_{SD}) range -100 V to 0 V with increasing negative gate-voltage (V_G) from 0 V to -100 V. As expected from OFETs, all devices showed typical transistors behaviour displaying some hole-mobilities in the linear and saturated regimes. All devices displayed output and transfer characteristics through applying different gate voltages within a fixed source-drain voltage window (output) or varying applied source-drain voltages at a fixed gate voltage range (transfer). Typical output and transfer characteristics graphs obtained for all devices are shown in Figure 4.3

and 4.4, respectively. Output characteristic graphs displayed two main components: a linear regime where the source-drain current is linearly dependent on the source-drain voltage[25] for small applied source-drain voltages. As the applied source-drain voltages increase, the charge carrier mobilities get to a plateau referred to as the saturated regime. On the other hand, the transfer characteristics show that the square root of resulting current is linearly dependent to the gate voltage of the saturation curve and extrapolation to the x-axis allows for the determination of the threshold voltage V_T,[26] the voltage at which the device gets to its "On" state and flow of charges starts. Because the mobility is gate-voltage dependent, only the linear portion of the curves was considered. Threshold voltage in turn depends on several factors that include total trap density (including dielectric/semiconductor bulk and dielectric/semiconductor interface trap densities), hole injection barrier between source/drain contact and polymers, and dielectric capacitance. The observed change in threshold voltage values is suggested to be due to not only the difference in the hole injection barrier coming from the difference in the Highest Occupied Molecular orbital (HOMO) levels of the polymers but also to the difference in the interface trap densities. Nevertheless, it is important to note that in all OFET structures, most of the device related parameters are based on the threshold voltage.[27] As it will be seen in the coming results, all devices exhibited p-type semiconductors behaviour.

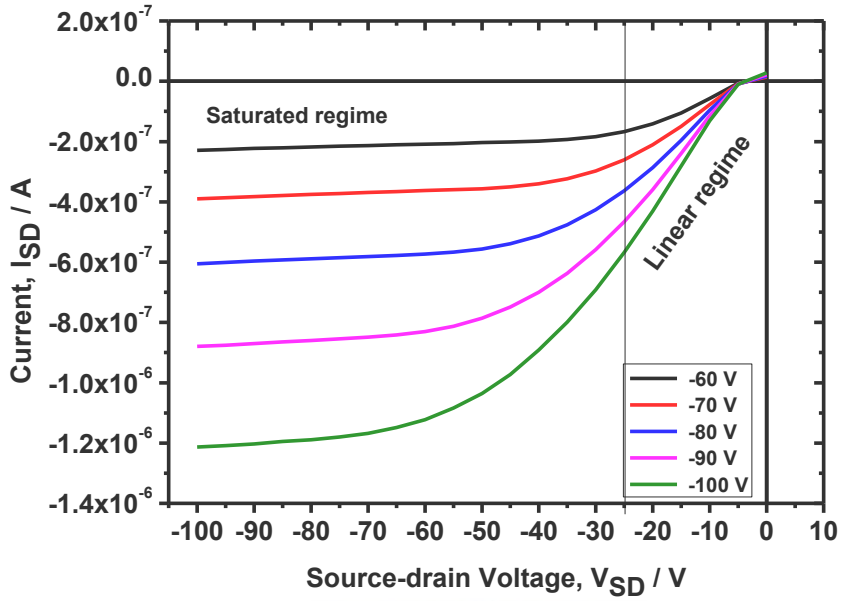

Figure 4.3 Output characteristics: Plot of I_{SD} vs V_{SD} of CEHTF8-c

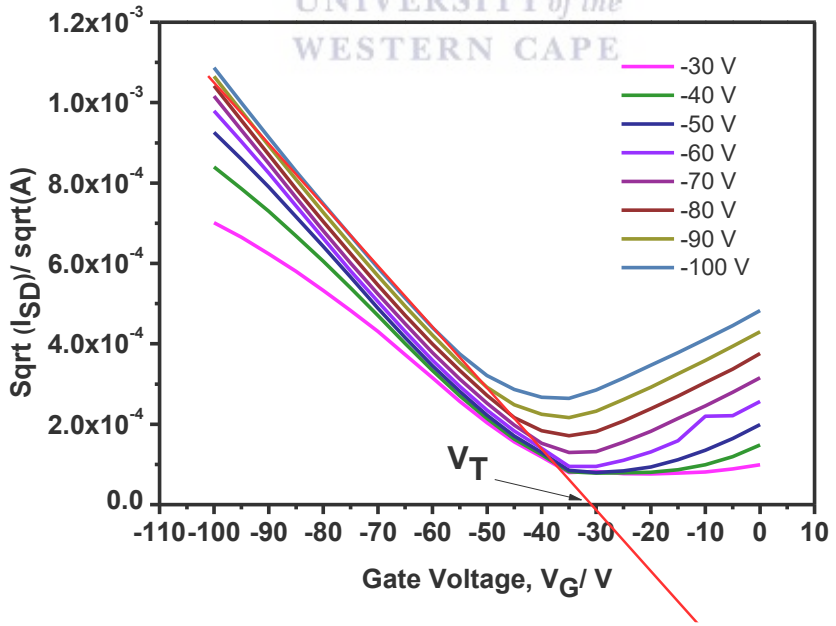

Figure 4.4 Transfer characteristics: Plot of sqrt (I_{SD}) vs V_G of CEHTF8-c

The mobilities were calculated by extracting the data from the graphs based on the Equations 4.1, 4.2, 4.3 and 4.4.[28]

For small V_{SD}, the mobility in the linear regime is calculated from Equation 4.1,

$$\mu_{lin} = \frac{L.g_{\mathrm{m}}}{W.C_{\mathrm{i}}.V_{SD}} \qquad \text{(Equation 4.1)}$$

Where,

$$g_{m=\frac{\partial I_{\mathrm{SD}}}{\partial V_{\mathrm{G}}}|_{V_D}} \qquad \text{(Equation 4.2)}$$

In the saturation regime, $V_{\mathrm{SD}} > (V_{\mathrm{G}}\text{-}V_{\mathrm{T}})$, is given by Equation 4.3

$$I_D = \frac{W\mu_{\mathrm{sat}}C_{\mathrm{i}}}{2L}(V_{\mathrm{G}} - V_{\mathrm{T}})^2 \qquad \text{(Equation 4.3)}$$

The mobility is calculated using Equation 4.3 above by solving Equation 4.4,

$$\mu_{sat} = \frac{2L}{WC_{\mathrm{i}}}\left(\frac{\partial\sqrt{I_{\mathrm{SD}}}}{\partial V_{\mathrm{G}}}\right)^2 \qquad \text{(Equation 4.4)}$$

where, L is length of the channel, g_m is the transconductance, W is the width of the channel, C_i is the capacitance of the dielectric layer, V_{SD} is the source-drain voltage, I_{SD} is the source-drain current and V_G is the gate-voltage.

4.3.1 Charge transport properties in the different copolymers.

4.3.1.1 Charge transport properties in CEHTF8 thin films

A series of devices based on CEHTF8 copolymers with octyl groups on the fluorene part and ethylhexyl groups on the thienothiadiazole, with different molecular weights (M_Ws) was prepared and characterized. Table 4.1 summarizes the obtained hole mobilities with respect to the molecular weight. All samples displayed approximately the same degree of dispersity, $Đ$ =1.45. It was found that increasing the molecular weight and as such the number of monomeric subunits accounts for an increase in the charge carrier transport; but it was also noted that this increase is not linearly proportional as sample CEHTF8-d_1, M_W = 63980 displayed a mobility μ_{sat} = 2.3 × 10^{-4} cm^2/Vs compared to sample CEHTF8-x with M_W 1.52 times higher and mobility 1.3 times greater and CEHTF8- c with molecular weight 3.5 times higher but the mobility was found to be greater by a factor of 2.9 only.

Table 4.1 Hole mobilities in CEHTF8 devices

Chemical structure	**Denotation**	M_w	$Đ$	μ_{lin}/ 10^{-4} cm^2/Vs	μ_{lsat}/ 10^{-4} cm^2/Vs
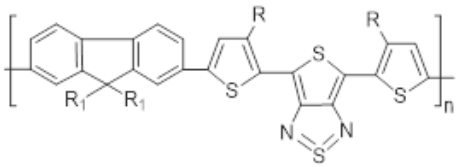	CEHTF8-d_1	63980	1.45	2.0	2.3
	CEHTF8-x	97790	1.45	2.0	3.0
R_1=n-C_8H_{17} R=2-ethylhexyl	CEHTF8-c	222300	1.44	6.4	6.7

4.3.1.2 Charge transport properties in CDTF thin films

A series of seven (7) devices prepared with samples where R_1 is an ethylhexyl group and R_2 is a dodecyl (-$C_{12}H_{25}$) group denoted CDTF was also investigated and all results are summarized in Table 4.2. These samples were prepared using different solvents and afforded various molecular weights with various dispersity, $Đ$. CDTF-1, CDTF-2, CDTF-3, CDTF-4, CDTF-5, CDTF-6, CDTF-7 with M_Ws ranging from 14920 g/mol to 48520g/mol exhibited mobilities of 1.3, 1.0, 1.5, 0.8, 0.5, 0.4 and 1.4 × 10^{-2} cm^2/Vs, respectively. In this batch of devices, it was very interesting to observe that $Đ$ played a very important role in the diffusion of the holes within the prepared polymers. Indeed, CDTF-1 the polymer with the lowest M_W but also with the smallest $Đ$ = 1.25

showed a mobility, $\mu_{sat} = 1.3 \times 10^{-2}$ cm^2/Vs compare to CDTF-7 with the highest M_W 48520 g/mol and $\mu_{sat} = 1.4 \times 10^{-2}$ cm^2/Vs but, $Đ = 1.67$. Also, CDTF-5 with the highest $Đ = 2.36$ and M_W 42770 g/mol exhibited a mobility $\mu_{sat} = 5.2 \times 10^{-3}$ cm^2/Vs. It was also interesting to notice that CDTF-6 with higher M_W 44920 g/mol and smaller $Đ = 1.83$ compare to CDTF-5 displayed a lower mobility, $\mu_{sat} = 4 \times 10^{-3}$ cm^2/Vs. We suggest that the reason being is, even though the $Đ$ is lower, there might be lost of planarity or unfavorable molecules packing when forming thin films, therefore hindering the continuous diffusion of charge carrier along the whole macromolecule. It therefore proves that to allow for a continuous flow of charge carrier, there must be a continuous π-π stacking that encourages intermolecular charge transfer and allows increased separation of charges[29], which is discontinued in macromolecules with increased $Đ$.[30] It is to be noted that CDTF group of devices exhibited the highest mobilities. This increased mobility is suggested to be caused by the conformational flexibility in these linear-substituted thienothiadiazole-fluorene [31]

Table 4.2 Hole mobilities in CDTF devices

Chemical structure	**Denotation**	**M_W**	**Đ**	**μ_{lin}/ 10^{-2} cm^2/Vs**	**μ_{sat}/ 10^{-2} cm^2/Vs**
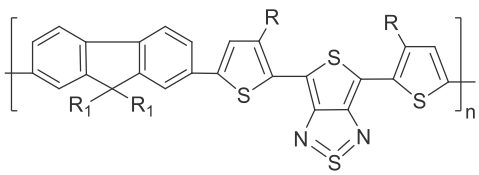 R_1= 2-ethylhexyl R=n-$C_{12}H_{25}$	CDTF-1	14920	1.25	1.2	1.3
	CDTF-2	32330	1.41	0.7	1.0
	CDTF-3	34330	1.43	1.2	1.5
	CDTF-4	35810	1.57	0.7	0.8
	CDTF-5	42770	2.36	0.5	0.5
	CDTF-6	44920	1.83	0.2	0.4
	CDTF-7	48520	1.67	1.3	1.4

4.3.1.3 Charge transport properties in CHTF thin films

Two devices were prepared using copolymer CHTF with ethylhexyl groups on the fluorene part and n-hexyl groups on the thienothiadiazole with two different molecular weights. The lowest molecular weight device CHTF-1 with *Đ*= 1.47 showed a saturated mobility $\mu_{sat} = 3 \times 10^{-3}$ cm^2/Vs; whereas CHTF -2 with a molecular weight almost three (3) times that of CHTF-1 showed a

saturated mobility of only $\mu_{sat} = 2 \times 10^{-3}$ cm^2/Vs. Again, it is suggested that the high molecular weight achieved inhibits proper π-π stacking in the conjugated polymer.

Table 4.3 Hole mobilities in CHTF devices

Chemical structure	**Denotation**	M_w	$Đ$	**μ_{lin}/ 10^{-3} cm^2/Vs**	**μ_{sat}/ 10^{-3} cm^2/Vs**
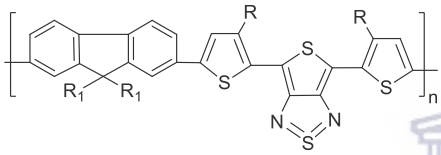	CHTF-1	21670	1.47	2	3
R_1= 2-ethylhexyl R= n-C_6H_{13}	CHTF-2	60200	2.69	1	2

4.3.1.4 Charge transport properties in CEHTF thin films

Devices based on CEHTF with ethylhexyl groups on the fluorene part and ethylhexyl groups on the thienothiadiazole exhibited the lowest charge transport properties. Indeed, CEHTF-1 with molecular weight, M_W 19500 g/mol and dispersity $Đ$= 1.43 only demonstrated saturated mobility of $\mu_{sat} = 2 \times 10^{-4}$ cm^2/Vs. The charge transport mobility was lowered by one order of magnitude to $\mu_{sat} = 7 \times 10^{-5}$ cm^2/Vs when the degree of polymerization was five (5) times increased (Table 4.4).

The poor performance exhibited by this group is suggested to be due to the branched nature of the substituents.

Table 4.4 Hole mobilities in CEHTF devices

Chemical structure	**Denotation**	M_w	Đ	μ_{lin} / 10^{-4} cm^2/Vs	μ_{sat}/ 10^{-4} cm^2/Vs
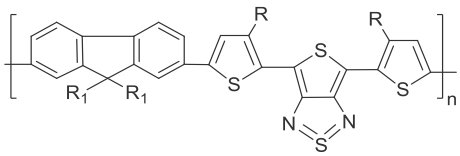 R_1= 2-ethylhexyl R=2-ethylhexyl	CEHTF-1	19500	1.43	2	2
	CEHTF-2	95000	3.00	0.5	0.7

4.3.2 Factors affecting the charge transport properties

4.3.2.1 Side-chain substituents

The four main groups of thienothiadiazole-fluorene copolymers with different alkyl chain substitutions CHTF, CDTF, CEHTF and CEHTF8 summarized in Table 4.5 were prepared and tested in OFETs. During charge transport investigation, it was noticed that the extent of hole mobilities in the devices is related to the type of substituents, branched or linear alkyl chains attached to the different components of the backbone. Indeed, we observed that all CEHTF

copolymers with ethylhexyl groups on both fluorene and thienothiadiazole components exhibited the poorest hole transport properties with saturated mobilities as low as $\mu_{sat} = 7 \times 10^{-5}$ cm^2/Vs. This saturated mobility is an order of magnitude lower than CEHTF8-based devices where the ethylhexyl groups on the fluorene was replaced by an n-octyl group. Another increase in order of magnitude to 10^{-3} cm^2/Vs compared to the CEHTF8 devices was observed when ehylhexyl groups were attached on fluorene but linear n-hexyl groups were attached on thienothiadiazole in CHTF-based devices. Further increase in the hole transport properties to as high as 1.5×10^{-2} cm^2/Vs was observed in CDTF-based OFETs devices where the n-hexyl groups on the thienothiadiazole was replaced by n-dodecyl groups. These results therefore demonstrate that branched or linear alkyl substitutions play a key role in the hole transport properties of these copolymers as the phase separation step is strongly dependent on these solubilizing side chains;[32] and that best mobilities are obtained with those polymers were the linear substitutions is on the thienothiadiazole. This behavior can be explained by the fact that branched alkyl side-chains are bulky and as such they distort the planarity of the macromolecules which result in lower π-π stacking strength. So, in CEHTF branched alkyls on both fluorene and thienothiadiazole unfavored π-π stacking which drastically hindered the hole mobilities. These findings can be correlated to the optical properties of these polymers. Indeed, Cimrova *et al*[23] observed that the maximal absorption of CEHTF with the branched alkyl chains are hypsochromic shifted compared to the absorption maxima of CHTF and CDTF copolymers with linear alkyls and suggested that the this could be as a result of the shielded stacking strength in bulkier branched ethylhexyl chains which hinders strong intermolecular interactions, while linear alkyl chains substitutions in these thienothiadiazole-fluorene copolymers enhances the stabilization of the supramolecular structure. Improved

structural order in CHTF and CDTF is therefore due to the intermolecular contacts caused by S–N interactions in the thin films.[21]

It was very interesting to note the large difference in the hole mobilities of these polymers, which was increased by three (3) order of magnitude despite their structural similarity. Which therefore suggests that the appropriate choice of alkyl side chains and their position on the different component of the polymer backbone has a significant effect on the transistors performance whose charge carrier mobilities strongly depend on interchain hopping[27] which in turn is actually dependent on the nature of the solid-state packing of these materials[33]

Table 4.5 Summary of hole mobilities of copolymers CHTF, CDTF, CEHTF, CEHTF8

Chemical structure of copolymer	**Denotation**	**R_1**	**R**	**μ_{sat}/ cm^2/Vs**
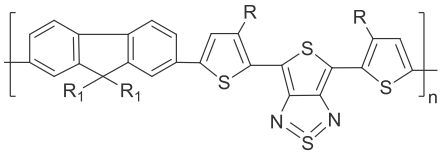	CEHTF	2-ethylhexyl	2-ethylhexyl	*7* x 10^{-5} (lowest μ_{sat})
	CEHTF8	n-C_8H_{17}	2-ethylhexyl	6.7 x 10^{-4}
	CHTF	2-ethylhexyl	n-C_6H_{13}	*3* x 10^{-3}
	CDTF	2-ethylhexyl	n-$C_{12}H_{25}$	*1.5*x 10^{-2}

4.3.2.2 Solvents used, molecular weight and dispersity

Even though there was a general observation that linear alkyl chain substituted thienothiadiazole-fluorene copolymers -linear substitution being on the thienothiadiazole part- exhibited the highest mobilities, it was also noticed that these mobilities are affected by the molecular weight. As a result, in CEHTF8 based devices, the hole mobilities increased with increasing molecular weight for these devices where the polymers used had approximately the same $Đ$= 1.45 (See Table 4.1). But this was not true for CEHTF, CHTF and CDTF-based devices where higher dispersity played an important role in the decrease of the mobilities even in polymers with high molecular weight. We can take the case of a CDTF- based devices where most of the polymers with high molecular weights, above 35000 g/mol were characterized by quite high dispersity, $Đ$ above 1.5, see Table 4.2 and exhibited saturated mobilities slightly lower than those with low molecular weights and low $Đ$. But again, it was interesting to notice that CDTF-7 with M_W 48520 g/mol had lower $Đ$ = 1.67 but high saturated mobility $\mu_{sat} = 1.4 \times 10^{-2}$ cm^2/Vs compared to CDTF-6 with M_W 44920, $Đ$ 1.83 but with a saturated hole mobility an order of magnitude lower, $\mu_{sat} = 4 \times 10^{-3}$ cm^2/Vs. Variations in these M_Ws were caused by the solvents used which in turn affected the $Đ$. This demonstrates that trapping should be one of the limiting charge transport steps caused by the lattice disorder in these high-molecular-weight semiconducting polymers[34] which disorder is highly related to the type of solvents involved in the copolymerization reaction. In addition, high molecular weight could also have an effect on the orientation of the polymers which could affect

the planarity.[35] Therefore, in order to ascertain good charge carrier properties a good $M_W/Đ$ regime must be established.[30]

4.3.2.3 Surface pre-treatment using hexamethyldisilazane (HMDS): case of CEHTF8-*c*

Many reports have shown the beneficial effects of self-assembled monolayer (SAM) treatment on the charge transport properties in OFETs stating that the increase in the mobilities was as a result of an improvement in the grain size of the thin films caused by the pre-treatment.[36] During device fabrication, the ITO substrate was pre-treated with HMDS before deposition of the CEHTF8-*c* layer with the highest M_W= 222300 g/mol on the ITO glass substrate, the obtained hole mobility of 7.4×10^{-4} cm^2/Vs (Table 4.6) shows that there is no significant increase in the mobilities (Figure 4.5).

Table 4.6 Saturated mobilities of CEHTF8 with and without HMDS treatment.

Chemical structure	**Denotation**	**HMDS**	**μ_{lin}/ 10^{-4} cm^2/Vs**	**μ_{Isat}/ 10^{-4} cm^2/Vs**
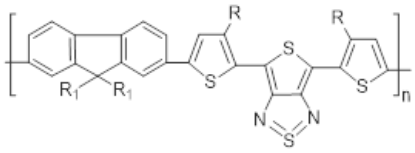 R_1=n-C_8H_{17} R=2-ethylhexyl	CEHTF8-c	No	6.4	6.7
		Yes	5.8	7.4

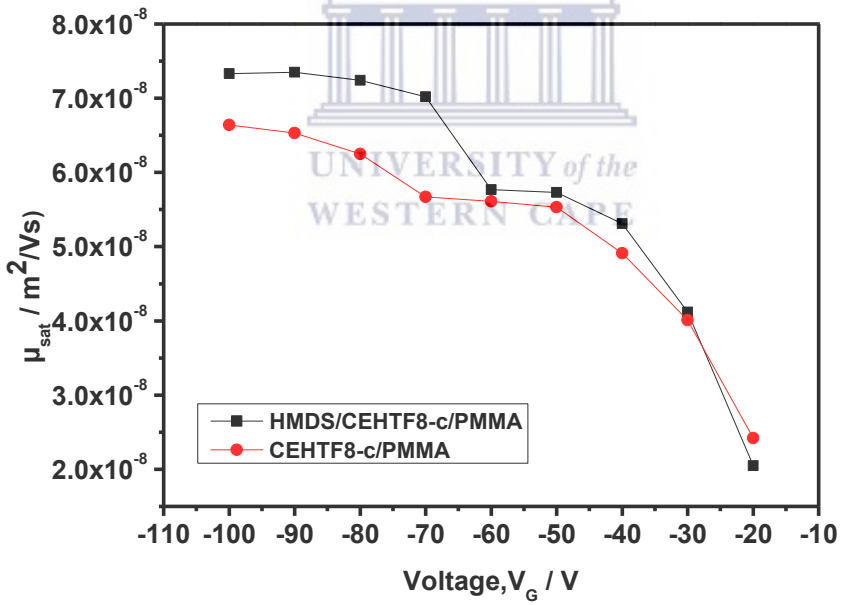

Figure 4.5 Plot of μ_{sat} vs V_G for the device configuration

ITO/HMDS/CEHTF8-c/PMMA/Ag and ITO/CEHTF8-c/PMMA/Ag

4.3.2.4 Other parameters affecting hole mobility: special investigation of CDTF-2 and CDTF-7

Special attention was given to CDTF polymers group as they exhibited the best transport properties. Indeed, various parameters such as polymer thickness, dielectric thickness, pre-treatment and annealing have been used/varied to investigate their effect on the hole transport properties. CDTFs were used to design devices either pre-treated with HMDS, with different dielectric thicknesses, or annealed. For CDTF-2, with molecular weight M_W 32330 g/mol and $Đ$ =1.41, saturated mobility was found to be $\mu_{sat} \approx 1.0 \times 10^{-2}$ cm^2/Vs as reported in Table 4.2. The device layer thickness is 84.3 nm and its dielectric layer thickness, 728.8 nm. Pre-treatment with HMDS did not change the hole mobilities. It has been reported that varying dielectric thickness and surface roughness can severely impact the mobility of OFET device with ultrathin gate dielectrics[37–39] due to the charge scattering that occurs at the rough surface.[40] But when the thickness of the layer was decreased to 80 nm and the dielectric layer PMMA also decreased to 507 nm, saturated mobility was found to be $\mu_{sat} \approx 1.4 \times 10^{-2}$ cm^2/Vs, a slight increase even though not significant. This is justified by the fact that the decrease in these layer's thicknesses was suitable for the diffusion of the holes. Pre-treatment using HMDS did not really influence the saturated mobility compare to the untreated one, but slightly affected the linear mobility which decreased from $\mu_{lin} \approx 1.5 \times 10^{-2}$ cm^2/Vs down to $\approx 1.2 \times 10^{-2}$ cm^2/Vs. A new device with PMMA thickness 560 nm was fabricated and no big change was observed either; saturated mobility was calculated to be $\mu_{sat} \approx 1.2 \times 10^{-2}$ cm^2/Vs. While the idea of annealing the device to high temperature of 200 ℃ was expected to result in an increase in the charge transport properties as heating is assumed to increase structural order in the thin films, annealing the device did not show any big

change neither and the saturated mobility was found to be $\mu_{sat} \approx 1.1 \times 10^{-2}$ cm^2/Vs. Increasing the thin film thickness by ca. 2.5 factor slightly changes the saturated mobility to $\mu_{sat} \approx 2.4 \times 10^{-2}$ cm^2/Vs. This slight increase is due to the big increase in thin film layers. But such result was not surprising if we consider the optical results[20] in which an increase in CDTF film thickness caused the absorption coefficient to decrease which resulted in a blue-shift of the longest wavelength maximum. Pre-treatment of this device with HMDS did not affect this mobility. On the other hand, OFETs based on CDTF-7 with higher molecular weight compared to CDTF-2 was also investigated. While the dielectric thickness was the same, the polymer layer thickness was few nanometers higher. This device exhibited similar charge transport compared to CDTF-2 despite the increase molecular weight and layer thickness and it is due the higher *Đ* of the polymer that results in a discontinuous flow of the charges along the conjugated backbone.

Table 4.7 Saturated mobilities when CDTF was subjected to different parameters variations

CDTF (Thickness)	**Dielectric thickness**	***M_w***	***Đ***	**μ_{lin}/ 10^{-2} cm^2/Vs**	**μ_{sat}/ 10^{-2} cm^2/Vs**
CDTF-2 (80 nm)	507 nm	32330	1.41	1.5	1.4
	507 nm and HMDS			1.2	1.3
	560 nm			1.4	1.2
	200 ^{o}C			1.1	1.1
CDTF-2 (84.3 nm)	728.8 nm	32330	1.41	0.7	1.0
	728.8 nm and HMDS			0.8	1.0
CDTF-2 (209.6 nm)	507 nm	32330	1.41	2.2	2.4
	507 and HMDS			2.1	2.3
CDTF-7 (107 nm)	507 nm	48520	1.67	1.3	1.3
	507 nm			1.1	1.3
	507 nm and HMDS			1.2	1.3

4.4 Conclusion

Organic field-effect transistors based on CEHTF, CEHTF8, CHTF and CDTF copolymers with either ethylhexyl or octyl substitutions on the fluorene component of the backbone and n-dodecyl, n-hexyl or ethylhexyl groups on the thienothiadiazole were successfully fabricated using top-gate,

bottom-contact architecture and different parameters were varied during these fabrications to investigate if they had any significant effect on the hole mobilities. While CDTFs with ethylhexyl groups on the fluorene and n-dodecyl side chain on the thienothiadiazole, exhibited the best performances with mobilities as high as 1.5×10^{-2} cm^2/Vs for as prepared devices without any parameter's variations, the lowest mobilities were observed from CEHTF comprising ethylhexyl side chain substitutions on both backbone components. Increase of hole mobilities by three orders of magnitude from CEHTF to CDTF was observed. Therefore, this demonstrates that best hole mobilities in these thienothiadiazole-fluorene copolymers are obtained from the linear alkyl-substituted polymers and most specifically those with straight alkyl substitutions on the thienothiadiazole component. A dependence of the hole mobilities on the molecular weights achieved by the polymers was also observed but the extent of this dependence is highly based on the lattice arrangement (dispersity, $Đ$) within these macromolecules. Indeed, a good $M_W/Đ$ regime needs to be met to obtain optimum charge transport properties. Further investigation by varying parameters such as polymers thickness, dielectric thickness, surface pre-treatment or annealing did not bring any significant change in the charge transport.

References

1. Luo, H., Yu, C., Liu, Z., Zhang, G., Geng, H., Yi, Y., Broch, K., Hu, Y., Sadhanala, A., Jiang, L., Qi, P., Cai, Z., Sirringhaus, H. & Zhang, D. Remarkable enhancement of charge carrier mobility of conjugated polymer field-effect transistors upon incorporating an ionic additive. *Science Advances* **2,** e1600076–e1600076 (2016).

2. Marques-Gonzalez, S. & Low, P. J. Molecular Electronics : History and Fundamentals. *Australian Journal of Chemistry* **69,** 244–253 (2016).

3. Hümmelgen, I. A. Organic electronic solid state device: electrochemistry of material preparation. *Journal of Solid State Electrochemistry* **21,** 1977–1985 (2017).

4. Amiri, I. S., Mohammadi, H. & Hosseinghadiry, M. Invention and Evaluation of Transistors and Integrated Circuits. In *Device Physics, Modeling, Technology, and Analysis for Silicon MESFET*, 1–9 (Springer International Publishing, 2019).

5. Phan, H., Ford, M. J., Lill, A. T., Wang, M., Bazan, G. C. & Nguyen, T.-Q. Electrical Double-Slope Nonideality in Organic Field-Effect Transistors. *Advanced Functional Materials* **28,** 1707221 (2018).

6. Larik, F. A., Faisal, M., Saeed, A., Abbas, Q., Kazi, M. A., Abbas, N., Thebo, A. A., Khan, D. M. & Channar, P. A. Thiophene-based molecular and polymeric semiconductors for organic field effect transistors and organic thin film transistors. *Journal of Materials Science: Materials in Electronics* **29,** 17975–18010 (2018).

7. Mittal, P., Negi, Y. S. & Singh, R. K. Mapping of performance limiting issues to analyze top and bottom contact organic thin film transistors. *Journal of Computational Electronics* **14,** 360–379 (2015).

8. Sirringhaus, H. 25th Anniversary Article: Organic Field-Effect Transistors: The Path Beyond Amorphous Silicon. *Advanced Materials* **26,** 1319–1335 (2014).

9. Lei, T., Dou, J. H. & Pei, J. Influence of alkyl chain branching positions on the hole mobilities of polymer thin-film transistors. *Advanced Materials* **24,** 6457–6461 (2012).

10. Liu, Y., Zhan, X. & Leu, Y. High-mobility conjugated polymers based on fused-thiophene building blocks. *Macromolecular Chemistry and Physics* **212,** 428–443 (2011).

11. Sun, B., Hong, W., Yan, Z., Aziz, H. & Li, Y. Record High Electron Mobility of 6.3 $cm^2V^{-1}s^{-1}$ Achieved for Polymer Semiconductors Using a New Building Block. *Advanced Materials* **26,** 2636–2642 (2014).

12. Nawaz, A., Kumar, A. & Hümmelgen, I. A. Ultra-high mobility in defect-free poly(3-hexylthiophene-2,5-diyl) field-effect transistors through supra-molecular alignment. *Organic Electronics: physics, materials, applications* **51,** 94–102 (2017).

13. Zhang, F., Hu, Y., Schuettfort, T., Di, C. A., Gao, X., McNeill, C. R., Thomsen, L., Mannsfeld, S. C. B., Yuan, W., Sirringhaus, H. & Zhu, D. Critical role of alkyl chain branching of organic semiconductors in enabling solution-processed N-channel organic thin-film transistors with mobility of up to 3.50 $cm^2V^{-1}s^{-1}$. *Journal of the American Chemical Society* **135,** 2338–2349 (2013).

14. Duan, C., Willems, R. E. M., Van Franeker, J. J., Bruijnaers, B. J., Wienk, M. M. & Janssen, R. A. J. Effect of side chain length on the charge transport, morphology, and photovoltaic performance of conjugated polymers in bulk heterojunction solar cells. *Journal of Materials Chemistry A* **4,** 1855–1866 (2016).

15. Hu, Y., Cao, D. X., Lill, A. T., Jiang, L., Di, C. A., Gao, X., Sirringhaus, H. & Nguyen, T. Q. Effect of Alkyl-Chain Length on Charge Transport Properties of Organic Semiconductors and Organic Field-Effect Transistors. *Advanced Electronic Materials* **4,** 1–8 (2018).

16. Kang, I., Yun, H.-J., Chung, D. S., Kwon, S.-K. & Kim, Y.-H. Record High Hole Mobility in Polymer Semiconductors via Side-Chain Engineering. *Journal of the American Chemical Society* **135,** 14896–14899 (2013).

17. Lim, B., Sun, H. & Noh, Y.-Y. Highly soluble small-molecule organic semiconductor with trihexylsilyloxy side chain for high-performance organic field-effect transistors with mobility of up to 3.10 cm2 V−1 s−1. *Dyes and Pigments* **142,** 17–23 (2017).

18. Kminek, I., Vyprachticky, D., Kriz, J., Dybal, J. & Cimrova, V. Low-band gap Copolymers Containing Thienothiadazole Units: Synthesis, Optical, and Electrochemical properties. *Journal of Polymer Science: Part A: Polymer Chemistry* **48,** 2743–2756 (2010).

19. Výprachticky, D., Kmínek, I., Pavlačková, P. & Cimrová, V. Syntheses of fluorene/carbazole-thienothiadiazole copolymers for organic photovoltaics. في *ECS Transactions* **33,** 111–118 (2011).

20. Cimrová, V., Kmínek, I. & Výprachtický, D. Novel soluble fluorene-thienothiadiazole and fluorene-carbazole copolymers for optoelectronics. في *Macromolecular Symposia* **295,** 65–70 (2010).

21. Cimrová, V., Kmínek, I., Pavlačková, P. & Výprachtický, D. Low-band gap donor-acceptor copolymers containing thienothiadiazole units for photovoltaics. في *ECS Transactions* **33,** 119–127 (2011).

22. Cimrová, V., Kmínek, I., Výprachtický, D. & Pokorná, V. Short-time synthesis of poly[4,6-bis(3′-(2-ethylhexyl)thien-2′-yl)thieno[3,4-c][1,2,5]thiadiazole-alt-9,9-dioctylfluorene], its photophysical, electrochemical and photovoltaic properties. *Polymer (United Kingdom)* **59,** 298–304 (2015).

23. Cimrová, V., Kmínek, I., Pavlačková, P. & Výprachtický, D. Low-bandgap donor-acceptor copolymers with 4,6-bis(3′-(2-ethylhexyl) thien-2′-yl)thieno[3,4-c][1,2,5]thiadiazole: Synthesis, optical, electrochemical, and photovoltaic properties. *Journal of Polymer Science, Part A: Polymer Chemistry* **49,** 3426–3436 (2011).

24. Cimrová, V., Výprachtický, D., Kmínek, I., Dzhabarov, V. & Pokorná, V. Photophysical and electrochemical properties of novel luminescent and photoconductive copolymers. في *ECS Transactions* **58,** 15–30 (2014).

25. Choi, D., Chu, P.-H., McBride, M. & Reichmanis, E. Best Practices for Reporting Organic Field Effect Transistor Device Performance. *Chemistry of Materials* **27,** 4167–4168 (2015).

26. Jiang, Y., Guo, Y. & Liu, Y. Engineering of Amorphous Polymeric Insulators for Organic

Field-Effect Transistors. *Advanced Electronic Materials* **3,** 1700157 (2017).

27. Usluer, Ö., Kästner, C., Abbas, M., Ulbricht, C., Cimrova, V., Wild, A., Birckner, E., Tekin, N., Sariciftci, N. S., Hoppe, H., Rathgeber, S. & Egbe, D. A. M. Charge carrier mobility, photovoltaic, and electroluminescent properties of anthracene-based conjugated polymers bearing randomly distributed side chains. *Journal of Polymer Science, Part A: Polymer Chemistry* **50,** 3425–3436 (2012).

28. Gupta, D., Katiyar, M. & Gupta, D. Mobility estimation incorporating the effects of contact resistance and gate voltage dependent mobility in top contact organic thin film transistors. *Proceedings of ASID* 425–428 (2006).

29. Yin-Hua, Z., Zhong-Feng, Y., Wei-Cai, W., Hai-Jian, X., Shan-Peng, W. & Wen-Jing, T. Solvent and electric field dependence of the photocurrent generation in donor:acceptor blend system. *Chinese Physics* **16,** 2136–2141 (2007).

30. Facchetti, A. π-Conjugated polymers for organic electronics and photovoltaic cell applications. *Chemistry of Materials* **23,** 733–758 (2011).

31. Dikundwar, A. G., Dutta, G. K., Row, T. N. G. & Patil, S. Polymorphism in opto-electronic materials with a benzothiazole-fluorene core: A consequence of high conformational flexibility of π-conjugated backbone and alkyl side chains. *Crystal Growth and Design* **11,** 1615–1622 (2011).

32. Li, W., Hendriks, K. H., Furlan, A., Roelofs, W. S. C., Meskers, S. C. J., Wienk, M. M. & Janssen, R. A. J. Effect of the fibrillar microstructure on the efficiency of high molecular

weight diketopyrrolopyrrole-based polymer solar cells. *Advanced Materials* **26,** 1565–1570 (2014).

33. Bronstein, H., Chen, Z., Shahid Ashraf, R., Zhang, W., Du, J., Durrant, J. R., Shakya Tuladhar, P., Song, K., Watkins, S. E., Geerts, Y., Wienk, M. M., J Janssen, R. A., Anthopoulos, T., Sirringhaus, H., Heeney, M. & McCulloch, I. Thieno[3,2-b]thiophene-diketopyrrolopyrrole-containing polymers for high-performance organic field-effect transistors and organic photovoltaic devices. *Journal of the American Chemical Society* **133,** 3272–3275 (2011).

34. Noriega, R. Efficient charge transport in disordered conjugated polymer microstructures. *Macromolecular Rapid Communications* **39,** 1800096:1–9 (2018).

35. Holliday, S., Donaghey, J. E. & McCulloch, I. Advances in charge carrier mobilities of semiconducting polymers used in organic transistors. *Chemistry of Materials* **26,** 647–663 (2014).

36. Horowitz, G., Lang, P., Mottaghi, M. & Aubin, H. Extracting parameters from the current-voltage characteristics of organic field-effect transistors. *Advanced Functional Materials* **14,** 1069–1074 (2004).

37. Yu, F., Wu, S., Wang, X., Zhang, G., Lu, H. & Qiu, L. Flexible and low-voltage organic phototransistors. *RSC Advances* **7,** 11572–11577 (2017).

38. Majewski, L. A., Schroeder, R., Grell, M., Glarvey, P. A. & Turner, M. L. High capacitance organic field-effect transistors with modified gate insulator surface. *Journal of Applied*

Physics **96,** 5781–5787 (2004).

39. Yang, C., Shin, K., Yang, S. Y., Jeon, H., Choi, D., Chung, D. S. & Park, C. E. Low-voltage organic transistors on a polymer substrate with an aluminum foil gate fabricated by a laminating and electropolishing process. *Applied Physics Letters* **89,** 153508: 1–3 (2006).

40. Saito, S., Torii, K., Shimamoto, Y., Tsujikawa, S., Hamamura, H., Tonomura, O., Mine, T., Hisamoto, D., Onai, T., Yugami, J., Hiratani, M. & Kimura, S. Effects of remote-surface-roughness scattering on carrier mobility in field-effect-transistors with ultrathin gate dielectrics. *Applied Physics Letters* **84,** 1395–1397 (2004).

CHAPTER FIVE

Poly[N,N'-bis(dodecyl)perylene-3,4,9,10-tetracarboxylic diimide-1,7-diyl-alt-9-(heptadecan-9-yl)carbazole-2,7-diyl]: synthesis and characterization

Abstract

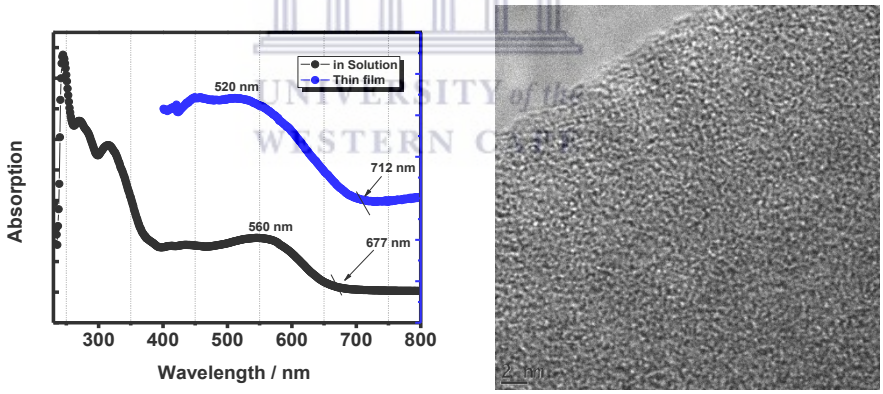

Graphical abstract: Absorption spectra of PDI-co-carbazole in solution and thin film (left) and HRTEM images of its thin film (right)

Poly[N,N'-bis(dodecyl)perylene-3,4,9,10-tetracarboxylic diimide-1,7-diyl-alt-9-(heptadecane-9-yl)carbazole-2,7-diyl] (PDI-co-Carbazole) was successfully prepared via Suzuki coupling

condensation reaction as confirmed by ^{1}H NMR and Fourier Transform IR spectroscopy, and exhibited good absorption properties in the visible spectral region. The amorphous morphology of the copolymer as shown by HRTEM images is as a result of the particle tendency to aggregate in liquid state as well as in thin films. The copolymer also exhibited good semiconducting properties with an optical band gap of 1.69 eV.

KEY WORDS: Band gap energy, carbazole, electron acceptor, perylene diimide.

5.1 Introduction

Bulk heterojunction (BHJ) active layers consisting of a blend of bi-continuous and interpenetrating electron donor (D) and electron acceptor(A) components in a bulk volume are typical solution-processed techniques currently used for the fabrication of cheap, environmentally-friendly and cost-effective organic photovoltaic cells (OPVs) on flexible large surface areas.[1] Dramatic increase in OPVs power conversion efficiency (PCE) to as high as 10% as reported in literature[2,3] can be attributed to the progress in these solution-processed BHJ OPVs. This continuous improvement enabled a better understanding of materials behavior and device fundamentals that include charge generation, separation, and transport; helped in improved control of materials structure and blend morphology. It has been noted that high record efficiencies in OPVs generally result from the design of new electron donor materials with improved properties such as better spectral absorption sensitivity, increased charge carrier mobility (hole transport) and appropriately tuned

HOMO/LUMO (highest occupied molecular orbital/lowest unoccupied molecular orbital) energy levels that correspond to those of well-known acceptors.[4] On the other hand, development of electron accepting materials has been lagging behind compared to the electron donating ones even though they are of the same importance in order to attain high performance OPVs. As electron acceptors, the materials should possess n-type semiconducting properties (basic properties): relatively low LUMO/HOMO energy levels and good inherent charge carrier mobility (electron transport ability).[5,6] To date, majority of the most successful solution-processed BHJ OPVs utilizes electron acceptor materials based on fullerenes and their derivatives, particularly 6,6-phenyl C_{61} butyric acid methyl ester ($PC_{61}BM$) and its C_{70}-based homologue ($PC_{71}BM$), thanks to their outstanding physical and electronic properties that include: (i) an increased electron affinity coupled to their high tendency to accept electrons from electron donating semiconductors; (ii) high charge carrier transport properties (electron mobility, μ_e) even when forming composites; (iii) their ease to form nanoscale interpenetrating networks with suitable donor materials; (iv) isotropy of charge transport; and (v) reversible electrochemical reduction.[1] Even though fullerene acceptors and derivatives are widely used, they present some important drawbacks.[7] For example, tuning the optical properties and electronic structures of fullerenes over a wide range of energy is difficult.[8–10] In addition, no general methods to allow for the enhancement of the absorption spectrum of the fullerene backbone in the visible and Near Infrared (NIR) regions have been established. Finally, the practical use of fullerenes and derivatives on a large scale is limited by their expensive cost.[11]

More emphasis has therefore been put on developing electron acceptors having totally different structures that will ascertain the good features of fullerenes while overcoming their insufficiencies, such as limited spectral breadth, weak visible light spectral absorption or and band gap tunability,

which are complex to achieve in fullerenes by chemical modification. Recent rapid development of electron-transporting materials with high performance for organic field-effect transistors (OFETs),[12–15] has triggered the interest of many researchers into exploring non-fullerene acceptors for solution-processed BHJ OPVs.[1,16,17] Introduction of electron-withdrawing building blocks has proved to be an effective and popular strategy for tailoring the properties of electron acceptors. Typical electron-withdrawing groups include cyano, perfluoroalkyl, carbonyl, imide or amide groups and their analogues. The addition of these electron-withdrawing units into π-conjugated semiconductors enables a decrease of the LUMO energy levels; indeed, as it is known, the π* energy level of the LUMO in a π-conjugated system is relatively close to that of the electron withdrawing unit. Therefore, the efficient mixing of these orbitals enables the stabilization of the LUMO energy. More and more interesting and novel electron-accepting materials, whether small or large molecules have been designed and synthesized for OPVs that were able to attain efficiencies of up to 6%.[1,18] The inability of non-fullerene electron-acceptors to fulfill their overall potential, is therefore justifying the continuous need for development of new electron-accepting materials. Among non-fullerene electron-acceptors that have been investigated, perylene diimide, a commercial dye, and its derivatives caught an important interest as alternative electron acceptors.[19,20,29,30,21–28] These materials exhibit good electron mobility in organic field-effect transistors, their molar absorptivity is high; also, they are easy to functionalize; and the starting materials are available commercially at affordable price.[7] In this chapter, I therefore report on the synthesis of a perylene-based donor-acceptor (D-A) copolymer in which the perylene backbone has been modified through substitution at the core positions by dodecyl groups; and attachment of a carbazole derivative at the bay-positions through Suzuki coupling.

5.2 Synthesis

5.2.1 Brominated 1,6- and 1,7- and 1,6,7- perylene-3,4,9,10-tetracarboxyic dianhydride

Bromination of perylene-3,4,9,10-tetracarboxyic dianhydride was confirmed by ^{1}H NMR spectroscopy analysis (600 MHz) in D_2SO_4 (98% H_2O). This spectroscopic result shows that there are three isomers 1,6, 1,7- and 1,6,7- present. In the region between 8.4 and 8.65 ppm three doublets are found; while the further upfield doublet is due to the coupling between neighboring H protons (C=CH-CH=C-C=O) in the 1,7- isomer, the other two doublets are from 1,6 and 1,6,7- isomers. Three singlets are found between 8.65 and 8.8 ppm. These bands are from the H protons that are isolated (C=CH-C-Br). Their polarization is different in the three isomers; as such, they have different chemical shifts. Further downfield, two doublets found between 9.25-9.50 ppm are due to the protons in (C=CH-CH=C-C=O) which are highly deshielded due to resonance effect of oxygen atom. This signals pattern confirms that 1,7- and 1,6-dibromoperylene bisanhydrides (1,7- and 1,6) and tri-brominated perylene 1,6,7- (Figure 5.1) were formed during the bromination of perylene bisanhydride. The integration areas of the doublets at 8.50, 8.55, and 8.58 ppm reveals that 1,7 and 1,6-PTCDA and the tri- 1,6,7-PTCDA are formed in a ratio of ca 70:15:15, respectively. The results obtained can be related to those reported in literature.[31]

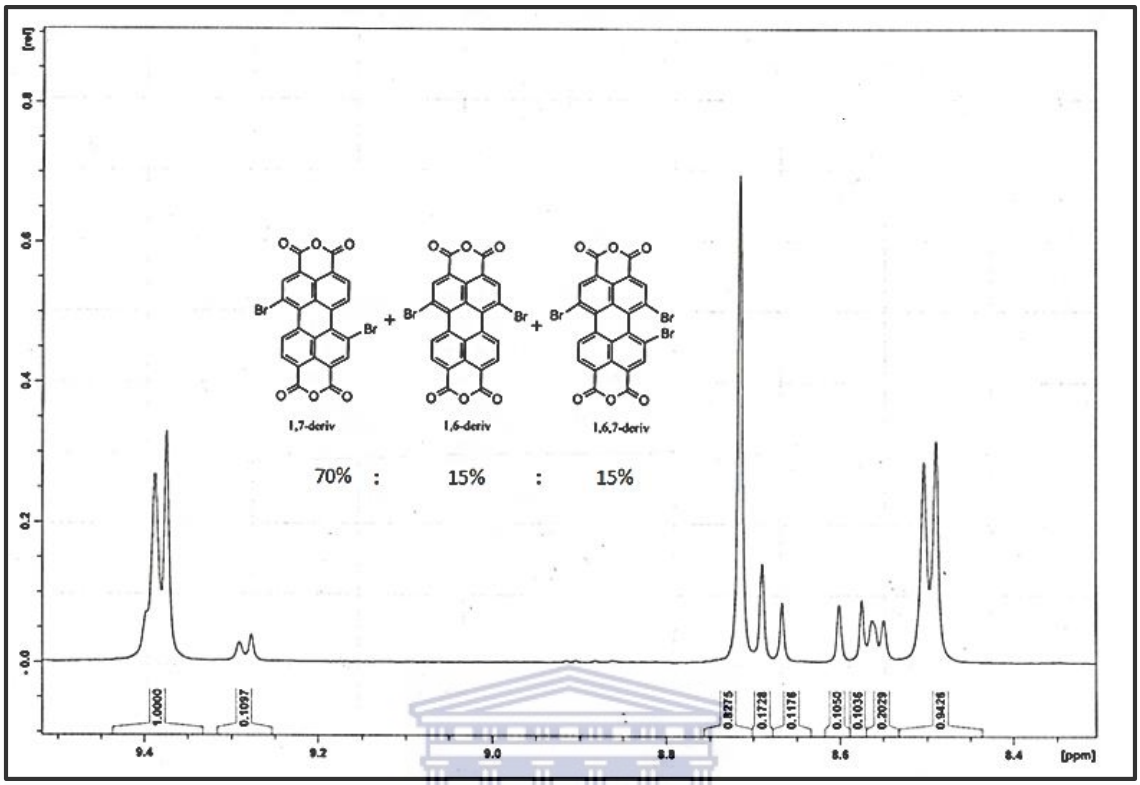

Figure 5.1 ^{1}H NMR of 1,7, 1,6-dibromo PTCDA and 1,6,7-tribromo PTCDA

5.2.2 N,N-bis(dodecyl)-1,7-dibromoperylene-3,4,9,10-tetracarboxylic diimide

Upon completion of imidization of brominated PTCDA, the material was subjected to ^{1}H NMR spectroscopy analysis (300 MHz) in $CDCl_3$ to confirm the imidized monomers were obtained. Bands characterizing the presence of methyl and methylene groups are observed. Chemical shifts, δ ppm 9.36-9.33 (d, 2H, perylene-H), 8.78 (s, 2H, perylene-H), 8.64–8.56 (d, 2H, perylene-H),

4.18 - 4.13 (m, 4H, $–CH_2–N$), 1.72–1.70 (m, 4H, alkyl-OCH_2-), 1.37–1.24 (m, 30H, alkyl-OCH_2-), 0.88–0.84 (m, 12H, alkyl-CH_3). Three other multiplet bands were found at δ ppm 3.42 – 3.38, 2.86 – 2.39 and 2.08-2.00. Results reveal that the three (3) isomers were successfully imidized (Figure 5.2).

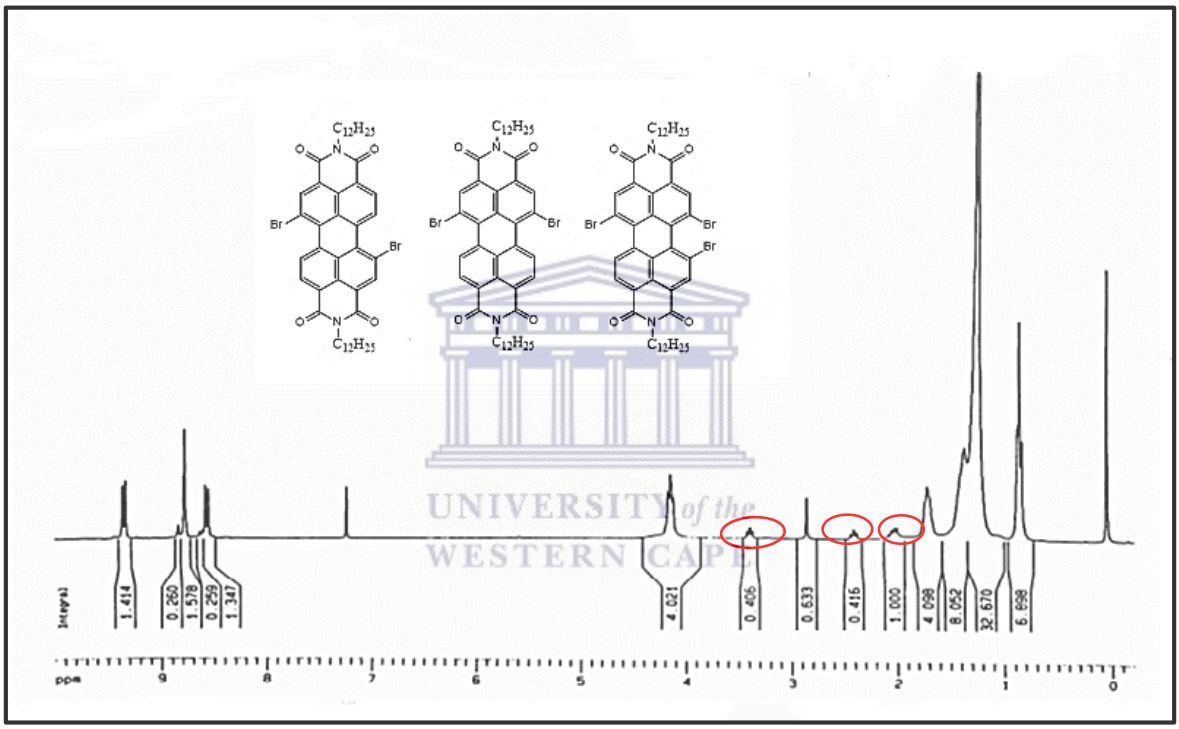

Figure 5.2 ^{1}H NMR of 1,7, 1,6-dibromo PDI and 1,6,7-tribromo PDI

The sample was then subjected to column chromatography to isolate 1,7-dibromoPDI. The purification/isolation was conducted in silica gel as stationery phase using a solvent system dichloromethane: hexane in a ratio 2:1. ^{1}H NMR spectroscopy (Figure 5.3) analysis (300 MHz) in

$CDCl_3$ was done to confirm the desired product.; δ ppm 9.39-9.37 (d, 2H, perylene-H), 8.82 (s, 2H, perylene-H), 8.62–8.59 (d, 2H, perylene-H), 4.19 - 4.14 (m, 4H, $–CH_2–N$), 1.73–1.67 (m, 4H, alkyl $-OCH_2-$), 1.37–1.24 (m, 30H, alkyl-OCH_2-), 0.88–0.83 (m, 12H, alkyl-CH_3). The obtained chemical shifts are in agreement with results reported in literature.[24,32]

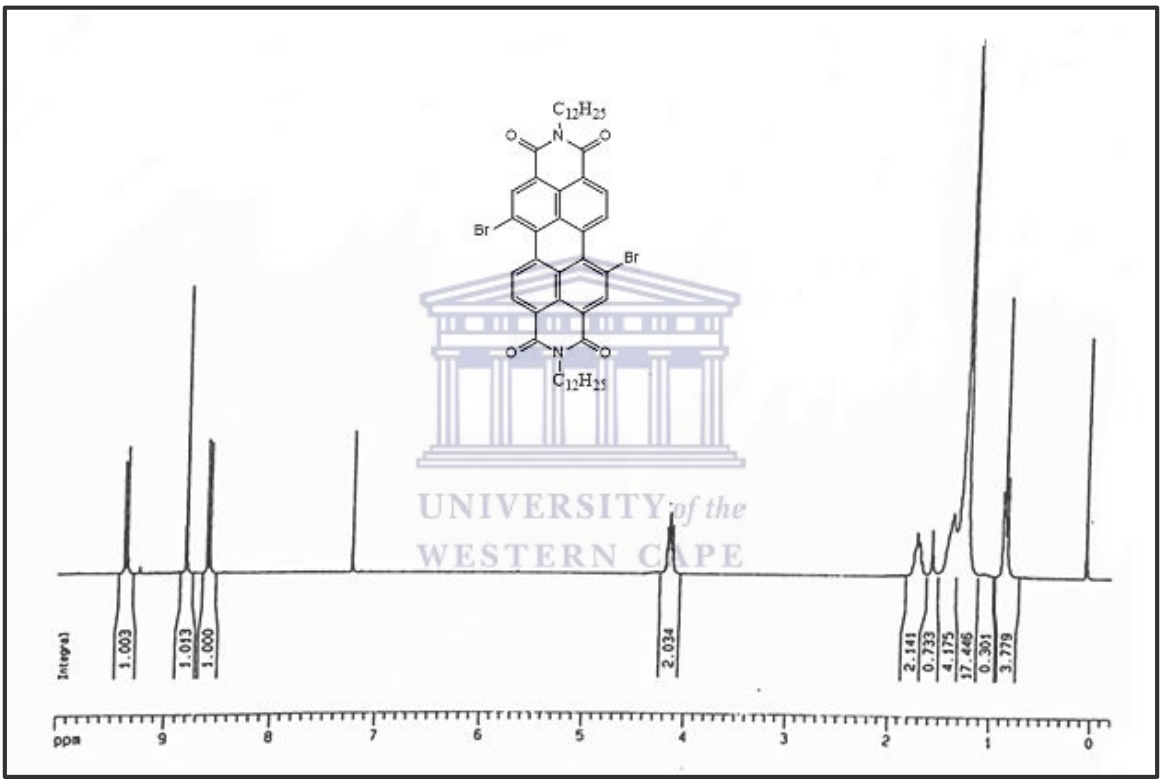

Figure 5.3 ^1H NMR of N,N-(bisdodecyl)-1,7-dibromoperylene-3,4,9,10-tetracarboxylic diimide (PDI-2Br)

5.3 Results and discussion

5.3.1 Nuclear Magnetic Resonance (NMR)

Poly[N,N'-bis(dodecyl)perylene-3,4,9,10-tetracarboxylic diimide-1,7-diyl-alt-9-(heptadecan-9-yl)carbazole-2,7-diyl] (PDI-co-Carbazole) ^{1}H NMR ($CDCl_3$, 400 MHz) was characterized by various chemical shifts δ(ppm): 8.79-8.77 (br, 2H), 8.17 (br, 2H) 7.98-7.96 (br, 4H), 7.78 (br, 2H), 7.50 (br, 2H), these broad bands are from the protons on the various aromatic rings; 6.99 (s, 5H), 4.53 (br, 1H), 4.15 (br, 4H), 3.71 (d, 8H), 2.28 (br, 1H) and 2.0-1.03 (m, 70 H), 0.84 (br, 18H). All these shifts assigned to the respective proton on the chemical structure of the copolymer, are found in Figure 5.4. The obtained chemical shifts can be related to the results obtained by Huo *et al*.[33]

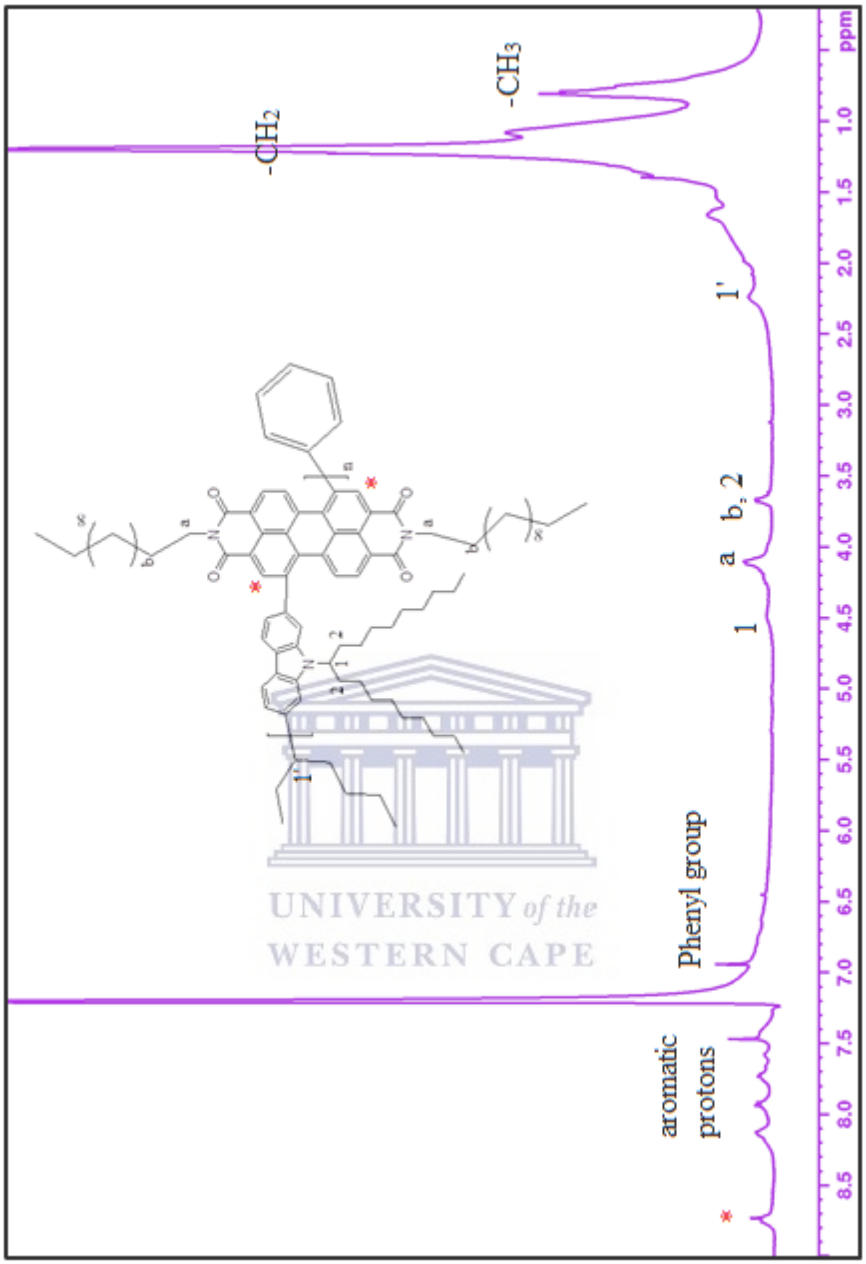

Figure 5.4 ^{1}H NMR of PDI-co-Carbazole

5.3.2 Fourier Transform Infrared spectroscopy

Figure 5.5 shows the infrared spectra of PDI-co-Carbazole with reference to carbazole and 1,7-dibromoPDI (PDI-2Br) as recorded using a PerkinElmer model Spectrum 100 series. It should be noted that this analysis was done in KBr pellets. The molecule vibrations characterizing the FTIR signals associated with the investigated polymer appear around, 2924-2854, 1714 - 1561, 1455, 1396, 1349, 1138, 1032, 850, and 750 cm^{-1}. The transmittance intensity of PDI-co-carbazole was very weak due to the low amount of material used; and as such the observed weak bands are relative to that small amount of material used. Vibrational band at 3071 cm-1 is suggested to be for the C- H on the aromatic ring.[34] Characteristic aliphatic -C-H stretching vibrations signals are observed in the region 2924 - 2854 cm^{-1}.[19] Around 1695 cm^{-1} is the vibrational stretching of C=O which was initially found at 1708 cm^{-1} in PDI-Br.[35] The spectrum shows a strong signal situated at 1455 cm^{-1}. This signal arises from the vibrational stretching of the unsaturated double bond within the conjugated aromatic rings (-C=C). The signals around 1396 cm^{-1} originate from the alkyl carbon-hydrogen vibrational bending (-C-H). At 1349 cm^{-1} is the vibrational stretching of -C-N bond while the quite intense signal at 750 cm^{-1} is suggested to be for the C- H phenyl substitution on the carbazole monomeric unit.[36] On the other hand, carbazole was characterized by many vibrational bands among which the strongest bands around 2950 cm^{-1} are due to the -C- H stretching in the heptadecanyl group attached to the N atom. PDI-2Br also displayed many vibrational modes among which are the stretching modes of C = C at 1432, 1466 cm^{-1}, C = O at 1708 cm^{-1} and the alkyl -C-H around 2924 – 2848 cm^{-1}.[34] All these data are summarized in Table 5.1 and in agreement with results obtained by Huo *et al*.[33]

Table 5.1 Vibrational modes in PDI-2Br, carbazole and PDI-co-Carbazole

Origin	**Group frequency / cm^{-1}**			**Vibrational mode**
	PDI-co-carbazole	**Carbazole**	**PDI-2Br**	
C-H	2924 - 2854	2924 - 2848	2924 - 2848	-C-H stretching
	1396	1261	1332	-C-H bending
	750	691	-	-C- H stretching, (phenyl substitution)
C=C	1455	1395	1390	-C=C stretching
C-N	1349	1344	1330	-C-N stretching
C=O	1695	-	1708	C = O stretching

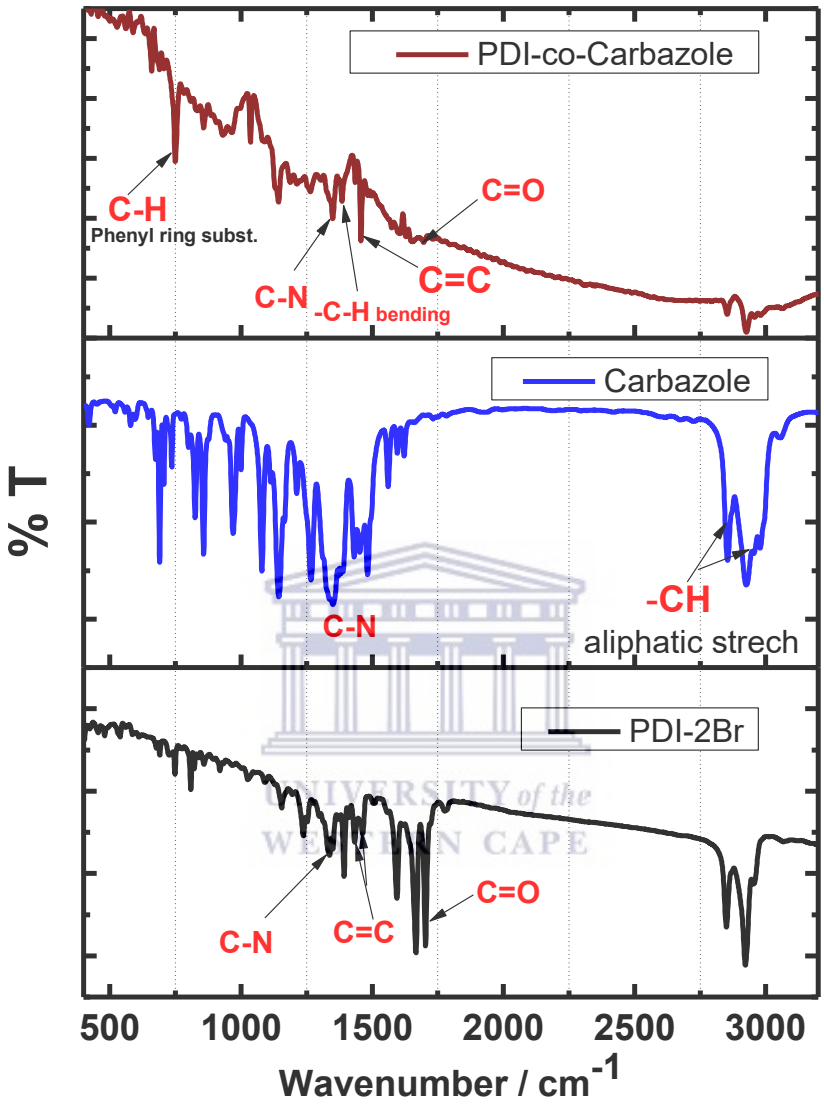

Figure 5.5 FTIR spectra of PDI-2Br, Carbazole and PDI-co-Carbazole with arrows marking the absorptions of functional group signals

5.3.3 Optical and photophysical studies

The photophysical properties of the D-A copolymer were studied by UV-Vis absorption and photoluminescence in chloroform or dichlorobenzene solution as well as in solid state. Results include the wavelength at the absorption maximum (λ_{max}), the onset absorption (λ_{onset}), the optical band gap energy (E_g^{opt}) calculated using the equation $1242/\lambda_{onset}$, the wavelength at the emission maximum (PL) as well as the Stokes' shift. All emission data were obtained by excitation at one or two wavelengths obtained in the main absorption spectrum.

5.3.3.1 UV-Vis spectroscopy

The absorption spectra of PDI-co-Carbazole have been recorded in solution from chloroform. (Figure 5.6) and in spin-coated thin films (Figure 5.7). All data are summarized in Table 5.2. The optical energy band gap (E_g^{opt}) value was calculated by determining the onset at the higher wavelength region. The electron donating group substitution at the bay region of the perylene diimide backbone resulted in a change of the optical characteristics of the PDI-2Br. Before copolymerization, PDI-2Br showed several absorption bands: two absorption maxima at 490 and 525 nm corresponding to S_0–S_1 transition with clear vibronic fine structure;[37] while the bands below 300 nm are due to the π – π* within the unsaturated aromatic ring.[32] Incorporation of

extended conjugated groups in the bay positions of PDI generally results in to bathochromical shift of the spectrum.[21] As such, the donor-acceptor copolymer, PDI-co-Carbazole, showed a red-shift to longer wavelength 580–680 nm with considerable peak broadening and low resolved vibronic fine structure due to the intramolecular transfer between the perylene diimide and the carbazole moieties.[38] In addition, the observed absorption bands at around 412 to 438 nm correspond to S_0–S_2 transition. Absorption maxima are observed at 244 and 271 nm due to the lowest π –π* electronic transition within the perylene or carbazole backbone.[39,40] The appearance of a new absorption band at 316 nm is suggested to be as a result of π – π* within the nitrogen containing ring in the carbazole moiety. The optical band gap, E_g^{opt} of liquid state PDI-co-carbazole was calculated to be 1.73 eV for an onset absorption at 720 nm, while it is found to be 1.9 eV in solid state. Similar E_g^{opt} was previously reported by Huo *et al.*, for a perylene-co-carbazole polymer denoted PPDIC in which the carbazole monomeric unit was 2- ethylhexylcarbazole-3,6-diyl.[33] On the hand, the shift in absorption maximum to shorter wavelength from 560 to 520 nm in PDI-co-Carbazole film is assumed to be due to H-aggregation that could be associated with factors such as twisting or deplanarization.[17]

Table 5.2 Optical data of PDI-co-carbazole in solution and in thin film

PDI-co-carbazole	**λ_{abs} (nm)**	**λ_{onset} (nm)**	**E_g^{opt} *(eV)***
In solution	244, 271, 316, 412,438,560	720	1.73
Thin film	455, 520	737	1.69

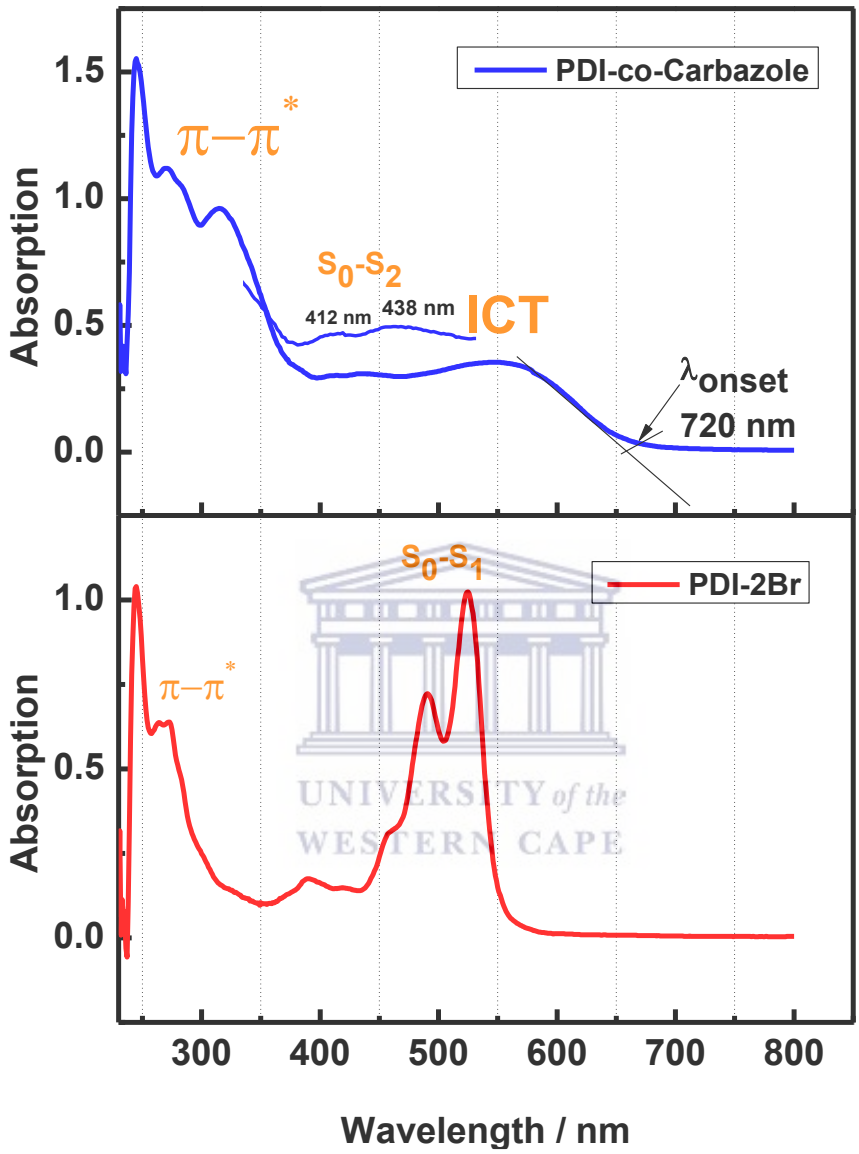

Figure 5.6 UV-Vis absorption of PDI-2Br and PDI-co-Carbazole in solution

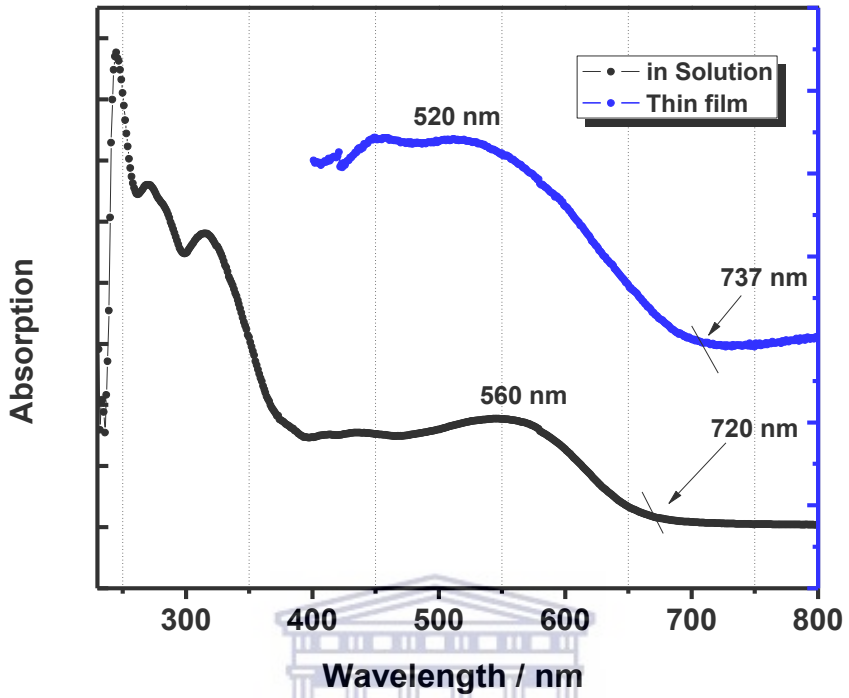

Figure 5.7 UV-Vis absorption of PDI-co-Carbazole film and in solution

5.3.3.2 Photoluminescence studies of PDI-co-Carbazole

PDI-co-Carbazole exhibited intense photoluminescence in solution upon excitation at wavelengths 316 nm and 560 nm. Figure 5.8 shows PL emission spectrum measured in dichlorobenzene solution using Horiba NanoLog™ - TRIAX (USA). Upon excitation at 316 nm, the emission spectrum exhibited five distinct emission bands 1' to 5'at 400, 503, 545, 633 and 665 nm,

respectively. A clear red-shift of all emission peaks with respect to their inherent absorption bands is observed. Excitation of electrons within the absorption broad peak 4 with maximum 560 nm resulted in two emission peaks 4' and 4'' at two different wavelengths 633 and 665 nm suggesting that the broad absorption band results from the overlapping and conjugation of the absorption of chromophores whose electrons get excited to different electronic states; as such when excited at 316 nm, the wavelengths at which those electrons emit are distinguishable. On the other hand, when the same electrons are excited at 560 nm, relaxation of the electrons only occur at 665 nm. This finding coupled to the Stokes' shifts between 73 and 125 nm therefore, confirm photo-induced intramolecular within the copolymer; but such large Stokes' shift could also be characteristics of aggregates or excimers in solid state.[41,42] Also, the emission in the longer wavelength region as compared to PDI-2Br is mainly due to the combination of intramolecular charge transfer (ICT) from electron-donating substituents to the electron-deficient perylene diimide core along with effective π-conjugation.[32]

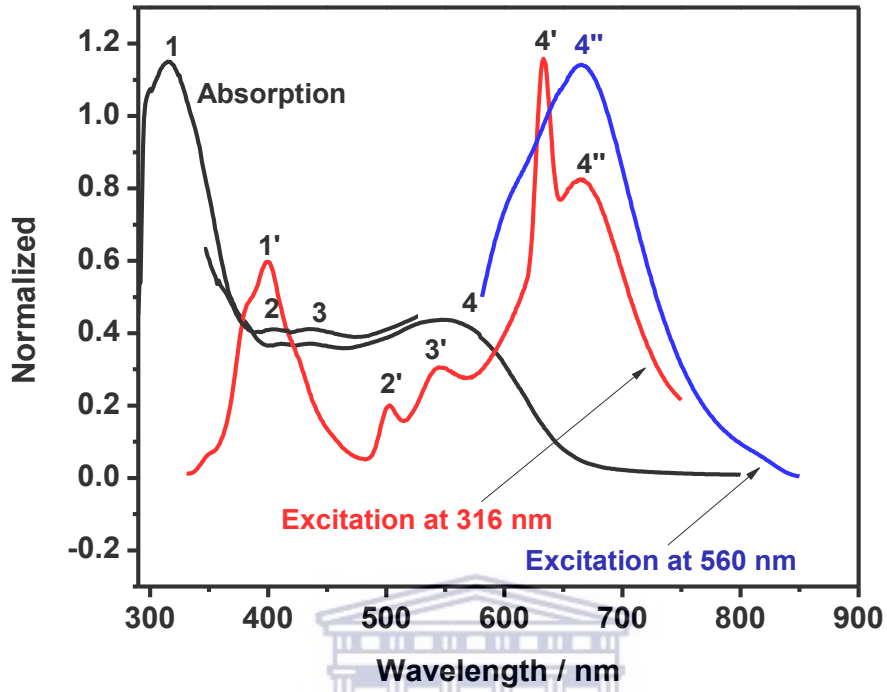

Figure 5.8 Photoluminescence of PDI-co-Carbazole in solution

5.3.4 Electrochemical studies

All electrochemical studies were carried out on a Pt disk in 0.1M Bu_4NPF_6 in acetonitrile at scan rate 50 mV/s using a three-electrode system where the counter electrode is a Pt wire and the reference electrode is Ag/Ag^+ ($AgNO_3$ in acetonitrile) electrode.

5.3.4.1 Cyclic Voltammetry (CV) And Square Wave Voltammetry (SWV)

Cyclic voltammetry (CV) was used to determine the electronic structure of PDI-co-Carbazole. Potential was applied to a thin film of PDI-co-Carbazole on a platinum electrode in acetonitrile solution of 0.1 M Bu_4NPF_6 (Bu = butyl) versus ferrocene at a scan rate of 50 mV/s. Representative CV curve of the thin copolymer film coated onto Pt disk electrode is displayed in Figure 5.9. The copolymer exhibited electrochemical quasi-reversible redox reactions. Two oxido-reduction couples were identified ip_{a1}, ip_{c1} with potential peaks at -1.06 and -1.54 V, respectively and ip_{a2}, ipc_2 with peak potentials at -1.75 and -1.88 V, respectively. Obtained data can be found in Table 5.3 which also include peak current values. The electronic properties were thus derived from these cyclic voltammograms. The ionization potential (HOMO level), E_{IP}, and electron affinity (LUMO level), E_A, were estimated from the onset potentials, E_{onset}, from the first oxidation and reduction peaks based on the reference energy level of ferrocene (4.8 eV below the vacuum level) using the equations below:

$$E_{\mathrm{A}}, LUMO = -e\left(E_{\mathrm{onset}}^{\mathrm{red}} - E_{\mathrm{ferr}}\right)V - 4.8\ eV| \qquad \text{(Equation 5.1)}$$

$$E_{\mathrm{IP}}, HOMO = -e(E_{\mathrm{onset}}^{\mathrm{ox}} - E_{\mathrm{ferr}})V - 4.8\ eV| \qquad \text{(Equation 5.2)}$$

$$E_g^{ec} = |E_{IP} - E_A|\ eV \qquad \text{(Equation 5.3)}$$

where, E_{ferr} = -0.03 V is the value for ferrocene vs. the Ag/Ag^+ electrode.

The E_{IP} and E_A were found to be 5.87 and 3.87 eV, respectively giving rise to an electrochemical band gap E_g^{ec} = 1.50 eV which is lower than to the optical band gap E_g^{opt} = 1.72 eV calculated from the absorption wavelength onset. The LUMO energy level as determined by CV was -3.87 eV, close to that of PCBM (-4.1 eV), indicating that the designed copolymer is a potential n-type polymer material for fabrication of a PSC.[33] The redox peaks obtained were ascertained by forward and reverse scans using square wave voltammetry technique (Figure 5.10).

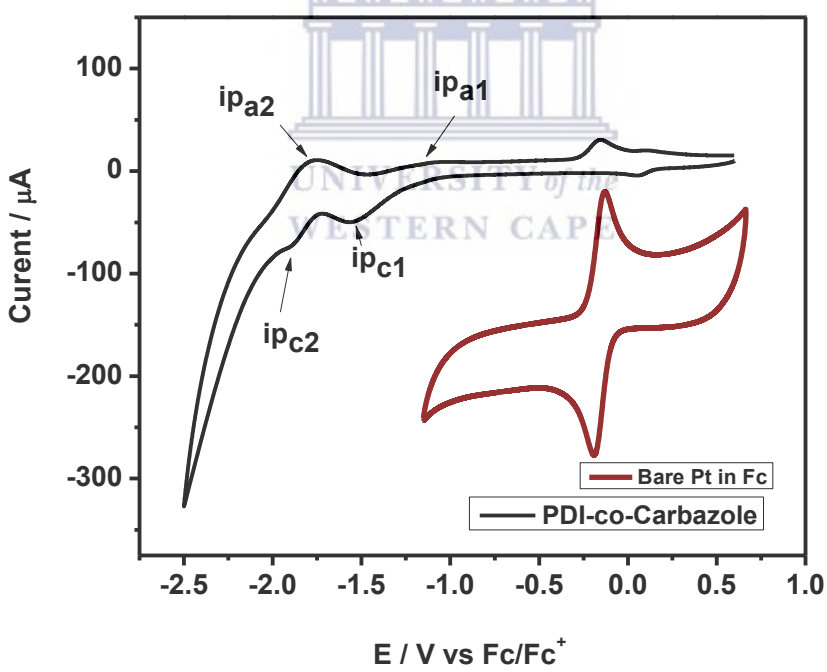

Figure 5.9 Cyclic voltammogram of PDI-co-Carbazole thin film on Pt electrode 0.1 M Bu_4NPF_6 in acetonitrile at scan rate 50 mV/s versus ferrocene in Ag/Ag^+ reference electrode

Table 5.3 Summary of redox potentials and peak currents for PDI-co-Carbazole

Materials	Ox^1	Red^1	E_1^o	Ox^2	Red^2	E_2^o
Potential (V)	-1.06	-1.54	-1.30	-1.79	-1.88	-1.84
|Ip| (µA)	9.26	47	-	10.9	72.7	-

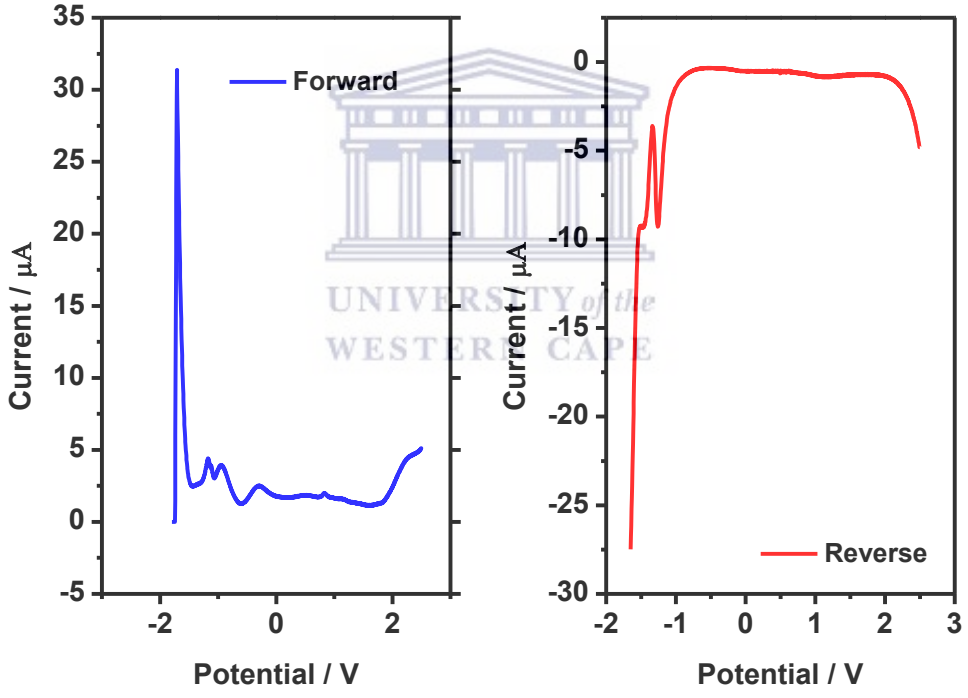

Figure 5.10 Forward and reverse square wave voltammograms of PDI-co-Carbazole in 0.1M Bu_4NPF_6 in acetonitrile at scan rate 50 mV/s

Table 5.4 HOMO, LUMO and band gap E_g^{ec} energy levels of PDI-co-Carbazole

Materials	E_{onset}^{ox1} **(V)**	E_{onset}^{red1} **(V)**	E_{IP} **(-E_{HOMO}) (eV)**	E_A **(-E_{LUMO}) (eV)**	E_g^{ec} **(eV)**	E_g^{opt} **(eV)**
PDI-co-Carbazole	0.54	-0.96	5.37	3.87	1.5	1.72

5.3.4.2 Electrochemical Impedance Spectroscopy (EIS)

Electrochemical impedance spectroscopy technique was used to determine the semi-conductive properties of the copolymer. A formal potential, E^o = -1.30 V was applied to PDI-co-Carbazole film in 0.1M Bu_4NPF_6 (acetonitrile) in 1-10^5 Hz frequency range. The material exhibited good semiconducting properties as confirmed by the obtained phase angle of ca. 60 degree (Figure 5.11). The copolymer was further investigated by varying the applied potentials and it is found that decreasing the applied potential, decrease the semi-conductive properties whereas increasing the applied potential increase this property (Figure 5.12).

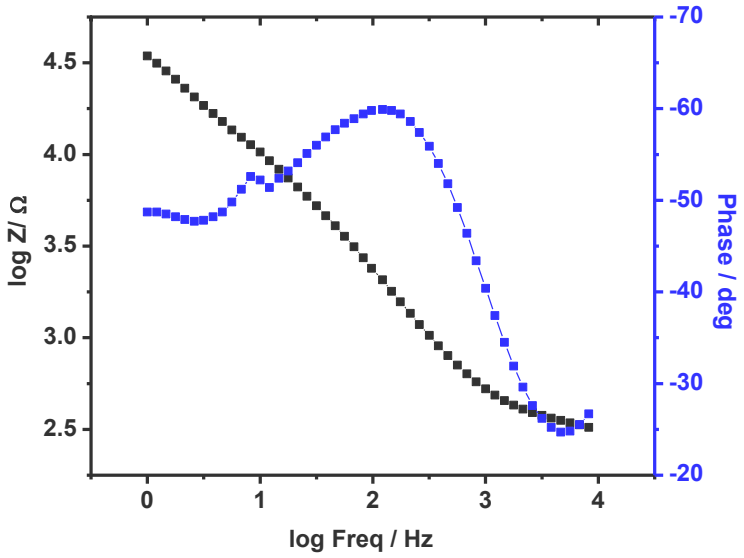

Figure 5.11 Bode plot of PDI-co-Carbazole in 0.1M Bu_4NPF_6 (acetonitrile) at -1.30 V

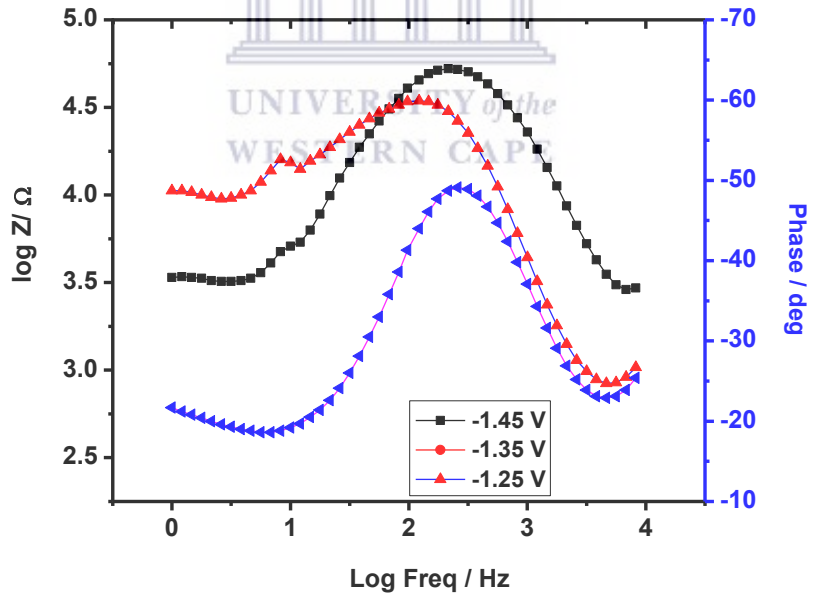

Figure 5.12 Bode plots of PDI-co-Carbazole in 0.1M Bu_4NPF_6 (acetonitrile) at different formal potentials

5.3.5 Morphological and particle size investigation of PDI-co-Carbazole

5.3.5.1 High-Resolution Transmission Electron Microscopy (HRTEM)

Morphological investigation of the copolymer was conducted using HRTEM. The results depicted on the images in Figure 5.13 represent the morphology of PDI-co-Carbazole thin film casted from chloroform. As it can be seen, PDI-co-Carbazole presents a rough with coarse (aggregate) phase demonstrating the amorphous nature of this copolymer which was confirmed by the SAED (Selected Area Electron Diffraction) images that do not show any crystallinity compared to Carbazole and PDI-2Br which showed some polycrystalline nature in their HRSEM images as confirmed by their SAED images which were characterized by more defined rings with white dots representing the crystal lattices. (Figure 5.14 and 5.15). Such results were predictable if we consider the obtained optical and photophysical results.

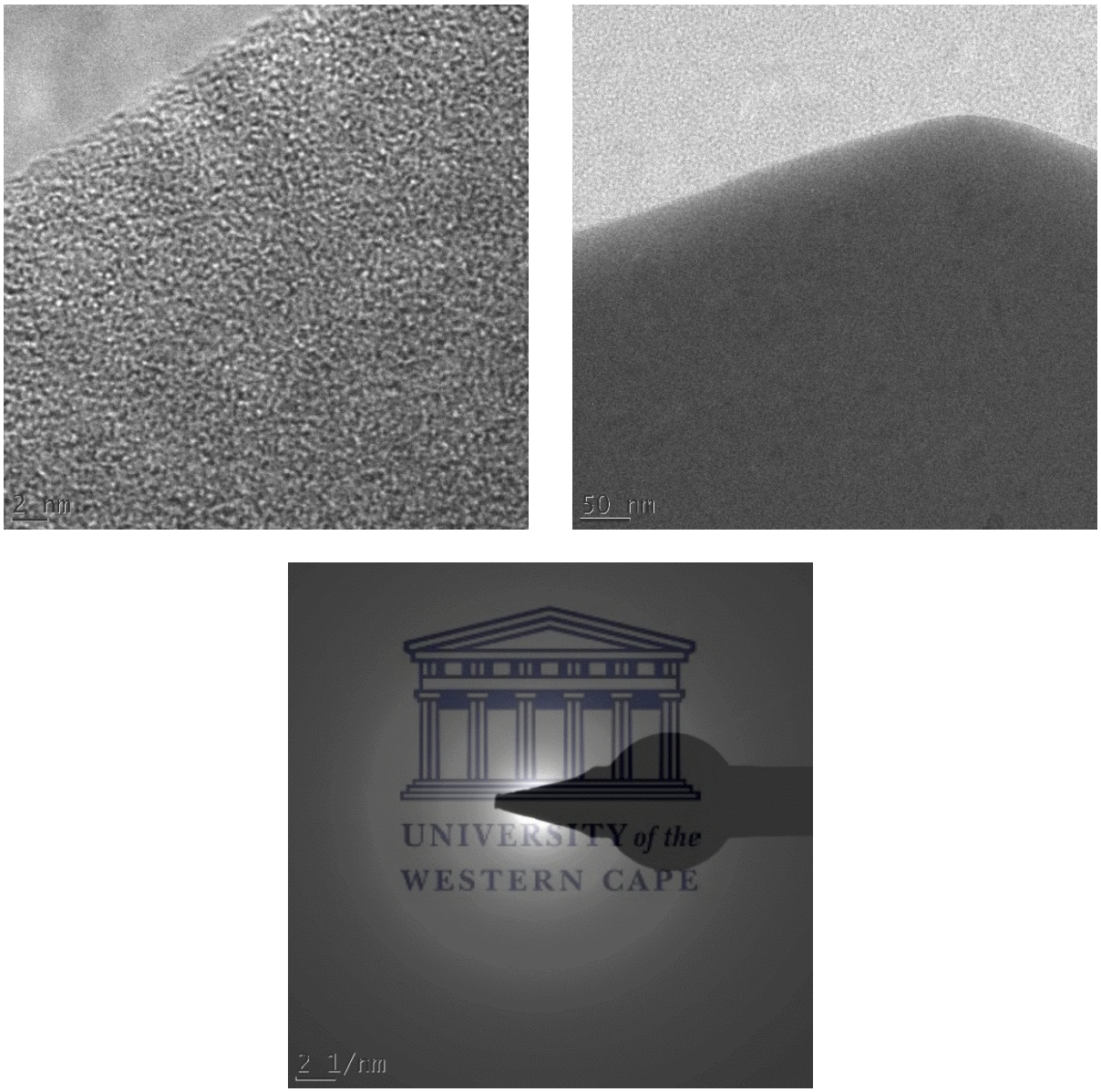

Figure 5.13 HRSEM and SAED images of PDI-co-Carbazole

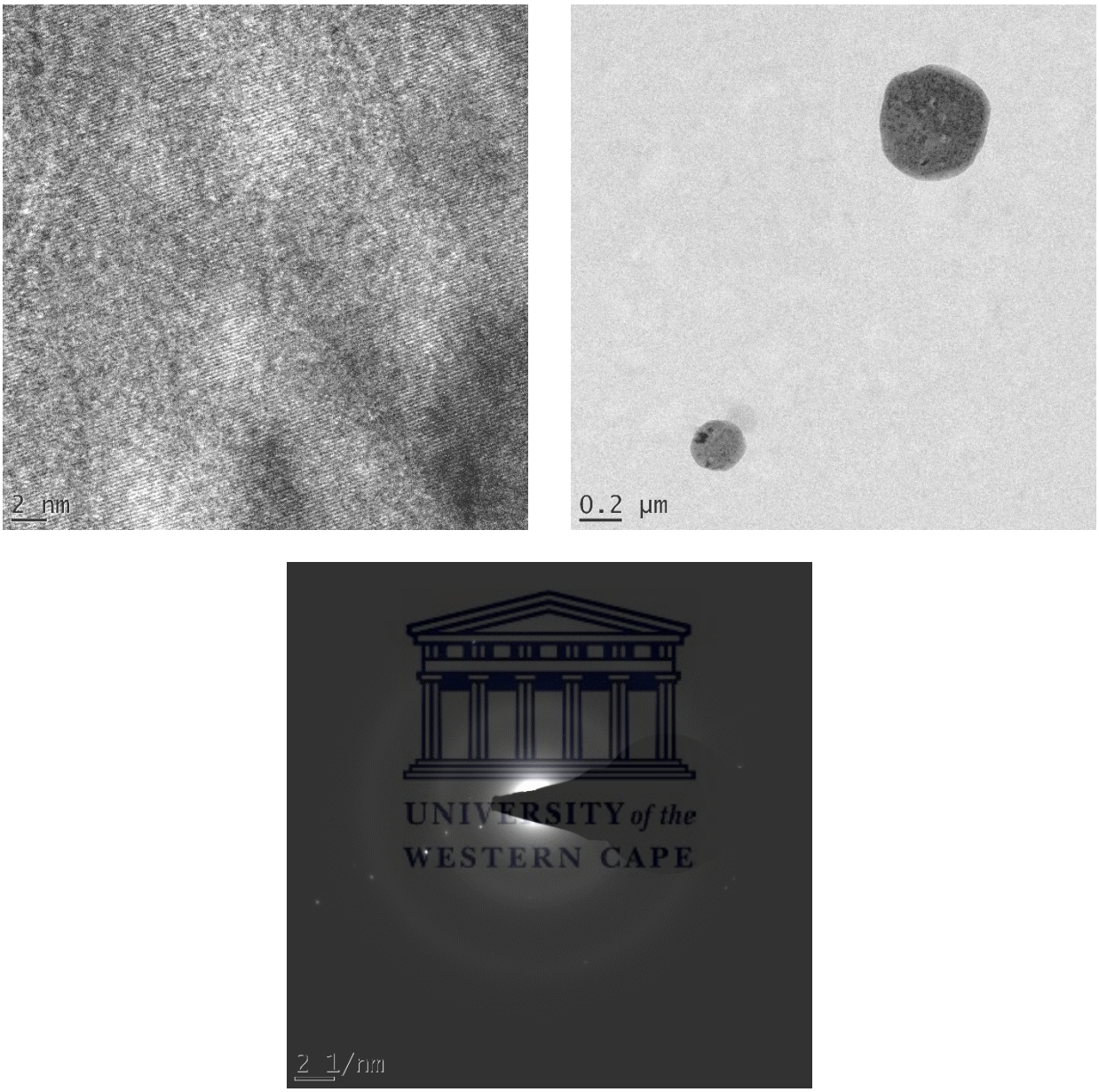

Figure 5.14 HRSEM and SAED images of Carbazole

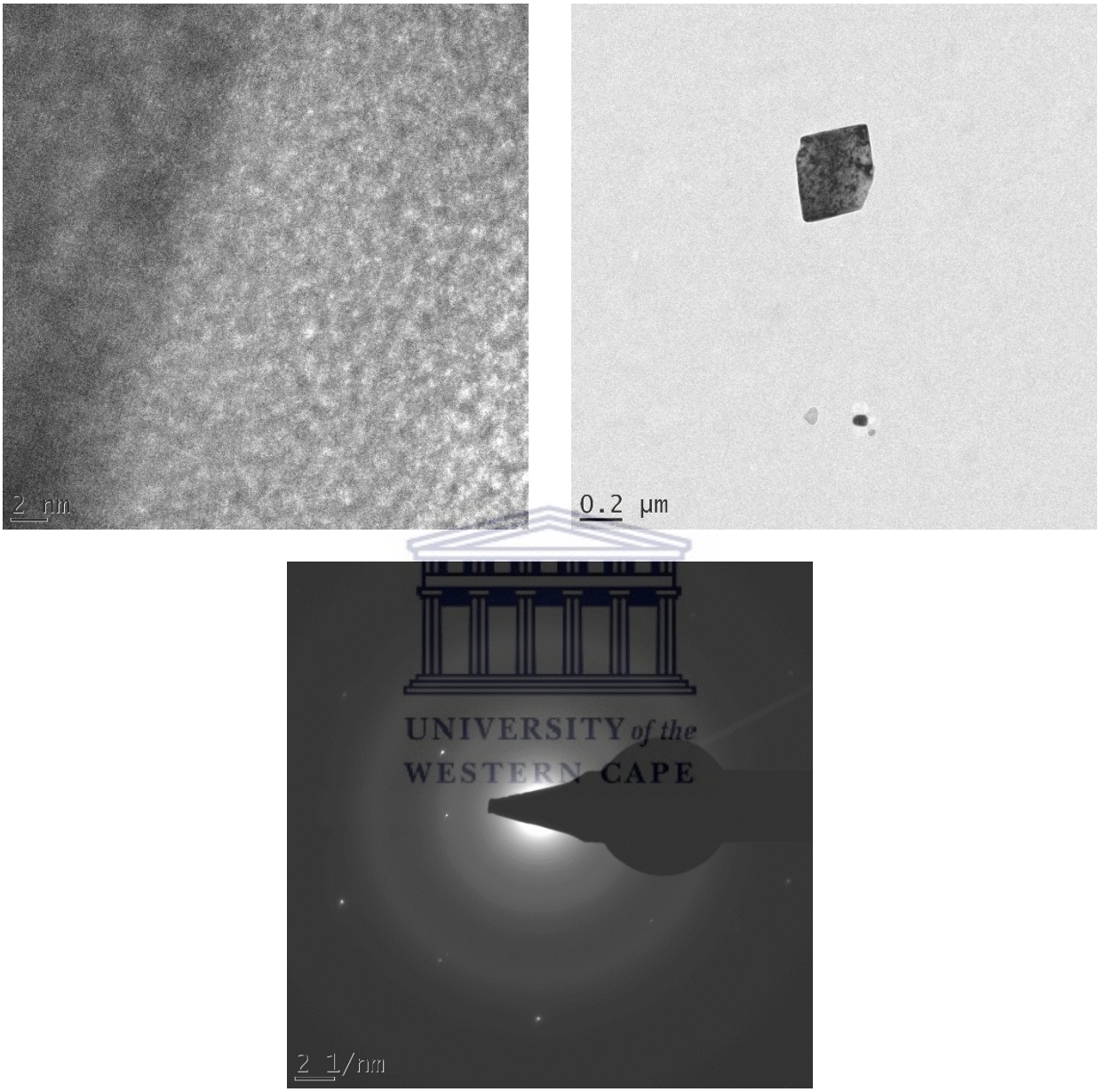

Figure 5.15 HRSEM and SAED images of PDI-2Br

5.3.5.2 Small-Angle X-ray Scattering (SAXS) analysis

Particle size investigation using SAXS analysis, a method used to determine the structure of particle systems in terms of averaged particle sizes or shapes, allowed to ascertain the shape and size of the prepared material. Indeed, the coarse morphology of PDI-co-Carbazole as observed on HRTEM images were confirmed by the shape of the graph of the free model, pair-distance distribution function (Figure 5.16). Indeed, the two consecutive peaks at 60 and 87 nm that proves of the aggregates shape of the particles.[43] The pair distance distribution functions of the nanoparticles in number-weighted particle size distributions are shown in Figure 5.17 with the volume-weighted particle size distribution as the inset. The scattering cross sections describe nanoparticles in the range of 1– 22 nm and 60 – 90 nm with a larger portion of the nanoparticles at 12 nm for the number-weighted distribution The volume-weighted particle size distribution shows the population of particles seen by their volume. It is commonly known that larger particles are "more seen" than the smaller particles[44] but here particles around 12 nm are more seen than those around 73 nm.

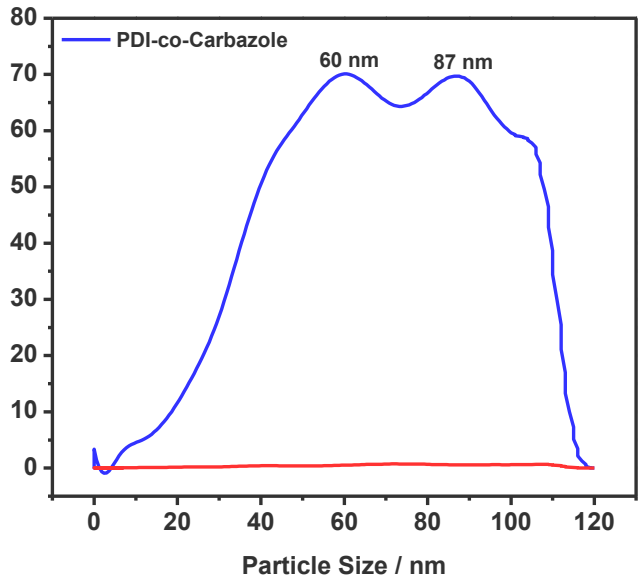

Figure 5.16 Pair-distance distribution function of PDI-co-Carbazole

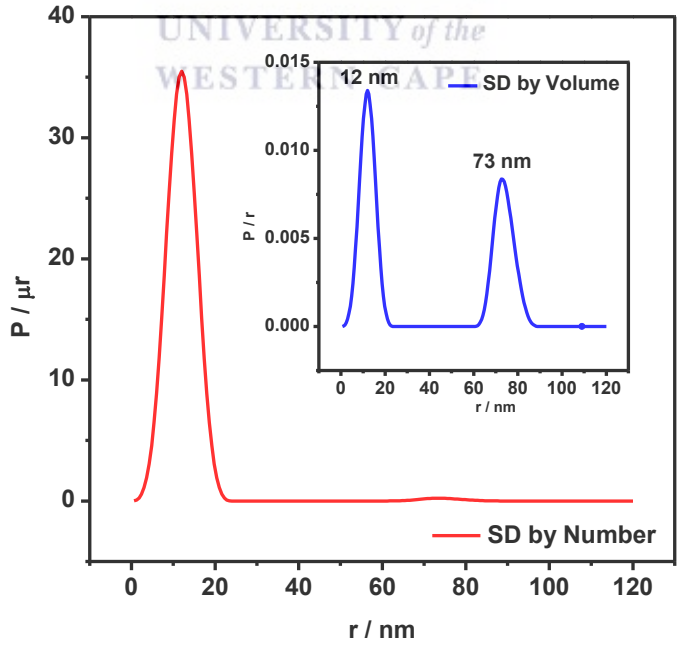

Figure 5.17 SAXS particle size distribution: by number and volume.

5.4 Conclusion

Poly[N,N'-bis(dodecyl)perylene-3,4,9,10-tetracarboxylic diimide-1,7-diyl-alt-9-(heptadecane-9-yl)carbazole-2,7-diyl] (PDI-co-Carbazole) with particle size in the ranges 1-22 nm and 60-90 nm was successfully synthesized. The copolymer exhibited good absorption properties in the UV-Vis region with an absorption onset shift to longer wavelength in thin film thereby decreasing the band gap energy to 1.69 eV. Photo-induced intramolecular charge transfer (ICT) which could be associated with the high- lying HOMO of the donor unit and the low-lying LUMO of the acceptor unit can also account for the reduced optical band gap. The decrease in thin film absorption maxima observed compared to co-monomer PDI-2Br, suggests that there is an aggregation in the solid-state. The LUMO energy level as determined by cyclic voltammetry of -3.87 eV, close to that of PCBM (-4.1 eV), indicates that the designed copolymer is a potential n-type polymer material for fabrication of an all-PSC.

References

1. Lin, Y. & Zhan, X. Non-fullerene acceptors for organic photovoltaics: An emerging horizon. *Materials Horizons* **1,** 470–488 (2014).

2. Chen, C. C., Chang, W. H., Yoshimura, K., Ohya, K., You, J., Gao, J., Hong, Z. & Yang, Y. An efficient triple-junction polymer solar cell having a power conversion efficiency exceeding 11%. *Advanced Materials* **26,** 5670–5677 (2014).

3. Liu, Y., Zhao, J., Li, Z., Mu, C., Ma, W., Hu, H., Jiang, K., Lin, H., Ade, H. & Yan, H. Aggregation and morphology control enables multiple cases of high-efficiency polymer solar cells. *Nature Communications* **5,** (2014).

4. Cheng, Y.-J., Yang, S.-H. & Hsu, C.-S. Synthesis of Conjugated Polymers for Organic Solar Cell Applications. *Chemical Reviews* **109,** 5868–5923 (2009).

5. Anthony, J. E., Facchetti, A., Heeney, M., Marder, S. R. & Zhan, X. N-Type organic semiconductors in organic electronics. *Advanced Materials* **22,** 3876–3892 (2010).

6. Zhao, X. & Zhan, X. Electron transporting semiconducting polymers in organic electronics. *Chemical Society Reviews* **40,** 3728 (2011).

7. Zhong, Y., Trinh, M. T., Chen, R. S., Wang, W., Khlyabich, P. P., Kumar, B., Xu, Q. Z., Nam, C. Y., Sfeir, M. Y., Black, C., Steigerwald, M. L., Loo, Y. L., Xiao, S. X., Ng, F., Zhu, X. Y. & Nuckolls, C. Efficient Organic Solar Cells with Helical Perylene Diimide Electron Acceptors. *Journal of the American Chemical Society* **136,** 15215–15221 (2014).

8. Lenes, M., Shelton, S. W., Sieval, A. B., Kronholm, D. F., Hummelen, J. C. & Blom, P. W. M. Electron trapping in higher adduct fullerene-based solar cells. *Advanced Functional Materials* **19,** 3002–3007 (2009).

9. Ross, R. B., Cardona, C. M., Guldi, D. M., Sankaranarayanan, S. G., Reese, M. O., Kopidakis, N., Peet, J., Walker, B., Bazan, G. C., Van Keuren, E., Holloway, B. C. & Drees, M. Endohedral fullerenes for organic photovoltaic devices. *Nature Materials* **8,** 208–212 (2009).

10. He, Y., Chen, H. Y., Hou, J. & Li, Y. Indene - C60 bisadduct: A new acceptor for high-performance polymer solar cells. *Journal of the American Chemical Society* **132,** 1377–1382 (2010).

11. Anctil, A., Babbitt, C. W., Raffaelle, R. P. & Landi, B. J. Material and energy intensity of fullerene production. *Environmental Science and Technology* **45,** 2353–2359 (2011).

12. Lim, B., Sun, H. & Noh, Y.-Y. Highly soluble small-molecule organic semiconductor with trihexylsilyloxy side chain for high-performance organic field-effect transistors with mobility of up to 3.10 cm2 V−1 s−1. *Dyes and Pigments* **142,** 17–23 (2017).

13. Cameron, J., Nanson, L., Blouin, N., Findlay, N. J., Inigo, A. R. & Skabara, P. J. Solution-processable 2,1,3-benzothiadiazole containing compound based on the novel 1-dodecyl-6-dodecoxynaphthyridine-2-one unit for organic field-effect transistors. *Organic Electronics: physics, materials, applications* **49,** 400–405 (2017).

14. Liang, N., Jiang, W., Hou, J. & Wang, Z. New developments in non-fullerene small molecule acceptors for polymer solar cells. *Materials Chemistry Frontiers* **1,** 1291–1303

(2017).

15. Choi, J., Kim, K. H., Yu, H., Lee, C., Kang, H., Song, I., Kim, Y., Oh, J. H. & Kim, B. J. Importance of Electron Transport Ability in Naphthalene Diimide-Based Polymer Acceptors for High-Performance, Additive-Free, All-Polymer Solar Cells. *Chemistry of Materials* **27,** 5230–5237 (2015).

16. Hwang, Y. J., Earmme, T., Courtright, B. A. E., Eberle, F. N. & Jenekhe, S. A. n-Type Semiconducting Naphthalene Diimide-Perylene Diimide Copolymers: Controlling Crystallinity, Blend Morphology, and Compatibility Toward High-Performance All-Polymer Solar Cells. *Journal of the American Chemical Society* **137,** 4424–4434 (2015).

17. Yang, J., Xiao, B., Tajima, K., Nakano, M., Takimiya, K., Tang, A. & Zhou, E. Comparison among Perylene Diimide (PDI), Naphthalene Diimide (NDI), and Naphthodithiophene Diimide (NDTI) Based n-Type Polymers for All-Polymer Solar Cells Application. *Macromolecules* **50,** 3179–3185 (2017).

18. Lin, Y., Li, Y. & Zhan, X. Small molecule semiconductors for high-efficiency organic photovoltaics. *Chemical Society Reviews* **41,** 4245–4272 (2012).

19. Mikroyannidis, J. A., Stylianakis, M. M., Sharma, G. D., Balraju, P. & Roy, M. S. A novel alternating phenylenevinylene copolymer with perylene bisimide units: Synthesis, photophysical, electrochemical, and photovoltaic properties. *Journal of Physical Chemistry C* **113,** 7904–7912 (2009).

20. Yuan, M. C., Su, M. H., Chiu, M. Y. & Wei, K. H. Synthesis and characterization of donor-bridge-acceptor alternating copolymers containing perylene diimide units and their

application to photovoltaic cells. *Journal of Polymer Science, Part A: Polymer Chemistry* **48,** 1298–1309 (2010).

21. Huang, C., Barlow, S. & Marder, S. R. Perylene-3,4,9,10-tetracarboxylic acid diimides: synthesis, physical properties, and use in organic electronics. *The Journal of Organic Chemistry* **76,** 2386–2407 (2011).

22. Nakabayashi, K., Takeuchi, Y. & Mori, H. Perylene bisimide-based donoracceptor materials incorporating oligothiophenes: Synthesis, characterization, thin-film properties, and nanomorphology. *Bulletin of the Chemical Society of Japan* **89,** 1063–1068 (2016).

23. Li, J., Dierschke, F., Wu, J., Grimsdale, A. C. & Müllen, K. Poly(2,7-carbazole) and perylene tetracarboxydiimide: A promising donor/acceptor pair for polymer solar cells. *Journal of Materials Chemistry* **16,** 96–100 (2006).

24. Do, J. Y., Kim, B. G., Kwon, J. Y., Shin, W. S., Jin, S. H. & Kim, Y. I. Soluble asymmetric perylene derivatives for organic solar cells. *Macromolecular Symposia* **249–250,** 461–465 (2007).

25. Kozma, E. & Catellani, M. Perylene diimides based materials for organic solar cells. *Dyes and Pigments* **98,** 160–179 (2013).

26. Sharenko, A., Gehrig, D., Laquai, F. & Nguyen, T. Q. The effect of solvent additive on the charge generation and photovoltaic performance of a solution-processed small molecule: Perylene diimide bulk heterojunction solar cell. *Chemistry of Materials* **26,** 4109–4118 (2014).

27. Zhi, C. & Dai, L. *Flexible energy conversion and storage devices*. (Wiley-VCH, 2018).

28. Fechtenko, A., Mu, K., Moons, E., Friend, R. H. & Mackenzie, J. D. Self-Organized Discotic Liquid Crystals for High-Ef ciency Organic Photovoltaics. *Science* **293,** 1119–1122 (2001).

29. Schmidt-Mende, L., Fechtenkötter, A., Müllen, K., Moons, E., Friend, R. H. & MacKenzie, J. D. Self-Organized Discotic Liquid Crystals for High-Efficiency Organic Photovoltaics. *Science* **293,** 1119–1122 (2001).

30. Tan, Z., Zhou, E., Zhan, X., Wang, X., Li, Y., Barlow, S. & Marder, S. R. Efficient all-polymer solar cells based on blend of tris(thienylenevinylene)-substituted polythiophene and poly[perylene diimide-alt-bis(dithienothiophene)]. *Applied Physics Letters* **93,** 173302: 1–1 (2008).

31. Würthner, F., Stepanenko, V., Chen, Z., Saha-Möller, C. R., Kocher, N. & Stalke, D. Preparation and characterization of regioisomerically pure 1,7-disubstituted perylene bisimide dyes. *Journal of Organic Chemistry* **69,** 7933–7939 (2004).

32. Vajiravelu, S., Ramunas, L., Juozas Vidas, G., Valentas, G., Vygintas, J. & Valiyaveettil, S. Effect of substituents on the electron transport properties of bay substituted perylene diimide derivatives. *Journal of Materials Chemistry* **19,** 4268–4275 (2009).

33. Huo, E. F., Zou, Y., Sun, H. Q., Bai, J. L., Huang, Y., Lu, Z. Y., Liu, Y., Jiang, Q. & Zhao, S. L. Synthesis and characterization of n-type conjugated copolymers bearing perylene diimide moieties. *Polymer Bulletin* **67,** 843–857 (2011).

34. Pakseresht, M., Bodapati, J. B. & Icil, H. A New π-conjugated 1,7-diphenoxy-perylene bisimide: Synthesis, characterization, photophysical and electrochemical properties. *Journal of Photochemistry and Photobiology A: Chemistry* **360,** 270–277 (2018).

35. Asir, S., Demir, A. S. & Icil, H. The synthesis of novel, unsymmetrically substituted, chiral naphthalene and perylene diimides: Photophysical, electrochemical, chiroptical and intramolecular charge transfer properties. *Dyes and Pigments* **84,** 1–13 (2010).

36. Mushtaq, A., Bin Mukhtar, H. & Mohd Shariff, A. FTIR Study of Enhanced Polymeric Blend Membrane with Amines. *Research Journal of Applied Sciences, Engineering and Technology* **7,** 1811–1820 (2014).

37. Zhao, L., Ma, T., Bai, H., Lu, G., Li, C. & Shi, G. Layer-by-layer deposited multilayer films of oligo(pyrenebutyric acid) and a perylene diimide derivative: Structure and photovoltaic properties. *Langmuir* **24,** 4380–4387 (2008).

38. Cimrová, V., Pokorná, V. & Výprachtický, D. Effects of alkyl or alkyloxy side chains in poly[4,6-bis(3′-dodecylthien-2′-yl)thieno-[3,4- c][1,2,5]thiadiazole-5′,5′-diyl- alt -2,5-di(alkyl or alkyloxy)-1,4-phenylene]: Synthesis, photophysics, and spectroelectrochemical and photovoltaic properties. *Polymer* **118,** 180–191 (2017).

39. Kozma, E., Kotowski, D., Catellani, M., Luzzati, S., Cavazzini, M., Bossi, A., Orlandi, S. & Bertini, F. Design of perylene diimides for organic solar cell: Effect of molecular steric hindrance and extended conjugation. *Materials Chemistry and Physics* **163,** 152–160 (2015).

40. Meena, S., Mohammad, T., Dutta, V. & Jacob, J. Design and synthesis of N-substituted

perylene diimide based low band gap polymers for organic solar cell applications. *RSC Advances* **8,** 30468–30480 (2018).

41. Cimrová, V., Výprachtický, D., Kmínek, I., Dzhabarov, V. & Pokorná, V. Photophysical and electrochemical properties of novel luminescent and photoconductive copolymers. في *ECS Transactions* **58,** 15–30 (2014).

42. Bouguerra, N., Ruìšžička, A., Ulbricht, C., Enengl, C., Enengl, S., Pokorná, V., Výprachtický, D., Tordin, E., Aitout, R., Cimrová, V. & Egbe, D. A. M. Synthesis and Photophysical and Electroluminescent Properties of Poly(1,4-phenylene-ethynylene)-alt-poly(1,4-phenylene-vinylene)s with Various Dissymmetric Substitution of Alkoxy Side Chains. *Macromolecules* **49,** 455–464 (2016).

43. Schnablegger, H. & Singh, Y. The SAXS Guide. (*Anton Paar GmbH*, 2013).

44. Ndipingwi, M. M, Ikpo, C. O., Hlongwa, N. W., Dywili, N., Djoumessi Yonkeu, A. L. & Iwuoha, E. I. Crystal chemistry and lithium-ion intercalation properties of lithium manganese silicate cathode for aqueous rechargeable Li-ion batteries. *Journal of Applied Electrochemistry* (2019). https://doi.org/10.1007/s10800-019-01296-0

CHAPTER SIX

Photophysical and electroanalytical investigation of highly crystalline chemically prepared poly(propylene thiophenoimine)-co-poly(3-hexylthiophene) star-copolymer

Abstract

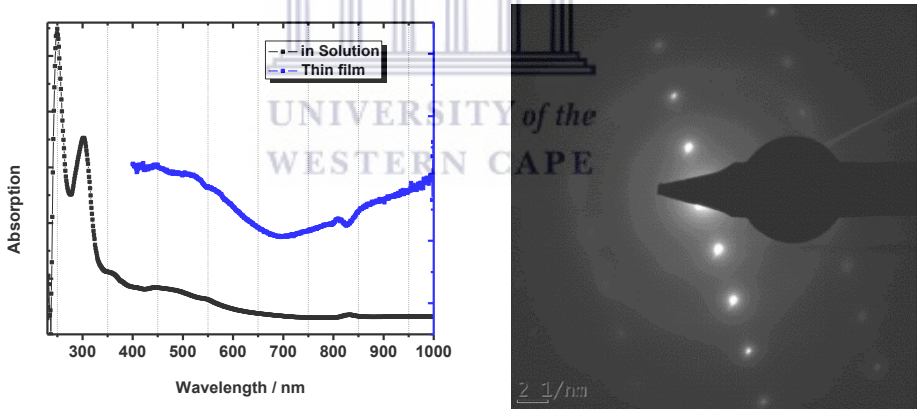

Graphical abstract: Absorption spectra of G1PPT-co-P3HT in solution and thin film (left) and HRTEM images of the thin film (right)

Highly crystalline generation 1 poly(propylene thiophenoimine)-co-poly(3-hexylthiophene) was prepared via simple oxidation reaction procedure. The prepared star copolymer spectroscopic

analyses showed that the macromolecule morphology is based on the mixed 'regioregular-regiorandom' nature of the poly(3-hexylthiophene) component of the material that accounts for the molecular ordering in G1PPT-co-P3HT structure. The copolymer is also characterized by good absorption properties in the UV-Vis into NIR spectral region with an optical bang gap as low as 1.43 eV. Conjugation of these properties, in addition to the highly electron-donating capability of the prepared material qualifies G1PPT-co-P3HT as a new type of donor polymer for optoelectronic devices in general and organic photovoltaics in particular.

KEY WORDS: Band gap energy, crystalline, dendritic star-copolymer, electron donor, semiconductor.

6.1 Introduction

The past recent years have seen an increasing number of investigations in organic bulk heterojunction solar cells (OBHJ) centered around the development of new materials[1] resulting in a rapid expansion of the field with numerous compounds being produced at a tremendously fast rate.[2–5] Four main categories can be distinguished when considering the different materials that have been designed, developed and/or investigated namely: conjugated polymers, dendrimers, oligomers, and small dye molecules.[6]

'Dendrimers' form a very interesting class of molecules[7,8] which have shown good applicability in organic optoelectronic applications.[9] Similarly to polymers, they consist of smaller repeating subunits, with the difference that instead of generating linear chains, the subunit grows out in a well-defined pattern (branches) from a main point. The synthesis of dendrimers have been reported to achieve (macro)molecules with high regularity and controlled molecular weight via either convergent or divergent methods;[10] therefore generating non-linear and covalent structures of this class of polymers that can be accurately controlled and inducing a broad range of studies.[8] Within 'dendrimers' group, π-conjugated dendrimers have been extensively investigated in organic light-emitting diodes and have shown to be efficient charge transporters mainly due to the high-quality films formed by the dendrimers.[11] They have also demonstrated good potential applications in organic photovoltaic devices (OPVs), organic field-effect transistors (OFETs), and non-linear photonics.[12] The strong co-facial π-π interactions within these molecules allow for a high degree of molecular ordering. The monodisperse nature of dendrimers help their film morphology, which in turn provide them with a potential advantage over polymers.[13] Indeed, polymers suffer from the difficulty of achieving low polydispersity index during their synthesis which is a big drawback during device fabrication as the charge carrier transport (mobility) within macromolecules strongly depends on their molecular weight.[14,15] The purification of these materials is easily achieved through simple processes such as column chromatography. These shape-persistent macromolecular materials with defined monodisperse structures therefore encompass the advantages of increased molecular weight of polymers with the chemical defined structures of oligomers.[16] Elements typically found in the structures of π-conjugated dendrimers include phenylenes,[17] phenylene-ethynylenes,[18,19],phenylene-vinylenes[20,21] carbazoles,[22–24] truxenes[25,26]

and thiophenes.[27–29] Among all materials, thiophene-based polymers, especially alkylated-polythiophenes exhibit excellent charge transport properties.[30] Poly-3-hexylthiophene (P3HT) specifically have been identified as the best electron-donating material due to its regioregularity, that leads to better crystallinity and higher the charge-carrier mobility;[31] and extensively studied for OPV applications.[15,31–33] This chapter, therefore focuses on the development and characterization of a star-copolymer consisting of generation1 poly(propylene thiophenoimine) and poly(3-hexylthiophene) as a new electron-donating material for OPVs.

6.2 Synthesis

6.2.1 Generation 1 poly(propylene thiophenoimine) (G1PPT)

Functionalization of generation 1 Poly(propyleneimine) tetramine dendrimer that produces generation 1 poly(propylene thiophenoimine), G1PPT was confirmed by ^{1}H NMR spectroscopy analysis (400 MHz) in $CDCl_3$ and the chemical shifts were compared to those found in the starting materials generation 1 poly(propyleneimine) tetramine and 2-thiophene carbaldehyde. Generation 1 poly(propyleneimine) tetramine was characterized by the following chemical shifts δ (ppm) 2.68-2.64 (t, 4H), 2.41-2.32 (2t, 16H), 1.57-1.49 (m, 12 H) and 1.33 (s, 8H) (Figure 6.1). On the other hand, 2-thiophene carbaldehyde had three (3) main bands at 9.92 (s, H), 7.77-7.74 (m, 2H) and 7.25-7.18(m, 1H) (see Figure 6.2). G1PPT on the other hand, showed a combination of the bands found in both starting materials with the difference that the chemical shifts of the dendrimer

moiety are deshielded by the attachment of thiophene ring and the formation of an imine group, -N=CH whose proton appears at 8.31. Furthermore, formation of this new bond results in a shielding effect of the thiophene protons b and d which appeared as a multiplet in 2-thiophene carbaldehyde have been splitted with proton-d appearing more downfield than proton-b (Figure 6.3)

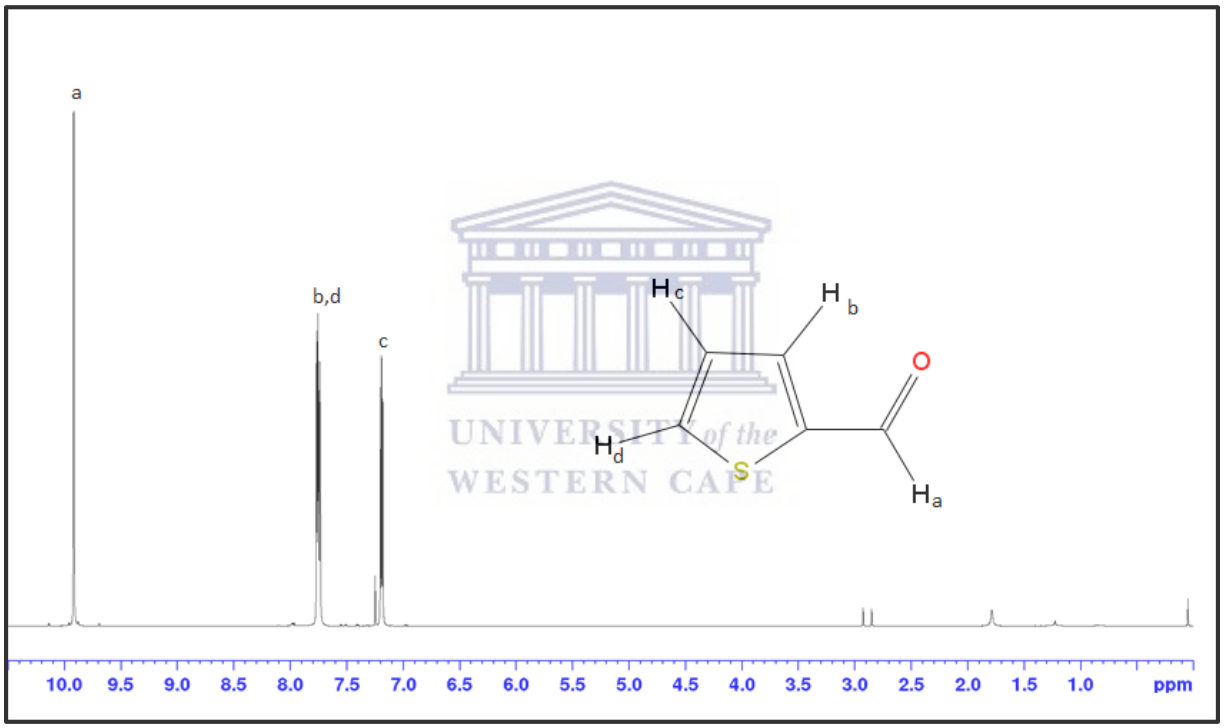

Figure 6.1 ^{1}H NMR of 2-thiophene carbaldehyde

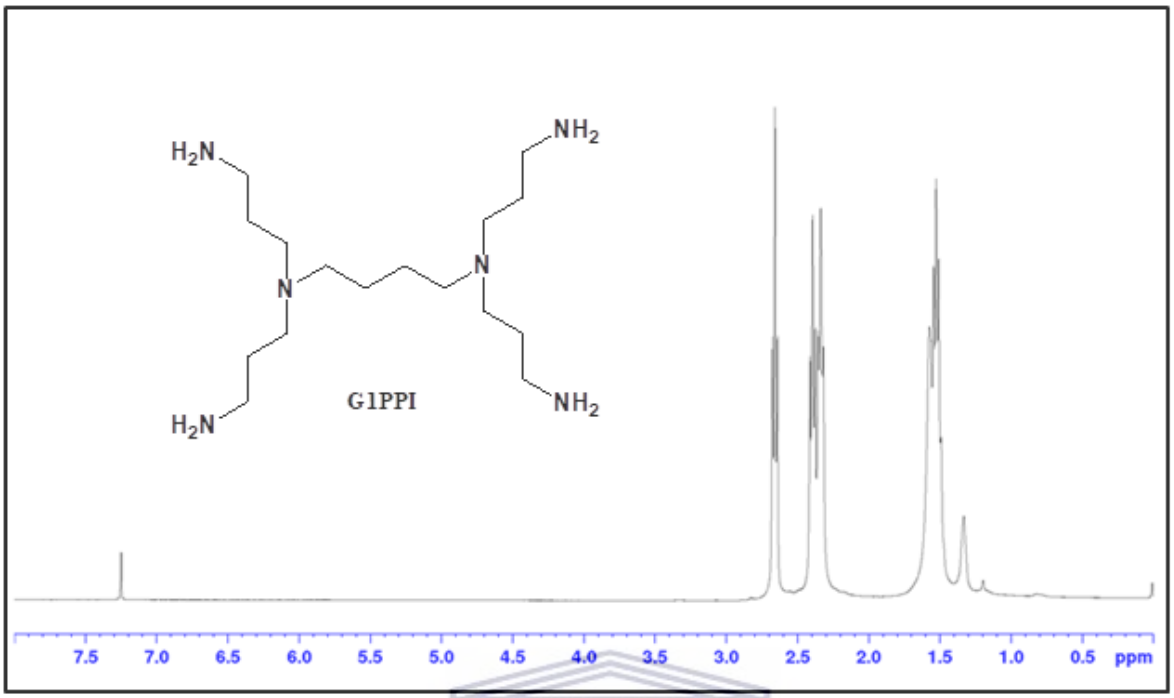

Figure 6.2 ^{1}H NMR of generation 1 poly(propyleneimine) tetramine

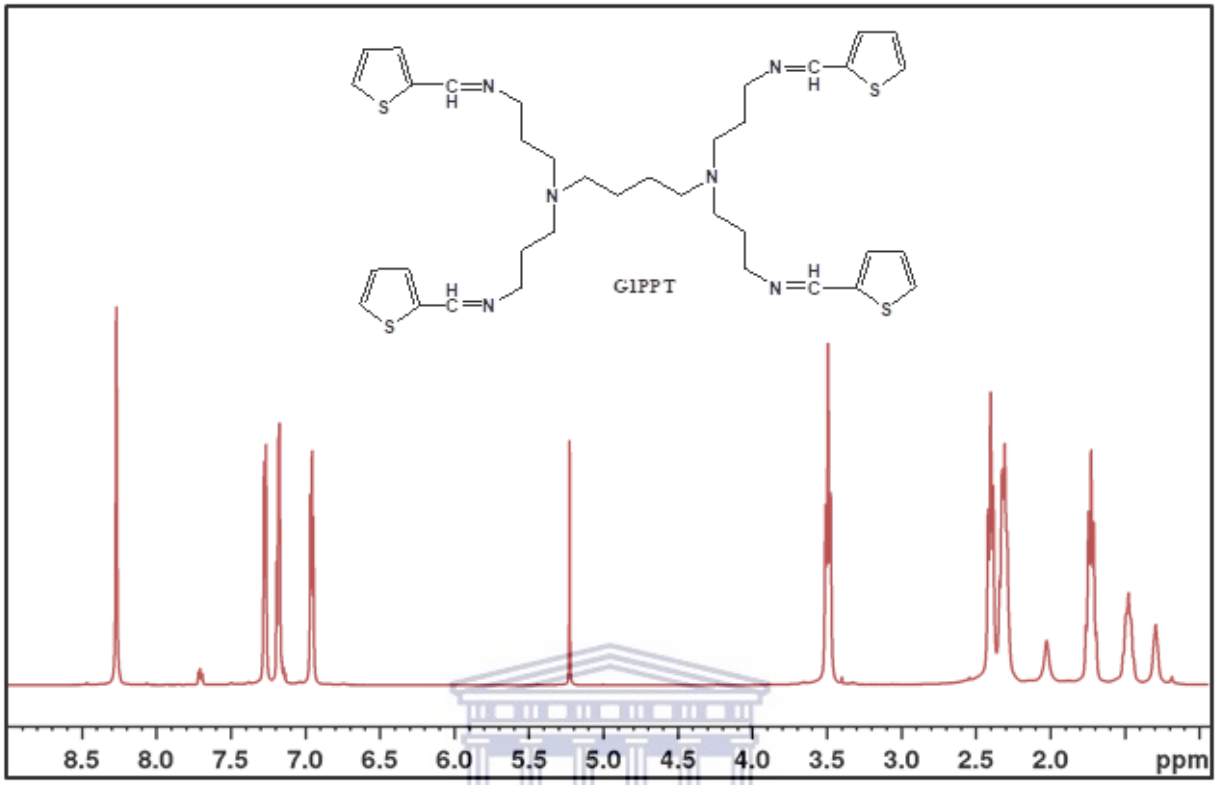

Figure 6.3 ^{1}H NMR of generation 1 poly(propylene thiophenoimine)

(Intense peak at 5.28 pm is due to CH_3OH)

6.3 Results and discussion

6.3.1 Nuclear Magnetic Resonance (NMR) and molecular weight determination.

^{1}H NMR ($CDCl_3$, 400 MHz) spectroscopy technique was used to ascertain the structure and purity of star-copolymer poly(propylene thiophenoimine)-co-poly(3-hexylthiophene) (G1PPT-co-P3HT). New signals were observed with respect to G1PPT (Figure 6.4). In general, extended

conjugation and resonance effects resulted in all bands being deshielded compared to the bands in the functionalized dendrimer and P3HT. The small peaks appearing at further downfield region (9.36 and 9.09 ppm) are due to the proton in the imine group (-N=CH) with is highly deshielded in the copolymer compared to the functionalized dendrimer due to the extended conjugation. The two peaks are suggested to be due to the cis and trans- conformations that the proton take. In the region 7.8-6.7 ppm, the protons on the non-alkylated and alkylated thiophene rings are found. The furthest last two downfield singlets are due to the two protons on the non-alkylated thiophene rings. While the other multiplets are from the poly(3-hexylpolythiophene) (P3HT). According to literature, regioregular P3HT in a head-to-tail (HT) configuration is characterized by the thiophene proton appearing at 6.98 ppm[34,35] whereas in the regiorandom P3HT where there is a combination of two or all of HT, head-to-head (HH), tail-to-tail (TT) configurations, more peaks are observed between 7.05-7.00 ppm.[36] This therefore suggests that we have a regiorandom P3HT in the star copolymer. Because we are dealing with a star copolymer with an imine group we, expect the protons on the thiophene rings to appear more downfield compared to normal thiopehene polymer. We suggest that the multiplet between 7.18-7.04 ppm is due to the resonance shifts downfield in the inner thiophene units. While the protons from the outermost shell of the thiophene rings also characterized by a multiplet, are located below 7.00 ppm.[27] Further upfield, around 4.15-3.91 are found the bands of the alkyl group protons α-positioned to the thiophene ring. Again, we observe three bands instead of one as in regioregular P3HT[36] conforming the regiorandom nature of P3HT in the star copolymer. But the intense band at 4.15ppm suggested that our copolymer comprises 84% regioregular P3HT. The other protons in the methylene of both dendrimer and attached to thiophene rings, and in methyl groups are found between 2.4-1.19 ppm (multiplets) and at 0.79

ppm (singlet), respectively. Number average molecular weight (M_n) and dispersity, $Đ$ were estimated from size exclusion chromatography, performed using HPLC grade dimethylformide (DMF) at a flow rate of 0.8 mL/min. M_n was found to be 16239 g/mol and the average molecular weight M_w 30315 g/mol. The dispersity, $Đ = M_w/M_n$ is calculated to be 1.87.

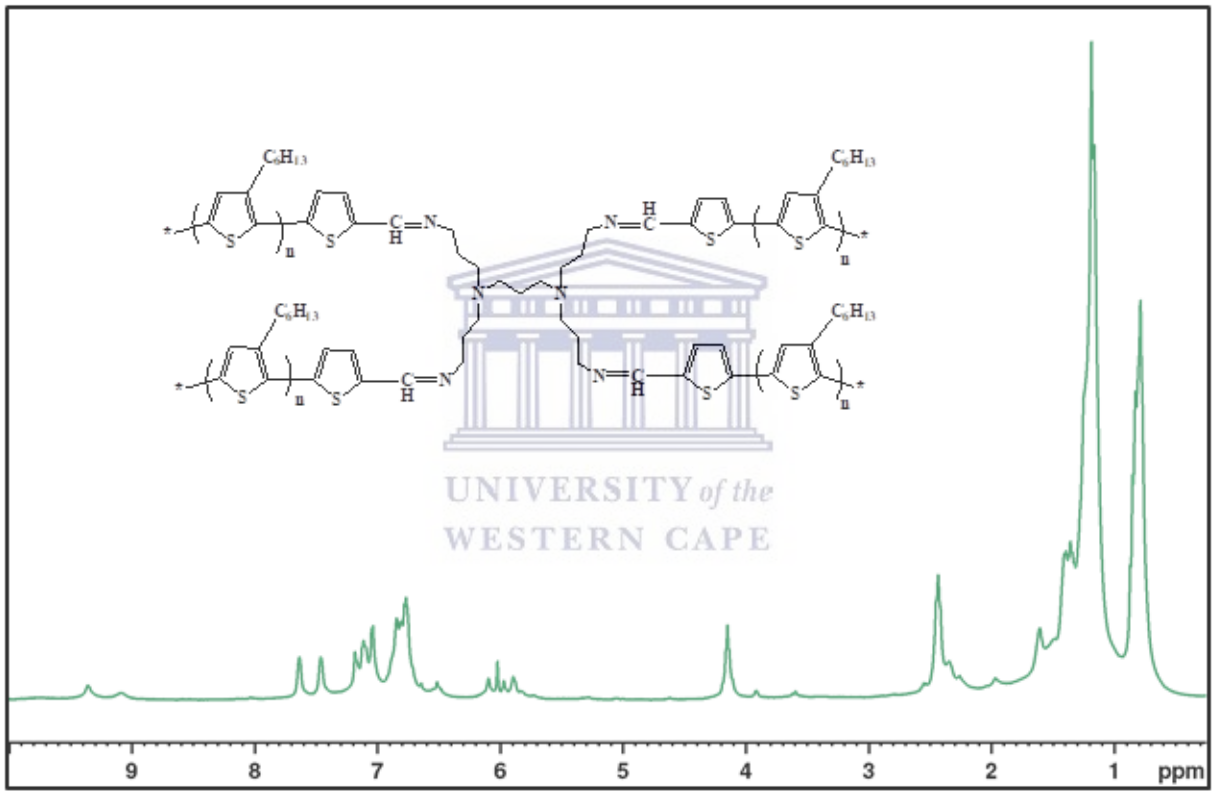

Figure 6.4 ^{1}H NMR of generation 1 poly(propylene thiophenoimine)-co-poly(3-hexylthiophene)

6.3.2 Fourier Transform Infrared Spectroscopy

The Fourier Transform infrared spectrum of G1PPT-co-P3HT is found in Figure 6.5 s with reference to 3-hexylthiophene (3-HT) and G1PPT. The star copolymer spectrum is characterized by many bands associated with the different molecular vibrations within the material which are found at 2954-2849, 1731, 1638, 1473, 1262, 802, 692 cm^{-1}. Bands in the spectral region 2954 - 2854 $cm^{-1}$are characteristics of aliphatic -C-H stretching signals of the hexyl group attached to the thiophene rings.[37] At 1731 and 1638 cm^{-1} are the bands resulting from the molecular vibrations of C=N-H and C=C, respectively; the same vibrations were observed in G1PPT at 1673 and 1632 $cm^{-1}$with high intensity.[38] The alkyl groups -C-H bending are found at 1473 cm^{-1} in G1PPT-co-P3HT. At 802 cm^{-1}, appears the C-S stretching within the thiophene rings that was also observed in 3-HT and G1PPT.[39] Finally, the lowest wavenumber band at 692 cm^{-1} in G1PPT-co-P3HT already present in G1PPT at 703 cm^{-1} is as a result of the bending vibrations of the proton at α-position to the non-alkylated thiophene ring and next to the imine bond.[40]

Table 6.1 Molecular vibrations in G1PPT-co-P3HT, 3-HT and G1PPT

Origin	**Group frequency (cm^{-1})**			**Vibrational mode**
	G1PPT-co-P3HT	**3-HT**	**G1PPT**	
C-H	2954 - 2849	2967 - 2855	2961 - 2801	-C-H stretching
	1473	1462	1432	-C-H bending
	692	-	703	-C- H bending, (α-position to the ring)
C=C	1638	1632, 1538 (weak)	1632	-C=C stretching
C=N	1731	-	1673	-C=N-H stretching

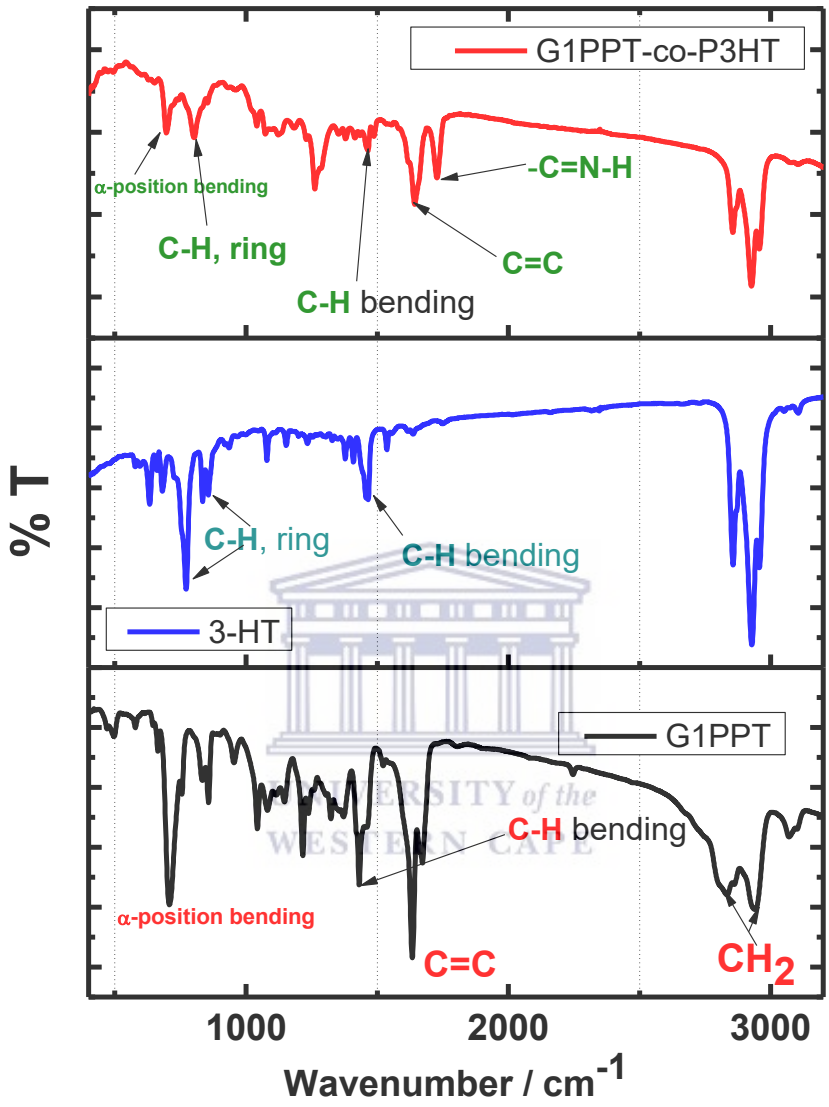

Figure 6.5 FTIR spectra of G1PPT-co-P3HT, 3-HT and G1PPT

6.3.3 Optical and photophysical studies of G1PPT-co-P3HT

The polymer photo-physical properties were studied in chloroform solution as well as in thin films. Maximal absorption wavelength (λ_{max}), onset absorption (λ_{onset}), the optical band gap energy (E_g^{opt}) calculated using the equation $^{1242}/_{\lambda_{onset}}$; as well as the wavelength at the emission maximum and the Stokes' shift are information found in this section.

6.3.3.1 UV-Vis spectroscopy

The absorption properties of G1PPT-co-P3HT were investigated in solution from chloroform as shown in Figure 6.6 and in spin-coated thin films (Figure 6.7). All data are summarized in Table 6.2. The optical bandgap (E_g^{opt}) value was calculated by determining the onset at the higher wavelength region. Oxidative copolymerization of 3-hexylthiophene to the functionalized dendrimer G1PPT resulted in the star copolymer G1PPT-co-P3HT that combined the absorption properties of G1PPT which showed two absorbance bands in the ultra-violet (UV) region with absorption maxima at 251 nm; and two new bands in the visible region. These two absorption peaks at higher frequency are due to the thiophene group[39] whereas the broad band from 423 nm to 676 nm is as a result on the π-π*intermolecular charge transfer due to the delocalization of the electrons caused by the extended conjugation.[41] This broad band has a maximum at ca. 465 nm. In

the NIR region, a new band is observed at 830 nm with an absorption onset at 870 nm giving rise to an optical band gap E_g^{opt} at ca. 1.43 eV. It is to be noted that the absorption of the star copolymer never quenches along the whole UV-Vis spectral region. On the other hand, solid-state G1PPT-co-P3HT demonstrated continuous absorption over the whole spectral range from 400 nm with a lowest absorption intensity recorded at 700 nm. The absorption maximum was red-shifted with broadened area owing to strong inter-chain interaction and π-π stacking in the solid state which are beneficial for charge transport.[42]

Table 6.2 Optical data of PDI-co-carbazole in solution and in thin film

PDI-co-carbazole	**λ_{abs} (nm)**	**λ_{onset} (nm)**	**E_g^{opt} *(eV)***
In solution	251, 302, 359, 465, 830	870	1.43
Thin film	443	875	1.42

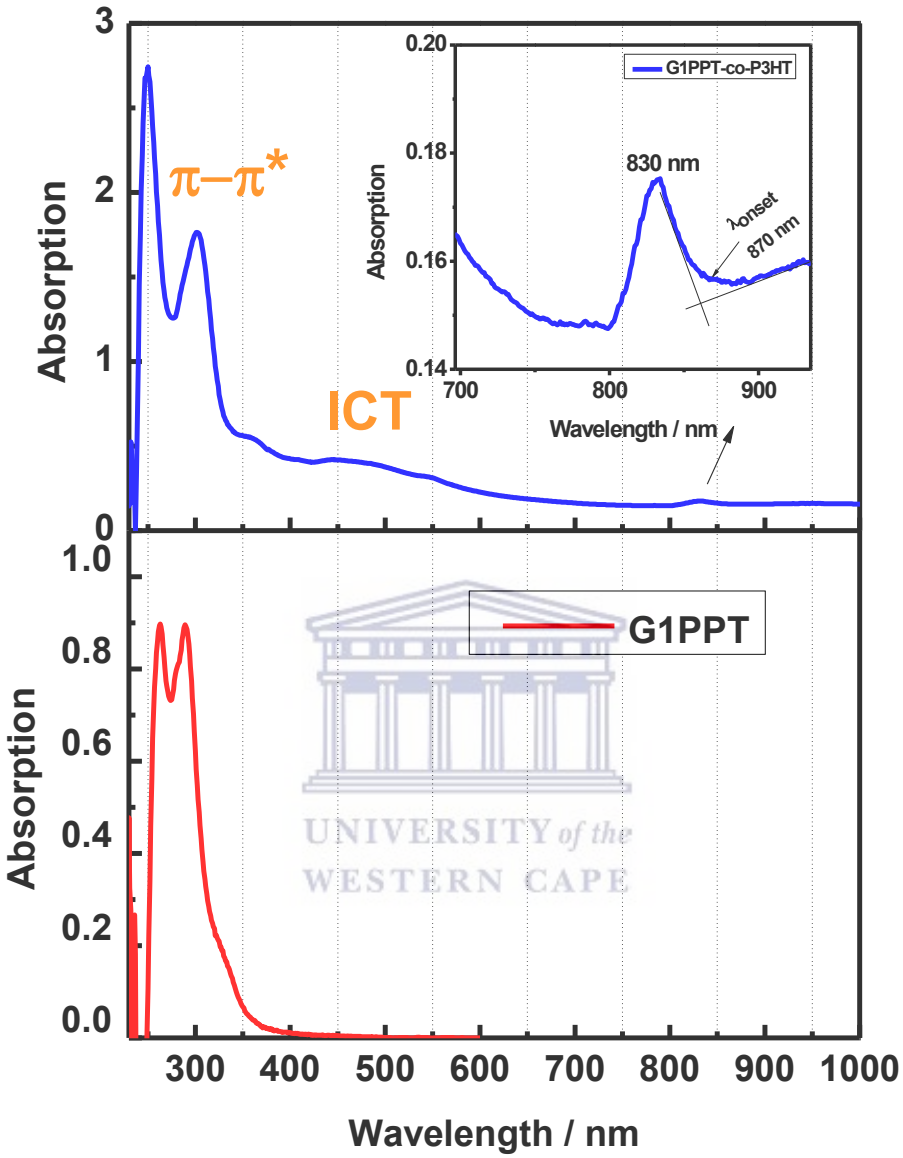

Figure 6.6 UV-Vis absorption of G1PPT-co-P3HT and G1PPT in chloroform solution

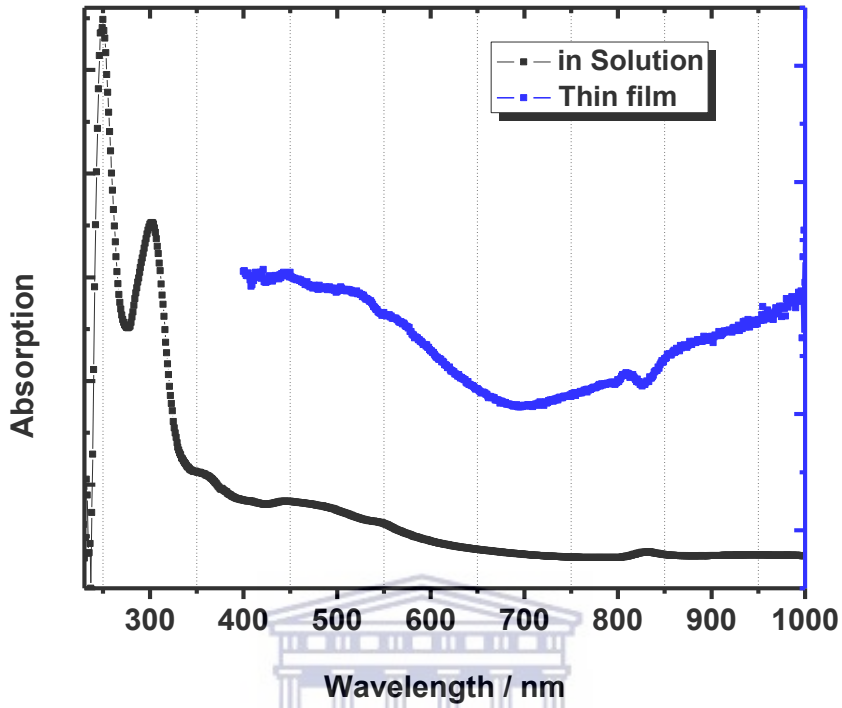

Figure 6.7 UV-Vis absorption of G1PPT-co-P3HT film and in solution

6.3.3.2 Photoluminescence studies

While the star copolymer demonstrated many absorption bands in the UV-Vis region into the NIR region, only one intense photoluminescence peak was observed when the material was exposed to monochromatic light-emitting diode light source of wavelength equals to 365 nm using an Ocean optics device. Upon excitation, the electrons were found to relapse to ground state via light

emission at 551 nm (Figure 6.8), causing a Stokes' shift of 300 nm. Such large Stokes' shift already predicts the formation of aggregates in solid state.[43,44] Emission at higher wavelength region results from intramolecular charge transfer (ICT) caused by effective π-conjugation.[45]

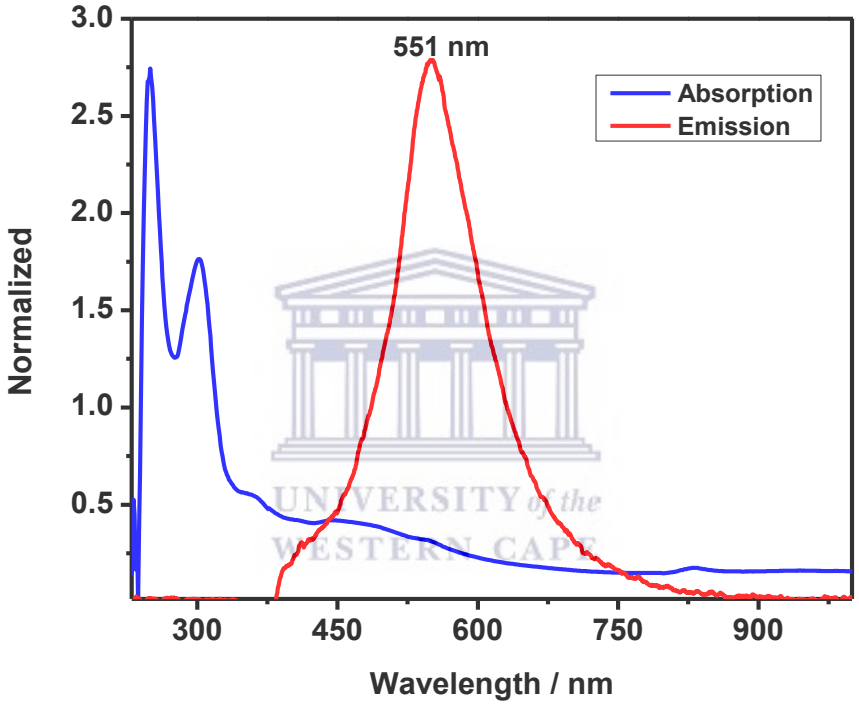

Figure 6.8 Photoluminescence of G1PPT-co-P3HT in chloroform

6.3.4 Electrochemical studies

6.3.4.1 Cyclic Voltammetry (CV) And Square Wave Voltammetry (SWV)

G1PPT-co-P3HT's electronic structure was determined by Cyclic voltammetry (CV). Electrochemical analyses of G1PPT-co-P3HT thin film on a gold working electrode using CV and SWV were carried out in 0.1M Bu_4NPF_6 (Bu = butyl) in acetonitrile versus ferrocene at 50 mV/s scan rate. A three-electrode system where the counter electrode is a Pt wire and the reference electrode is Ag/Ag^+ (0.1 M $AgNO_3$ in acetonitrile) electrode was used. Representative CV curve of the star copolymer is depicted in Figure 6.9. The copolymer exhibited electrochemical quasi-reversible redox reactions, found in the region (-2.5 V) – (-0.5 V). Two redox couples were identified ip_{a1}, ip_{c1} with potential peaks at -0.9 and -1.3 V, respectively and ip_{a2}, ipc_2 with peak potentials at -1.7 and -2.0 V, respectively. Peak currents and potentials are found in Table 6.3. The electronic properties were also derived from these cyclic voltammograms. The ionization potential energy (HOMO energy level), E_{IP}, and electron affinity energy (LUMO energy level), E_A, were estimated from the respective first oxidation and reduction onset potentials, E_{onset}, based on the reference energy level of ferrocene (4.8 eV below the vacuum level) using the equations

$$E_A, LUMO = -e\left(E_{\text{onset}}^{\text{red}} - E_{\text{ferr}}\right)V - 4.8eV \qquad \text{(Equation 6.1)}$$

$$E_{\text{IP}}, HOMO = -e(E_{\text{onset}}^{\text{ox}} - E_{\text{ferr}})V - 4.8eV \qquad \text{(Equation 6.2)}$$

$$E_g^{ec} = |E_{IP} - E_A| \quad \text{(Equation 6.3)}$$

Where, E_{ferr}= -0.03V is the value for ferrocene vs. the Ag/Ag^+ electrode.

The E_{IP} and E_A were found to be 5.53 and 3.6 eV, respectively, giving rise to an electrochemical band gap E_g^{ec} = 1.93 eV slightly higher than the optical band gap E_g^{opt} = 1.43 eV calculated from the absorption wavelength onset.

Table 6.3 Summary of redox potentials and peak currents for G1PPT-co-P3HT

Materials	Ox^1	Red^1	E_1^o	Ox^2	Red^2	E_2^o
Potential/ V	-0.9	-1.3	-1.7	-1.7	-2.0	-1.84
|Ip| /µA	2.5	5	-	1.9	8.7	-

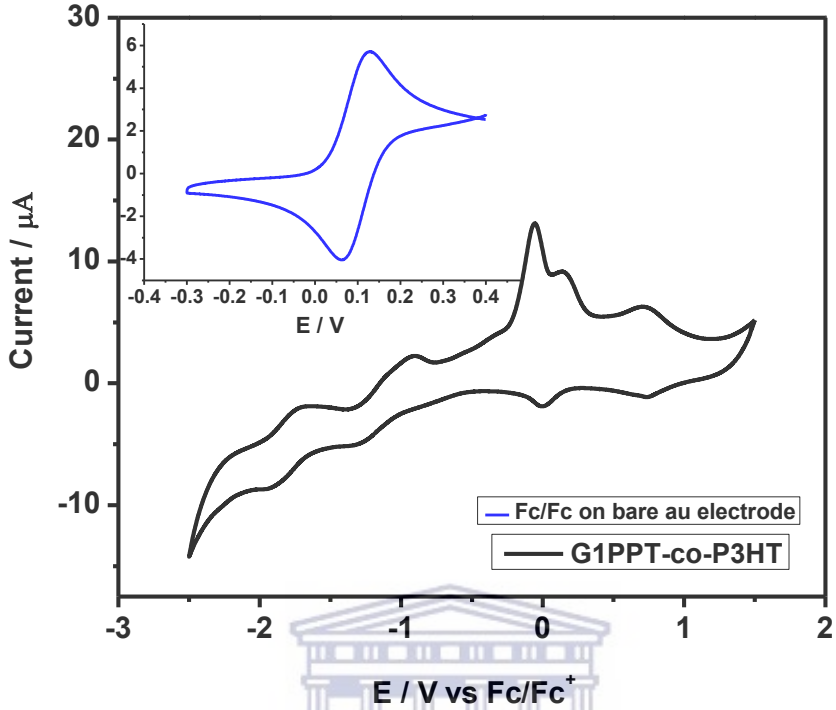

Figure 6.9 Cyclic voltammogram of G1PPT-co-P3HT in 0.1M Bu_4NPF_6 in acetonitrile at scan rate 50 mV/s versus Ferrocene using Ag/Ag+ reference electrode

Table 6.4 HOMO, LUMO and band gap E_g^{ec} energy levels of G1PPT-co-P3HT

Materials	E_{onset}^{ox1} **(V)**	E_{onset}^{red1} **(V)**	E_{IP} **(-E_{HOMO}) (eV)**	E_A **(-E_{LUMO}) (eV)**	E_g^{ec} **(eV)**	E_g^{opt} **(eV)**
PDI-co-Carbazole	-0.63	-2.2	5.53	3.6	1.93	1.43

The copolymer was also investigated using Ag/AgCl reference electrode. Upon application of a potential voltage in the range 0 - 2.5 V, two redox couples are observed. The two oxidation peaks i_{pa1} and i_{pa2} are found at 1.38 and 1.73 V, respectively, and the two reduction peaks i_{pc1} and i_{pc2} at 0.97 and 1.21 V, respectively (Figure 6.10). The first redox couple i_{pa1} and i_{pc1} are suggested to be due to the insertion and removal of Bu_4N^+ ion, while the second redox couple i_{pa2} and i_{pc2} is assumed to be due to insertion and removal of PF_6^- ion. These pairs of oxidation and reduction peaks were confirmed by square wave voltammetry technique (Figure 6.11) using the same parameters as in CV.

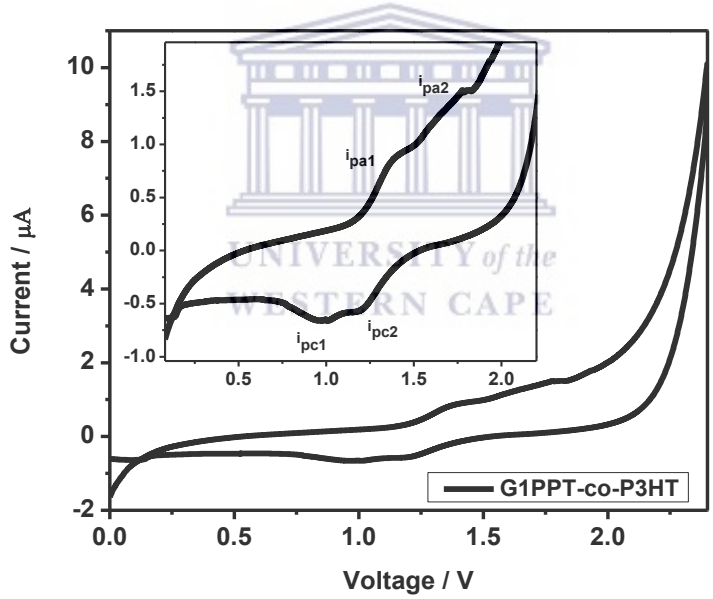

Figure 6.10 Cyclic voltammogram of G1PPT-co-P3HT in 0.1M Bu_4NPF_6 in acetonitrile at scan rate 50 mV/s using Ag/AgCl reference electrode

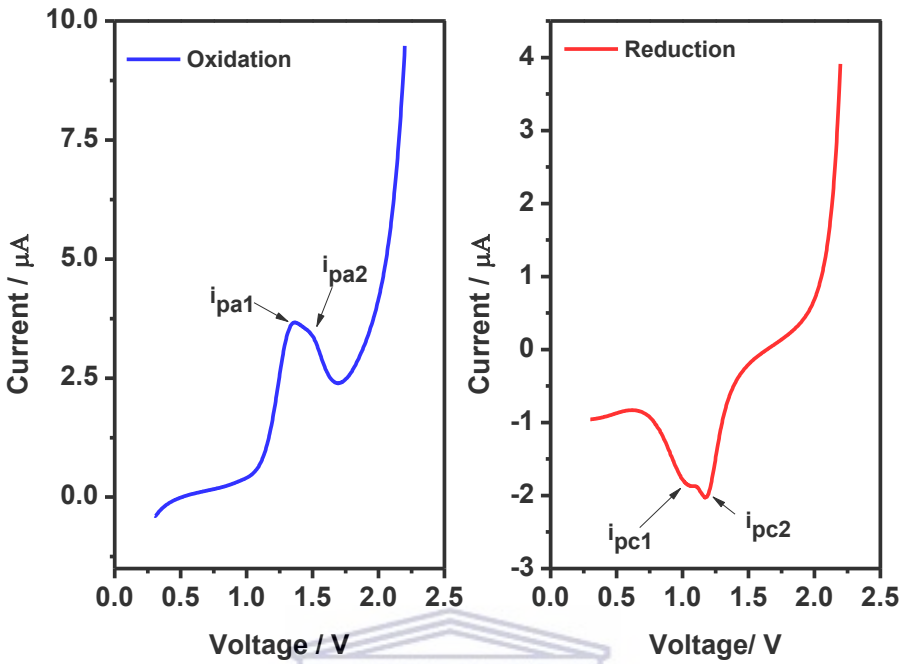

Figure 6.11 Forward and reverse square wave voltammograms of G1PPT-co-P3HT in 0.1M Bu_4NPF_6 (acetonitrile) at scan rate 50 mV/s using Ag/AgCl reference electrode

6.3.4.2 Electrochemical Impedance Spectroscopy (EIS)

Bode plot of G1PPT-co-P3HT (Figure 6.12) was extracted from electrochemical impedance spectroscopy study. The star copolymer was again deposited on a working gold electrode disc in 0.1M Bu4NPF6 in acetonitrile at scan rate 50 mV/s using a three-electrode system where the counter electrode is a Pt wire and the reference electrode is Ag/AgCl electrode with an applied

potential of 1.182 V. The acquired data allowed for the determination of the phase angle at ca. 75 degree which demonstrates the relatively good semiconducting nature of the star copolymer.

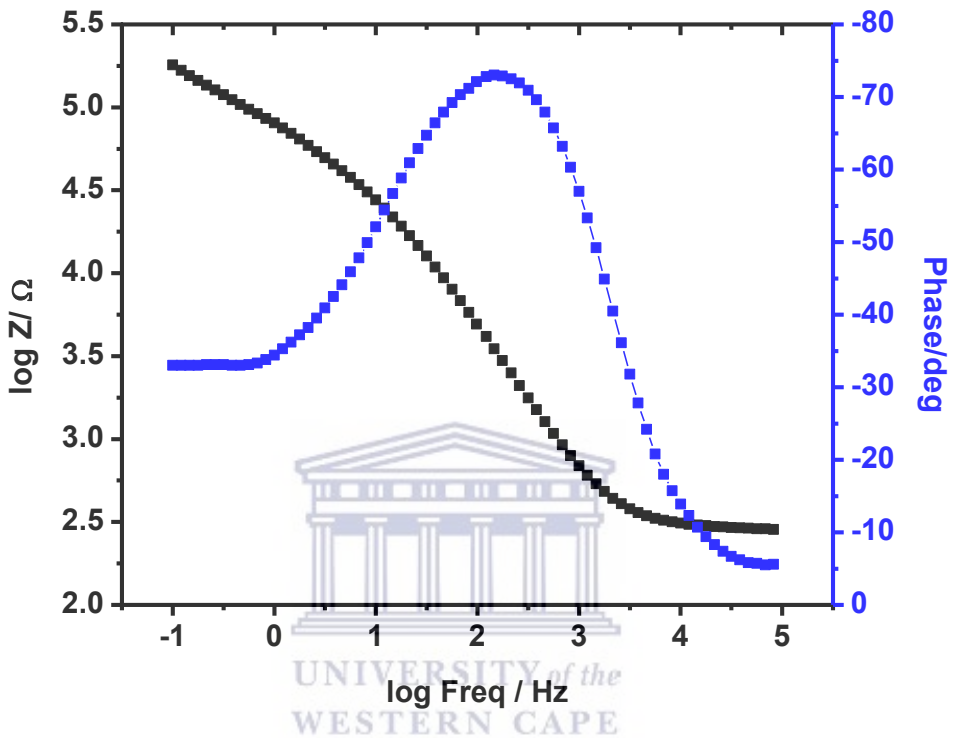

Figure 6.12 Bode plot of G1PPT-co-P3HT in 0.1M Bu_4NPF_6 in acetonitrile at 1.182 V

6.3.5 Morphological and particle size investigation

6.3.5.1 High-Resolution Transmission Electron Microscopy (HRTEM)

HRTEM was used as the technique of choice for the morphological investigation of the star copolymer. The results depicted on the images in Figure 6.13 represent the morphology of G1PPT-co-P3HT thin film casted from chloroform. Despite the mixed 'regiorandom-regioregular' nature of the star copolymer as demonstrated by ^{1}H NMR spectroscopy, G1PPT-co-P3HT showed a highly crystalline nature with well-defined lattice fringes as observed on the HRTEM image. This crystallinity of the star copolymer was confirmed by the SAED (Selected Area Electron Diffraction) image in which well-patterned crystal lattice arrays are observed; therefore, confirming our hypothesis from NMR data that P3HT component in the star copolymer is composed of a higher ratio of regioregular P3HT compared to regiorandom P3HT. G1PPT was polycrystalline (Figure 6.14) and 3-HT was quite amorphous with coarse nature (Figure 6.15), we therefore believe that copolymerization of 3-HT to the functionalized dendrimer aided in the molecular ordering of the star copolymer. Since crystallinity is a very important and critical factor that affects the properties of optoelectronic films, the achieved degree of crystallinity could ascertain good organic photovoltaic performances.[46]

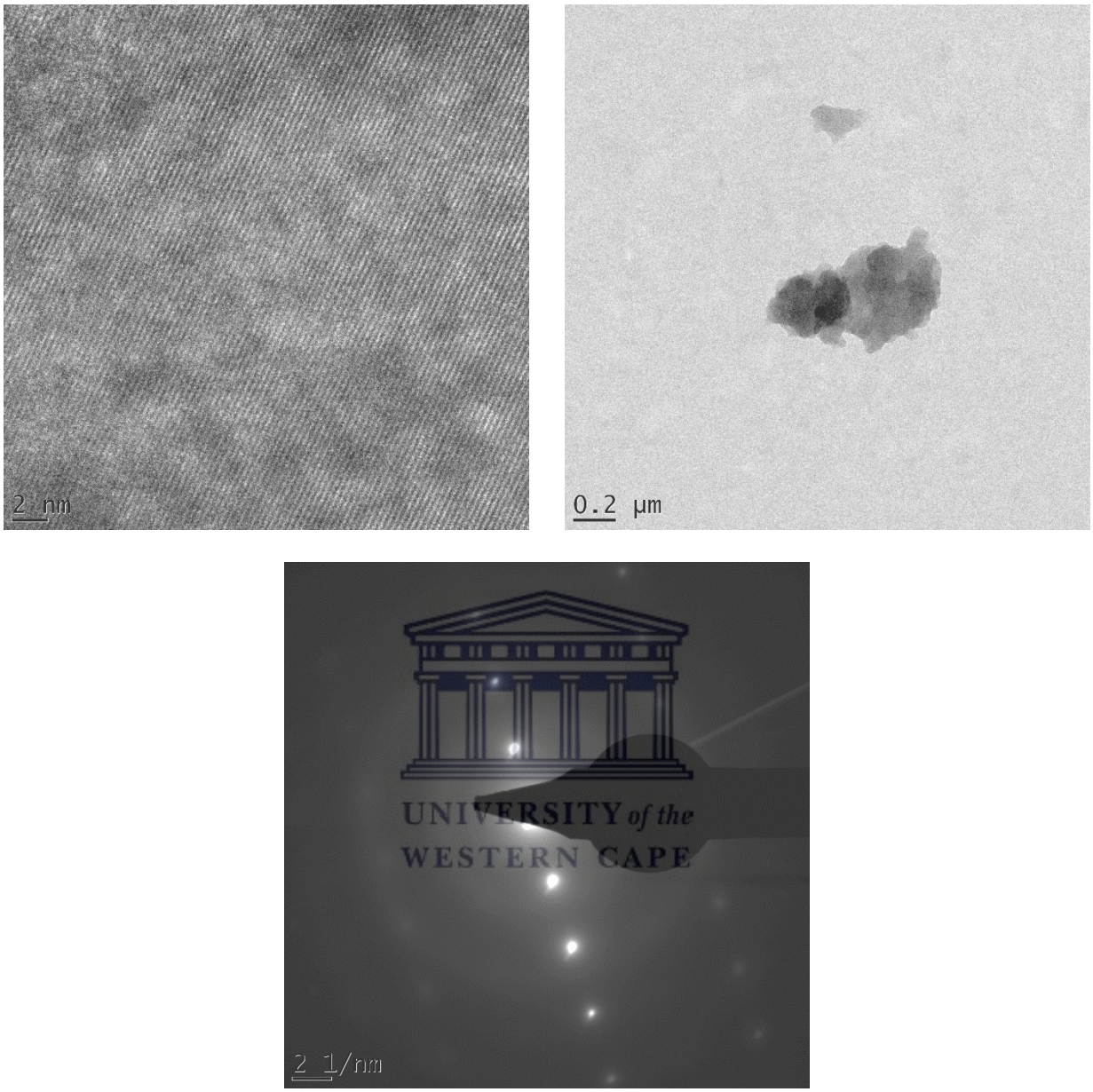

Figure 6.13 HRSEM and SAED images of G1PPT-co-P3HT

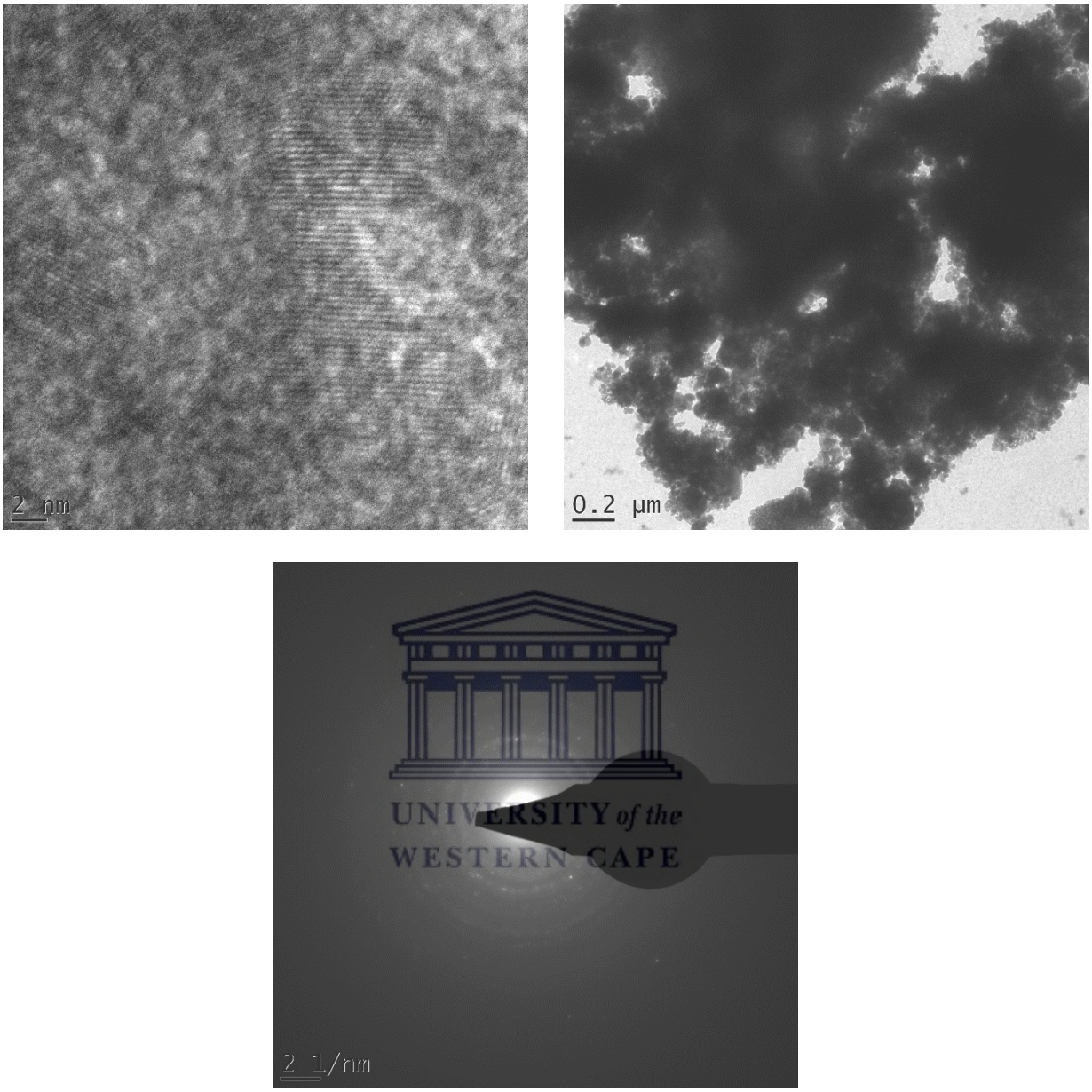

Figure 6.14 HRSEM and SAED images of G1PPT

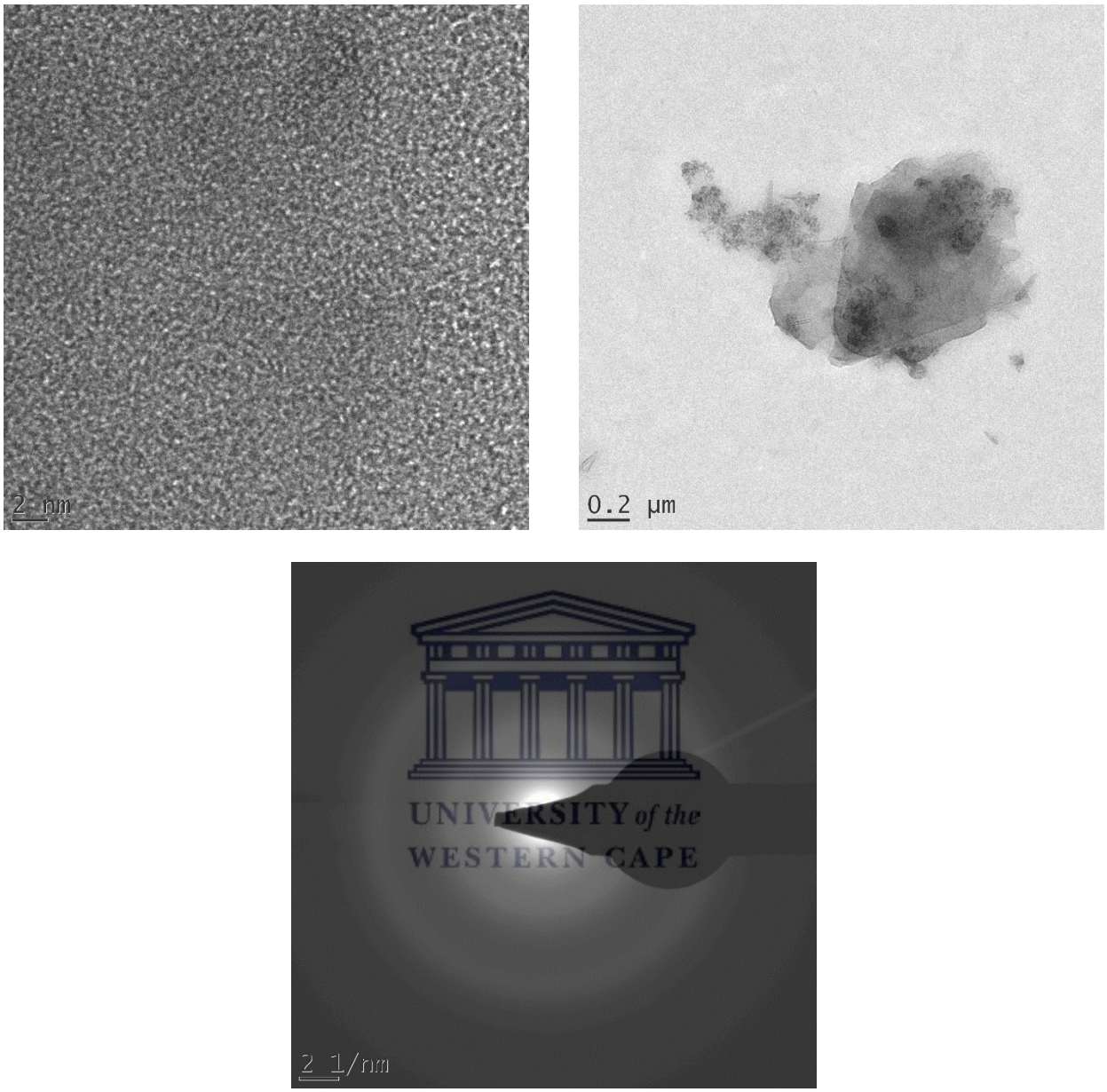

Figure 6.15 HRSEM and SAED images of 3-hexylthiophene

6.3.8 Small-angle X-ray Scattering (SAXS) analysis

Small-angle X-ray scattering (SAXS) was used to obtain the particle size distribution of G1PPT-co-P3HT. The free-model pair distance distribution function of the star copolymer depicted in Figure 6.16 shows that G1PPT-co-P3HT is mostly in aggregate form with maximum particle sizes around 80 nm. The pair distance distribution functions of the nanoparticles in number-weighted particle size distributions are shown in Figure 6.17 with the volume-weighted particle size distribution as the inset. Nanoparticles in the ranges of 2– 23 nm and 55 – 76 nm are described by scattering cross sections, with a larger portion of the nanoparticles at 12 nm for the number-weighted distribution The volume-weighted particle size distribution shows the population of particles seen by their volume. Particles around 12 nm are more seen than those around 65 nm. This result is in contradiction with the concept that larger particles are "more seen" than smaller particles.[47]

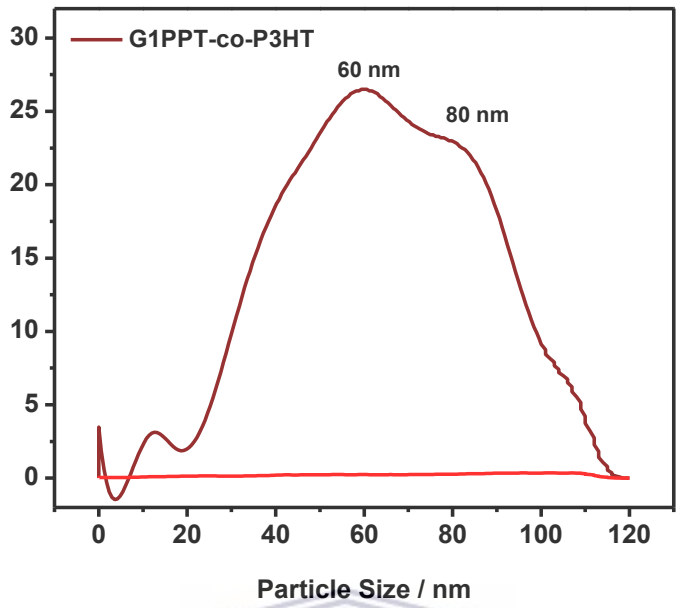

Figure 6.16 Pair-distance distribution function of G1PPT-co-P3HT

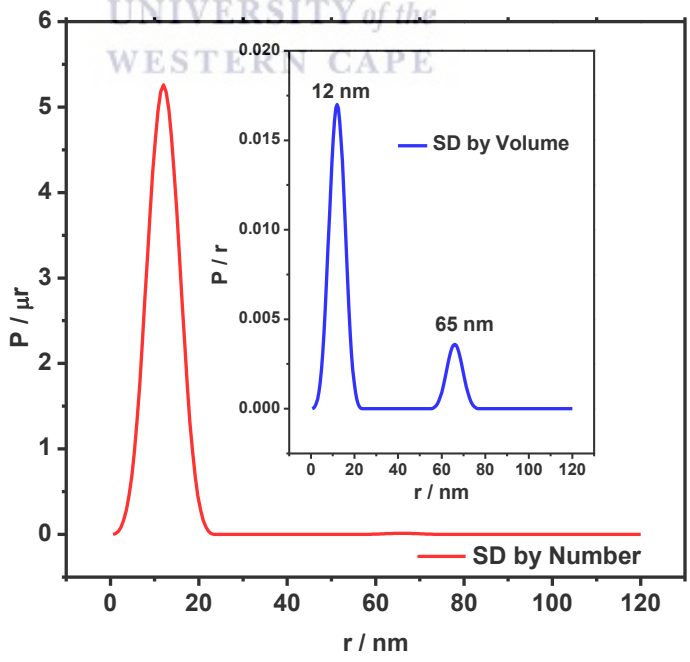

Figure 6.17 SAXS particle size distribution: by number and volume.

6.4 Conclusion

Oxidative copolymerization of G1PPT to 3-HT in chloroform in the presence of $FeCl_3$ was successfully achieved as confirmed by the ^1H NMR spectroscopy analysis of G1PPT- co-P3HT which demonstrated several characteristic bands associated with the regiorandom and regioregular nature usually observed in poly(3-hexylthiophene) coupled to the characteristic of the functionalized dendrimer. Low-band gap of 1.43 eV was achieved by the star copolymer that exhibits good absorption properties in the UV-Vis to NIR spectral region. The star copolymer also exhibited good electrochemical properties with two well-defined quasi-reversible redox couples and very good semiconducting properties as revealed by the Bode plot. The highly crystalline nature of the prepared copolymer coupled to the above-mentioned other properties suggests that G1PPT-co-P3HT could be a good candidate as electron-donating material in organic photovoltaic devices.

References

1. Boudreault, P. L. T., Najari, A. & Leclerc, M. Processable low-bandgap polymers for photovoltaic applications. *Chemistry of Materials* **23,** 456–469 (2011).

2. Mishra, A. & Bäuerle, P. Small molecule organic semiconductors on the move: promises for future solar energy technology. *Angewandte Chemie - International Edition* **51,** 2020–2067 (2012).

3. Cheng, Y.-J., Yang, S.-H. & Hsu, C.-S. Synthesis of conjugated polymers for organic solar cell applications. *Chemical Reviews* **109,** 5868–5923 (2009).

4. Persano, L., Camposeo, A. & Pisignano, D. Active polymer nanofibers for photonics, electronics, energy generation and micromechanics. *Progress in Polymer Science* **43,** 48–95 (2015).

5. Ogawa, S. *Organic Electronics Materials and Devices*. (Springer, 2015).

6. Schulz, G. L., Mastalerz, M., Ma, C. Q., Wienk, M., Janssen, R. & Bäuerle, P. Synthesis and photovoltaic performance of pyrazinoquinoxaline containing conjugated thiophene-based dendrimers and polymers. *Macromolecules* **46,** 2141–2151 (2013).

7. Tomalia, D. A. & Frechet, J.M.J. Dendrimers and other dendritic polymers (Wiley, 2001).

8. Astruc, D. & Boisselier, E. Dendrimers designed for functions : from physical , photophysical , and supramolecular properties to applications in sensing , catalysis , molecular electronics , photonics , and nanomedicine. 1857–1959 (2010).

9. Kopidakis, N., Mitchell, W. & Bozell, J. Bulk heterojunction organic photovoltaic devices using dendrimers. *2005 DOE Solar Energy Technologies* (2005).

10. Gupta, V. & Nayak, S. K. Dendrimers : a review on synthetic approaches. **5,** 117–122 (2015).

11. Anthopoulos, T. D., Markham, J. P. J., Namdas, E. B., Samuel, I. D. W., Lo, S.-C. & Burn, P. L. Highly efficient single-layer dendrimer light-emitting diodes with balanced charge transport. *Applied Physics Letters* **82,** 4824–4826 (2003).

12. Wang, J. L., He, Z., Wu, H., Cui, H., Li, Y., Gong, Q., Cao, Y. & Pei, J. Solution-processed bulk-heterojunction photovoltaic cells based on dendritic and star-shaped D-π-A organic dyes. *Chemistry - An Asian Journal* **5,** 1455–1465 (2010).

13. Kopidakis, N., Mitchell, W. J., Van De Lagemaat, J., Ginley, D. S., Rumbles, G., Shaheen, S. E. & Rance, W. L. Bulk heterojunction organic photovoltaic devices based on phenyl-cored thiophene dendrimers. *Applied Physics Letters* **89,** 1–4 (2006).

14. Kline, R. J., McGehee, M. D., Kadnikova, E. N., Liu, J. & Fréchet, J. M. J. Controlling the field-effect mobility of regioregular polythiophene by changing the molecular weight. *Advanced Materials* **15,** 1519–1522 (2003).

15. Schilinsky, P., Asawapirom, U., Scherf, U., Biele, M. & Brabec, C. J. Influence of the molecular weight of poly(3-hexylthiophene) on the performance of bulk heterojunction solar cells. *Chemistry of Materials* **17,** 2175–2180 (2005).

16. John, H., Bauer, R., Espindola, P., Sonar, P., Heinze, J. & Müllen, K. 3D-hybrid networks

with controllable electrical conductivity from the electrochemical deposition of terthiophene-functionalized polyphenylene dendrimers. *Angewandte Chemie - International Edition* **44,** 2447–2451 (2005).

17. Andreitchenko, E. V., Clark, C. G., Bauer, R. E., Lieser, G. & Müllen, K. Pushing the synthetic limit: polyphenylene dendrimers with "exploded" branching units - 22-nm-diameter, monodisperse, stiff macromolecules. *Angewandte Chemie - International Edition* **44,** 6348–6354 (2005).

18. Fernández-Lázaro, F., Zink-Lorre, N. & Sastre-Santos, Á. Perylenediimides as non-fullerene acceptors in bulk-heterojunction solar cells (BHJSCs). *Journal of Materials Chemistry A* **4,** 9336–9346 (2016).

19. Ondarse-Alvarez, D., Oldani, N., Roitberg, A. E., Kleiman, V., Tretiak, S. & Fernandez-Alberti, S. Energy transfer and spatial scrambling of an exciton in a conjugated dendrimer. *Physical Chemistry Chemical Physics* **20,** 29648–29660 (2018).

20. Itami, K., Tonogaki, K., Nokami, T., Ohashi, Y. & Yoshida, J. I. Palladium-catalyzed convergent synthesis and properties of conjugated dendrimers based on triarylethene branching. *Angewandte Chemie - International Edition* **45,** 2404–2409 (2006).

21. Chen, Z., Jeffery, C. J., Morshedi, M., Moxey, G. J., Barlow, A., Yang, X., Babgi, B. A., Dalton, G. T., Randles, M. D., Smith, M. K., Zhang, C., Samoc, M., Cifuentes, M. P. & Humphrey, M. G. Syntheses, electrochemical, linear optical, and cubic nonlinear optical properties of ruthenium-alkynyl-functionalized oligo(phenylenevinylene) stars. *ChemPlusChem* **80,** 1329–1340 (2015).

22. Thongkasee, P., Thangthong, A., Janthasing, N., Sudyoadsuk, T., Namuangruk, S., Keawin, T., Jungsuttiwong, S. & Promarak, V. Carbazole-dendrimer-based donor-π-acceptor type organic dyes for dye-sensitized solar cells: Effect of the size of the carbazole dendritic donor. *ACS Applied Materials and Interfaces* **6,** 8212–8222 (2014).

23. Albrecht, K., Matsuoka, K., Fujita, K. & Yamamoto, K. Carbazole dendrimers as solution-processable thermally activated delayed-fluorescence materials. *Angewandte Chemie - International Edition* **54,** 5677–5682 (2015).

24. Cho, Y. J., Kim, S. Y., Son, M. R., Son, H. J., Cho, D. W. & Kang, S. O. Time-resolved spectroscopic analysis of the light-energy harvesting mechanism in carbazole-dendrimers with a blue-phosphorescent Ir-complex core. *Physical Chemistry Chemical Physics* **19,** 20093–20100 (2017).

25. Shi, K., Wang, J. Y. & Pei, J. π-conjugated aromatics based on truxene: Synthesis, self-assembly, and applications. *Chemical Record* **15,** 52–78 (2015).

26. Jiang, Y., Wang, J. Y., Ma, Y., Cui, Y. X., Zhou, Q. F. & Pei, J. Large rigid blue-emitting π-conjugated stilbenoid-based dendrimers: synthesis and properties. *Organic Letters* **8,** 4287–4290 (2006).

27. Xia, C., Fan, X., Locklin, J., Advincula, R. C., Gies, A. & Nonidez, W. Characterization, supramolecular assembly, and nanostructures of thiophene dendrimers. *Journal of the American Chemical Society* **126,** 8735–8743 (2004).

28. Gao, W., Wang, J., Luo, Q., Lin, Y., Ma, Y., Dou, J., Tan, H., Ma, C. Q. & Cui, Z. Tuning the optical and electrochemical properties of conjugated all-thiophene dendrimers via core

functionalization with a benzothiadiazole unit. *RSC Advances* **7,** 1606–1616 (2017).

29. Stoltzfus, D. M., Ma, C. Q., Nagiri, R. C. R., Clulow, A. J., Bäuerle, P., Burn, P. L., Gentle, I. R. & Meredith, P. Thiophene dendrimer-based low donor content solar cells. *Applied Physics Letters* **109,** 103302:1–4 (2016).

30. Ma, C. Q., Fonrodona, M., Schikora, M. C., Wienk, M. M., Janssen, R. A. J. & Bäuerle, P. Solution-processed bulk-heterojunction solar cells based on monodisperse dendritic oligothiophenes. *Advanced Functional Materials* **18,** 3323–3331 (2008).

31. Dang, M. T., Hirsch, L. & Wantz, G. P3HT:PCBM, best seller in polymer photovoltaic research. *Advanced Materials* **23,** 3597–3602 (2011).

32. Hrostea, L., Girtan, M., Mallet, R. & Leontie, L. Optical and Morphological Properties of P3HT and P3HT: PCBM Thin Films Used in Photovoltaic Applications. In *IOP Conference Series: Materials Science and Engineering* **374,** 1–6 (2018).

33. Hauch, J. A., Schilinsky, P., Choulis, S. A., Childers, R., Biele, M. & Brabec, C. J. Flexible organic P3HT:PCBM bulk-heterojunction modules with more than 1 year outdoor lifetime. *Solar Energy Materials and Solar Cells* **92,** 727–731 (2008).

34. Wu, P. T., Xin, H., Kim, F. S., Ren, G. & Jenekhe, S. A. Regioregular poly(3-pentylthiophene): synthesis, self-assembly of nanowires, high-mobility field-effect transistors, and efficient photovoltaic cells. *Macromolecules* **42,** 8817–8826 (2009).

35. Rudenko, A. E., Wiley, C. A., Stone, S. M., Tannaci, J. F. & Thompson, B. C. Semi-random P3HT analogs via direct arylation polymerization. *Journal of Polymer Science, Part A:*

Polymer Chemistry **50,** 3691–3697 (2012).

36. Qu, S., Yao, Q., Shi, W., Wang, L. & Chen, L. The Influence of Molecular Configuration on the Thermoelectrical Properties of Poly(3-hexylthiophene). *Journal of Electronic Materials* **45,** 1389–1396 (2016).

37. Makelane, H. R., John, S. V., Waryo, T. T., Baleg, A., Mayedwa, N., Rassie, C., Wilson, L., Baker, P. & Iwuoha, E. I. AC voltammetric transductions and sensor application of a novel dendritic poly(propylene thiophenoimine)-co-poly(3-hexylthiophene) star co-polymer. *Sensors and Actuators, B: Chemical* **227,** 320–327 (2016).

38. Baleg, A. A., Jahed, N., Yonkeu, A. L. D., Njomo, N., Mbambisa, G., Molapo, K. M., Fuku, X. G., Fomo, G., Makelane, H., Tsegaye, A., Waryo, T. T., Baker, P., Vilakazi, S., Tshikhudo, R. & Iwuoha, E. I. Impedimetry and microscopy of electrosynthetic poly(propylene imine)-co-polypyrrole conducting dendrimeric star copolymers. *Electrochimica Acta* **128,** 448–457 (2014).

39. Ganesamoorthy, R., Sathiyan, G., Thangamuthu, R. & Sakthivel, P. Synthesis and characterization of bay substituted perylene diimide small molecule for organic solar cell application. In *Recent Trends in Materials Science and Applications*, 401–415 (Springer, 2017).

40. Makelane, H. R., Tovide, O., Sunday, C. E., Waryo, T. & Iwuoha, E. I. Electrochemical interrogation of G3-poly(propylene thiophenoimine) dendritic star polymer in phenanthrene sensing. *Sensors* **15,** 22343–22363 (2015).

41. Heo, H., Kim, H., Lee, D., Jang, S., Ban, L., Lim, B., Lee, J. & Lee, Y. Regioregular D1-

A-D2-A terpolymer with controlled thieno[3,4-b]thiophene orientation for high-efficiency polymer solar cells processed with nonhalogenated solvents. *Macromolecules* **49,** 3328–3335 (2016).

42. Meena, S., Mohammad, T., Dutta, V. & Jacob, J. Design and synthesis of N-substituted perylene diimide based low band gap polymers for organic solar cell applications. *RSC Advances* **8,** 30468–30480 (2018).

43. Cimrová, V., Výprachtický, D., Kmínek, I., Dzhabarov, V. & Pokorná, V. Photophysical and electrochemical properties of novel luminescent and photoconductive copolymers. *ECS Transactions* **58,** 15–30 (2014).

44. Bouguerra, N., Ruišžička, A., Ulbricht, C., Enengl, C., Enengl, S., Pokorná, V., Výprachtický, D., Tordin, E., Aitout, R., Cimrová, V. & Egbe, D. A. M. Synthesis and photophysical and electroluminescent properties of poly(1,4-phenylene-ethynylene)-alt-poly(1,4-phenylene-vinylene)s with various dissymmetric substitution of alkoxy side chains. *Macromolecules* **49,** 455–464 (2016).

45. Vajiravelu, S., Ramunas, L., Juozas Vidas, G., Valentas, G., Vygintas, J. & Valiyaveettil, S. Effect of substituents on the electron transport properties of bay substituted perylene diimide derivatives. *Journal of Materials Chemistry* **19,** 4268–4275 (2009).

46. Zhou, C., Chen, Z., Zhang, G., McDowell, C., Luo, P., Jia, X., Ford, M. J., Wang, M., Bazan, G. C., Huang, F. & Cao, Y. Toward high efficiency polymer solar cells: rearranging the backbone units into a readily accessible random tetrapolymer. *Advanced Energy Materials* **8,** 1–9 (2018).

47. Ndipingwi, M. M., Ikpo, C. O., Hlongwa, N. W., Dywili, N., Djoumessi Yonkeu, A. L. & Iwuoha, E. I. Crystal chemistry and lithium-ion intercalation properties of lithium manganese silicate cathode for aqueous rechargeable Li-ion batteries. *Journal of Applied Electrochemistry* (2019). https://doi.org/10.1007/s10800-019-01296-0

CHAPTER SEVEN

The photophysical and photovoltaic characteristics of generation 1 poly(propylene thiephenoimine)-co-poly(3-hexylthiophene):poly[N,N'-bis(dodecyl)perylene-3,4,9,10-tetracarboxylic diimide-1,7-diyl-alt-9-(heptadecan-9-yl)carbazole-2,7-diyl] nanocomposites

Abstract

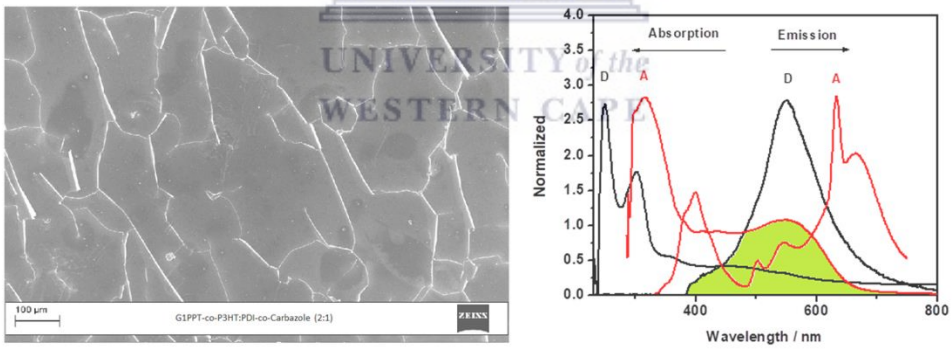

Graphical abstract: HRSEM images (left) and FRET (right) of G1PPT-co-P3HT:PDI-co-Carbazole BHJ blend

Bulk heterojunction systems of G1PPT-co-P3HT:PDI-co-Carbazole were successfully prepared and exhibited good optical properties in the UV-Vis region. Addition of PDI-co-Carbazole into pristine G1PPT-co-P3HT resulted in blue shift of the intermolecular vibronic band with respect to

pristine PDI-co-Carbazole, characterizing the distortion of the molecular structure of the highly crystalline G1PPT-co-P3HT. Upon excitation of these blends, an increase in the acceptor fluorescence intensity was observed which demonstrated that Förster resonance energy transfer occurs, suggested to be accompanied by non-radiative charges recombination. The blend exhibited poor photovoltaic performances due to the evident defect/trap in the morphology of the active layer.

KEY WORDS: All-polymer solar cell, bulk heterojunction, nanocomposite, photoluminescence, photovoltaic.

7.1 Introduction

Polymer solar cells (PSCs), in which the active layer typically consists of an electron donating polymer and a small molecule or a polymer as an electron accepting counterpart, have caught a lot of attention in the recent past years for their supreme advantages such as light weight, inexpensiveness and ease to manufacture through potential roll-to-roll production on flexible substrates. In this type of solar cells, the p-type and n-type semiconducting materials are physically intermixed in a bulk heterojunction (BHJ) architecture.[1] All-polymer solar cells (all-PSCs), in which the electron accepting material is an n-type semiconducting polymer rather than the conventional widely used fullerene and its derivatives have some unique attributes over polymer/fullerene BHJs for many reasons. These include the photons absorption within the

spectral region of visible light that can be extended into NIR region. Also, there is the possibility for fine tuning of the energy levels of n-type polymers, thanks to their structural variety; which is a key aspect in achieving high performances in PSCs.[2] BHJ polymer/polymer solar cells with power conversion efficiency (PCE) exceeding 4% and up to above 7% have been reported.[3–5] The photovoltaic properties and efficiencies of these PSCs strongly depend on the molecular weight and molecular weight distribution, nature of the alkyl chains, purity and regioregularity of the conjugated polymers.[6–9] Unfortunately, in most cases, molecular weight and molecular weight distribution are difficult to control, affecting the overall devices efficiencies and often resulting in the challenge of obtaining reproducible PCEs for the same polymers.[10] Even though organic solar cells device fabrication and photovoltaic process (refer to Chapter 2, Figure 2.2) appears to be relatively easy, the biggest challenge lies in finding the optimal donor-acceptor conjugated polymers pair and ascertaining the most appropriate morphology; which in turn depends on many parameters that include choice of solvent, deposition technique, annealing temperature and ultimately, the blend ratio. As a primary requirement, the semiconducting polymers must be air-stable. This implies that the HOMO (highest occupied molecular orbital) should be below -5.2 eV (approximately the air-oxidation threshold). Secondly, there must be effective electron transfer between the LUMO (lowest unoccupied molecular orbital) of the donor and the LUMO of the acceptor; an energy difference between the two LUMO energy levels of 0.3 eV is required to achieve such electron transfer (see Figure 7.1). This is also true if the electron transfer occurs through the HOMO energy levels. Lastly, since the open circuit voltage, V_{OC} is mostly based on the difference between the LUMO of the acceptor and the HOMO of the donor, it is desirable that the HOMO energy level of the electron-donating polymer remains as low as possible.[11]

Organic photovoltaic cells consisting of rylene diimide-based acceptor polymers, more recently developed, are among the most efficient polymer solar cells.[12] This class of rylenes are interesting because they exhibit good electron transport behavior and the molecular electronic properties can be tuned through varying substituents on the imide nitrogen atoms or on the rylene 'bay' position. Also, they exhibit high electron mobilities, excellent chemical, thermal and photochemical stabilities as well as relatively high electron affinities.[13,14] On the other hand, the molecular ordering coupled to the good electron donating properties, whose transport happen in all directions, [15] observed in star-shaped dendrimers and dendritic polymers, notably thiophene-based dendrimers have made them good candidates as electron donor in OPVs.[16,17] In this chapter, we are therefore going to prepare a novel BHJ active layer of poly(propylene thiophenoimine)-co-poly(3-hexylthiophene)/ poly[N,N'-bis(dodecyl)perylene-3,4,9,10-tetracarboxylic diimide-1,7-diyl-alt-9-(heptadecane-9-yl)carbazole-2,7-diyl], denoted G1PPT-co-P3HT/PDI-co-Carbazole; study the optical and photophysical properties of the nanocomposite and investigate its photovoltaic characteristics. Each of the constituting polymer of this nanocomposite, whether donor or acceptor, will also be investigated in a BHJ active layer with the worldwide used best reported acceptor and donor, fullerene ($PC_{61}BM$) and poly(3-hexylthiophene),[18] respectively.

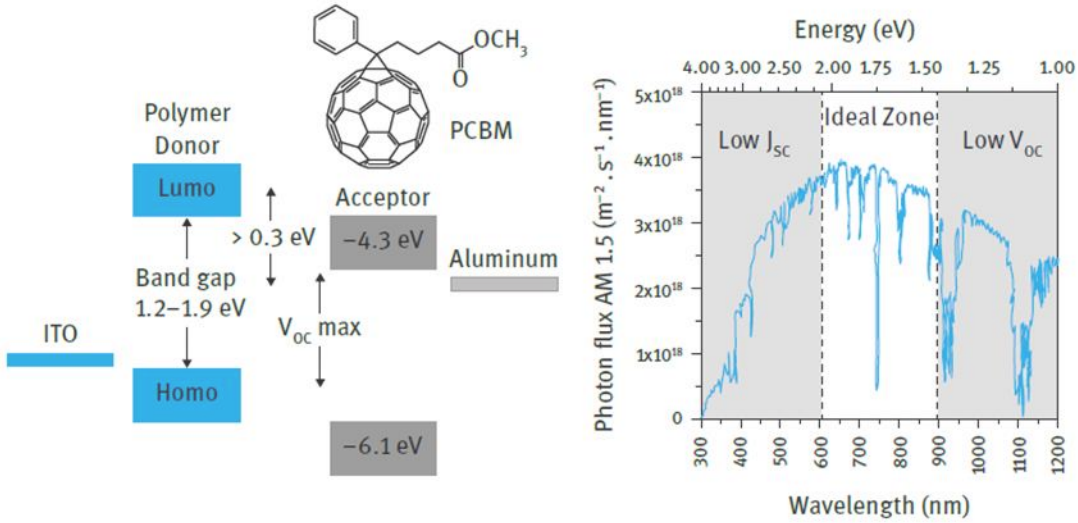

Figure 7.1 Properties of conjugated polymers in OPVs (right) and sun spectrum (left)[11]

(here the electron acceptor is fullerene)

7.2 Optical and photophysical investigation of G1PPT-co-P3HT/PDI-co-Carbazole bulk heterojunction blends

7.2.1 Optical studies of G1PPT-co-P3HT/PDI-co-Carbazole bulk heterojunction blends

G1PPT-co-P3HT:PDI-co-Carbazole bulk heterojunction blends optical absorption properties were studied in chloroform in the UV-Vis-NIR spectral region using Nicolet Evolution 100 UV–visible spectrometer (Thermo Electron, UK) depicted in Figure 7.2. The blends were prepared in the ratio 1:1, 1:2 and 1:3 and investigated with reference to pristine donor G1PPT-co-P3HT (donor) and pristine acceptor PDI-co-Carbazole (acceptor). The blends displayed combined optical behavior of both pristine polymers (refer to Chapter 5, Figure 5.6 and Chapter 6, Figure 6.6 for more details) with strong absorption in the UV-Vis spectral region and onset absorption around 675 nm. It was

interesting to note that for all BHJ blends, the absorption maxima, λ_{max} for the broad band between 470 – 680 nm corresponding to the intermolecular charge transfer (ICT)[19] shifted to shorter wavelength (blue shift) with respect the pristine PDI-co-Carbazole and to longer wavelength with respect to pristine G1PPT-co-P3HT. Indeed, as the amount of PDI-co-Carbazole with respect to G1PPT-co-P3HT was increased in these ratios 1:1, 1:2 and 1:3, the red shift of the blends with respect to the donor were 57, 69 and 75 nm in 1:1, 1:2 and 1:3, respectively. This therefore suggests that there is effective electron transfer between the electron donating polymer and the electron accepting PDI-co-Carbazole. On the other hand, the blue shift of the blends with respect to pristine PDI-co-Carbazole with the 1:1 ratio having 38 nm blue shift, suggests that addition of the later to the pristine G1PPT-co-P3HT results in the deplanarization of PDI-co-Carbazole;[20] but further addition of the accepting polymer might favor strong co-facial π-π interactions that create some molecular ordering.[17]

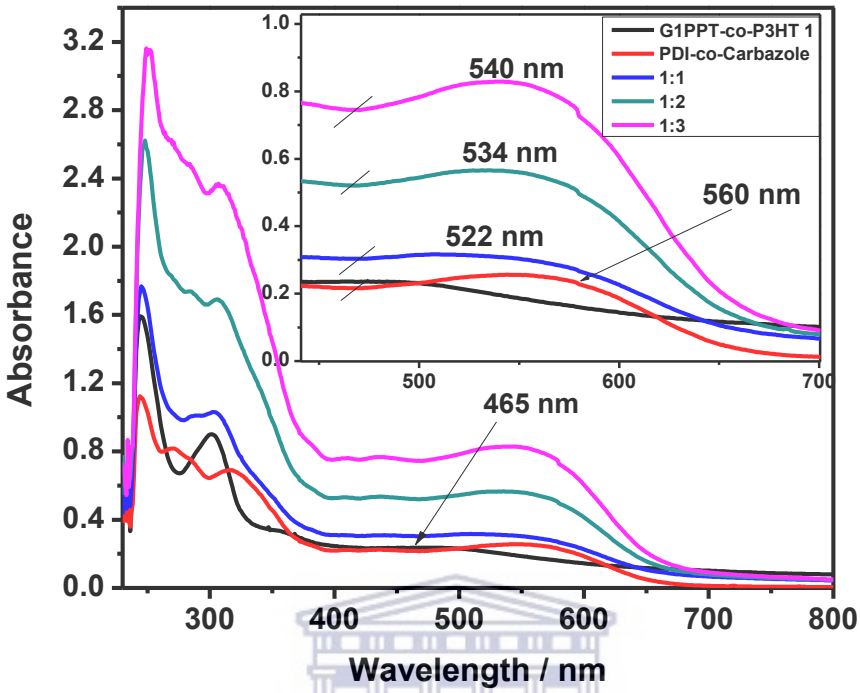

Figure 7.2 UV-Vis absorption of G1PPT-co-P3HT/PDI-co-Carbazole at different ratio

7.2.2 Photoluminescence quenching effects of PDI-co-carbazole on G1PPT-co-P3HT and Förster resonance energy Transfer (FRET)

G1PPT-co-P3HT/PDI-co-Carbazole different bulk heterojunction blends photophysical properties were also investigated using Photoluminescence spectroscopic technique. The nanocomposite fluorescence properties were studied using Ocean Optics device. Fluorescence of pristine G1PPT-

co-P3HT and PDI-co-Carbazole have been fully discussed in Chapter 6, Section 6.3.3.1 and Chapter 5, Section 5.3.3.1, so in this section, we will only focus of the fluorescence of the blends. Upon excitation of D-A blends, total quenching of the donor is observed, characterized by the complete disappearance of the G1PPT-co-P3HT fluorescence emission peak initially exhibited by the pristine material at 551 nm, an indication that there is essentially no radiative exciton decay in the blend.[21] This can be as result of the photo-induced electron transfer between the electron donating G1PPT-co-P3HT and the electron accepting PDI-co-Carbazole which is the desired process in photovoltaic devices. Also, while a red shift (20 nm) of the emission peak of the blends is observed, from 665 nm in pristine PDI-co-Carbazole to 685 nm in the blends, an increase in peak intensity with increasing content of PDI-co-carbazole is also to be noted (Figure 7.3). The total disappearance of the donor fluorescence peak coupled to the increase in acceptor intensity peaks suggest that there is also a Fluorescence or Förster resonance energy transfer (FRET) from the donor to the acceptor.[22] This is further confirmed by the emission spectrum of the donor overlapping the acceptor absorption spectrum[23] as shown in Figure 7.4. We also suspect that this energy transfer is followed by non-radiative recombination[22] considering the increase in acceptor peak intensity above-mentioned.

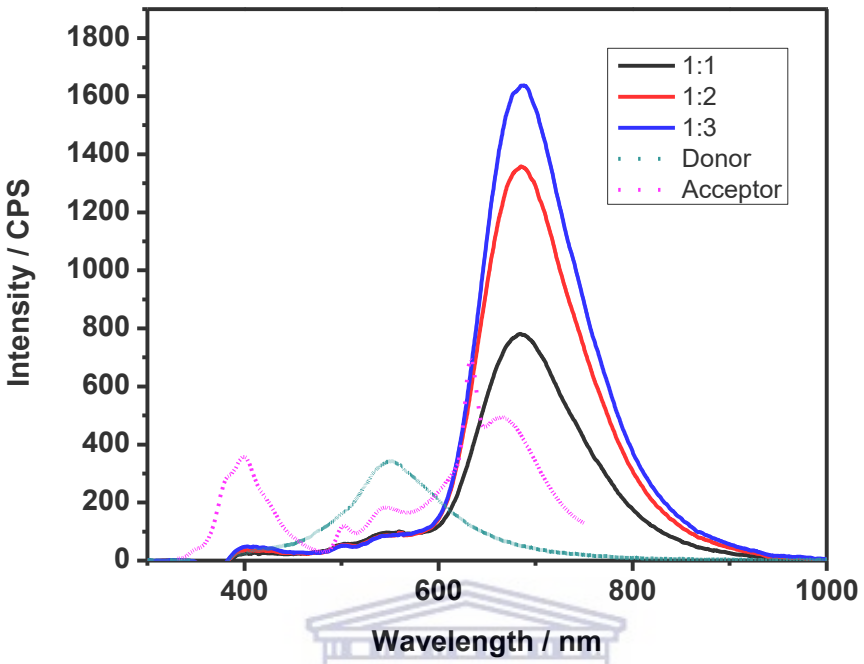

Figure 7.3 Emission spectra of G1PPT-co-P3HT, PDI-co-Carbazole and their blends

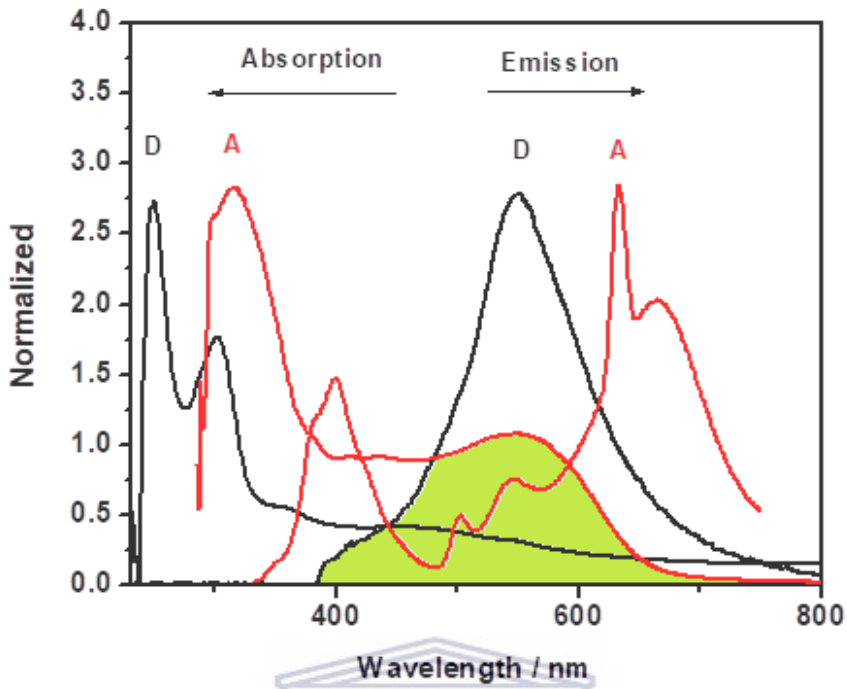

Figure 7.4 Absorption and emission spectra of G1PPT-co-P3HT (D) and PDI-co-Carbazole (A) (green area represents the spectral overlap of donor emission and acceptor absorption characterizing the Förster resonance energy transfer)

7.3 Device fabrication and characterization

7.3.1 Device fabrication

Photovoltaic devices were fabricated according to the following procedure, where the device configuration used was glass/ indium tin oxide (ITO)/poly(3,4- ethylenedioxythiphene): poly(styrenesulphonate) (PEDOT:PSS)/ BHJ active layer/Al with a pixel area of ~0.0256 cm^2.

Prior to fabrication, the patterned ITO-coated glass substrates with resistance 20 Ω / square, were cleaned. The cleaning procedure was as follows: the substrates were sonicated in Hellmanex solution for 15 min and rinsed twice in boiling water; then sonicated for 15 min in N, N-isopropanol and rinse again twice in boiling water. Afterwards, the substrates were dried under an argon gas stream. After the cleaning process, the hole transporting layer, PEDOT:PSS (Heraeus Clevios PH-1000) was deposited on the ITO surface by spin coating at 5000 rpm for 30 s; then dried on a hot plate at 150 °C for 5 min. PEDOT-PSS was used to reduce the roughness of the ITO and acts as electron blocking layer between the ITO and the active layer. PEDOT-PSS was gently wiped away from the etched part of the ITO using de-ionized water with a cotton bud to enhance contact with the electrode. The prepared donor:acceptor solutions in chloroform (50 µL) were spin coated on the PEDOT-PSS at 900 rpm for 105 s, dried on a hot plate at 80 °C for 10 min and the edges were cleaned using chloroform. Finally, the top electrode Al layer (103 nm) deposition was done by thermal evaporation on the glass/ITO/PEDOT-PSS/BHJ active layer substrate to complete the device fabrication. A drop of encapsulation epoxy was deposited on a glass substrate and used to seal the device; that was then dried under UV lamp to avoid oxidation from air contact.

Even though the main device of interest is the one based on G1PPT-co-P3HT/PDI-co-Carbazole (2:1) bulk heterojunction blend, four other devices based on P3HT: PDI-co-Carbazole (2:1), G1PPT-co-P3HT: $PC_{61}BM$ (1:2), PDI-co-Carbazole:$PC_{61}BM$ (1:2), P3HT:$PC_{61}BM$ (2:1) bulk heterojunction blends were also fabricated to investigate the photovoltaic characteristics of each prepared copolymer with respect to well-known widely used P3HT and PCBM as donor and acceptor, respectively.

7.3.2 I-V characteristics evaluation: morphology – device performance relationship.

Current voltage (I-V) curves of the devices were recorded in the dark and under illumination using a solar simulator. All characteristics measurements were carried out at ambient air. The I-V characteristics of the BHJ PSCs as shown in Figures 7.5 to 7.9 were recorded under simulated solar illumination of AM 1.5 with an incident power density of 100 mW/cm^2 from -0.2 to 1 V using a Keithley output Reader. The parameters of the PSCs are summarized in Table 7.1. All devices exhibited very poor performances except for P3HT:PC$_{61}$BM that achieved a power conversion efficiency of 1.5 % for V_{OC} = 140 mV, J_{SC} = 17.85 µA, Fill factor, *FF* = 0.26. G1PPT-co-P3HT:PDI-co-Carbazole (2:1) exhibited the poorest characteristics with V_{OC} = 5 mV, J_{SC} = 2.65 µA, Fill factor, *FF* = 0.11 and almost an extremely low power conversion of 2.1 x 10^{-5} %. This is suggested to be due to the recombination of the separated charges immediately after their excitation - through light absorption. Such result confirms the findings obtained from fluorescence studies where we observed a spectral overlap of the donor, G1PPT-co-P3HT emission spectrum and the acceptor, PDI-co-carbazole absorption characterizing an energy transfer; and mostly the increase in fluorescence intensity peak of the acceptor, which suggested that non-radiative recombination occurs.[24] In addition, the tendency of PDI-co-Carbazole to self-aggregate during film deposition can also account for the isolation/trapping of the charges within the macromolecule lattices which will inhibit proper charge transport.[25,26] Device *FF* of 0.11, smaller than those of other devices may be due to short-conjugated length and amorphous structure of PDI-co-Carbazole. Low *FF*s (below 0.4) of solutions processed OPVs are also associated with large series resistance and small shunt resistance.[27] In OPVs, the device performance is strongly dependent on free charge carrier

generation, transport in the active layer, and collection at corresponding electrodes. The I-V characteristics of most devices exhibit strong electric field dependence (Figure 7.6, 7.7 and 7.8) associated with recombination processes. This is probably induced by the energetically close positions of G1PPT-co-P3HT and PDI-co-Carbazole,[27] thereby reducing the selectivity of the negative contact to separate holes and electrons. Such behavior appears to be a typical feature of transport limitation.

Table 7.1 Summary of photovoltaic device performances.

Device structure: ITO/PEDOT:PSS/Active layer/Al

Active layer	***V*oc (V)**	***J*sc (μA/cm^2)**	***FF***	***PCE*/ (1 x 10^{-3}%)**
P3HT: PDI-co-Carbazole (2: 1)	0.18	62	0.26	3.0
G1PPT-co-P3HT: $PC_{61}BM$ (1:2)	0.08	15	0.24	3
G1PPT-co-P3HT:PDI-co-Carbazole (2: 1)	0.05	2.65	0.11	0.021
PDI-co-Carbazole:$PC_{61}BM$ (1:2)	0.14	17.85	0.26	7
P3HT:$PC_{61}BM$ (2: 1)	0.51	7.7 E^3	0.38	1.5 x 10^3

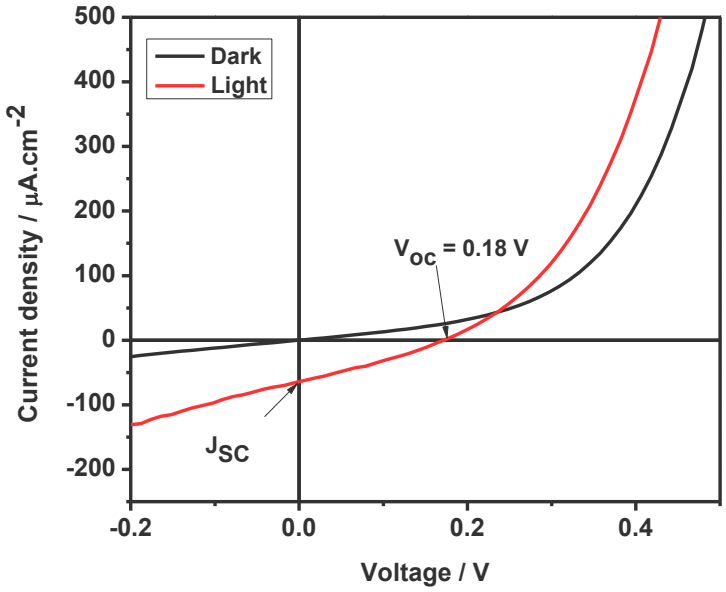

Figure 7.5 I-V Characteristics of P3HT: PDI-co-Carbazole (2: 1)

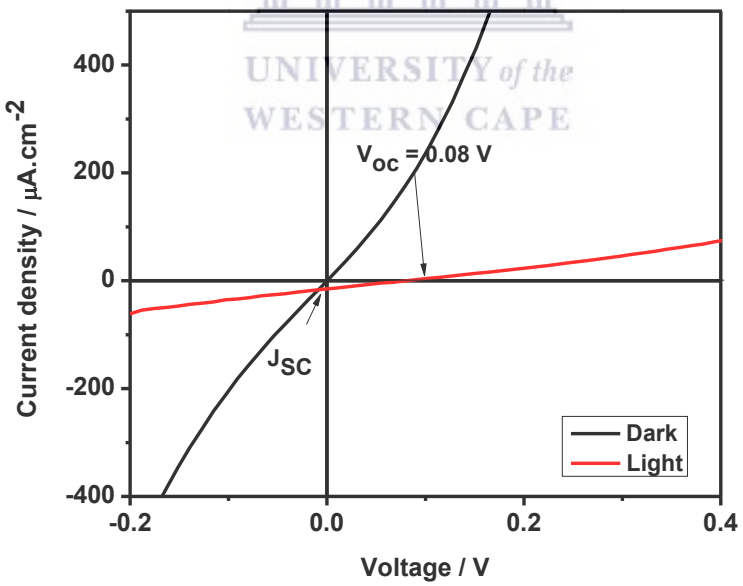

Figure 7.6 I-V Characteristics of G1PPT-co-P3HT: $PC_{61}BM$ (1:2)

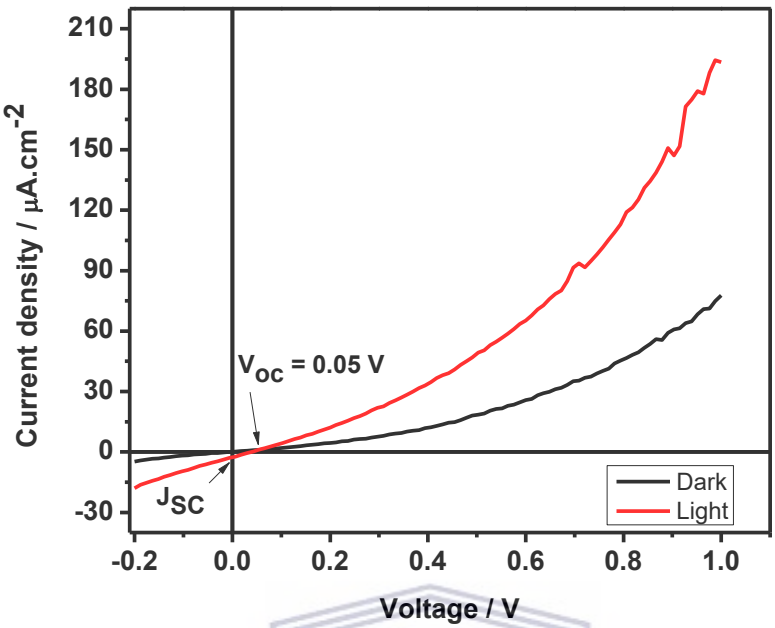

Figure 7.7 I-V Characteristics of G1PPT-co-P3HT/PDI-co-Carbazole (2:1)

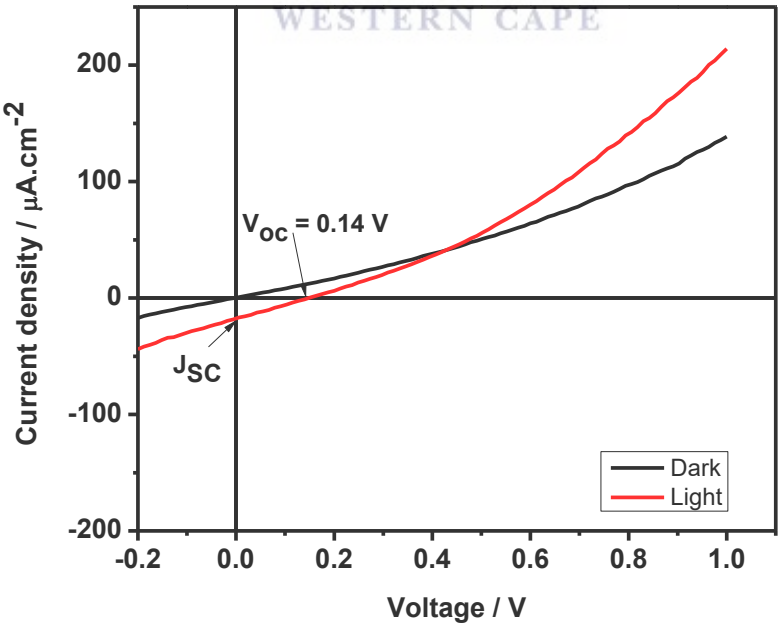

Figure 7.8 I-V Characteristics of PDI-co-Carbazole:$PC_{61}BM$ (1:2)

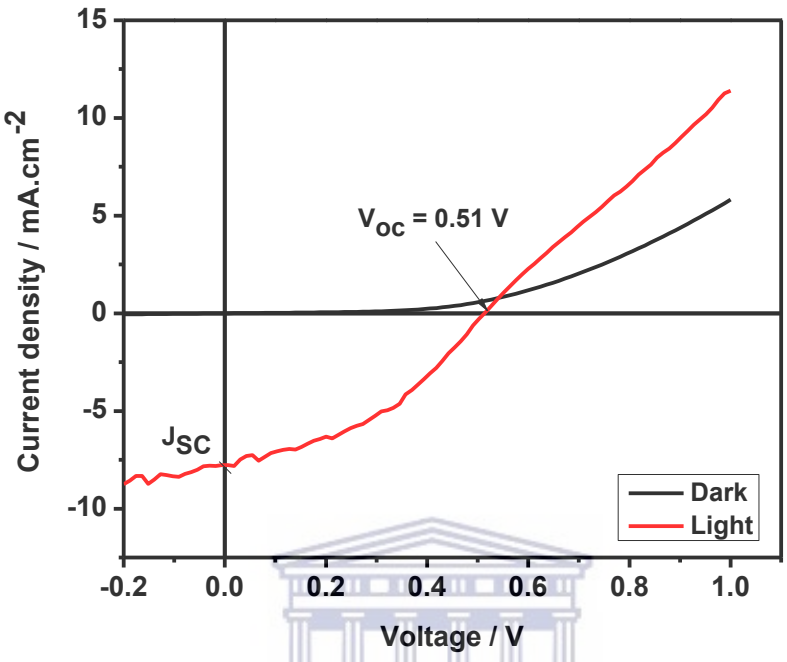

Figure 7.9 I-V Characteristics of P3HT: $PC_{61}BM$ (1:2)

7.3.3 Morphological investigation of the BHJ layers

Various studies have demonstrated that organic photovoltaic device performances are strongly dependent on the BHJ blend morphology.[28,29] It is therefore imperative to understand the relation between them. In order to achieve good charge carrier generation, the interface between the donor and the acceptor should be large enough and efficient charge extraction should be allowed by the

networks blend of donor and acceptor polymers.[30] Also, the capacity of both components to exhibit crystalline ordering on length scales of several nanometers could be beneficial for carrier transport and device efficiency.[16,17] The five devices morphology were investigated using Scanning Electron Microscopy (SEM) and the images on Figures 7.10 to 7.14 show that in most devices, the blends were characterized by evident defects that act as charge trapping and inhibit continuous flow of the charges to the respective electrodes. Precise morphology parameters, including the van der Waals crystal packing of the donor and acceptor polymers; and the formation of nanoscale domains of the two phases, are strongly dependent on donor and acceptor blend ratio, the solvents used, processing conditions and finally post-production treatment. The use of chloroform as the casting solvent could therefore have played a detrimental effect on the morphology of the devices as the fast evaporation of the solvent resulted in material clustering. Also, the low BHJ active layer thickness as see on the image of G1PPT-co-P3HT: $PC_{61}BM$ (Figure 7.11) affected the device performance.

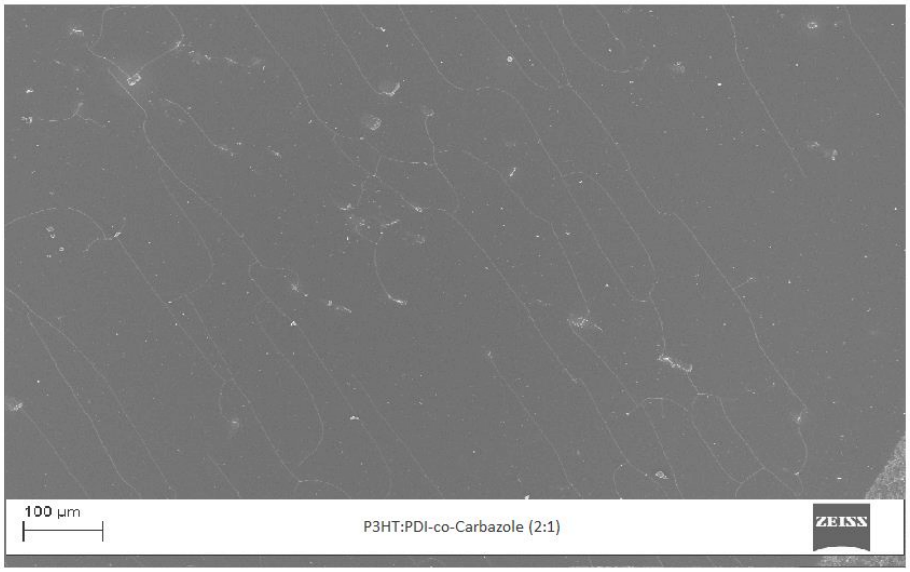

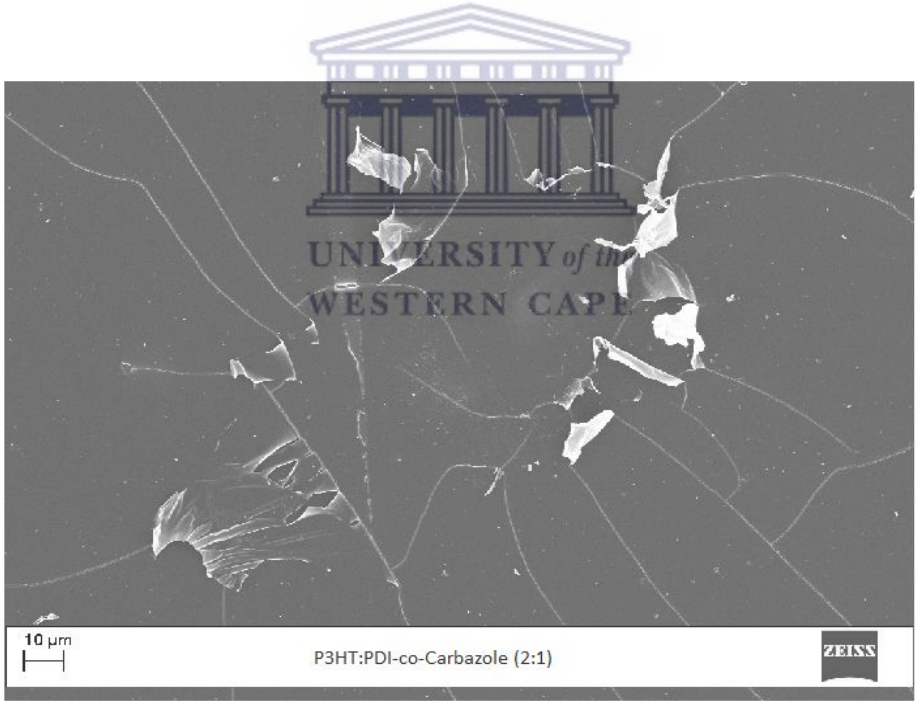

Figure 7.10 SEM images of P3HT:PDI-co-Carbazole (2:1) on 100 µm and 10 µm scale

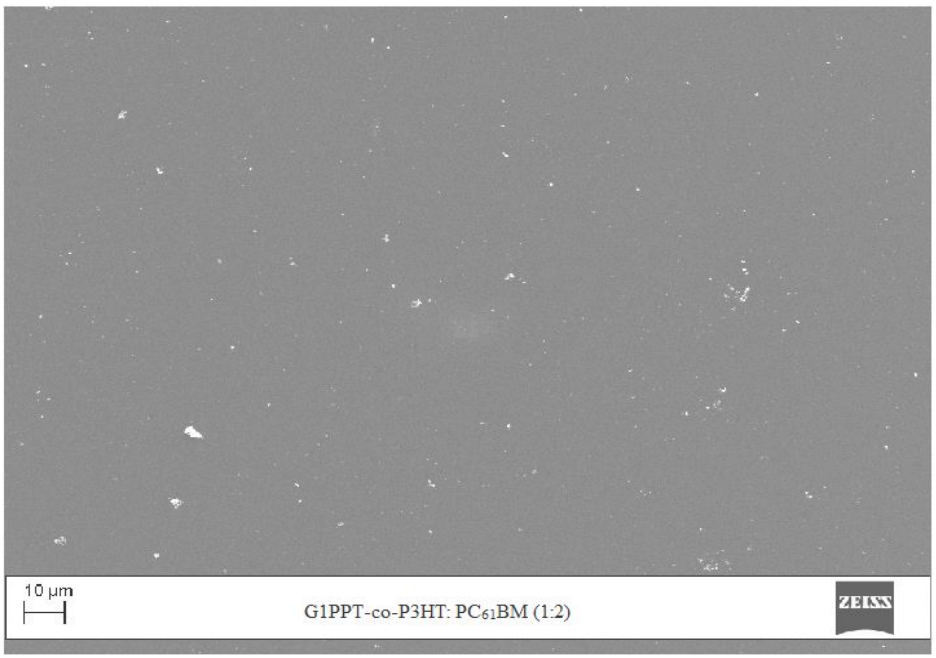

Figure 7.11 SEM images of G1PPT-co-P3HT:$PC_{61}BM$ (1:2) on 10 µm scale

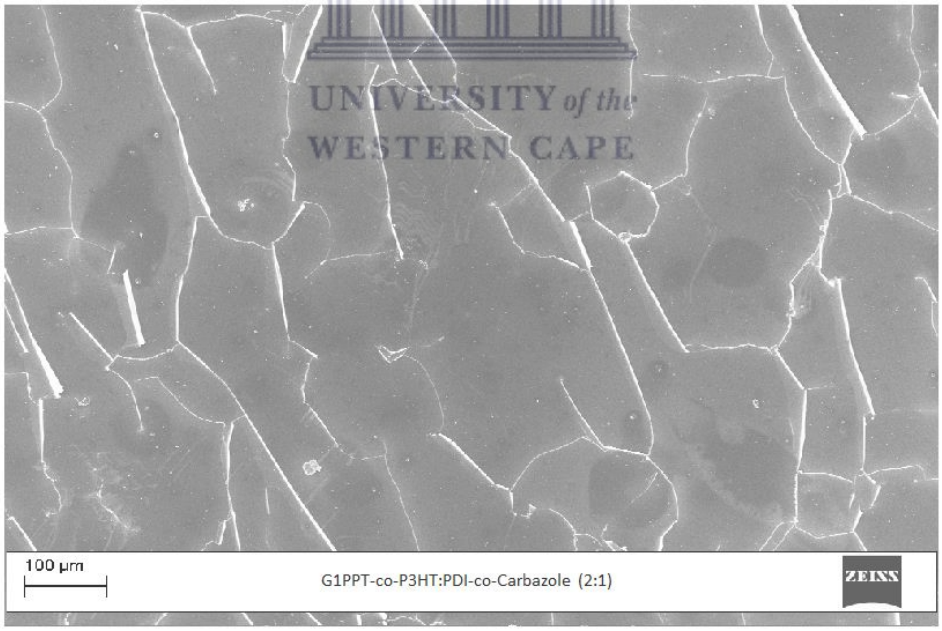

Figure 7.12 SEM images of G1PT-co-P3HT:PDI-co-Carbazole (2:1) on 100 µm scale

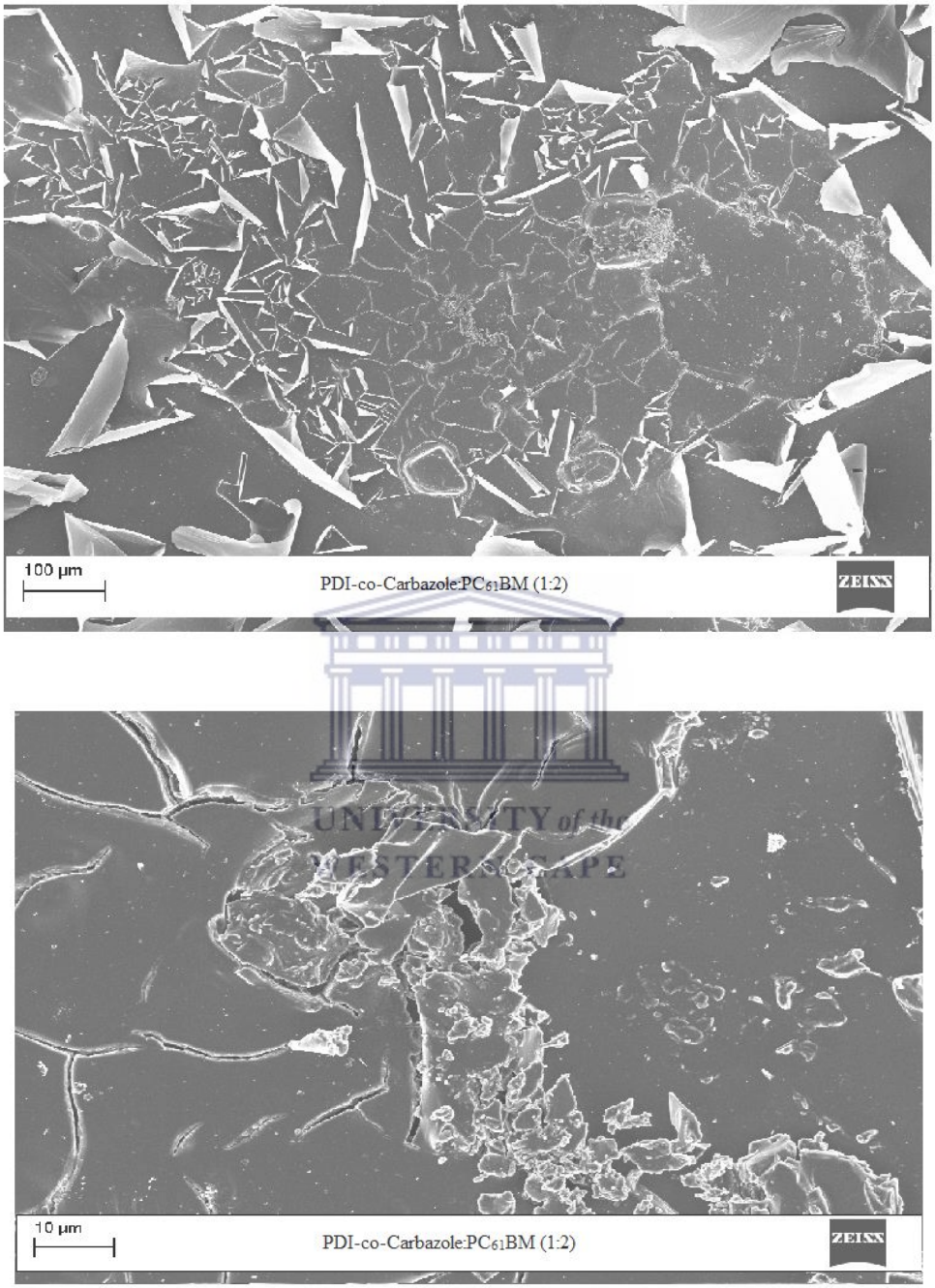

Figure 7.13 SEM images of PDI-co-Carbazole:$PC_{61}BM$ (1:2) on 100 µm and 10 µm scale

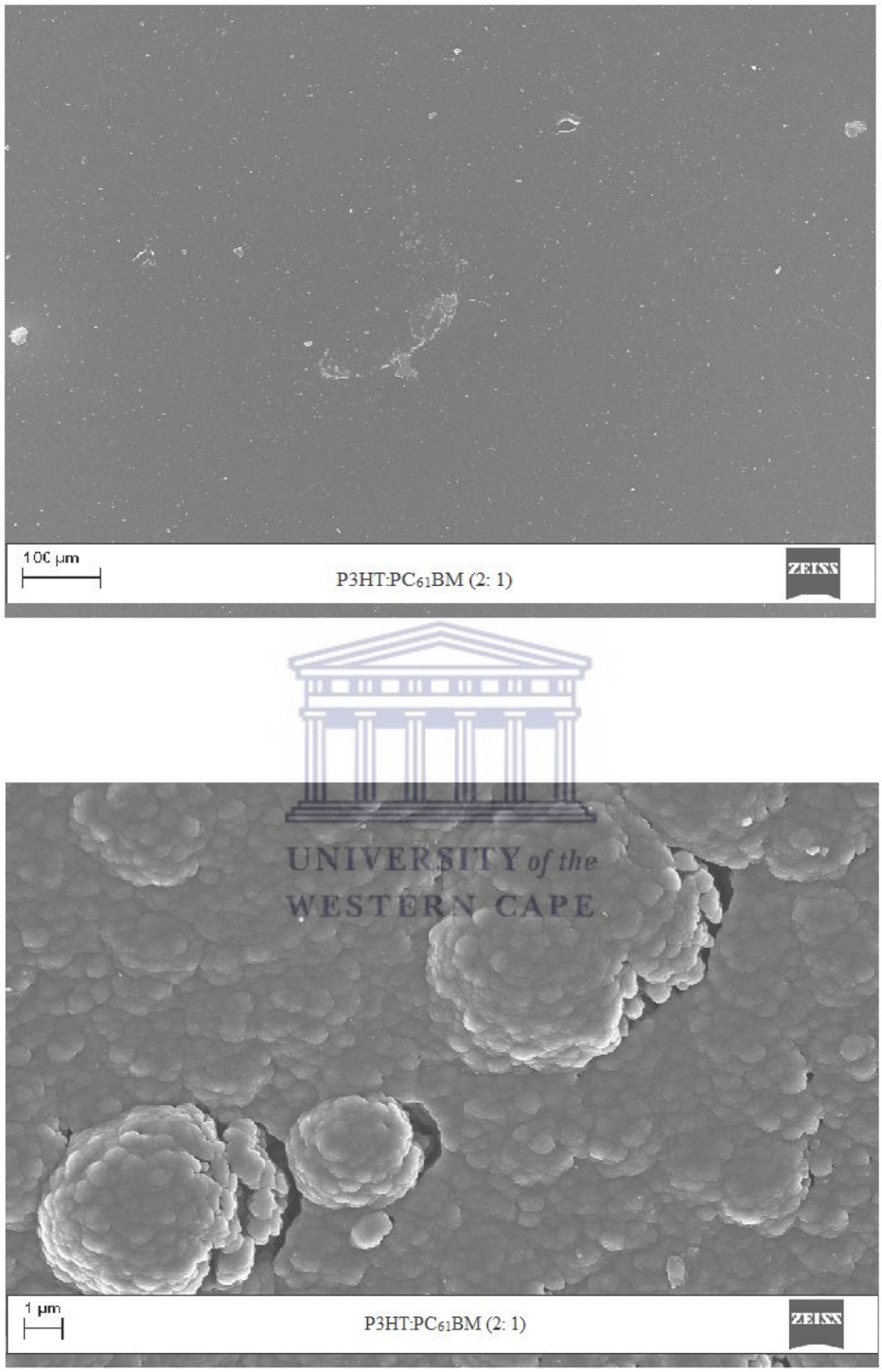

Figure 7.14 SEM images of P3HT:$PC_{61}BM$ (2:1) on 100 µm and 10 µm scale

7.4 Conclusion

Due to parameters used, the multipolymer architecture of G1PPT-co-P3HT:PDI-co-Carbazole was limited to a random arrangement of subunits that consequently hindered its propensity for achieving ordered phases. This resulted in all devices exhibiting relatively poor photovoltaic performance characteristics. Since molecular ordering characterized by crystallinity is a key factor influencing the film optoelectronic properties, important effort has to be put toward synthesizing highly ordered multipolymers that could achieve a greater degree of molecular arrangement and thus improved performance compare to their random counterparts as it was observed in G1PPT-co-P3HT:PDI-co-Carbazole blends.

References

1. Zhou, C., Chen, Z., Zhang, G., McDowell, C., Luo, P., Jia, X., Ford, M. J., Wang, M., Bazan, G. C., Huang, F. & Cao, Y. Toward High Efficiency Polymer Solar Cells: Rearranging the Backbone Units into a Readily Accessible Random Tetrapolymer. *Advanced Energy Materials* **8,** 1–9 (2018).

2. Zhou, E., Cong, J., Wei, Q., Tajima, K., Yang, C. & Hashimoto, K. All-polymer solar cells from perylene diimide based copolymers: Material design and phase separation control. *Angewandte Chemie - International Edition* **50,** 2799–2803 (2011).

3. Wu, Y., Li, G., Tsai, S.-T., Yu, L., Xu, Z., Ray, C., Liang, Y. & Xia, J. For the Bright Future-Bulk Heterojunction Polymer Solar Cells with Power Conversion Efficiency of 7.4%. *Advanced Materials* **22,** E135–E138 (2010).

4. Chen, H.-Y., Hou, J., Zhang, S., Liang, Y., Yang, G., Yang, Y., Yu, L., Wu, Y. & Li, G. Polymer solar cells with enhanced open-circuit voltage and efficiency. *Nature Photonics* **3,** 649–653 (2009).

5. Lin, Y. & Zhan, X. Non-fullerene acceptors for organic photovoltaics: an emerging horizon. *Materials Horizons* **1,** 470–488 (2014).

6. Bundgaard, E. & Krebs, F. C. Low band gap polymers for organic photovoltaics. *Solar Energy Materials and Solar Cells* **91,** 954–985 (2007).

7. Wang, D., Kopidakis, N., Reese, M. O. & Gregg, B. A. Treating Poly(3-hexylthiophene)

with Dimethylsulfate Improves Its Photoelectrical Properties. *Chemistry of Materials* **20,** 6307–6309 (2008).

8. Piliego, C., Holcombe, T. W., Douglas, J. D., Woo, C. H., Beaujuge, P. M. & Fréchet, J. M. J. Synthetic control of structural order in N-alkylthieno[3,4- c]pyrrole-4,6-dione-based polymers for efficient solar cells. *Journal of the American Chemical Society* **132,** 7595–7597 (2010).

9. Günes, S., Neugebauer, H. & Sariciftci, N. S. Conjugated polymer-based organic solar cells. *Chemical Reviews* **107,** 1324–1338 (2007).

10. Lin, Z., Bjorgaard, J., Yavuz, A. G. & Köse, M. E. Low band gap star-shaped molecules based on benzothia(oxa)diazole for organic photovoltaics. *Journal of Physical Chemistry C* **115,** 15097–15108 (2011).

11. Allard, N. & Leclerc, M. Conjugated polymers for organic electronics. In functional materials: for energy, sustainable development and biomedical sciences, 121–138 (De Gruyter, 2014).

12. Facchetti, A. Polymer donor-polymer acceptor (all-polymer) solar cells. *Materials Today* **16,** 123–132 (2013).

13. Zhan, X., Facchetti, A., Barlow, S., Marks, T. J., Ratner, M. A., Wasielewski, M. R. & Marder, S. R. Rylene and related diimides for organic electronics. *Advanced Materials* **23,** 268–284 (2011).

14. Wang, B. Organic π-Stacking Semiconducting Material : Design , Synthesis and the

Analysis of Structure and Properties. Dissertation, The City University of New York (2014).

15. Ma, C. Q., Fonrodona, M., Schikora, M. C., Wienk, M. M., Janssen, R. A. J. & Bäuerle, P. Solution-processed bulk-heterojunction solar cells based on monodisperse dendritic oligothiophenes. *Advanced Functional Materials* **18,** 3323–3331 (2008).

16. Kopidakis, N., Mitchell, W. J., Bozell, J. J., Piris, J., Ginley, D. S., Rumbles, G. & Shaheen, S. E. Bulk Heterojunction Organic Photovoltaic Devices Using Dendrimers. DOE Solar Energy Technologies (2005).

17. Kopidakis, N., Mitchell, W. J., Van De Lagemaat, J., Ginley, D. S., Rumbles, G., Shaheen, S. E. & Rance, W. L. Bulk heterojunction organic photovoltaic devices based on phenyl-cored thiophene dendrimers. *Applied Physics Letters* **89,** 1–4 (2006).

18. Dang, M. T., Hirsch, L. & Wantz, G. P3HT:PCBM, best seller in polymer photovoltaic research. *Advanced Materials* **23,** 3597–3602 (2011).

19. Heo, H., Kim, H., Lee, D., Jang, S., Ban, L., Lim, B., Lee, J. & Lee, Y. Regioregular D1-A-D2-A terpolymer with controlled thieno[3,4-b]thiophene orientation for high-efficiency polymer solar cells processed with nonhalogenated solvents. *Macromolecules* **49,** 3328–3335 (2016).

20. Yang, J., Xiao, B., Tajima, K., Nakano, M., Takimiya, K., Tang, A. & Zhou, E. Comparison among perylene diimide (PDI), naphthalene diimide (NDI), and naphthodithiophene diimide (NDTI) based n-type polymers for all-polymer solar cells application. *Macromolecules* **50,** 3179–3185 (2017).

21. Lu, S., Niu, J., Li, W., Mao, J. & Jiang, J. Photophysics and morphology investigation based on perylenetetracarboxylate/polymer photovoltaic devices. *Solar Energy Materials and Solar Cells* **91,** 261–265 (2007).

22. Berney, C. & Danuser, G. *FRET or No FRET: A Quantitative Comparison*. *Biophysical Journal* **84,** 3992–4010 (2003).

23. Fomo, G., Achadu, O. J. & Nyokong, T. One-pot synthesis of graphene quantum dots–phthalocyanines supramolecular hybrid and the investigation of their photophysical properties. *Journal of Materials Science* **53,** 538–548 (2018).

24. Shinde, K. N., Dhoble, S. J., Swart, H. C. & Park, K. Basic Mechanisms of Photoluminescence. In *Phosphate Phosphors for Solid-State Lighting*, 41–60 (Springer, 2012).

25. Allen, N. S. Photochemistry and Photophysics Of Polymer Materials (Wiley, 2010).

26. Li, M., An, C., Pisula, W. & Müllen, K. Cyclopentadithiophene-benzothiadiazole donor-acceptor polymers as prototypical semiconductors for high-performance field-effect transistors. *Accounts of Chemical Research* **51,** 1196–1205 (2018).

27. Winder, C. Sensitization of low bandgap polymer bulk heterojunction solar cells. *Thin Solid Films* **403–404,** 373–379 (2002).

28. Duan, C., Willems, R. E. M., Van Franeker, J. J., Bruijnaers, B. J., Wienk, M. M. & Janssen, R. A. J. Effect of side chain length on the charge transport, morphology, and photovoltaic performance of conjugated polymers in bulk heterojunction solar cells. *Journal of Materials*

Chemistry A **4,** 1855–1866 (2016).

29. Gu, K. L., Zhou, Y., Gu, X., Yan, H., Diao, Y., Kurosawa, T., Ganapathysubramanian, B., Toney, M. F. & Bao, Z. Tuning domain size and crystallinity in isoindigo/PCBM organic solar cells via solution shearing. *Organic Electronics: physics, materials, applications* **40,** 79–87 (2017).

30. Yang, X. & Loos, J. Toward high-performance polymer solar cells: The importance of morphology control. *Macromolecules* **40,** 1353–1362 (2007).

CHAPTER EIGHT

Conclusion and future work

8.1 Summary of findings

This work reports on the first-time chemical preparation of low-band gap, air-stable and highly crystalline generation 1 poly (propylene thiophenoimine)-co-poly(3-hexylthiophene) (G1PPT-co-P3HT) as a donor material for bulk heterojunction organic photovoltaic cells (OPVs). The star copolymer was synthesized at room temperature in chloroform, via oxidative copolymerization in the presence of ferric chloride ($FeCl_3$) under a gentle nitrogen stream for 48 h. Synthesis achieved a high molecular weight star copolymer (M_w 30315 g/mol) with dispersity, $Đ$= 1.87. Confirmation of the isolated pure macromolecule was done via ^{1}H NMR and FTIR spectroscopy. Results obtained from ^{1}H NMR demonstrated that the star copolymer was constituted of 84 % regioregular poly(3-hexylthiophene) which accounted for the molecular ordering observed in the HRSEM images that showed one-directional lattice fringes; confirmed by the clear, well-aligned crystal lattices in Small -Angle energy diffraction (SAED) images. Regioregularity of polymers is a very important feature when designing organic photovoltaic devices as the molecular ordering in the materials films allows for appropriate charges separation and continuous transport to the respective electrodes. Particles size within the nanometer range found in this copolymer (2– 23 and 55 – 76 nm); as evaluated by small angle x-ray scattering (SAXS) analysis will definitely aid the flow of

electrons in the conjugated chain. This dendritic polymer also exhibited excellent absorption properties in the UV-Vis into NIR spectral region; a very important characteristic of donor material in OPVs, with an onset absorption above 850 nm that allowed for an optical band gap E_g^{opt} around 1.43 eV. Indeed, upon copolymerization to 3-hexylthiophene, two new bands are observed. The broad band between 400-680 nm is as result of intramolecular transfer due to the extended conjugation in the alkylated thiophene chain, and another small band at 830 nm is assumed to be due to n-π* transition. Such low optical band gap is an added advantage towards photovoltaic device fabrication as when combined to the suitable acceptor material, there will be proper "jump" of the electrons to the lowest unoccupied molecular orbital (LUMO) of the acceptor. G1PPT-co-P3HT demonstrated good semiconducting properties with quasi-reversible electrochemical behavior in 0.1 M Bu_4NPF_6 (acetonitrile) at 50 mV/s scan rate. The electronic parameters, E_{IP} (-E_{HOMO}), E_A (-E_{LUMO}) and electrochemical bag gap E_g^{ec} of the material as determined by cyclic voltammetry on the reference of ferrocene energy level were 5.53, 3.6 and 1.93 eV respectively. All these optical, electronic and morphological results qualify G1PPT-co-P3HT as a good electron donor for photovoltaic applications. But also allow for the consideration of this dendritic star copolymer in optoelectronic notably organic light-emitting diodes (OLEDs) in which molecular ordering is of outermost importance.

On the other hand, poly[N,N'-bis(dodecyl)perylene-3,4,9,10-tetracarboxylic diimide-1,7-diyl-alt-9-(heptadecan-9-yl)carbazole-2,7-diyl] (PDI-co-Carbazole), an electron acceptor copolymer was also synthesized. A lot of effort has been put in the designing of non-fullerene based photovoltaic devices and perylene diimides have been identified as good electron accepting semiconductors.

Perylene diimide copolymerized to carbazole have received a lot of attention but most of these types of copolymers being studied consist of branched alkyl or other functionalized substituents at the imide (core) positions. Here we designed a copolymer based on perylene diimide and carbazole via the well-known Suzuki coupling with dodecyl substituents at the imide positions. The copolymer was successfully prepared as confirmed by spectroscopic techniques and exhibited good absorption properties in the UV-Vis spectral region with optical band gap, E_g^{opt} = 1.73 eV. The morphology of the material was found to be amorphous with aggregate formation of particle size between 1– 22 nm and 60 – 90 nm. Electrochemical band gap, E_g^{ec} as determined using cyclic voltammetry investigation of the copolymer deposited on a platinum electrode disk in in 0.1 M Bu_4NPF_6 (acetonitrile) at 50 mV/s scan rate on the reference of ferrocene was found to be slightly higher than the optical band gap. The semiconducting properties of the material were ascertained by means of electrochemical impedance spectroscopy. The later technique revealed that this copolymer is very sensitive to the applied potential as decreasing the formal potential resulted in a decrease of the semi-conductive behavior through an increase of charge transfer resistance.

The two prepared materials, star copolymer donor G1PPT-co-P3HT and polymer acceptor PDI-co-Carbazole, were then mixed in bulk heterojunction blends of different ratios (1:1, 1:2 and, 1:3), an architecture that allow for three-dimensional internetworking of the electron donating and electron accepting materials. The optical studies of these blends revealed that the tendency of PDI-co-Carbazole to aggregate was increased when mixed with G1PPT-co-P3HT as there was an evident blue shift of the blends' wavelength with respect to pristine PDI-co-Carbazole. Studies of the fluorescence properties demonstrated that photo-induced electron transfer characterized by the

total disappearance of fluorescence peak of G1PPT-co-P3HT was accompanied by Förster resonance energy transfer. Indeed, a pronounced spectral overlap of the emission of the donor GPPT-co-P3HT with the absorption of the acceptor PDI-co-Carbazole was observed. This resonance energy transfer suggested to be followed by non-radiative, germinate recombination of the charges, was confirmed by the poor photovoltaic performances of their blend. Indeed, five photovoltaic devices based on the following BHJ active layers, G1PPT-co-P3HT:PDI-co-Carbazole (2:1), P3HT: PDI-co-Carbazole (2:1), G1PPT-co-P3HT: $PC_{61}BM$ (1:2), PDI-co-Carbazole:$PC_{61}BM$ (1:2), P3HT:$PC_{61}BM$ (2:1) were fabricated. The architecture followed this configuration, glass/ITO/PEDOT: PSS/active layer/Al where, PEDOT:PSS was deposited by spin-coating followed by annealing at 150 °C for 5 min, then the active layer was spin-coated from chloroform solution and annealed at 80 °C for 10 min and Al layer was thermally evaporated as the cathode electrode. All devices exhibited poor photovoltaic characteristics except from P3HT:$PC_{61}BM$ that demonstrated a power conversion efficiency PCE of 1.5 %. G1PPT-co-P3HT:PDI-co-Carbazole exhibited the poorest device performance with an open-circuit voltage V_{OC} of only 5 mV compare to 510 mV for the P3HT: $PC_{61}BM$ -based device. Investigation of the morphology revealed that the high amount of defects in the structure of the blends act as trap of charges, prevent their transport to the electrodes and allow for charges recombination. Also, the inherent tendency of PDI-co-Carbazole to aggregate has aided in the poor homogeneity of the thin film. In addition, we suspect that the choice of chloroform as the casting solvent played a detrimental role on these performances as chloroform quick evaporation time does not give sufficient appropriate time for homogeneous film forming.

This work also included the evaluation of the charge carrier transport of some thienothiadiazole/fluorene copolymers in organic field-effect transistors (OFETs). As charge separation and transport is a crucial step in the photovoltaic performances, it is important to investigate these parameters in photovoltaic polymer materials. The synthesis of these thienothiadiazole/fuorene materials was done by Cimrova and co-workers and is reported in literature (see Chapter 4 for references). Side-chain engineering through alkyl substitution is usually used during optoelectronic and photovoltaic polymers design as a way to increase the solubility of the materials, tune their morphology, optical and photophysical properties; which therefore influence their device performances. The materials under our investigation were prepared with different alkyl chains on either thienothiadiazole or fluorene component of the backbone and are denoted CEHTF, CEHTF8, CHTF and CDTF. These organic field-effect transistor devices were successfully fabricated using top-gate, bottom-contact architecture with silver (Ag) top-electrode and poly(methymethacrylate) (PMMA) as dielectric gate. Different parameters were varied during these device fabrications to investigate if they had any significant effect on the hole mobilities. Because these polymers are electron donors, hole mobilities were evaluated in the source-drain voltage (V_{SD}) range -100 V to 0 V with increasing negative gate-voltage (V_G) from 0 V to -100 V. All, devices demonstrated typical transistors behaviour characterized by linear and saturated regimes. The best performance, with saturated mobility, μ_{sat} as high as 2.4 x 10^{-2} cm^2/Vs was exhibited by CDTF copolymer with ethylhexyl groups on the fluorene and n-dodecyl side chain on the thienothiadiazole and with the highest layer thickness; whereas, the lowest mobilities were observed from CEHTF comprising ethylhexyl side chain substitutions on both backbone components. An increase of the hole mobilities by three orders of magnitude from CEHTF to

CDTF through CEHTF8 and CHTF was observed. This demonstrates that the best hole mobilities in these thienothiadiazole/fluorene copolymers are obtained from the linear alkyl-substituted polymers and most specifically those with straight alkyl substitutions on the thienothiadiazole component. These polymers also demonstrated hole mobilities dependence on the molecular weights; but the extent of this dependence is highly based on the dispersity, *Đ* of these macromolecules. Indeed, a good M_W/ *Đ* regime needs to be met to obtain optimum charge transport properties. Further investigation by varying parameters such as dielectric thickness, surface pre-treatment or annealing did not bring any significant change in the charge transport. Summary of the hole mobilities can be found in Table 8.1

Table 8.1 Hole mobilities summary for CEHTF, CEHTF8, CHTF and CDTF

Chemical structure of copolymer	Denotation	R_1	R	μ_{sat} cm^2/Vs
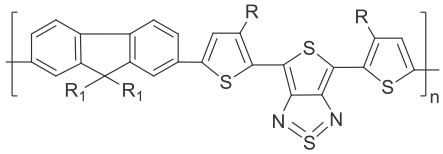	CEHTF	2-ethylhexyl	2-ethylhexyl	*7* x 10^{-5} (lowest μ_{sat})
	CEHTF8	n-C_8H_{17}	2-ethylhexyl	6.7 x 10^{-4}
	CHTF	2-ethylhexyl	n-C_6H_{13}	*3* x 10^{-3}
	CDTF	2-ethylhexyl	n-$C_{12}H_{25}$	2.4 x 10^{-2} (highest μ_{sat})

8.2 Recommendations and future work

It is evident that the overall device performances were far from good, but these materials present good properties for OPVs and there is room for optimization of their photovoltaic characteristics. It is critical to study the fundamental processes of charge transfer and charge carrier recombination across the donor– acceptor interfaces. The band gap offset between donor and acceptor must be optimized to yield the highest possible photovoltage from the device. Also, ways to reduce contact resistance between layers must be found in order to reduce the device series resistance, which is important in determining the fill factor, *FF* and thus the power conversion efficiency, PCE. It is also important to increase the active layer thickness while minimizing charge carrier recombination and keeping the series resistance of the device low in order to obtain higher charge carrier mobilities. In addition, strategies to develop BHJ active layers that self-assemble into ordered phases with pathways for efficient charge transport is a promising route to obtaining higher carrier mobilities.

Future work therefore consists in designing ways to address issues such as control of the morphologies, and improving the optoelectronic properties of the light-absorbing and charge-transporting materials through optimization of the active layer thickness, use of other solvents, temperature and solvent annealing, use of additives, use of different cathode electrode. This will therefore include:

1. Detailed qualitative and quantitative investigations of the photo-physical and morphological properties of the co-polymers G1PPT-co-P3HT, PDI-co-Carbazole and their bulk heterojunction thin films through TOF, AFM, XPS and mobility studies will be worthwhile to better understand how the materials interact and can be better engineered in the bulk heterojunctions systems to avoid recombination process.

2. Varying the ratio of donor:acceptor, device engineering such as thickness optimization, pre- and/or post-solvent and thermal annealing which usually have varying influence on the morphology which in turn will affect morphological and photovoltaic properties of the material is recommended.

3. Investigation of other electrodes in place of Al in the device configuration.

4. Furthermore, it is obvious that despite the good optical properties of G1PPT-co-P3HT and PDI-co-Carbazole, their photovoltaic properties are far from being enhanced. Reaction conditions should be optimized through addition of different side-chains or varying the alkyl substituents in order to suppress the aggregation issue.

5. Contact resistance in the thienothiadiazole/fluorene –based organic field-effect transistors devices performances should be investigated in order to understand their effect on the charge transport properties.